

POLYELECTROLYTE MULTILAYERS FOR TUNABLE
RELEASE OF ANTIBIOTICS AND OTHER THERAPEUTICS

by

Helen F. Chuang

B.S. Chemical Engineering
California Institute of Technology, 2003

SUBMITTED TO THE DEPARTMENT OF CHEMICAL ENGINEERING IN PARTIAL
FULFILLMENT OF THE REQUIREMENT FOR THE DEGREE OF

DOCTOR OF PHILOSOPHY IN CHEMICAL ENGINEERING
AT THE
MASSACHUSETTS INSTITUTE OF TECHNOLOGY

SEPTEMBER 2008

©2008 Massachusetts Institute of Technology. All rights reserved.

Signature of Author: _____
Department of Chemical Engineering
July 30, 2008

Certified by: _____
Paula T. Hammond
Professor of Chemical Engineering
Thesis Supervisor

Accepted by: _____
William M. Deen
Professor of Chemical Engineering
Graduate Officer

Abstract

Polyelectrolyte multilayers (PEMs) were fabricated via the layer-by-layer (LbL) deposition process, incorporating hydrolytically degradable poly(β -amino esters) to result in biodegradable PEMs that can release active ingredients in a dosage- and rate-tunable fashion. Specifically, PEMs incorporating several types of antibiotics, ranging from aminoglycosides to antimicrobial peptides (AmPs), were fabricated and characterized; these coatings are intended for applications onto biomedical device surfaces for infection control. *In vitro* efficacy against *Staphylococcus aureus* and nontoxicity towards pre-osteoblasts MC3T3 were demonstrated. *In vivo* evaluations involving a rabbit osteomyelitis model were undertaken as well.

Aside from the development of antimicrobial PEMs, additional projects pursued under this thesis, all in the context of PEM-based drug delivery, include [1] demonstration of the sequential release of two species, [2] assessment of the *in vitro* activity of anti-coagulant films, [3] delivery of siRNAs, [4] evaluation of the biocompatibility of poly(β -amino esters), [5] incorporation of cyclodextrins for the purpose of small molecule delivery, [6] incorporation of poly(lactic-*co*-glycolic acid) (PLGA) nanoparticles encapsulating gentamicin, [7] evaluation of film sterilizability via FDA-approved methods, and [8] design and characterization of a multi-drug coating for orthopedic implants for dual antimicrobial and tissue regenerative actions.

Acknowledgements

This thesis and my graduate school experience would not have been possible without the support and encouragement of many. First and foremost, I wish to give my deepest gratitude to Professor Paula Hammond, for not only her guidance on my research, but also her supportive and cheerful attitude towards all my pursuits in and out of the laboratory. My thesis experience has been multifarious and engaging because of the variety of projects and activities that she has generously allowed me to pursue.

I also wish to thank my thesis committee members, Professors Robert Langer, Myron Spector, and K. Dane Wittrup, for providing me very constructive feedback on my research and career planning. Myron was especially helpful in developing my project towards the orthopedic implant application and provided invaluable guidance on my animal studies. I also want to give my gratitude to Professor William Deen, my first advisor at MIT, for being a very caring mentor during my time in his group and for his understanding of my need to pursue a different project.

I also want to thank Professor David Lynn at University of Wisconsin, Madison and members of his group, for being great collaborators and friends over the course of my thesis. Backtracking a bit, I would also like to acknowledge my professors at Caltech and mentors on my summer internships for the preparation and support they provided me towards graduate school attendance. I want to especially acknowledge Professors Mark Davis, Frances Arnold, and Zheng-Gang Wang at Caltech, as well as Dr. Brett Cruden at NASA Ames Research Center.

Everyone in the Hammond group past and present had been a critical part of my thesis, both as a research collaborator and as a friend. I would like to especially thank Kris Wood, for training me on numerous aspects of my project and being a fantastic mentor throughout my thesis. I also want to thank individuals on the drug delivery project for their collaborative efforts and insightful discussions – Mara Macdonald, Renée Smith, Anita Shukla, Byeong-Su Kim, and Daniel Schmidt. I also want to acknowledge Josh Moskowitz for being a diligent “apprentice”. Many other past and present members including Jodie Lutkenhaus, Nicole Zacharia, Piljin Yoo, Kevin Krogman, and Eric Verploegen also helped with various aspects of my project. Nathan Ashcraft has been a fun cubicle mate over the years so deserves a mention here.

This thesis was completed to its extent with the assistance from many wonderful undergraduate students – Yamicia Connor, Jenny Yeh, Alia Carter, Matt Clancy, Michelle Wilson, Andrew Hoy, HyeMee Shin, and Jeff Easley. Jenny, Michelle, HyeMee, and Jeff were especially hardworking. Jeff in particular was invaluable in my last year of research, and I hope the experience will pay him back during his thesis.

For my animal studies, I want to thank Dr. Hu-Ping Hsu for performing the surgeries, teaching me surgical techniques, preparing the histology samples, and sharing his insights on our surgical observations and other data. Dr. Larry Madoff was extremely helpful throughout the study with his inputs on our infection model. Dr. Jean Lee took over

Larry's part and provided valuable inputs on the future directions of the model. Drs. Scott Martin and Mitch Harris helped to shape the overall approach to the model. I also want to give deep thanks to all the staff at the E25 animal facility and MIT DCM, especially Alison Hayward, Sylvia Lesnikowski, Katie Madden, Chris Autieri, and Ellen Buckley – for their assistance on animal care, facility logistics, and data evaluation.

Many thanks also go to members of the Robert Langer group, past and present, for being both wonderful friends and valuable advisors on my research and business ventures. Karen Daniel, David Berry, Yoon Yeo, David Nguyen, Greg Zugates, Jason Fuller, Jordan Green, Frank Gu, Jeff Karp, Dan Kohane, William Neeley, Grace Kim, and Naushad Hossain have all helped with my project in some way, and I would still like to thank many more for their friendships.

My antimicrobial peptide project would not have been possible without Chris Loose and Tanguy Chau. I wish to especially thank Chris for proposing the collaboration, training me on various antimicrobial testing protocols, and being a close collaborator. Chris also generously assisted me with my business ventures. Speaking of which, I also want take this opportunity to acknowledge “MAD Nanolayers” team members- Lakshman Pernenkil, Eileen Peng, Chris Bettinger, Benoit Elichabe, and Ken Messier, for their dedication towards the business project.

Certainly my thesis could not have progressed smoothly without the help of numerous administrative staff. I want to especially thank Linda Mousseau, for not only handling all my complicated administrative requests but also being a good friend. Members of the student office – Suzanne Easterly, Mary Wesolowski, and Iris Chang, have also been great help and fun. Katie Foster, Alina Haverty, Connie Beal, Gwen Wilcox, Don McGaffigan, and many other staff members of the department have also been tremendously helpful at one point or another.

For funding, I wish to acknowledge NIH, MIT Deshpande Center for Innovation, the DoD, NSF, and MIT Office of the Provost for their research grants and fellowships. I would like to thank the Deshpande Center for going far beyond funding and helping to bring my project out into the entrepreneurial scene in Boston.

Of course, no endeavor in my life would be possible without my family and friends. My husband David Moore deserves a standing ovation for enduring all my research complaints over the years. He has provided me the kind of understanding and support that no one else can. I want to thank my parents for always being there for me whether they with my decisions or not. They have shown an extraordinary level of care and concern for me. My siblings Jody and Frank have been great sounding boards on college and graduate school experiences, and my grandmother has remained an unparalleled caregiver since the day I was born. My friends from college and high school have provided me essential mental and emotional boosts throughout these years.

Despite the lengthiness of this acknowledgement, it is by no means comprehensive. So much has gone into my thesis that perhaps I should sum it up with “thank you, world”.

Biography

Helen Fei-Lun Chuang was born in Taipei, Taiwan on February 24, 1981. She spent her first fourteen years of life in Taiwan, undergoing a variety of urban, suburban, and even farmland living. She was an avid artist in her early life but eventually found her passion in the math and sciences through her participation of a magnet program in elementary school. In 1995, she immigrated to the U.S. with her sister Jody, and began life in the new world at Monta Vista High School in Cupertino, CA. Her nerdy character persisted in the new country, leading to her continual participation on the math and science teams and, eventually, to the California Institute of Technology (Caltech). To prove to her unconvinced parents that she could handle the rigor of Caltech, Helen chose the allegedly toughest major there – chemical engineering – and fortunately survived. The college years proved to be extremely important in her life – she found her passion in the chemical engineering discipline, met her husband David Christopher Moore, and established lasting bonds with the fantastic faculty and students there.

As if one Institute of Technology was not enough, Helen and David decided to attend MIT for their Ph.D. degrees beginning 2003, in the chemical engineering and computer science programs, respectively. During this process, Helen not only affirmed her interest in engineering technology development, but also discovered a new interest in entrepreneurship. She participated in various business classes and events and got the opportunity to work with a wonderful team of MBA and Ph.D. students in crafting a business plan around a technology stemming out of her research. Her combination of research and venture experiences from MIT led to her decision to pursue a career in entrepreneurship, and she is very excited to begin her life after school with a business-oriented role at a biotech start-up in sunny Southern California.

Table of Contents

BIOGRAPHY	5
TABLE OF CONTENTS	6
LIST OF FIGURES.....	8
LIST OF TABLES.....	12
CHAPTER 1. INTRODUCTION	13
1.1 CONTROLLED RELEASE.....	13
1.2 SURFACE RELEASE FROM ORTHOPEDIC IMPLANTS: AN UNMET NEED IN CONTROLLED RELEASE .	15
1.2.1 <i>Current implant surface treatment options</i>	16
1.2.2 <i>Current sequential release methods</i>	17
1.3 LAYER-BY-LAYER (LBL) ASSEMBLY AS A SOLUTION FOR SEQUENTIAL RELEASE	18
1.3.1 <i>Introduction</i>	18
1.3.2 <i>Applications to drug delivery</i>	19
1.3.3 <i>Beyond drug delivery: degradable LbL films for other applications</i>	24
1.3.4 <i>Previous work in LbL drug delivery</i>	25
1.4 OVERVIEW OF THESIS	25
1.4.1 <i>Background on materials and methods</i>	25
1.4.2 <i>Previous work</i>	27
1.4.3 <i>Initial objectives</i>	29
1.4.4 <i>Revised objectives</i>	30
1.4.5 <i>Summary of thesis progression</i>	32
1.4.6 <i>Concurrent LbL drug delivery projects</i>	35
1.5 OUTLOOK: OTHER LbL DRUG DELIVERY SYSTEMS	36
1.5.1 <i>Electrochemically degradable LbL films</i>	36
1.5.2 <i>Reductively degradable LbL films</i>	38
1.6 REFERENCES	40
CHAPTER 2. INCORPORATION OF POLYSACCHARIDES	50
2.1 SEQUENTIAL RELEASE OF POLYSACCHARIDES	50
2.1.1 <i>Introduction</i>	50
2.1.2 <i>Materials and Methods</i>	51
2.1.3 <i>Results and Discussion</i>	55
2.1.4 <i>Conclusion</i>	64
2.2 IN VIVO ASSESSMENT OF HEPARIN FILMS.....	65
2.2.1 <i>Introduction</i>	65
2.2.2 <i>Materials and Methods</i>	66
2.2.3 <i>Results and Discussion</i>	67
2.2.4 <i>Conclusion</i>	77
REFERENCES.....	78
CHAPTER 3. BIOCOMPATIBILITY ASSESSMENT OF POLY X'S.....	80
3.1 INTRODUCTION.....	80
3.2 MATERIALS AND METHODS.....	81
3.3 RESULTS AND DISCUSSION.....	81
3.4 CONCLUSION.....	95
CHAPTER 4. INCORPORATION OF CYCLODEXTRINS FOR SMALL MOLECULE ENCAPSULATION	98
4.1 INTRODUCTION.....	98

4.2	MATERIALS AND METHODS	101
4.3	RESULTS AND DISCUSSION.....	103
4.4	CONCLUSION.....	114
CHAPTER 5. POLYELECTROLYTE MULTILAYERS FOR TUNABLE RELEASE OF ANTIBIOTICS 118		
5.1	FABRICATION AND CHARACTERIZATION	118
5.1.1	<i>Introduction</i>	118
5.1.2	<i>Materials and Methods</i>	123
5.1.3	<i>Results and Discussion</i>	130
5.1.4	<i>Conclusion</i>	151
5.2	SUPPLEMENTS TO INVESTIGATIONS ON [(POLY 1/HA)(GS/HA)] _N	153
5.2.1	<i>Chitosan substitution of Poly 1 to probe release mechanism</i>	153
5.2.2	<i>Alternative polyanion and influence of MW</i>	155
5.3	PHYSICOCHEMICAL PROPERTIES OF [(POLY 1/HA)(GS/HA)] _N	159
5.3.1	<i>Introduction</i>	159
5.3.2	<i>Materials and Methods</i>	159
5.3.3	<i>Results and Discussion</i>	160
5.3.4	<i>Conclusion</i>	166
5.4	PLGA ENCAPSULATION OF GENTAMICIN.....	167
5.4.1	<i>Introduction</i>	167
5.4.2	<i>Materials and Methods</i>	167
5.4.3	<i>Results and Discussion</i>	170
5.4.4	<i>Conclusion</i>	174
5.5	METHODS FOR FILM STERILIZATION.....	176
5.5.1	<i>Introduction</i>	176
5.5.2	<i>Materials and Methods</i>	180
5.5.3	<i>Results and Discussion</i>	182
5.5.4	<i>Conclusion</i>	194
CHAPTER 6. GENTAMICIN-PROTEIN COMBINATION FILMS..... 208		
6.1	INTRODUCTION.....	208
6.2	MATERIALS AND METHODS	210
6.3	RESULTS AND DISCUSSION.....	216
6.4	CONCLUSION.....	229
CHAPTER 7. ANTIMICROBIAL PEPTIDE (AMP) DELIVERY..... 235		
7.1	INTRODUCTION.....	235
7.2	MATERIALS AND METHODS.....	237
7.3	RESULTS AND DISCUSSION.....	243
7.4	CONCLUSION.....	268
CHAPTER 8. IN VIVO EVALUATION: DESIGN AND DEVELOPMENT OF MODEL..... 272		
8.1	INTRODUCTION.....	272
8.2	MATERIALS AND METHODS	278
8.3	RESULTS AND DISCUSSION.....	293
8.4	CONCLUSION.....	321
CHAPTER 9. INCORPORATION OF SIRNAS..... 325		
9.1	INTRODUCTION.....	325
9.2	MATERIALS AND METHODS	327
9.3	RESULTS AND DISCUSSION.....	331
9.4	CONCLUSION.....	346
CHAPTER 10. APPENDICES..... 366		

List of Figures

FIGURE 2.1 - ASSEMBLY OF LBL FILMS INCORPORATING HEPARIN AND DEXTRAN.	50
FIGURE 2.2 - HEPARIN (BASE, ◆) AND DEXTRAN SULFATE (TOP, ▲)-LOADED PEM WITHOUT DIVIDING LAYERS.	51
FIGURE 2.3 - SCHEMATIC DEPICTING STRATEGIES EMPLOYED IN THIS STUDY TO CONSTRUCT PHYSICAL BARRIERS TO CONTROL INTERLAYER DIFFUSION IN MULTICOMPONENT FILMS.	55
FIGURE 2.4 - DS (BASE LAYER, ▲) AND HEP (SURFACE LAYER, ◆)-LOADED PEM SEPARATED BY A SINGLE, CROSSLINKED LAYER OF (PAH/PAA), EXHIBITING SEQUENTIAL RELEASE.	56
FIGURE 2.5 - RELEASE OF HEPARIN FROM A PEM CAPPED WITH A SINGLE CROSSLINKED LAYER OF PAH/PAA.	57
FIGURE 2.6 - HEPARIN AND DEXTRAN RELEASE FROM FILMS FORMULATED WITH VARIOUS TYPES OF NON-COVALENT BARRIER LAYERS.	59
FIGURE 2.7 - RELEASE OF DEXTRAN FROM PEMs CAPPED WITH A SINGLE LAYER OF (PAH/PAA) CROSSLINKED FOR DIFFERENT AMOUNTS OF TIME.	61
FIGURE 2.8 - NORMALIZED INITIAL AVERAGE RELEASE RATE (MG/HR-CM ²) FROM BASE FILMS CONTAINING DS (A) AND HEP (B).	63
FIGURE 2.9 - KINETICS AND DOSAGE OF HEPARIN (LEFT) AND DEXTRAN (RIGHT) RELEASE FROM (<i>POLY I</i> /HEPARIN, DEXTRAN) _N FILMS IN PBS AT 25°C.	68
FIGURE 2.10 - KINETICS OF HEPARIN RELEASE FROM (<i>POLY I</i> /HEP) ₄₀ FILMS IN PBS AT VARIOUS TEMPERATURES.	68
FIGURE 2.11 - KRIS WOOD'S MAY 2005 DATA ON HEPARIN RELEASE FROM (<i>POLY I</i> /HEP) _N FILMS.	69
FIGURE 2.12 - KINETICS OF HEPARIN RELEASE FROM (<i>POLY I</i> /HEP) ₂₀ FILMS AT 37°C IN VARIOUS MEDIA.	70
FIGURE 2.13 - F32 CELL PROLIFERATION RESPONSE TO HEPARIN ADMINISTERED VIA DIFFERENT MEANS.	72
FIGURE 2.14 - F32 CELL PROLIFERATION RESPONSE TO HEPARIN ADMINISTERED VIA DIFFERENT MEANS AT VARIOUS CONCENTRATIONS.	73
FIGURE 2.15 - F32 CELL PROLIFERATION UNDER VARIOUS AMOUNTS OF <i>POLY I</i> SUPPLEMENTATION.	74
FIGURE 2.16 - F32 PROLIFERATION UNDER VARIOUS AMOUNTS OF HEPARIN AND/OR <i>POLY I</i> /2 SUPPLEMENTATION.	75
FIGURE 2.17 - F32 PROLIFERATION UNDER VARIOUS AMOUNTS OF <i>POLY I</i> /2 SUPPLEMENTATION.	77
FIGURE 3.1 - METABOLIC RESPONSE OF MC3T3 CELLS TO <i>POLY I</i> SOLUTIONS AFTER A 48-HOUR EXPOSURE.	82
FIGURE 3.2 - METABOLIC RESPONSE OF MC3T3 CELLS TO VARIOUS CONCENTRATIONS OF DIACRYLATE AND DIAMINE MONOMERS OF <i>POLY I</i>	84
FIGURE 3.3 - METABOLIC RESPONSE OF MC3T3 CELLS TO <i>POLY I</i> SOLUTIONS AFTER VARIOUS EXPOSURE TIMES.	86
FIGURE 3.4 - METABOLIC RESPONSE OF MC3T3 CELLS TO "FRESH" VS. "DEGRADED" <i>POLY I</i> SOLUTIONS OVER VARIOUS EXPOSURE TIMES.	87
FIGURE 3.5 - METABOLIC RESPONSE OF MC3T3 CELLS TO CHITOSAN SOLUTIONS AND FRESH VS. DEGRADED <i>POLY I</i> SOLUTIONS OVER VARIOUS EXPOSURE TIMES.	88
FIGURE 3.6 - SHORT-EXPOSURE MONITORING OF METABOLIC RESPONSE OF MC3T3 CELLS TO FRESHLY PREPARED <i>POLY I</i> SOLUTIONS.	89
FIGURE 3.7 - METABOLIC RESPONSE OF MC3T3 CELLS TO VARIOUS COMBINATIONS OF <i>POLY I</i> WITH HEPARIN OR DEXTRAN, WITH OVERNIGHT (18 HRS) EXPOSURE.	90
FIGURE 3.8 - METABOLIC RESPONSE OF COS-7 CELLS TO FRESH VS. DEGRADED <i>POLY I</i> SOLUTIONS OVER 5-HR TO 3-DAY EXPOSURE TIMES.	92
FIGURE 3.9 - COMPARISON OF METABOLIC RESPONSES OF MC3T3 AND COS-7 CELLS TO FRESH VS. DEGRADED <i>POLY I</i>	93
FIGURE 3.10 - SHORT-TIME MONITORING OF METABOLIC RESPONSE OF COS-7 CELLS TO FRESHLY PREPARED <i>POLY I</i> SOLUTIONS.	95
FIGURE 4.1 - STRUCTURE OF UNMODIFIED B-CYCLODEXTRIN.	98
FIGURE 4.2 - SCHEMATICS OF LBL DRUG INCORPORATION METHODS VIA CYCLODEXTRIN INCLUSION COMPLEXES.	100
FIGURE 4.3 - STRUCTURES OF THE THERAPEUTICS USED IN THIS STUDY.	101

FIGURE 4.4 – STRUCTURE OF METHYL ORANGE.....	101
FIGURE 4.5 – GROWTH CURVE OF $(POLY I/S-CyD)_N$ FILMS.....	104
FIGURE 4.6 – PRE-UPTAKE OF AMP.....	106
FIGURE 4.7 –POST-UPTAKE OF AMPICILLIN.....	107
FIGURE 4.8 – PRE-UPTAKE OF DEXAMETHASONE.....	109
FIGURE 4.9 – POST-UPTAKE OF DEXAMETHASONE.....	111
FIGURE 4.10 – CUMULATIVE RELEASE OF DEXAMETHASONE FROM $(POLY I/S-B-CyD)_{60}$ AFTER 9-HR UPTAKE IN ETHANOL.....	112
FIGURE 4.11 – POST-UPTAKE OF GENTAMICIN.....	113
FIGURE 5.1 - STRUCTURE OF GENTAMICIN.....	130
FIGURE 5.2 - STRUCTURES OF $POLY X$ USED IN THIS STUDY.....	132
FIGURE 5.3 - GROWTH CURVES FOR $[(POLY X/HA)_1(GS/HA)_1]_N$	133
FIGURE 5.4 – TOTAL GENTAMICIN LOADING VS. NUMBER OF TETRALAYERS FOR $[(POLY X/HA)_1(GS/HA)_1]_N$	135
FIGURE 5.5 - NORMALIZED CUMULATIVE GENTAMICIN RELEASE FROM 50-TETRALAYER FILMS MADE WITH DIFFERENT $POLY X$ 'S.....	137
FIGURE 5.6 – NORMALIZED <i>IN SITU</i> FILM EROSION AND GENTAMICIN RELEASE FROM A $POLY 2$ FILM.....	138
FIGURE 5.7 – CUMULATIVE AMOUNT OF GENTAMICIN RELEASED FROM $POLY 1$ FILMS WITH VARIATIONS IN FILM ARCHITECTURE AND NUMBER OF DEPOSITED LAYERS.....	142
FIGURE 5.8 – NORMALIZED DENSITY OF <i>S. AUREUS</i> LIQUID CULTURES AFTER TREATMENT WITH ELUTION BUFFERS OF $[(POLY X/HA)(GS/HA)]_{100}$	145
FIGURE 5.9 - COMBINED DATA ON <i>IN VITRO</i> EFFICACY AND NONTOXICITY OF $[(POLY 1, 2/HA)_1(GS/HA)_1]_{100}$	150
FIGURE 5.10 – NORMALIZED RELEASE OF GENTAMICIN FROM $[(X/HA)(GS/HA)]_{100}$ IN M-SBF AT 37°C, WITH X BEING EITHER $POLY 1$ OR CHITOSAN.....	154
FIGURE 5.11 – RELEASE OF GENTAMICIN FROM $[(POLY 1/PAA)(GS/PAA)]_{100}$ IN M-SBF AT 37°C, WITH PAA OF DIFFERENT MWS.....	156
FIGURE 5.12 - RELEASE OF GENTAMICIN FROM $[(POLY 1/HA)(GS/HA)]_{100}$ IN M-SBF AT 37°C, WITH A MW 64kDa HA.....	157
FIGURE 5.13 – OVERLAY OF DSC SPECTRA OF $[(POLY 1/HA)(GS/HA)]_{100}$ AND INDIVIDUAL FILM COMPONENTS.....	161
FIGURE 5.14 – SEM IMAGES OF THE SURFACE OF A $[(POLY 1/HA)(GS/HA)]_{100}$ FILM.....	162
FIGURE 5.15 – SAXS IMAGES OF $[(POLY 1/HA)(GS/HA)]_{100}$ AND ITS INDIVIDUAL FILM COMPONENTS.....	163
FIGURE 5.16 – WAXS DATA ON $[(POLY 1/HA)(GS/HA)]_{100}$ AND INDIVIDUAL FILM COMPONENTS.....	165
FIGURE 5.17 - MW VERSUS IV CORRELATION FOR A 50:50 PLGA COPOLYMER.....	168
FIGURE 5.18 - GENTAMICIN RELEASE FROM FILMS MADE WITH FREE OR PRE-ENCAPSULATED GENTAMICIN, IN COMPARISON TO TETRALAYERS INCORPORATING NON-MODIFIED GENTAMICIN.....	173
FIGURE 5.19 - COMPARING GENTAMICIN RELEASE FROM UNTREATED VERSUS AUTOCLAVED $[(POLY 1/HA)(GS/HA)]_{100}$	183
FIGURE 5.20 - NORMALIZED GENTAMICIN RELEASE FROM UNTREATED VS. DRY HEATED $[(POLY 1/HA)(GS/HA)]_{100}$	185
FIGURE 5.21 - NORMALIZED GENTAMICIN RELEASE FROM ETO-TREATED VS. UNTREATED $[(POLY 1/HA)(GS/HA)]_{100}$	187
FIGURE 5.22 - COMPARING GENTAMICIN RELEASE FROM Γ -IRRADIATED VS. UNTREATED $[(POLY 1/HA)(GS/HA)]_{100}$	190
FIGURE 5.23 - COMPARING GENTAMICIN RELEASE FROM $[(POLY 1/HA)(GS/HA)]_{100}$ FILMS THAT ARE EITHER UNTREATED, OR IMMERSSED IN 70% ETHANOL FOR 30 MIN OR 24 HRS.....	192
FIGURE 6.1 - STRUCTURES OF $POLY X$ USED IN THIS STUDY.....	211
FIGURE 6.2 – GROWTH CURVE (A) $[(POLY 1/HEP)(FGF/HEP)]_N$, AND (B) $[(POLY 1/HEP)(FGF/HEP)]_{50} + [(POLY1/HA)(GS/HA)]_N$	218
FIGURE 6.3 – CUMULATIVE RELEASE OF GENTAMICIN IN M-SBF, 37°C FROM (A) $[(POLY 1/HA)(GS/HA)]_N$ FILMS, AND (B) $[(POLY 1/HEP)(FGF/HEP)]_{50} + [(POLY 1/HA)(GS/HA)]_N$ FILMS.....	220
FIGURE 6.4 – CUMULATIVE RELEASE OF GENTAMICIN IN M-SBF, 37°C, ZOOMED INTO THE INITIAL 2.5 HOURS, FROM (A) $[(POLY 1/HA)(GS/HA)]_N$ FILMS, AND (B) $[(POLY 1/HEP)(FGF/HEP)]_{50} + [(POLY1/HA)(GS/HA)]_N$ FILMS.....	221

FIGURE 6.5 - CUMULATIVE RELEASE OF GENTAMICIN IN RELEASE MEDIUM FROM [(POLY I/HEP)(FGF/HEP)] ₅₀ + [(POLY I/HA)(GS/HA)] _N FILMS.....	222
FIGURE 6.6 – TOTAL LOADING AND LOADING DENSITY OF GENTAMICIN INTO COMBINATION FILMS AS A FUNCTION OF NUMBER OF [(POLY I/HA)(GS/HA)] TETRALAYERS DEPOSITED ON TOP OF [(POLY I/HEP)(FGF/HEP)] ₅₀	224
FIGURE 6.7 - NORMALIZED CUMULATIVE RELEASES OF GENTAMICIN (GS) AND FGF FROM A [(POLY I/HEP)(FGF/HEP)] ₅₀ + [(POLY I/HA)(GS/HA)] ₁₀₀ FILM, WITH ACCOMPANYING FILM EROSION CURVE.	225
FIGURE 6.8 – MACRODILUTION ASSAY OF [(POLY I/HEP)(FGF/HEP)] ₅₀ + [(POLY I/HA)(GS/HA)] ₁₀₀ FILM AGAINST <i>S. AUREUS</i>	227
FIGURE 6.9 –NET KIRBY-BAUER DIAMETERS OF VARIOUS COMBINATION FILM SAMPLES IN CORRELATION TO THE ESTIMATED TOTAL GENTAMICIN WITHIN THE SAMPLE. CONTROLS WERE BD SENSI-DISC®.	229
FIGURE 7.1 - STRUCTURES OF POLY X USED IN THIS STUDY.....	243
FIGURE 7.2 – RELEASE OF RNAIII-INHIBITING PEPTIDE (RIP) FROM A BILAYER CONSTRUCT WITH HYALURONIC ACID: (A) RELEASE CURVES ZOOMED IN TO THE INITIAL 0.5 DAY TO COMPARE THE BURST RELEASE PROFILES BETWEEN THE TWO TYPES OF FILMS, AND (B) OVERALL RELEASE CURVES AS ASSESSED OVER 9 DAYS.	245
FIGURE 7.3 - RELEASE OF DERMASEPTIN (DERM) FROM A BILAYER CONSTRUCT WITH ALGINATE AND HYALURONIC ACID/.....	247
FIGURE 7.4 - RELEASE OF DERMASEPTIN (DERM) FROM A 50-BILAYER VERSUS 50-TETRALAYER CONSTRUCTS WITH POLY I AND HYALURONIC ACID.	249
FIGURE 7.5 - GROWTH CURVES FOR [(POLY X/HA)(AMP/HA)] _N AT THE EARLY REGIME WITH VARIOUS POLY XS AND AMPs.	250
FIGURE 7.6 – CUMULATIVE RELEASE OF DERMASEPTIN FROM [(POLY X/HA)(DERM/HA)] _N FILMS FORMULATED WITH VARIOUS POLY XS, EACH ASSESSED AT BOTH ROOM TEMPERATURE (25°C) AND PHYSIOLOGICAL TEMPERATURE (37°C).	252
FIGURE 7.7 – CUMULATIVE DERMASEPTIN RELEASE FROM 20-TETRALAYER FILMS MADE WITH DIFFERENT POLY X's.	253
FIGURE 7.8 – CALIBRATION OF RF SIGNALS FROM FTIC-DERM SAMPLES SYNTHESIZED IN DIFFERENT BATCHES.....	254
FIGURE 7.9 – EVOLUTION OF RF SIGNAL FROM FTIC-DERM STANDARDS AT 20 UG/ML.	254
FIGURE 7.10 – BCA CALIBRATION CURVE FOR FITC-DERM.	255
FIGURE 7.11 - CUMULATIVE DERMASEPTIN AND MELITTIN RELEASES FROM (POLY I/HA)(AMP/HA)] ₁₀₀ . RELEASE ASSESSMENT WAS BASED ON BCA RATHER THAN FITC SIGNAL.	256
FIGURE 7.12 - GROWTH CURVES OF [(POLY I/HA)(DERM/HA)] _N AT DIFFERENT pHs.....	257
FIGURE 7.13 – RELEASE OF DERMASEPTIN FROM [(POLY 2/HEP)(FGF/HEP)] ₂₀ + [(POLY I/HA)(DERM/HA)] ₁₀₀	258
FIGURE 7.14 – BCA CALIBRATION CURVE FOR PONERICIN.	259
FIGURE 7.15 - RELEASE OF PONERICIN (PON) FROM [(POLY I/HA)(PON/HA)] ₂₅	260
FIGURE 7.16 – ACTIVITY OF VARIOUS LEVELS AND COMBINATIONS OF POLYMERS ON PROLIFERATION OF <i>S. AUREUS</i> , NORMALIZED TO NEGATIVE CONTROLS.	262
FIGURE 7.17 – EFFECT OF VARIOUS LEVELS AND COMBINATIONS OF POLYMERS ON ACTIVITY OF PONERICIN AT 2X MIC TOWARDS <i>S. AUREUS</i> , NORMALIZED TO POSITIVE AND NEGATIVE CONTROLS:.....	264
FIGURE 7.18 – ACTIVITY OF PONERICIN AGAINST <i>S. AUREUS</i> PROLIFERATION AS ADMINISTERED IN TWO FORMS.....	265
FIGURE 7.19 - EFFECT OF VARIOUS AMP TREATMENTS ON MC3T3 METABOLIC ACTIVITY LEVEL AT VARIOUS CONCENTRATIONS: (A) MELITTIN, (B) CECROPIN-A-MELITTIN, AND (C) PONERICIN.	267
FIGURE 8.1 - MODEL FEMUR BONE SHOWING: (LEFT) DEFECT SITE AT THE MEDIAL FEMORAL CONDYLE, ALONG WITH WIRED BONE CEMENT RODS AND 8MM DRILL BIT, (RIGHT) BONE CEMENT ROD PLACED INTO THE MODEL DEFECT TO CHECK FIT.....	284
FIGURE 8.2 - SCHEMATIC OF THE CUSTOM-MADE PMMA RODS FOR ROUND 4 STUDIES.....	288
FIGURE 8.3 – PHOTOGRAPH OF PMMA RODS USED TO SIMULATE FOREIGN IMPLANT OBJECT.....	288
FIGURE 8.4 - RESULT OF THE ASSESSMENT ON SURFACE COLONIZATION OF BONE CEMENT RODS BY <i>S. AUREUS</i>	296
FIGURE 8.5 – IMAGES FROM 07-174'S 1 ST SURVIVAL SURGERY.....	297

FIGURE 8.6 – LATERAL (LEFT) AND AP (ANTERIOR-POSTERIOR, RIGHT) RADIOGRAPHS OF RABBIT 07-174 AFTER 1 ST SURVIVAL SURGERY, SHOWING DRILLED DEFECT AND INSERTED BONE CEMENT ROD.	297
FIGURE 8.7 – IMAGES FROM 07-170’S TISSUE HARVEST, SHOWING (LEFT) VISIBLE SOFT TISSUE INFECTION BUT (MIDDLE) NO DEFINITIVE SIGN OF BONE INFECTION.	298
FIGURE 8.8 – IMAGES FROM 07-172’S SACRIFICE.	299
FIGURE 8.9 - IMAGES FROM 07-175’S 2 ND SURVIVAL SURGERY.	300
FIGURE 8.10 – LATER (LEFT) AND AP (RIGHT) RADIOGRAPHS OF RABBIT 07-175 AFTER 2 ND SURVIVAL SURGERY, SHOWING ENLARGED DEFECT WITH A FORM-FITTING IMPLANT IN PLACE.	300
FIGURE 8.11 – IMAGES OF SPLIT BONE FROM TISSUE HARVESTS OF 07-171 (LEFT) AND 07-175 (RIGHT), BOTH OF WHICH RECEIVED A COATED IMPLANT AT 2 ND SURVIVAL SURGERY.	301
FIGURE 8.12 – REFERENCE SAMPLES FROM ALT <i>ET AL.</i> ¹⁴¹ TO DEMONSTRATE SIGNS OF OSTEOMYELITIS UNDER HISTOLOGY.	302
FIGURE 8.13 – SAMPLE HISTOLOGY ON 07-170’S JOINT CAPSULE SLICES.	303
FIGURE 8.14 – SAMPLE HISTOLOGY ON 07-172’S DEEP SOFT TISSUE (LEFT) AND 07-174’S SUPERFICIAL SOFT TISSUE (RIGHT), BOTH OF WHICH DISPLAYING DENSE PRESENCE OF DARK COLONIES SIMILAR TO THOSE OBSERVED IN 07-170’S JOINT CAPSULE STAINING (FIGURE 8.13).	303
FIGURE 8.15 - POST-OP HEALTH STATS OF RABBITS 07-179 TO 07-182.	304
FIGURE 8.16 – LATERAL RADIOGRAPH OF 07-179 PRIOR TO SACRIFICE.	305
FIGURE 8.17 – IMAGES FROM 07-181’S SACRIFICE.	306
FIGURE 8.18 – IMAGES FROM 07-179, 07-180, AND 07-182’S SACRIFICES (FROM LEFT TO RIGHT), SHOWING SPLIT FEMUR BONES REVEALING THE DEFECT SITE (CIRCLED).	306
FIGURE 8.19 – LATERAL RADIOGRAPHS OF 07-223.	308
FIGURE 8.20 - RESULT OF THE ASSESSMENT ON SURFACE COLONIZATION OF BONE PMMA RODS BY <i>S. AUREUS</i>	309
FIGURE 8.21 - 3MM X 10MM DEFECT AT THE MEDIAL FEMORAL CONDYLE BEFORE (LEFT) AND AFTER (RIGHT) COLONIZED ROD INSERTION, SHOWING GOOD FIT OF THE MODEL.	310
FIGURE 8.22 - POST-OP LATERAL RADIOGRAPH OF THE DEFECT SITE FROM RABBIT 08-042, SHOWING PLACEMENT OF THE IMPLANT WITH THE SMALL WIRE AT THE TOP.	311
FIGURE 8.23 – IMAGES FROM 08-042’S TISSUE HARVEST, 13 DAYS AFTER FIRST SURGERY.	312
FIGURE 8.24 – IMAGES FROM 08-044’S TISSUE HARVEST.	314
FIGURE 8.25 - IMAGES FROM 08-045’S TISSUE HARVEST.	314
FIGURE 8.26 – AVERAGE SALINE COUNT OF <i>S. AUREUS</i> AS SONICATED OFF SURFACES OF COLONIZED PMMA RODS AFTER VARIOUS LENGTHS OF STORAGE AT -80°C.	319
FIGURE 9.1 - siRNA CALIBRATION BY UV ABSORBANCE.	332
FIGURE 9.2 - (<i>POLY X</i> /siRNA) _n GROWTH CURVES IN THICKNESS AND ABS ₂₆₀	333
FIGURE 9.3 - REFLECTION OPTICAL IMAGE OF (<i>POLY X</i> /siRNA) ₄₀ DEPOSITED ON SILICON.	336
FIGURE 9.4 – AFM IMAGES OF (<i>POLY I</i> /siRNA) ₄₀ (ON ISLAND PORTIONS OF THE FILM) OVER A COURSE OF INCUBATION IN NUCLEASE-FREE PBS BUFFER AT 37°C.	339
FIGURE 9.5 – (<i>POLY I</i> /siRNA) ₄₀ FILM EROSION AND siRNA RELEASE.	340
FIGURE 9.6 - COMPARING EROSION AND RELEASE OF (<i>POLY I</i> /siRNA) ₄₀ FILMS ON SILICON VS. QUARTZ SUBSTRATES.	342
FIGURE 9.7 – (<i>POLY 6</i> /siRNA) ₄₀ FILM EROSION AND siRNA RELEASE.	344
FIGURE 9.8 - COMPARING EROSION AND RELEASE OF (<i>POLY 6</i> /siRNA) ₄₀ FILMS ON SILICON VS. QUARTZ SUBSTRATES.	346
FIGURE 10.1. POLY I, A POLY(B-AMINO ESTER) WHICH IS OUR PROTOTYPICAL HYDROLYTICALLY-DEGRADABLE POLYCATION.	ERROR! BOOKMARK NOT DEFINED.
FIGURE 10.2. BIS(B-AMINO ACID) DEGRADATION PRODUCT OF POLY I	ERROR! BOOKMARK NOT DEFINED.

List of Tables

TABLE 1 - THICKNESS, GENTAMICIN DOSAGE, AND VERTICAL GENTAMICIN LOADING DENSITY OF [(POLYX/HA)(GS/HA)] _N FILMS, AS A FUNCTION OF THE NUMBER OF TETRALAYERS.	136
TABLE 2 –QUALITATIVE ASSESSMENT OF VARIOUS FILM SUBSTRATE IN INHIBITING GROWTH OF <i>S.AUREUS</i> IN LIQUID CULTURE.	143
TABLE 3 – ZONE OF INHIBITION (ZOI) OF NEGATIVE CONTROLS FILMS AND THOSE ESTIMATED TO CONTAIN 10 UG OF GENTAMICIN.	147
TABLE 4 - ZOI OF <i>POLY 2</i> TETRALAYER FILMS ON SILICON WITH VARYING GENTAMICIN DOSAGES.	147
TABLE 5 - PLGA NANOENCAPSULATION PROCEDURE PARAMETERS.	168
TABLE 6 – KIRBY-BAUER DIAMETERS OF [(POLY I/HEP)(FGF/HEP)] ₅₀ + [(POLY I/HA)(GS/HA)] ₂₅ SUBSTRATES AND 10 μG BD SENSI-DISC® CONTROLS. SUBSTRATE SIZES WERE CHOSEN TO YIELD GS LOADINGS OF ~10 UG PER SAMPLE.	228
TABLE 7 - LIST OF ANTIMICROBIAL PEPTIDES USED IN THIS STUDY.	238
TABLE 8 - SUMMARY OF SCHEDULE AND OPERATING PARAMETERS	289
TABLE 9 - COMPLETE BLOOD COUNT (CBC) RESULTS FOR ALL RABBITS.....	293
TABLE 10 - MICROBIOLOGY RESULTS FOR BLOOD, BONE TISSUES, AND IMPLANTS.....	293
TABLE 11 - MICROBIOLOGY RESULTS FOR SOFT TISSUES AND OTHER MATERIALS EXTERIOR TO DEFECT SITE	294
TABLE 12 – SUMMARY OF QUANTITATIVE PMMA ROD COLONIZATION EVALUATION.	319

Chapter 1. Introduction

*Portions adopted with permission from “Polyelectrolyte Multilayers for Tunable Release of Antibiotics” by Helen F. Chuang, Renee C. Smith, and Paula T. Hammod. *Biomacromolecules*, 9 (6), 1660–1668, 2008. 10.1021/bm800185h, © 2008 American Chemical Society.

1.1 Controlled Release

Controlled release is defined as drug delivery at a predetermined rate for an extended period of time, typically 12 hrs or longer¹. Controlled release can improve efficacy and decrease toxicity/side effects by holding the drug concentration at the optimal level. It can also reduce the required number of drug administrations, thus improving patient compliance. Consequently, controlled release has been a centerpiece of drug delivery research since its introduction 30 years ago². In particular, polymer-based systems have dominated research in *controlled release* due to the functionalizability, blendability, cost and ease of synthesis, and a well-established set of research tools for these materials.

There are two types of controlled release, temporal and distributional². In temporal control, the drug is delivered over an extended duration or at specific times. Such temporal control is especially beneficial for drugs that are rapidly metabolized or have a very narrow window of efficacious concentration^a. In distributional control,

^a For example, opioid painkiller³. Falk, R.; Randolph, T. W.; Meyer, J. D.; Kelly, R. M.; Manning, M. C., Controlled release of ionic compounds from poly (-lactide) microspheres produced by precipitation with a compressed antisolvent. *Journal of Controlled Release* **1997**, 44, (1), 77-85. 4. Johnson, O. L.; Cleland, J. L.; Lee, H. J.; Charnis, M.; Duenas, E.; Jaworowicz, W.; Shepard, D.; Shihzamani, A.; Jones, A. J. S.; Putney, S. D., A month-long effect from a single injection of microencapsulated human growth hormone. *Nature Medicine* **1996**, 2, (7), 795-799, 5. Chluba, J.; Voegel, J.-C.; Decher, G.; Erbacher, P.; Schaaf, P.;

the drug is delivered to a precise region in the body (*e.g.* a tumor, the intestines, or a surgical wound). Such *targeting* is needed if the drug causes major side reactions to other parts of the body or if the drug cannot reach the target site by natural distribution^b. Distributional control can be achieved by either an implant at the site^{10, 13-15} or a colloidal polymeric formulation capable of targeting the site of action¹⁶⁻¹⁹. Aside from controlling the release of drugs, polymeric encapsulation can also raise efficacy by preserving the active form of the drug within its protective microenvironment²⁰.

Polymer-based controlled release systems can be further distinguished based on their mechanisms of release¹. The first is diffusion, which is the dominant mechanism for such systems as drug encapsulation within polymer capsules^{16-18, 21, 22} or uniform drug dispersion within polymer matrices¹³. The second is chemical reaction, such as degradation of the polymer by solvents²³⁻²⁵ or enzymes²⁶. The third is solvent activation, in which the drug is entrapped in the polymer until either

Ogier, J., Peptide Hormone Covalently Bound to Polyelectrolytes and Embedded into Multilayer Architectures Conserving Full Biological Activity. *Biomacromolecules* **2001**, 2, (3), 800-805, 6. Misra, G. P.; Siegel, R. A., New mode of drug delivery: long term autonomous rhythmic hormone release across a hydrogel membrane. *Journal of Controlled Release* **2002**, 81, (1-2), 1-6., and vaccines⁷. McGee, J. P.; Davis, S. S.; O'Hagan, D. T., The immunogenicity of a model protein entrapped in poly(lactide-co-glycolide) microparticles prepared by a novel phase separation technique. *Journal of Controlled Release* **1994**, 31, (1), 55-60, 8. Qiu, L. Y.; Zhu, K. J., Design of a core-shelled polymer cylinder for potential programmable drug delivery. *International Journal of Pharmaceutics* **2001**, 219, (1-2), 151-160. can all benefit from temporal control.

^b Examples are chemotherapeutic agents⁹. Dang, W.; Colvin, O. M.; Brem, H.; Saltzman, W. M., Covalent coupling of methotrexate to dextran enhances the penetration of cytotoxicity into a tissue-like matrix. *Cancer Research* **1994**, 54, (7), 1729-1735, 10. Brem, H.; Gabikian, P., Biodegradable polymer implants to treat brain tumors. *Journal Of Controlled Release: Official Journal Of The Controlled Release Society* **2001**, 74, (1-3), 63-67. and anti-inflammatory¹¹. Conforti, A.; Bertani, S.; Lussignoli, S.; Grigolini, L.; Terzi, M.; Lora, S.; Caliceti, P.; Marsilio, F.; Veronese, F. M., Anti-inflammatory activity of polyphosphazene-based naproxen slow-release systems. *Journal of Pharmacy and Pharmacology* **1996**, 48, (5), 468-473, 12. Benkirane-Jessel, N.; Schwinte, P.; Falvey, P.; Darcy, R.; Haikel, Y.; Schaaf, P.; Voegel, J.-C.; Ogier, J., Build-up of Polypeptide Multilayer Coatings with Anti-Inflammatory Properties Based on the Embedding of Piroxicam-Cyclodextrin Complexes. *Advanced Functional Materials* **2004**, 14, (2), 174-182. drugs.

the solvent swells the polymer^{6, 27} or water imbibement generates osmotic pressure²⁸. The fourth is by externally applied stimuli, such as electrochemical²⁹, magnetic³⁰, or ultrasonic controls³¹. Mechanisms one through three are *passive controls* because the drug release cannot be externally intervened. On the other hand, releases by external stimuli are *active controls*. While active controls offer the flexibility of human intervention, they also carry the drawback of having to implement the control device (*e.g.* a voltage generator), which could be inconvenient and uncomfortable to the patient.

1.2 Surface release from orthopedic implants:

an unmet need in controlled release

Arthroplasty, or the surgical repair of a joint, is often performed on disabled arthritic patients and those who suffer from other forms of bone degeneration. Total joint replacement, particularly of the hip and knee, has become one of the most frequent prosthetic surgeries due to its success in restoring mobility to these patients. It is estimated that a million joint placements are performed worldwide each year³², about half of which are in the U.S.. Unfortunately, due to surgical and implant-derived complications, about 10% such joint replacements eventually fail and require a *revision arthroplasty*³³, in which the patient may undergo more than two additional surgeries. Such revisions cost over \$1 billion yearly in the U.S.³⁴, and the revision cost to the patient can more than double that of the primary arthroplasty³⁵. Therefore, reductions to primary failures and improvements in revision success are of utmost importance.

There are many sources to implant failures, including infection^{32, 33, 36, 37}, *aseptic loosening*³³, and long term implant rejection. Other complications that do not directly contribute to implant removal but still need to be addressed are pain, inflammation, and other discomforts to the patient. Additionally, implants have been known to cause *thromboembolism* (blood clotting and embolic migration)³⁸⁻⁴⁰, *ischemia* (lowered blood flow) to the lower extremities⁴¹, and tumor^{42, 43} or cyst⁴⁴ formations.

1.2.1 Current implant surface treatment options

There are several technologies currently available for joint implant surface modification to address some of the problems above. For example, *Implant Sciences Corp.* (Wakefield, MA) offers surface treatments to implants to impart specific properties such as durability, adhesion, and ease of visualization. A similar technology is practiced by *Spire Biomedical Corp.* (Bedford, MA) which uses ionic treatment of the surface via processes such as ionic bombardment. The surface treatment methods are highly directional and cannot produce uniform surface modification on a highly porous or otherwise complex surface. Such surface treatments also cannot release therapeutic agents to address complications such as pain and infection.

An emerging technology for implant surface treatment is exemplified by *Bacterin, Inc.* (Belgrade, MT), which developed block copolymers to fabricate thin-film coatings loaded with anti-microbial agents that can be applied to orthopaedic

implants and other medical devices. However, this block copolymer based coating cannot sequentially release multiple therapeutics, and the copolymer casting process may involve harsh solvents or operating conditions that can significantly inactivate many drugs.

1.2.2 Current sequential release methods

Several devices do exist which can deliver multiple drugs sequentially. The most prominent example is the microchip delivery device pioneered by the Langer group⁴⁵⁻⁴⁸. These microchips have multiple microreservoirs, each covered by a separate membrane that can be independently dissolved to release the drug content underneath. The initial prototypes were silicon microchips with gold membranes that required external electrochemical stimuli to dissolve^{47, 48}.

Current efforts are directed towards bioresorbable microchips made from poly(lactic acid) (PLA) with poly(lactic-co-glycolic acid) (PLGA) membranes⁴⁶ that passively dissolve, eliminating the needs for external interfaces and surgeries to remove the device. While these microchips can release multiple agents in a sequential, controlled manner, they cannot be deposited onto implants, stents, or sutures. Thus, their implementation would require the insertion of an extra foreign object into the patient. Furthermore, the microchips cannot sustain release over a large or extended surface area, and it would be difficult to implement them in oral or intravenous dosage forms. Last but not least, these microchips require clean-room fabrication that is laborious and costly.

Other biodegradable, multi-agent, and sequential delivery systems have been investigated, including a dual-encapsulation polymeric matrix^{15, 49} and double-layered gelatin coatings⁵⁰. The former system involves encapsulating one drug agent directly into a PLGA matrix while the second agent is pre-encapsulated in microspheres that are in turn incorporated into the said matrix. The latter system is composed of two-layer heterogeneously-loaded and crosslinked gelatin coatings. While both were demonstrated to release two agents in a controlled, sequential fashion, neither appears capable of delivering more than two agents, and, similar to the bioresorbable microchips, these systems also lack conformality and ease of fabrication. In addition, there are fewer degrees of control for the release profiles.

1.3 Layer-by-layer (LbL) assembly as a solution for sequential release

1.3.1 Introduction

Sequential, alternating build-up of multilayers based on electrostatic interactions was first conducted in 1991 by Decher *et al.* with bipolar amphiphiles⁵¹. They subsequently pioneered the use of polyelectrolytes (PELs), polymers with repeated charged units, for multilayer assembly⁵². Today, the process of alternate depositions of oppositely charged PELs to build multilayers is often referred to as layer-by-layer (LbL) self-assembly. Aside from the ease of this technique, LbL assembly offers flexibility in substrate geometry and the amenability for multifunctionalization by other molecules, through either covalent attachment to the

PEL building block or nonspecific adsorption during the buildup process.

Furthermore, film properties such as thickness and density can be easily tuned by factors such as the pH and ionic strength of the deposition buffer. In short, LbL thin films can be constructed with nanoscaled control over surface properties, morphology, and molecular architecture⁵³.

LbL films have numerous applications, including gas separation⁵⁴, electrochromics^{55, 56}, nanoreactors⁵⁷, sensors⁵⁸⁻⁶¹, solid-state electrolytes⁶², and nanomechanical thin films⁶³. LbL assembly on the mesoscale, using microparticles such as polystyrene latex beads^{64, 65} and metal particles^{66, 67}, led to the creation of high-surface-area thin films, electromagnetically active films, and catalytic films. LbL assembly can also be used to create patterned films⁶⁸ and 3D structures⁶⁹, eliminating the labor and expense of photolithography. Aside from traditional synthetic polymers, one can fabricate LbL thin films using biopolymers such as proteins^{58, 70, 71}, nucleic acid⁶¹, and even charged bionanoparticles such as viruses and lipid vesicles²². This opens the door to countless biological applications including arterial wall repair⁷², patterned cell arrays⁷³, bioactive coatings⁵, biosensors^{58-61, 71}, and ultimately drug delivery.

1.3.2 Applications to drug delivery

As LbL films are conformal and can be deposited onto any surface geometry, applications can range from coated small particles for oral or intravenous administrations to coated implants, stents, and sutures for localized delivery.

1.3.2.1 Medical devices

One of the most promising applications, in terms of both medical and commercial impacts, is functionalization of orthopaedic implant surfaces, as discussed previously. Two implant failures that an LbL coating can readily address are infection and aseptic loosening. In fact, the use of PEMs as wear-resistant coatings for orthopaedic implants has already been explored by Cohen *et al.* at MIT⁷⁴, and their tested (PAA/PAH) multilayers can be incorporated into our device as a non-degradable base layer. This permanent base layer will reduce incidences of aseptic loosening. In terms of antibiotic elution, two prominent candidates are gentamicin and tobramycin⁷⁵, both of which are cationic polysaccharides and can be incorporated in our model PEM via the construction of heterostructures or by pre-encapsulation into nanocomposites. The conformality of LbL deposition will ensure thorough coverage of all microscopic crevices of the implant surface, addressing the previously unsolvable problem of bacterial growth within these compartments.

On top of reducing implant-associated illnesses, we can incorporate growth factors into our multilayers to promote bone regeneration and implant integration. Both the osteoinductive agent BMP-2 (bone morphogenetic protein-2)⁷⁶⁻⁸¹ and the angiogenetic agent VEGF (vascular endothelial growth factor)⁸²⁻⁸⁵ have been well-studied *in vitro* and *in vivo* to have positive therapeutic impact on bone regeneration. They are both net positively charged at pH 7.4, so they may be incorporated via heterostructures. The incorporation of large

biomolecules such as proteins into PEMs is well-documented in the literature^{58, 70, 86}. We can also implement proteins via pre-encapsulation by PLGA.

Other potential applications include improved drug-eluting stents, patches or implants to aid wound healing, intraocular lens for cataract treatment, and local cancer therapy. Current drug-eluting stents can only release one drug, typically a cytostatic agent to prevent restenosis. We can improve upon this by delivering a more complex schedule of drugs, beginning with antibiotics plus anti-inflammatories (immediate to several days), followed by cytostatic agents (up to 6 months), and possibly concluding with a gene therapy to reprogram the arterial cell tissue for better long term response (weeks to months). In terms of therapeutic angiogenesis, a sequential delivery of vascular endothelial growth factor (VEGF)-165 followed by platelet-derived growth factor (PDGF)-BB was found to be more effective than either alone or both simultaneously⁴⁹.

Therefore, we could make wound dressings or subcutaneous implants which deliver a complex schedule of antibiotics, anti-inflammatory agents, and sequentially angiogenic factors.

Another area that may benefit from sequential delivery of multiple drugs is recovery from cataract surgery. Cataract is a clouding of the normally clear lens of the eye, and the only treatment is to surgically remove the cataract and replace it with an intraocular lens (IOL) implant. Patients are usually given eye drops containing anti-inflammatories and immunosuppressants. However,

proper administration of these agents requires high patient compliance. A practical alternative is to coat the IOL for immediate and concurrent release of dexamethasone (anti-inflammatory)⁸⁷ and cyclosporine or azathioprine (immunosuppressant)⁸⁸, possibly followed by a slower, sustained release of pilocarpine to suppress development of glaucoma, which is a common complication of cataract surgery. Such a self-dosing IOL will eliminate issues of patient compliance or patient error (*e.g.* applying the wrong amount of eye drops) and can also increase therapeutic efficacy by maintaining a constant release at the surgical site.

1.3.2.2 Other localized releases

Perhaps the most prominent example of localized cancer treatment is the FDA-approved Gliadel® wafer. It is used to treat high-grade malignant gliomas (a form of brain tumor) and implanted along the floor and walls of the cavity left by tumor removal. Gliadel® can only deliver one chemotherapeutic agent, carmustine, or BCNU. While that is effective against malignant gliomas, other forms of cancer may require a complex schedule of multiple agents for optimal treatment. For example, it was found that for locoregionally advanced nasopharyngeal carcinoma (an upper respiratory tract cancer), sequential administrations of paclitaxel and carboplatin, followed by cisplatin and concurrent radiotherapy, may be optimal⁸⁹. Ovarian cancer has also been found to require sequential administrations of multiple active agents⁹⁰.

1.3.2.3 Oral and IV applications

Aside from large-area coatings on implants or patches, LbL films can also be deposited onto pills or nanospheres for oral and intravenous administrations, allowing the LbL technology to be applied to drugs that need to be systemically rather than locally administered. For example, the DTP (diphtheria, tetanus, and pertussis) vaccine is given as a multi-dose series to an infant at 2, 4, 6, and 15-18 months of age, with a final follow-up at 4-6 years of age⁹¹. To increase parental compliance and reduce stress on infants, one could administer a single shot of LbL-coated nanospheres that would automatically release the antibodies with the desired schedule of dosage. Aside from illustrating flexibility in the route of delivery, this example also highlights the potential impact LbL films can make by delivering a single agent with a complex, controlled profile; its versatility is not restricted to the delivery of multiple agents. These complex profiles may involve combinations of distinct profiles, such as constant, pulsatile^c, and periodic, all potentially achievable by an LbL device through the proper layerings of appropriate PELs.

^c Another example of single-drug delivery with complex profile is *pulsatile* release, by which pulses of drugs are delivered at variable time intervals. This release method may be superior in some cases because it better mimics the way human body produces certain hormones⁴⁸. Santini, J. T.; Richards, A. C.; Scheidt, R.; Cima, M. J.; Langer, R., Microchips as Controlled Drug-Delivery Devices. *Angewandte Chemie International Edition* **2000**, 39, (14), 2396-2407.. For example, plasma insulin concentration has been found to pulsate with a natural period of about 14 minutes⁹². Matthews, D. R.; Lang, D. A.; Burnett, M. A.; Turner, R. C., Control of pulsatile insulin secretion in man. *Diabetologia* **1983**, 24, (4), 231-237.. Hormones of the anterior pituitary gland, such as gonadotropin (regulates reproduction), are also produced by the body in a pulsatile fashion⁴⁸. Santini, J. T.; Richards, A. C.; Scheidt, R.; Cima, M. J.; Langer, R., Microchips as Controlled Drug-Delivery Devices. *Angewandte Chemie International Edition* **2000**, 39, (14), 2396-2407.. Pulsatile drug administration has found success in treating women with gonadotropin releasing hormone (GnRH) deficiency, who cannot ovulate normally⁹³. Reid, R. L.; Fretts, R.; Van Vugt, D. A., The theory and practice of ovulation induction with gonadotropin-releasing hormone. *American Journal Of Obstetrics And Gynecology* **1988**, 158, (1), 176-185.. In fact, therapies involving constant sustained release of GnRH has been found to actually suppress gonadotropin release⁹⁴. Kuret, J. A.; Murad, F., In *Goodman and Gilman's the Pharmacological Basis of Therapeutics*, 8

1.3.3 Beyond drug delivery: degradable LbL films for other applications

The study of degradable LbL multilayers can benefit fields far beyond biomedicine. One example is the field of agriculture, which can benefit from controlled release of pesticides, nutrients, and growth promoters into soils. One could make LbL-coated particles that release a complex schedule of chemicals appropriate for a given crop. Efforts are already underway in terms of polymer delivery of pesticides⁹⁵, but current systems lack the multi-agent and conformal versatility of degradable LbL coatings. Similar to agriculture, the food and cosmetic industry has employed controlled release for such products as flavors, fragrances, and colorants⁹⁶⁻⁹⁸. The LbL technology will open the door to such novel products as a “chameleon perfume” that alters its scent throughout the day or an all-in-one blemish cream which sequentially delivers the exfoliant, antibiotic, and anti-inflammatory for optimal acne treatment.

Aside from contributing to a myriad of potential applications, the knowledge gained from studying degradable multilayers can be invaluable to the entire field of LbL self-assembly or even to polymer science in general. The underlying science of molecular interactions is fundamental to many disciplines, and full comprehension of it will have far-reaching contributions.

ed.; Gilman, A. G.; Rall, T. W.; Niles, A. S.; Taylor, P., Eds. McGraw-Hill: New York, 1990; pp 1334-1360.. Thus, pulsatile release profiles are essential for certain drug deliveries, and the LbL architecture can deliver such a profile by alternating high-loading layers with empty spacer layers.

1.3.4 Previous work in LbL drug delivery

LbL assemblies for drug delivery have already been considered by many groups^{12, 17, 19, 25, 99-103}. However, each of these existing systems has a major drawback. For example, systems from Dubas *et al.*¹⁰⁰ and Schuler *et al.*¹⁷ require un-physiologically high salt concentrations^d to degrade, while Sukhishvili *et al.*'s polymers require un-physiological pH (3.6-6.9) to degrade^{25, 104}. Several others suffer from undesirable release behaviors such as unsustainable release (*i.e.* less than one hour)⁹⁹ or initial burst¹⁹. Some require specific enzymes for polymer degradation¹⁰¹, a characteristic which could be advantageous under very particular delivery needs but is unsuitable for general applications. Most importantly, none of these systems addresses the delivery of multiple agents in a sequential, controlled manner.

1.4 Overview of Thesis

1.4.1 Background on materials and methods

Each LbL assembly or polyelectrolyte multilayers (PEMs) requires a prudent selection of the polyanion(s) and polycation(s) to be deposited. For my initial studies, the polyanion will be the drug to be delivered (and will thus be varied from one study to another), while the polycation will always be a member of the hydrolytically degradable poly(β -amino ester) family serving as the structural backbone. The polycation will be referred to as “*Poly X*” for short, where X is a

^d >0.6M NaCl for Dubas *et al.* and >5M NaCl for Schuler *et al.*

number that denotes a particular chemistry. **Error! Reference source not found.** shows an example of *Poly X*, in particular *Poly I*. Due to the hydrolytic degradability of *Poly X*, LbL films formulated with *Poly X* will be a passive release system via the mechanism of chemical reaction, with both temporal and spatial controls. Temporal control comes from the chemistry of *Poly X* and the process by which the LbL films are deposited, while spatial control comes from the choice of substrate being deposited, be it a medical device, patch, catheter, pill, or even micro- and nanoparticles.

Poly X is chosen as our model structural component due to its lack of cytotoxicity^e and its passive degradability under physiological conditions²³. Many polycations that have been traditionally popular as transfection vectors, such as poly(lysine) and poly(ethylene imine) (PEI), have been found to be somewhat cytotoxic^{105, 106}, while others are not readily biodegradable¹⁰⁷. *Poly X* was developed by Lynn and Langer²³ in an effort to create a DNA delivery vehicle that was not only biocompatible and physiologically degradable but also easily synthesized^f. *Poly X* was among a series of three poly(β -amino esters) synthesized in that endeavor. Its synthesis is based on the conjugate addition of bis(secondary amine) monomers to diacrylate esters. This procedure requires no independent preparation of specialized monomers or the use of expensive coupling

^e As determined by the MTT/thiazolyl blue dye reduction assay using the NIH 3T3 cell line.; see Lynn and Langer 23. Lynn, D. M.; Langer, R., Degradable Poly(amino esters): Synthesis, Characterization, and Self-Assembly with Plasmid DNA. *J. Am. Chem. Soc.* **2000**, 122, (44), 10761-10768. .

^f *Poly I* was found to condense plasmid DNA into nanometer-sized structures, with transfection efficiencies exceeding those of PEI under certain conditions²³. Ibid., as determined using luciferase (Promega) and cell protein assay (Pierce) kits. However, we are not concerned with the gene delivery potential of *Poly I* at this point.

agents, these being drawbacks to other attractive drug-delivering polycations^{24, 108, 109}. In addition, both monomers are commercially available in a variety of chemical structures, allowing for an easy “mix and match” synthesis to create a large combinatorial library of poly(β -amino esters), each with a distinct backbone structure. Such a library would allow for rapid screening for a *Poly X* with a particular desired property.

Poly X degrades exclusively to 1,4-butanediol and a bis(β -amino acid)(**Error! Reference source not found.**), neither of which is cytotoxic²³. As an example of *Poly X*'s hydrolytic degradability, free *Poly I* was found to degrade completely within 5 hrs in PBS at 37°C, with a half-life of less than an hour. Due to its hydrolysis by the basic mechanism, the degradation proceeds more slowly at lower pH. For instance, under pH 5.1, it degrades with a half-life of ~8 hrs²³. Actual half-life of *Poly I* within a PEM will depend on many factors, including properties of the counter polyanion and the pH/ionic strength of the deposition buffers.

1.4.2 Previous work

Vazquez *et al.* made the first set of PEMs that incorporated *Poly I*¹¹⁰. They investigated two model polyanions, poly(styrene sulfonate) (PSS), a strong polyanion, and poly(acrylic acid) (PAA), a weak polyanion. Each assembly consisted of ten bilayers on top of a nondegradable base layer^g. The resulting

^g The nondegradable base layer consisted of 10 bilayers of linear poly(ethylene imine) (LPEI)/PSS or poly(dimethyldiallylammonium chloride) (PDAC)/PAA. This base layer ensures a suitably charged base surface for the adsorption of *Poly I*[5. Chluba, J.; Voegel, J.-C.; Decher, G.; Erbacher, P.; Schaaf, P.;

films were smooth^h and degraded by gradual top-down erosion rather than bulk deconstructionⁱ. This study demonstrated not only that *Poly I* can build up PEMs that predictably erode under physiological conditions but also that the degradation timescale can be easily controlled by the choice of polyanion. However, Vazquez's multilayer constructs did not contain any model drug molecule.

Zhang, Lynn, *et al.* established the drug delivery potential of *Poly I* by constructing PEMs consisting of *Poly I* and DNA¹¹¹; in this case, the DNA served as the polyanion. Eight bilayers were deposited onto each substrate, with a resulting multilayer stack of ~100nm in thickness^j. The PEM eroded gradually over 30 hrs without signs of bulk erosion^k with a concomitant continual release of DNA. Subsequent studies established mechanisms of release¹¹²⁻¹¹⁵, various control handles for release rates^{116, 117}, *in vitro* transfection efficacy^{112, 118}, and *in vivo* evaluation using a stent model is currently under way. While Lynn's studies demonstrated the ability of *Poly I* to support sustained DNA release under physiological conditions, the results cannot be generalized to other drug molecules, especially those that are not polyanionic.

Wood *et al.* supplemented Zhang's study by incorporating three polysaccharides: heparin, low-MW heparin, and chondroitin sulfate, into separate PEMs with *Poly*

Ogier, J., Peptide Hormone Covalently Bound to Polyelectrolytes and Embedded into Multilayer Architectures Conserving Full Biological Activity. *Biomacromolecules* **2001**, 2, (3), 800-805.

^h The films were 100nm and 600nm in total thickness for the PSS and PAA assemblies, respectively

ⁱ In PBS buffer, pH 7.4, [NaCl]=150mM, 37°C, bilayers of PSS degraded over 40 hrs, while those of PAA degraded over 9 hrs.

^j When the deposition was carried out in 100mM sodium acetate buffer, pH 5.1. Film thickness was significantly lower (~10nm over 8 bilayers) when *Poly I* and DNA were deposited in DI water.

^k In PBS, pH 7.4, 137mM NaCl, 37°C; erosion was monitored by ellipsometry and UV spectrophotometry.

1. Twenty bilayers of each (*Poly I*/polysaccharide) pair were deposited¹, resulting in total film thickness of ~100nm for all three systems. Exponential film growth was observed¹¹⁹. While the PEMs eroded with pseudo-first order kinetics, the release of heparin (the only drug studied for release) showed a power-law profile with larger amounts released at the beginning. This could be a consequence of the exponential film growth, as the outermost layer had the highest loading. Subsequently, Wood, Chuang, *et al.* established the sequential release of model drugs dextran and heparin¹²⁰, as to be discussed in a subsequent chapter.

1.4.3 Initial objectives

The original objectives proposed for my thesis were:

1. *Elucidate mechanisms of film buildup and drug release for various PEM constructs and establish a set of prognostic guidelines.*
2. *Enable the incorporation of therapeutic agents of any charge, size, and conformation.*
3. *Enhance the controllability of multi-agent delivery through the use of spacer layers and other chemical means.*

Per objective 1, I would study the film buildup behavior by examining total thickness versus bilayers deposited. Complementarily, I would examine drug release from each construct and correlate the release profiles with the observed buildup mechanism, with the ultimate goal of establishing a set of rigorous

¹ Similar to Vazquez *et al.*, there is an (LPEI/PSS)₁₀ base layer. Depositions were carried out in 100mM acetate buffer, pH 5.1.

guidelines that would predict growth/release behaviors through the physicochemical properties of the PEM constituents.

Objective 2 was identified to address the limitation of LbL assembly in incorporating only charged species. Initial effort would be focused on pre-encapsulation of drugs in nanoparticles that have a negatively charged surface. These nanocomposites should be less mobile than the naked drug, thus retarding diffusion between layers and advancing Objective 3. Dissolution of these nanoparticles would present an additional degree of release control which can be coordinated with the PEM degradation for complex release profiles. Due to drug diffusion, polymer rearrangement, and other potential factors that could reduce the stratification of PEMs, 'as-made' PEMs might not demonstrate perfectly controllable sequential release. Thus, Objective 3 aimed to identify simple, cost-effective ways to improve release control through the use of spacer layers, cleavable diffusion-retarding tags, and other chemical means.

1.4.4 Revised objectives

Soon after delving into my thesis, I realized the unrealistic breadth of the original objectives and the need to focus the chosen application, *i.e.* multi-therapeutic coating for orthopedic implants. With additional literature research and preliminary experiments, I decided to focus on the development of antibiotic component, as infection was the most serious complication to medical devices. Infections not only cause device failure but could also spread systemically ¹²¹.

This problem is critical and escalating, and it should be either prevented prophylactically or eradicated remedially.

Most of the antimicrobial orthopedic implant coatings under development, such as dip coating of hydroxyapatite¹²² or collagen¹²³, direct incorporation of antibiotics into glass implants¹²⁴, bone cement¹²⁵, PLGA-based coatings¹²⁶, or nitric oxide-releasing sol-gel coatings¹²⁷, cannot be easily tuned with regard to drug dosage or release rate. In some cases, residual foreign materials are left behind, which may induce long-term immunogenic responses. A biodegradable coating that can be tuned to deliver the desired dosage of drugs over a specified amount of time, while leaving no residual material on the implant surface, would address both problems. Such an antimicrobial coating would also be applicable towards other implanted devices such as dental implants¹²⁸, catheters^{129, 130}, shunts¹³¹, and guide wires¹³².

As bacteria can be introduced either during the surgical process onto the implant surface or post-surgically from the patient's blood, an antimicrobial coating should both discourage bacteria attachment and impose antimicrobial action on the tissues and fluids immediately surrounding the implant. Such a dual action would effectively prevent biofilm formation, the major source of implant surface infection^{129, 130, 133-136}. Due to the widely differing timescales and severities in device infections that range from rapid acute infections to longer term chronic modes¹³⁶⁻¹³⁸, antimicrobial coatings with adjustable dosages and release rates are needed. Therefore, a coating with controls over both parameters would be highly

desirable. Hence, we seek to develop an antimicrobial coating that can both discourage bacteria attachment to the implant surface and be able to release antibiotics into the surrounding tissues at a tunable dosage and rate. This can be achieved through a biodegradable coating that controllably sheds from its surface to release antibiotics. Specifically, we wish to construct a hydrolytically degradable thin film via the layer-by-layer (LbL) deposition technique encapsulating gentamicin, an antibiotic commonly used to treat device infections^{121, 139-141}.

While LbL systems incorporating antimicrobial agents, such as cetrimide and silver¹⁴²⁻¹⁴⁴, have been developed, there is significant concern over the toxicity of some of these agents¹⁴⁵. These agents may also be ineffective against bacterial colonization of orthopedic implants¹⁴⁶. Hence, my revised objectives were:

1. Establish an LbL coating that encapsulates an antibiotic agent already in use for orthopedic infections,
2. Establish controls on dosage and release rate of this antibiotic,
3. Demonstrate *in vitro* efficacy and biocompatibility,
4. (Exploratory) Establish multi-release coating with other therapeutics,
5. (Exploratory) Demonstrate *in vivo* efficacy and biocompatibility.

1.4.5 Summary of thesis progression

Initial experiments focused on the encapsulation of polysaccharides, as these are naturally polyanionic and hence “low-hanging fruits” for LbL incorporation.

Working closely with Kris Wood, I examined various types of barrier layers to

separate heparin and dextran to establish true sequential release, while also investigating mechanisms of film growth and erosion in these systems.

Once sequential release was established¹²⁰, I wanted to demonstrate *in vitro* activity of heparin films and begin work on the encapsulation of my therapeutic of interest – antibiotics. With assistance from Kris Wood and David Berry, I conducted a series of *in vitro* assays demonstrating activity of heparin-releasing films in promoting the proliferation of F32 cells.

On the antibiotic side, since most of the accepted antimicrobial agents were small molecules, I began by attempting formation of cyclodextrin inclusion complexes to go into LbL assemblies. In the process I also examined encapsulation of an anti-inflammatory, dexamethasone, since it was another therapeutic of interest for the orthopedic implant application. Unfortunately little success was achieved using cyclodextrins, but during this time I also noticed that gentamicin could directly go into a PEM without any pre-modification. In order to construct a tunable release system that incorporates our unique poly(β -amino esters), I came up with the heterostructure $[(Poly X/PA)(gentamicin/PA)]_n$ in which PA can be any biocompatible polyanion. This system was found to incorporate and release gentamicin in a highly tunable and *in vitro* active fashion¹⁴⁷.

During the development of the gentamicin coatings, I also worked on a side collaborative project with Dr. James Quattrochi of Harvard Medical School. The

goal was to establish PEMs on nanospheres to sequentially release siRNAs then carbachol. While there was little success in constructing PEMs on nanospheres due to aggregation, I did establish tunable buildup and release of siRNAs from a planar substrate using a simple bilayer structure with *Poly I*.

Despite having excellent dosage tunability and *in vitro* activity, the gentamicin films had not achieved the multi-day release necessary for full infection control on medical devices. Hence, I undertook several projects in attempt to establish a general method for extending small molecule release. They included alterations of PEM components, PLGA encapsulation of gentamicin, insertion of non-degradable layers, crosslinking of film, and inclusion of co-excipients. Most of these yielded unsatisfactory results, although the inclusion of protein co-excipients showed some promise. This finding led to a new project in establishing a gentamicin-protein co-release film. Overall, I learned from these experiments that in order to establish truly sustained and highly controllable release rate, more involved approaches such as synthetic prodrug designs and sophisticated carrier systems would need to be used.

Yet another alternative for achieving more sustained release of antibiotics was the use of naturally polymeric antibiotics. In particular, antimicrobial peptides (AmPs) were excellent candidates due to their broad-spectrum, potent activity and a charged, oligomeric structure. While I was still developing the gentamicin films, Chris Loose of the Greg Stephanopoulos group approached our group for a

potential collaboration on the incorporation of his AmPs into LbL thin films for slow release. Both sides agreed this is a feasible and promising idea, and hence a long-term AmP incorporation project was initiated that began to dominate the latter half of my thesis. A variety of AmPs were examined, and various protocols for incorporation and diagnostic assays were established.

Another project that took shape in the later phase of my thesis was *in vivo* evaluation of the antimicrobial coatings. After establishing *in vitro* efficacy and non-toxicity, we believed that we were ready for *in vivo* evaluation. An osteomyelitis model was designed based extensive research into the literature and advice from our consultants. However, establishing an effective, reproducible osteomyelitis model turned out to be more challenging than anticipated. Hence, the *in vivo* evaluation evolved into a study on osteomyelitis models, and after several rounds of modification, we eventually developed a working model that can now be used for future evaluations.

At this point, efforts are ongoing in fine-tuning the osteomyelitis model, improving the AmP-released thin films, and characterizing a dual-therapy coating that co-releases gentamicin and bFGF for simultaneous infection control and bone regeneration.

1.4.6 Concurrent LbL drug delivery projects

Several projects on LbL drug delivery are under active investigation in the Hammond group. They include but are not limited to:

1. Tissue engineering coating for grafts and medical devices (Mara Macdonald),

2. Therapeutic coating for intraocular lens (Renee Smith), with focus on the delivery of anti-inflammatory agents,
3. Wound dressing coating for battlefield trauma (Anita Shukla), with hemostatic, antimicrobial, and possibly tissue regenerative therapies,
4. Delivery of small hydrophobic drugs via designed micelles¹⁴⁸ (Byeong-Su Kim),
5. Delivery of small hydrophilic drugs (Josh Moskowitz), via liposomes, micelles, or prodrugs,
6. Optimizing poly(β -amino ester) chemistry (Renee Smith),
7. Spray-misting of LbL coatings for more sustained, sequential release (Mara Macdonald, Anita Shukla, and Kevin Krogman),
8. Electrochemically degradable thin film, to be described below (Daniel Schmidt),
9. Antimicrobial coating incorporating novel synthetic bacteriocidal polymers (Jessie Wong).

1.5 Outlook: Other LbL drug delivery systems

1.5.1 Electrochemically degradable LbL films

The specific polymer used in constructing electrochemically-degradable PEMs is Prussian blue (PB), which is a transition metal hexacyanoferrate complex. *Non-degradable* PEMs incorporating this compound have been extensively studied in the Hammond group for electrochromic applications^{29, 149, 150}. In one of these studies, Dean DeLongchamp found that constant switching of the applied voltage

between 0.6V and 1.5V resulted in controlled dissolution of his (LPEI/PB) multilayers^{m29}. Additional studies by Nicole Zacharia *et al.* confirmed that both a constant voltage of 1.5V and a cycling between 0 and 1.5V can result in controlled film dissolution and concomitant model drug release (data unpublished). PB was found to be non-toxic and was even considered as a remedial drug to radioactive contamination¹⁵¹.

Unlike passive release by hydrolytic degradation, PB-based drug delivery systems are actively controlled by externally applied voltage. While this approach minimizes unexpected or uncontrollable drug releases, it carries the drawback of having to implement an interface for external intervention. However, for applications such as cancer therapy, active control could be especially advantageous as doctors can administer the optimal schedule of chemotherapeutic agents based on the observed progress.

Further investigations into the release kinetics of this system will be needed. The quantitative effects of voltage cycling speed and amplitude should also be characterized, and stability of these multilayers under physiological conditions must be addressed. Long-term endeavors in this system will be similar to those planned for *Poly I*, namely expanding the range of encapsulatable drugs and fine-tuning complex delivery schedules of multiple drugs. As the PB nanocomposites used in the LbL assemblies are anionic, the natural drug candidates for

^m DeLongchamp and Hammond postulated that at 1.5V, PB exists in a form that possesses no surface or interior ionization, therefore unable to shield its adjacent LPEI layers from electrostatic repulsion.

encapsulation are polycationic. This is opposite to *Poly 1* systems, although the two systems are rather dissimilar in control mechanisms and may not be natural supplements for each other.

1.5.2 Reductively degradable LbL films

Our inspiration for a reductively-degradable PEM came from Oupicky *et al.*'s reductively cleavable linear polycations (RPC) synthesized from oxidative polycondensation of Cys(Lys)₁₀Cys with dimethyl sulfoxide¹⁵². It is degraded by intracellular glutathione and is thus stable in the extracellular environment. This system is ideal for delivering drugs that should only be released within a cell, such as plasmids for gene therapy. However, one must deposit the PEMs onto a particle small enough for efficient cellular uptake. Kris Wood has conducted proof-of-concept studies in which [Cys(Lys)₁₀Cys]_n were synthesized via Oupicky *et al.*'s protocol and layered with polyanionic heparin in a 20-bilayer film. He demonstrated that film degradation only occurred in the presence of glutathione. The films were smooth with a near-linear degradation profile. However, heparin release kinetics has not been studied.

Similar to the electrochemically degradable system, in-depth characterization of this system's release kinetics is necessary. *In vitro* release in plasma and cell lysate solution should be conducted to verify that drug release only occurs in the intracellular environment. In addition, we must demonstrate that there is efficient cell uptake of our chosen delivery vehicle.

While the two systems above are promising candidates for drug delivery, the hydrolytically degradable system still holds the most potential as it has been more extensively characterized and has a broader range of prospective applications. Nevertheless, the electrochemical and reductive systems, if successfully developed, will be valuable additions to our library of PEMs as they have unique features, namely active control and intracellular targeting. The opportunity to study these two systems is certainly an exciting prospect, and these additional pursuits may offer insights into LbL drug delivery systems not available from the hydrolytic system.

1.6 *References*

- (1) Langer, R. *Acc. Chem. Res.*, **1993**, *26*, 537-542
- (2) Uhrich, K. E., Cannizzaro, S. M., Langer, R. S. and Shakesheff, K. M. *Chemical Reviews*, **1999**, *99*, 3181-3198
- (3) Falk, R., Randolph, T. W., Meyer, J. D., Kelly, R. M. and Manning, M. C. *Journal of Controlled Release*, **1997**, *44*, 77-85
- (4) Johnson, O. L., Cleland, J. L., Lee, H. J., Charnis, M., Duenas, E., Jaworowicz, W., Shepard, D., Shihzamani, A., Jones, A. J. S. and Putney, S. D. *Nature Medicine*, **1996**, *2*, 795-799
- (5) Chluba, J., Voegel, J.-C., Decher, G., Erbacher, P., Schaaf, P. and Ogier, J. *Biomacromolecules*, **2001**, *2*, 800-805
- (6) Misra, G. P. and Siegel, R. A. *Journal of Controlled Release*, **2002**, *81*, 1-6
- (7) McGee, J. P., Davis, S. S. and O'Hagan, D. T. *Journal of Controlled Release*, **1994**, *31*, 55-60
- (8) Qiu, L. Y. and Zhu, K. J. *International Journal of Pharmaceutics*, **2001**, *219*, 151-160
- (9) Dang, W., Colvin, O. M., Brem, H. and Saltzman, W. M. *Cancer Research*, **1994**, *54*, 1729-1735
- (10) Brem, H. and Gabikian, P. *Journal Of Controlled Release: Official Journal Of The Controlled Release Society*, **2001**, *74*, 63-67
- (11) Conforti, A., Bertani, S., Lussignoli, S., Grigolini, L., Terzi, M., Lora, S., Caliceti, P., Marsilio, F. and Veronese, F. M. *Journal of Pharmacy and Pharmacology*, **1996**, *48*, 468-473
- (12) Benkirane-Jessel, N., Schwinte, P., Falvey, P., Darcy, R., Haikel, Y., Schaaf, P., Voegel, J.-C. and Ogier, J. *Advanced Functional Materials*, **2004**, *14*, 174-182
- (13) Gopferich, A. *Journal of Controlled Release*, **1997**, *44*, 271-281
- (14) Sershen, S. and West, J. *Advanced Drug Delivery Reviews*, **2002**, *54*, 1225-1235
- (15) Brekke, J. H. and Gubbe, J. H. *Journal*, **2004**,
- (16) Caruso, F. and Schuler, C. *Langmuir*, **2000**, *16*, 9595-9603

- (17) Schuler, C. and Caruso, F. *Biomacromolecules*, **2001**, 2, 921-926
- (18) Shi, X. and Caruso, F. *Langmuir*, **2001**, 17, 2036-2042
- (19) Khopade, A. J. and Caruso, F. *Nano Letters*, **2002**, 2, 415-418
- (20) Cohen, S., Yoshioka, T., Lucarelli, M., Hwang, L. H. and Langer, R. *Pharmaceutical Research*, **1991**, 8, 713-720
- (21) Sukhorukov, G. B., Brumen, M., Donath, E. and Möhwald, H. *J. Phys. Chem. B*, **1999**, 103, 6434-6440
- (22) Sukhorukov, G. B. *Journal*, **2002**, 5, 111-147
- (23) Lynn, D. M. and Langer, R. *J. Am. Chem. Soc.*, **2000**, 122, 10761-10768
- (24) Lim, Y.-b., Kim, C.-h., Kim, K., Kim, S. W. and Park, J.-s. *J. Am. Chem. Soc.*, **2000**, 122, 6524-6525
- (25) Sukhishvili, S. A. and Granick, S. *Macromolecules*, **2002**, 35, 301-310
- (26) Etienne, O., Schneider, A., Taddei, C., Richert, L., Schaaf, P., Voegel, J.-C., Egles, C. and Picart, C. *Biomacromolecules*, **2005**, 6, 726-733
- (27) Hiller, J. A. and Rubner, M. F. *Macromolecules*, **2003**, 36, 4078-4083
- (28) Tanaka, S., Yamakoshi, K., Kamiya, A., Shimazu, H. and Togawa, T. *Medical & Biological Engineering & Computing*, **1986**, 24, 371-374
- (29) DeLongchamp, D. M. and Hammond, P. T. *Advanced Functional Materials*, **2004**, 14, 224-232
- (30) Hsieh, D. S., Langer, R. and Folkman, J. *Proceedings Of The National Academy Of Sciences Of The United States Of America*, **1981**, 78, 1863-1867
- (31) Kost, J., Leong, K. and Langer, R. *Proceedings Of The National Academy Of Sciences Of The United States Of America*, **1989**, 86, 7663-7666
- (32) Bernard, L., Hoffmeyer, P., Assal, M., Vaudaux, P., Schrenzel, J. and Lew, D. *J. Antimicrob. Chemother.*, **2004**, 53, 127-129
- (33) Bauer, T. W. and Schils, J. *Skeletal Radiology*, **1999**, 28, 483-497
- (34) Lavernia, C. J., Drakeford, M. K., Tsao, A. K., Gittelsohn, A., Krackow, K. A. and Hungerford, D. S. *Clin. Orthop.*, **1995**, 311, 136-141

- (35) Saleh, K. J., Rand, J. A. and McQueen, D. A. *J Bone Joint Surg Am*, **2003**, 85, S18-20
- (36) Bourne, R. B. *The Journal of Arthroplasty*, **2004**, 19, 69-72
- (37) Fluckiger, U. and Zimmerli, W. *Der Orthopade*, **2004**, 33, 416-423
- (38) Bottner, F., Sculco, T. P., Sharrock, N. E., Westrich, G. H. and Steinbeck, J. *Der Orthopade*, **2001**, 30, 890-896
- (39) Heisel, C., Clarius, M., Schneider, U. and Breusch, S. J. *Zeitschrift fur Orthopadie und ihre Grenzgebiete*, **2001**, 139, 221-228
- (40) Dahl, O. E. *Drugs*, **2004**, 64, 17-25
- (41) Patil, S., Allan, D. B. and Quin, R. *The Journal of Arthroplasty*, **2002**, 17, 882-886
- (42) Cole, B. J., Schultz, E., Smilari, T. F., Hajdu, S. I. and Krauss, E. S. *Skeletal Radiology*, **1997**, 26, 559-563
- (43) Ganapathi, M., Lake, D. N. W. and Griffiths, A. P. *The Journal of Arthroplasty*, **2001**, 16, 229-232
- (44) Korkala, O. and Syrj nen, K. J. *Archives of Orthopaedic and Trauma Surgery*, **1998**, 118, 113-115
- (45) Grayson, A. C. R., Voskerician, G., Lynn, A., Anderson, J. M., Cima, M. J. and Langer, R. *Journal of Biomaterials Science. Polymer Edition*, **2004**, 15, 1281-1304
- (46) Richards-Grayson, A. C., Choi, I. S., Tyler, B. M., Wang, P. P., Brem, H., Cima, M. J. and Langer, R. *Nature Materials*, **2003**, 2, 767-772
- (47) Santini, J. T., Cima, M. J. and Langer, R. *Nature*, **1999**, 397, 335-338
- (48) Santini, J. T., Richards, A. C., Scheidt, R., Cima, M. J. and Langer, R. *Angewandte Chemie International Edition*, **2000**, 39, 2396-2407
- (49) Richardson, T. P., Peters, M. C., Ennett, A. B. and Mooney, D. J. *Nature Biotechnology*, **2001**, 19, 1029-1034
- (50) Raiche, A. T. and Puleo, D. A. *Biomaterials*, **2004**, 25, 677-685
- (51) Decher, G. and Hong, J. D. *Makromolekulare Chemie, Macromolecular Symposia*, **1991**, 46, 321-327

- (52) Decher, G. and Hong, J. D. *Berichte der Bunsen-Gesellschaft*, **1991**, 95, 1430-1434
- (53) Decher, G. *Science*, **1997**, 277, 1232-1237
- (54) Stroeve, P., Vazquez, V., Coelho, M. A. N. and Rabolt, J. F. *Thin Solid Films*, **1996**, 285, 708-712
- (55) Balasubramanian, S., Wang, X., Wang, H. C., Yang, K., Kumar, J. and Tripathy, S. K. *Chemistry of Materials*, **1998**, 10, 1554-1560
- (56) Lindsay, G. A., Roberts, M. J., Chafin, A. P., Hollins, R. A., Merwin, L. H., Stenger-Smith, J. D., Yee, R. Y., Zarras, P. and Wynne, K. J. *Chemistry of Materials*, **1999**, 11, 924-929
- (57) Joly, S., Kane, R., Radzilowski, L., Wang, T., Wu, A., Cohen, R. E., Thomas, E. L. and Rubner, M. F. *Langmuir*, **2000**, 16, 1354-1359
- (58) Caruso, F., Niikura, K., Furlong, D. N. and Okahata, Y. *Langmuir*, **1997**, 13, 3427-3433
- (59) Constantine, C. A., Mello, S. V., Dupont, A., Cao, X., David Santos, J., Osvaldo N. Oliveira, J., Strixino, F. T., Pereira, E. C., Cheng, T.-C., Defrank, J. J. and Leblanc, R. M. *J. Am. Chem. Soc.*, **2003**, 125, 1805-1809
- (60) Forzani, E. S., Otero, M., Pérez, M. A., Teijelo, M. L. and Calvo, E. J. *Langmuir*, **2002**, 18, 4020-4029
- (61) Sukhorukov, G. B., Montrel, M. M., Petrov, A. I., Shabarchina, L. I. and Sukhorukov, B. I. *Biosensors and Bioelectronics*, **1996**, 11, 913-922
- (62) DeLongchamp, D. M. and Hammond, P. T. *Langmuir*, **2004**, 20, 5403-5411
- (63) Rouse, J. H. and Lillehei, P. T. *Nano Letters*, **2003**, 3, 59-62
- (64) Fulda, K.-U., Kampes, A., Krasemann, L. and Tieke, B. *Thin Solid Films*, **1998**, 327-329, 752-757
- (65) Iler, R. K. *Journal of Colloid Interface Science*, **1966**, 21, 569-594
- (66) Dokoutchaev, A., James, J. T., Koene, S. C., Pathak, S., Prakash, G. K. S. and Thompson, M. E. *Chemistry of Materials*, **1999**, 11, 2389-2399
- (67) Liu, Y. J., Wang, Y. X. and Claus, R. O. *Chemical Physics Letters*, **1998**, 298, 315-319
- (68) Hammond, P. T. and Whitesides, G. M. *Macromolecules*, **1995**, 28, 7569-7571

- (69) Clark, S. L. and Hammond, P. T. *Advanced Materials*, **1998**, *10*, 1515-1519
- (70) Lvov, Y. M. and Sukhorukov, G. B. *Membrane Cell Biology*, **1997**, *11*, 277-303
- (71) Onda, M., Lvov, Y. M., Ariga, K. and Kunitake, T. *Biotechnology and Bioengineering*, **1996**, *51*, 163-166
- (72) Groth, T. and Lendlein, A. *Angewandte Chemie International Edition*, **2004**, *43*, 926-928
- (73) Berg, M. C., Yang, S. Y., Hammond, P. T. and Rubner, M. F. *Langmuir*, **2004**, *20*, 1362-1368
- (74) Pavoov, P. V., Gearing, B. P., Bellare, A. and Cohen, R. E. *Wear*, **2004**, *256*, 1196-1207
- (75) van de Belt, H., Neut, D., Schenk, W., van Horn, J. R., van der Mei, H. C. and Busscher, H. J. *Acta Orthopaedica Scandinavica*, **2001**, *72*, 557-571
- (76) Ono, I., Tateshita, T., Inoue, M. and Kuboki, Y. *Journal of Bone and Mineral Metabolism*, **1998**, *16*, 81-87
- (77) Li, R. H., Bouxsein, M. L., Blake, C. A., D'Augusta, D., Kim, H., Li, X. J., Wozney, J. M. and Seeherman, H. J. *Journal of Orthopaedic Research*, **2003**, *21*, 997-1004
- (78) Geiger, M., Li, R. H. and Friess, W. *Advanced Drug Delivery Reviews*, **2003**, *55*, 1613-1629
- (79) Keskin, D. S., Tezcaner, A., Korkusuz, P., Korkusuz, F. and Hasirci, V. *Biomaterials*, **2005**, *26*, 4023-4034
- (80) Kroese-Deutman, H. C., Ruhe, P. Q., Spauwen, P. H. M. and Jansen, J. A. *Biomaterials*, **2005**, *26*, 1131-1138
- (81) Kaito, T., Myoui, A., Takaoka, K., Saito, N., Nishikawa, M., Tamai, N., Ohgushi, H. and Yoshikawa, H. *Biomaterials*, **2005**, *26*, 73-79
- (82) Tabata, Y., Miyao, M., Ozeki, M. and Ikada, Y. *Journal of Biomaterials Science, Polymer Edition*, **2000**, *11*, 915-930
- (83) Yamamoto, M., Ikada, Y. and Tabata, Y. *Journal of Biomaterials Science, Polymer Edition*, **2001**, *12*, 77-88
- (84) Carano, R. A. D. and Filvaroff, E. H. *Drug Discovery Today*, **2003**, *8*, 980-989

- (85) Gu, F., Amsden, B. and Neufeld, R. *Journal of Controlled Release*, **2004**, 96, 463-472
- (86) Kotov, N. A. *Nanostructured Materials*, **1999**, 12, 789-796
- (87) Wadood, A. C., Armbrecht, A. M., Aspinall, P. A. and Dhillon, B. *Journal of Cataract & Refractive Surgery*, **2004**, 30, 761-768
- (88) Baeyens, V., Percicot, C., Zignani, M., Deshpande, A. A., Kaltsatos, V. and Gurny, R. *Advanced Drug Delivery Reviews*, **1997**, 28, 335-361
- (89) Prevention, C. f. D. C. a. *Journal*, **2001**,
- (90) Matthews, D. R., Lang, D. A., Burnett, M. A. and Turner, R. C. *Diabetologia*, **1983**, 24, 231-237
- (91) Reid, R. L., Fretts, R. and Van Vugt, D. A. *American Journal of Obstetrics and Gynecology*, **1988**, 158, 176-185
- (92) Kuret, J. A. and Murad, F. *Journal*, **1990**, 1334-1360
- (93) Chan, A. T. C., Ma, B. B. Y., Lo, Y. M. D., Leung, S. F., Kwan, W. H., Hui, E. P., Mok, T. S. K., Kam, M., Chan, L. S., Chiu, S. K. W., Yu, K. H., Cheung, K. Y., Lai, K., Lai, M., Mo, F., Yeo, W., King, A., Johnson, P. J., Teo, P. M. L. and Zee, B. *J Clin Oncol*, **2004**, 22, 3053-3060
- (94) Herzog, T. J. *Clin Cancer Res*, **2004**, 10, 7439-7449
- (95) Kost, J. and Langer, R. *Trends in Biotechnology*, **1992**, 10, 127-131
- (96) Levy, R., Nichols, M. A. and Miller, T. W., Jr. *ACS Symposium Series*, **1993**, 520, 202-212
- (97) Bouzeloc, S., Creutz, S. and Leaym, T. M. *Journal*, **2004**,
- (98) Brannon-Peppas, L. *ACS Symposium Series*, **1993**, 520, 42-52
- (99) Dees, C. H. *Journal*, **2003**,
- (100) Chung, A. J. and Rubner, M. F. *Langmuir*, **2002**, 18, 1176-1183
- (101) Dubas, S. T. and Schlenoff, J. B. *Macromolecules*, **2001**, 34, 3736-3740
- (102) Hahn, S. K. and Hoffman, A. S. *Biotechnology and Bioprocess Engineering*, **2004**, 9, 179-183

- (103) Sukhorukov, G. B., Mohwald, H., Decher, G. and Lvov, Y. M. *Thin Solid Films*, **1996**, 284-285, 220-223
- (104) Thierry, B., Winnik, F. M., Merhi, Y., Silver, J. and Tabrizian, M. *Biomacromolecules*, **2003**, 4, 1564-1571
- (105) Sukhishvili, S. A. and Granick, S. *J. Am. Chem. Soc.*, **2000**, 122, 9550-9551
- (106) Choksakulnimitr, S., Masuda, S., Tokuda, H., Takakura, Y. and Hashida, M. *Journal of Controlled Release*, **1995**, 34, 233-241
- (107) Zauner, W., Ogris, M. and Wagner, E. *Advanced Drug Delivery Reviews*, **1998**, 30, 97-113
- (108) Roberts, J. C., Bhalgat, M. K. and Zera, R. T. *Journal of Biomedical Materials Research*, **1996**, 30, 53-65
- (109) Barrera, D. A., Zylstra, E., Peter T. Lansbury, J. and Langer, R. *J. Am. Chem. Soc.*, **1993**, 115, 11010-11011
- (110) Putnam, D. and Langer, R. *Macromolecules*, **1999**, 32, 3658-3662
- (111) Vazquez, E., Dewitt, D. M., Hammond, P. T. and Lynn, D. M. *J. Am. Chem. Soc.*, **2002**, 124, 13992-13993
- (112) Zhang, J., Chua, L. S. and Lynn, D. M. *Langmuir*, **2004**, 20, 8015-8021
- (113) Jewell, C. M., Zhang, J., Fredin, N. J. and Lynn, D. M. *Journal of Controlled Release*, **2005**, 106, 214-223
- (114) Zhang, J., Fredin, N. J. and Lynn, D. M. *Langmuir*, **2007**, 23, 11603-11610
- (115) Zhang, J., Montanez, S. I., Jewell, C. M. and Lynn, D. M. *Langmuir*, **2007**, 23, 11139-11146
- (116) Fredin, N. J., Zhang, J. and Lynn, D. M. *Langmuir*, **2005**, 21, 5803-5811
- (117) Liu, X., Yang, J. W., Miller, A. D., Nack, E. A. and Lynn, D. M. *Macromolecules*, **2005**,
- (118) Zhang, J. and Lynn, D. M. *Macromolecules*, **2006**, 39, 8928-8935
- (119) Jewell, C. M., Zhang, J., Fredin, N. J., Wolff, M. R., Hacker, T. A. and Lynn, D. M. *Biomacromolecules*, **2006**, 7, 2483-2491

- (120) Wood, K. C., Boedicker, J. Q., Lynn, D. M. and Hammond, P. T. *Langmuir*, **2005**, *21*, 1603-1609
- (121) Wood, K. C., Chuang, H. F., Batten, R. D., Lynn, D. M. and Hammond, P. T. *PNAS*, **2006**, *103*, 10207-10212
- (122) Schmidmaier, G., Lucke, M., Wildemann, B., Haas, N. P. and Raschke, M. *Injury*, **2006**, *37*, S105-S112
- (123) Bauer, T. W. and Schils, J. *Skeletal Radiology*, **1999**, *28*, 483-497
- (124) Stigter, M., Bezemer, J., de Groot, K. and Layrolle, P. *Journal of Controlled Release*, **2004**, *99*, 127-137
- (125) Humphrey, J. S., Mehta, S., Seaber, A. V. and Vail, T. P. *Clinical Orthopaedics And Related Research*, **1998**, 218-224
- (126) L. Meseguer-Olmo, M. J. R.-N., M. Clavel-Sainz, V. Vicente-Ortega, M. Alcaraz-Baños, A. Lax-Pérez, D. Arcos, C. V. Ragel, M. Vallet-Regí,. *Journal of Biomedical Materials Research*, **2002**, *61*, 458-465
- (127) Johannes G.E. Hendriks, D. N., Jim R. van Horn, Henny C. van der Mei, Henk J. Busscher,. *Journal of Biomedical Materials Research Part B: Applied Biomaterials*, **2003**, *64B*, 1-5
- (128) Price, J. S., Tencer, A. F., Arm, D. M. and Bohach, G. A. *Journal of Biomedical Materials Research*, **1996**, *30*, 281-286
- (129) Nablo, B. J., Rothrock, A. R. and Schoenfisch, M. H. *Biomaterials*, **2004**, *26*, 917-924
- (130) Chung, R.-J., Hsieh, M.-F., Huang, C.-W., Perng, L.-H., Wen, H.-W. and Chin, T.-S. *Journal of Biomedical Materials Research Part B: Applied Biomaterials*, **2006**, *76B*, 169-178
- (131) Balaban, N., Gov, Y., Bitler, A. and Boelaert, J. R. *Kidney International*, **2003**, *63*, 340-345
- (132) Danese, P. N. *Chemistry & Biology*, **2002**, *9*, 873-880
- (133) Bayston, R., Ashraf, W. and Bhundia, C. *J. Antimicrob. Chemother.*, **2004**, *53*, 778-782
- (134) Camiel C. L. Peerlings, H. H. L. H., Raymond T. J. Bevers, Erik J. H. Boelen, Bram J. Stelt, Eva J. M. Korthagen, Leo H. Koole,. *Journal of Biomedical Materials Research*, **2002**, *63*, 692-698

- (135) Belt, H. v. d., Neut, D., Schenk, W., Horn, J. R. v., Mei, H. C. v. d. and Busscher, H. J. *Acta Orthopaedica Scandinavica*, **2001**, 72, 557-571
- (136) Ramage, G., Tunney, M. M., Patrick, S., Gorman, S. P. and Nixon, J. R. *Biomaterials*, **2003**, 24, 3221-3227
- (137) Harris, L. G. and Richards, R. G. *Injury*, **2006**, 37, S3-S14
- (138) Lynch, A. S. and Robertson, G. T. *Annual Review of Medicine*, **2008**, 59, 415-428
- (139) Costerton, J. W., Khoury, A. E., Ward, K. H. and Anwar, H. *The International Journal of Artificial Organs*, **1993**, 16, 765-770
- (140) Esposito, S. and Leone, S. *International Journal of Antimicrobial Agents*, **2007**, 29, 494-500
- (141) Lucke, M., Schmidmaier, G., Sadoni, S., Wildemann, B., Schiller, R., Haas, N. P. and Raschke, M. *Bone*, **2003**, 32, 521-531
- (142) Hanssen, A. D. and Spangehl, M. J. *Clinical Orthopaedics And Related Research*, **2004**, 79-85
- (143) Alt, V., Bitschnau, A., Osterling, J., Sewing, A., Meyer, C., Kraus, R., Meissner, S. A., Wenisch, S., Domann, E. and Schnettler, R. *Biomaterials*, **2006**, 27, 4627-4634
- (144) Cook, G., Costerton, J. W. and Darouiche, R. O. *International Journal of Antimicrobial Agents*, **2000**, 13, 169-173
- (145) Gosheger, G., Harges, J., Ahrens, H., Streitburger, A., Buerger, H., Erren, M., Gonsel, A., Kemper, F. H., Winkelmann, W. and von Eiff, C. *Biomaterials*, **2004**, 25, 5547-5556
- (146) Grunlan, J. C., Choi, J. K. and Lin, A. *Biomacromolecules*, **2005**, 6, 1149-1153
- (147) Hollinger, M. A. *Critical Reviews in Toxicology*, **1996**, 26, 255-260
- (148) Sheehan, E., McKenna, J., Mulhall, K. J., Marks, P. and McCormack, D. *Journal of Orthopaedic Research*, **2004**, 22, 39-43
- (149) Sax, H. and Lew, D. *Current Infectious Disease Reports*, **1999**, 1, 261-266
- (150) Waldvogel, F. A. and Papageorgiou, P. S. *New England Journal of Medicine*, **1980**, 303, 360-370
- (151) Goldenberg, D. L. *Lancet*, **1998**, 351, 197-202

- (152) Hamed, K. A., Tam, J. Y. and Prober, C. G. *Clinical Pharmacokinetics*, **1996**, *31*, 156-163
- (153) Tam, V. H., Kabbara, S., Vo, G., Schilling, A. N. and Coyle, E. A. *Antimicrob. Agents Chemother.*, **2006**, *50*, 2626-2631
- (154) Schafer, J. A., Hovde, L. B. and Rotschafer, J. C. *J. Antimicrob. Chemother.*, **2006**, *58*, 108-111
- (155) Stallmann, H. P., Faber, C., Bronckers, A. L. J. J., Nieuw Amerongen, A. V. and Wuisman, P. I. J. M. *J. Antimicrob. Chemother.*, **2004**, *54*, 472-476
- (156) Schultheis, K. H., Rehm, K. E., Voelkel, W., Schiefer, H. G., Schulz, A. and Kahl, M. *Chirurgisches Forum fuer Experimentelle und Klinische Forschung*, **1983**, 127-131
- (157) Kotlus, B. S., Wymbs, R. A., Vellozzi, E. M. and Udell, I. J. *American Journal of Ophthalmology*, **2006**, *142*, 721-726
- (158) Edmiston, C. E., Goheen, M. P., Seabrook, G. R., Johnson, C. P., Lewis, B. D., Brown, K. R. and Towne, J. B. *American Journal of Surgery*, **2006**, *192*, 344-354
- (159) Chuang, H. F., Smith, R., xe, C and Hammond, P. T. *Biomacromolecules*, **2008**, *ASAP Article*,
- (160) Kim, B.-S., Park, S. W. and Hammond, P. T. *ACS Nano*, **2008**, *2*, 386-392
- (161) DeLongchamp, D. M. and Hammond, P. T. *Polymer Preprints*, **2003**, *44*, 649-650
- (162) DeLongchamp, D. M. and Hammond, P. T. *Chemistry of Materials*, **2004**, *16*, 4799-4805
- (163) Pearce, J. *Food and Chemical Toxicology*, **1994**, *32*, 577-582
- (164) Oupick, D., Parker, A. L. and Seymour, L. W. *J. Am. Chem. Soc.*, **2002**, *124*, 8-9

Chapter 2. Incorporation of Polysaccharides

2.1 Sequential release of polysaccharides

Reproduced in part with permission from Kris C. Wood, Helen F. Chuang, Robert D. Batten, David M. Lynn, and Paula T. Hammond. Controlling interlayer diffusion to achieve sustained, multiagent delivery from layer-by-layer thin films. *PNAS* **103**(27):10207-10212, 2006.

© 2006 National Academy of Sciences, with the addition of supplemental data.

2.1.1 Introduction.

A drug species that was found to build exponentially growing films with *Poly 1* was thought to be a “diffusing” species¹⁵³, while one that built linear films would be non-diffusing. Examples of diffusing and non-diffusing model drugs are heparin and dextran, respectively, of which the growth curves and structures are shown in Figure 2.1.

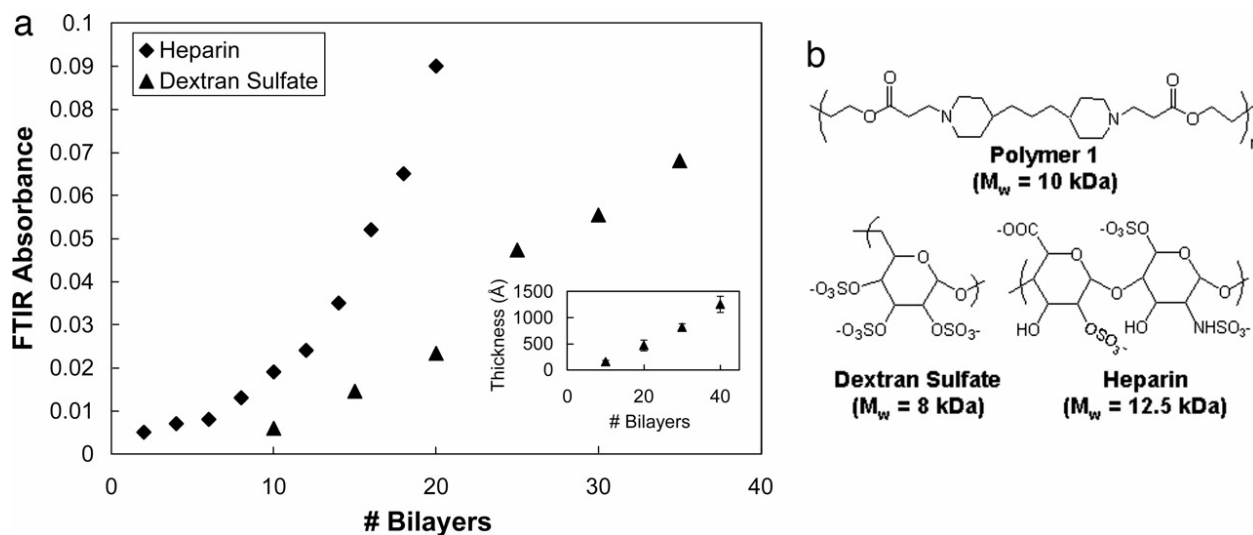


Figure 2.1 - Assembly of LbL films incorporating heparin and dextran.

(a) A plot of FTIR absorbance versus number of thin-film bilayers demonstrates LbL assembly of polymer 1/HEP (◆) and polymer 1/DS (▲) films exhibiting exponential and linear growth, respectively. (Inset) Thickness versus number of bilayers for polymer 1/DS films. (b) Chemical structures of degradable polymer and model drugs used in this study.

Kris *et al.* observed that a direct sequential layering of the non-diffusing dextran beneath heparin would still result in concurrent release (see **Figure 2.2**). Hence, we decided that it would be necessary to deposit “barrier layers” between different therapeutics to impose greater control on sequentiality. In a series of experiments with Kris Wood and Robert Batten, I examined several types of barrier layers, varying both thickness and degree of crosslinking, for their ability to prevent interdiffusion of the drugs between layers.

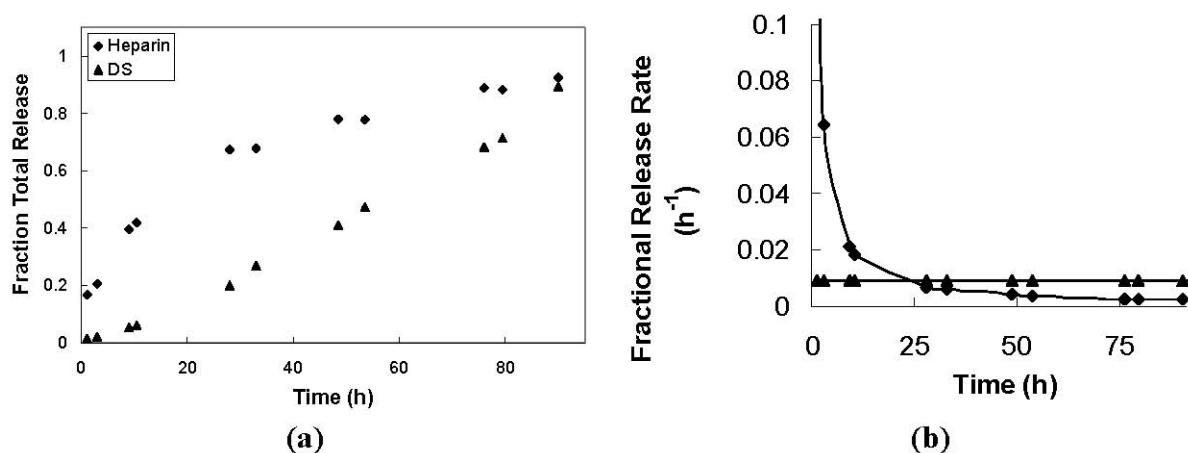


Figure 2.2 - Heparin (base, \blacklozenge) and dextran sulfate (top, \blacktriangle)-loaded PEM without dividing layers. (a) Fraction of mass release versus degradation time (error bars are small). (b) Fractional release rate versus time. Simultaneous release was observed.

2.1.2 Materials and Methods.

Materials. Polymer 1 [$M_n = 10,000$ (M_n is number-average molecular weight)] was synthesized as previously described²³. HEP sodium salt ($M_n = 12,500$) was obtained from Celsus Laboratories (Cincinnati). DS sodium salt ($M_n = 8,000$), poly(sodium 4-styrenesulfonate) ($M_n = 1$ million), PAH ($M_n = 70,000$), and PDAC ($M_n = 100,000$) were obtained from Sigma–Aldrich. Linear poly(ethylenimine) ($M_n = 25,000$) and PAA ($M_n = 90,000$) were purchased from Polysciences. Silicon wafers

(test grade n-type) were purchased from Silicon Quest (Santa Clara, CA). [^3H]HEP sodium salt [1 mCi (1 Ci = 37 GBq), 0.30 mCi/mg, $M_n = 12,500$] and [^{14}C]DS sodium salt (100 μCi , 1.5 mCi/g, $M_n = 8,000$) were obtained from American Radiolabeled Chemicals (St. Louis). Radiolabeled and corresponding unlabeled polymers were chosen with similar molecular weights and polydispersities to mimic the behavior of the unlabeled species as closely as possible. All materials and solvents were used as received without further purification.

General Considerations. A Harrick PDC-32G plasma cleaner was used to etch silicon substrates (3 x 2 cm) after they were rinsed with methanol and deionized water and dried under a stream of dry nitrogen. LbL thin films were deposited with an automated Zeiss HMS-series programmable slide stainer. Absorbances from growing films were measured by FTIR with a Nicolet Magna IR 550 Series II spectrometer. Zinc selenide substrates used for transmission FTIR analysis were prepared by the same method used for silicon substrates. Ellipsometric measurements for film thickness were conducted by using a Gaertner variable angle ellipsometer (6,328 nm, 70° incident angle) and GEMP 1.2 (Gaertner Ellipsometer Measurement Program) software interface. The release of radiolabeled polymers was quantified by using a Tri-Carb liquid scintillation counter (model U2200, Packard). The amount of radiolabel in each sample vial was measured by using ^3H , ^{14}C , and dual counting protocols, each of which were shown to be both consistent and highly accurate over a broad concentration range (30–100,000 dpm/ml) in calibration experiments performed before drug release. Thermal crosslinking of

PAH/PAA films was performed by incubating films in a Yamato DVS400 gravity convection oven at 215°C for the time intervals indicated in Figure 2.8.

Thin-Film Fabrication. All films were constructed from dilute aqueous solutions (2–10 mM) using the alternating dipping method⁵³. All polymers used in degradable thin films were prepared in 100 mM acetate buffer at pH 5.. Nondegradable base layers were deposited from dipping solutions of linear poly(ethylenimine) and poly(sodium 4-styrenesulfonate) in deionized water pH adjusted to 4.25 and 4.75, respectively. Deionized water used to prepare all solutions was obtained via a Milli-Q Plus (Millipore) at 18.2 M Ω . For degradation experiments, 1x PBS buffer (137 mM NaCl/2.7 mM KCl/10 mM Na₂HPO₄, pH 7.4) was used. Films used in this study were constructed on either silicon (for ellipsometry and degradation studies) or zinc selenide (for transmission-mode FTIR) planar substrates. In all cases, degradable, polymer 1-based films were constructed directly on top of 10 bilayer, nondegradable base films containing linear poly(ethylenimine) and SPS to ensure uniform adhesion to the substrate. After deposition, films were removed from rinsing baths and dried thoroughly under a stream of dry nitrogen to avoid premature degradation.

Thin-Film Degradation Studies. All film degradation studies were performed as follows. Films were immersed in 20 ml of the appropriate buffer solution in a screw-top glass vial and tightly sealed. At designated times, films were removed and dried thoroughly under a stream of dry nitrogen, and thickness was measured

using ellipsometry at 10 predetermined locations on the film surface (measurements were performed in triplicate). After the measurements were taken, the films were reimmersed in buffer solutions and resealed.

Release Studies. For drug-release experiments, radiolabeled LbL thin films were first constructed by alternately depositing polymer 1 and the indicated radiolabeled drug(s). Radiolabeled deposition solutions containing [^3H]HEP were prepared by combining 1 ml of 50 $\mu\text{Ci/ml}$ [^3H]HEP (0.30 mCi/mg, $M_n = 12,500$) with 35 ml of 100 mM acetate buffer. Unlabeled HEP ($M_n = 12,500$) was added to bring the total concentration of HEP (unlabeled plus labeled) to 2 mg/ml (1.5–2 $\mu\text{Ci/ml}$ ^3H).

Radiolabeled deposition solutions containing [^{14}C]DS were similarly prepared by combining [^{14}C]DS (1.5 mCi/g, $M_n = 8,000$), unlabeled DS ($M_n = 8,000$), and 100 mM acetate buffer to yield a total concentration of DS to 2 mg/ml (1 $\mu\text{Ci/ml}$ ^{14}C). After fabrication of the indicated films, drug-release experiments were performed by immersing each film in 50 ml of 1x PBS buffer in a 200-ml screw-top vial. A 1-ml sample was extracted at various predetermined time points and analyzed by adding 5 ml of ScintiSafe Plus 50% (Fisher Scientific) before measurement.

Degradation vials were tightly capped between sample extractions to prevent evaporation of the buffer solution. Raw data (given in disintegrations per minute) were converted to micrograms of drug released using the conversion factor $2.2 \times 10^6 \text{ DPM} = 1 \mu\text{Ci}$, the specific radioactivity of the drug, and our knowledge of the ratio of total drug to labeled drug in the deposition solution¹¹⁹.

2.1.3 Results and Discussion.

Controlling Interlayer Diffusion to Modulate Multiagent Release Profiles. Our first set of experiments involved 20–40 base layers of polymer 1/HEP, followed by a set of "barrier" layers consisting of either polymer 1/sulfonated poly(styrene) (SPS) (degradable), poly(diallyldimethylammonium chloride) (PDAC)/SPS (nondegradable), thermally crosslinked poly(allylamine hydrochloride) (PAH)/poly(acrylic acid) (PAA), or nothing at all. Finally, we constructed a set of 20–40 surface layers of polymer 1/DS. In a similar fashion, we also constructed films identical to the others, except that the order of the labeled components was reversed (DS base layers and HEP surface layers) (see Figure 2.3).

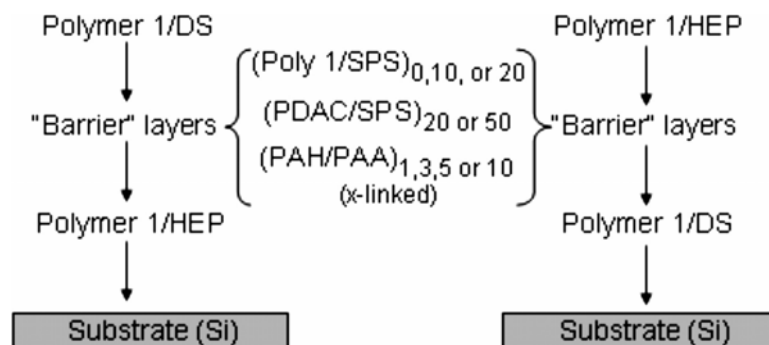


Figure 2.3 - Schematic depicting strategies employed in this study to construct physical barriers to control interlayer diffusion in multicomponent films.

As shown in Figure 2.4, when a base layer of polymer 1/DS was coated with a single bilayer of PAH/PAA (covalently crosslinked for 20 min at 215°C), followed by the deposition of polymer 1/HEP, we observed a multistage, serial release of first the surface HEP followed by the underlying DS. Thus, the use of a single covalently crosslinked PAH/PAA layer was sufficient to separate the two components when deposited onto the surface of the linearly growing polymer 1/DS

system, as evidenced by the two-stage release profile. After the ≈ 25 -h time delay, underlying DS was released with a linear profile. Interestingly, the average rate of DS release was $\approx 60\%$ slower than that observed in corresponding films without covalently crosslinked barrier layers. Additional experiments using single and multiple crosslinked PAH/PAA barrier layers show that the duration of the release delay and the rate of release after this delay can be broadly controlled under this approach. For example, multiple layers of PAH/PAA crosslinked for longer than 1.5 h (at 215°C) virtually halted the release of all underlying DS (no release of DS was observed for up to 45 days). This result may have important and direct applications in drug delivery, because it suggests that both the timing and rate of release of an underlying species can be broadly controlled using as little as a single crosslinked bilayer.

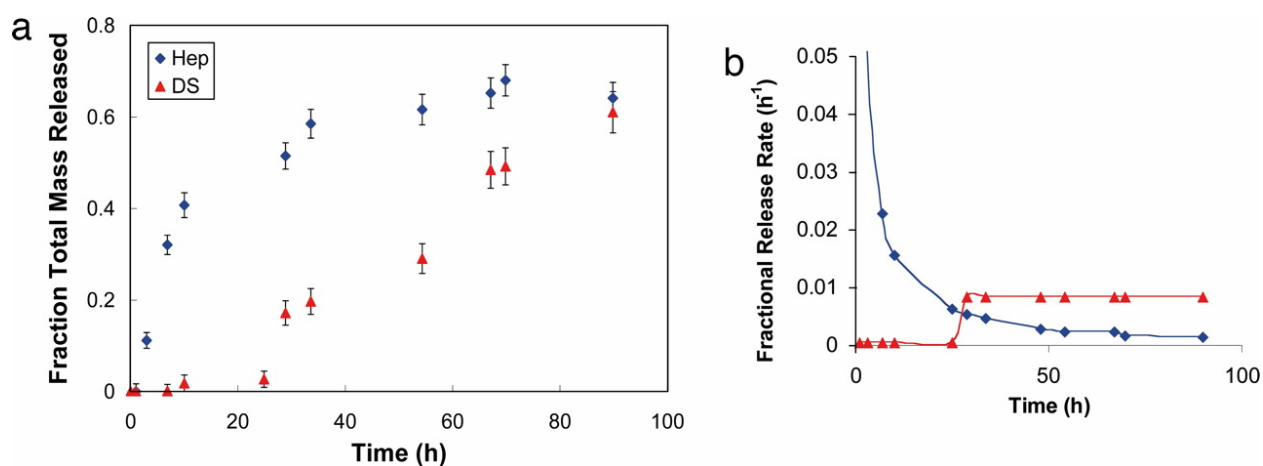


Figure 2.4 - DS (base layer, \blacktriangle) and HEP (surface layer, \blacklozenge)-loaded PEM separated by a single, crosslinked layer of (PAH/PAA), exhibiting sequential release.

(a) Fraction of mass-released versus degradation time. (b) Fractional release rate versus time.

Interestingly, we also found that when the order of the two labeled components was reversed (HEP as the base layer and DS as the surface layer) it was no longer

possible to achieve serial release of the two components using crosslinked spacer layers, suggesting that the nature of the base film onto which the crosslinked barrier layer is absorbed influences the final properties of the barrier layer (see Figure 2.5).

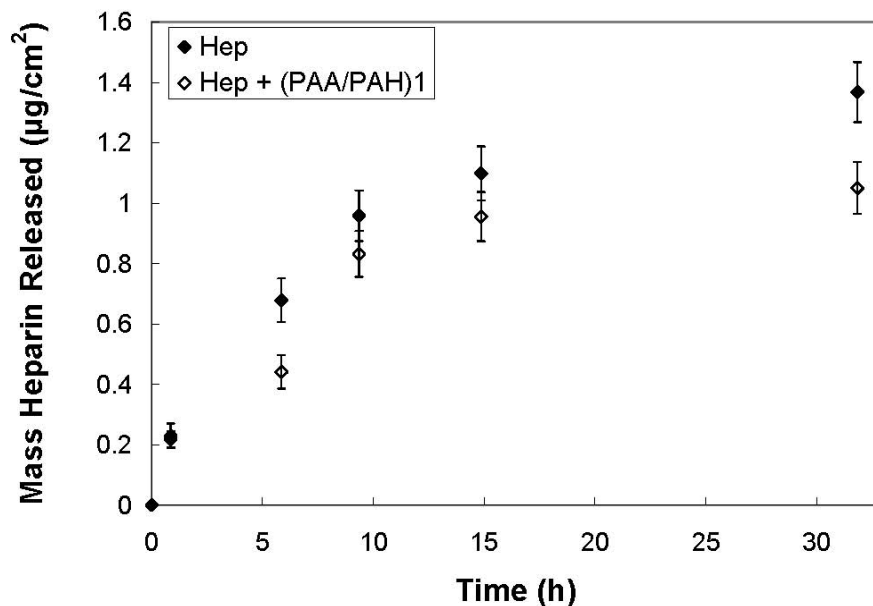
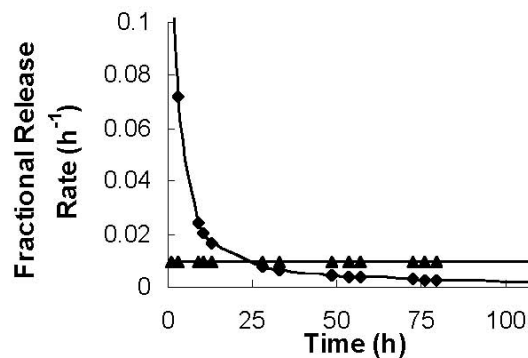
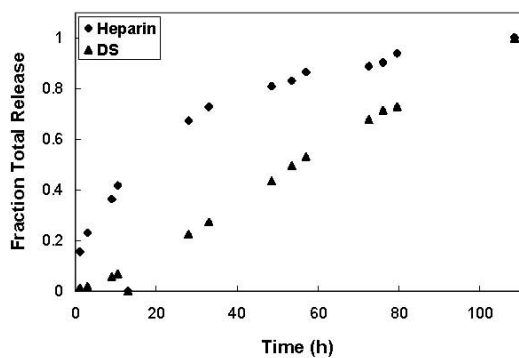


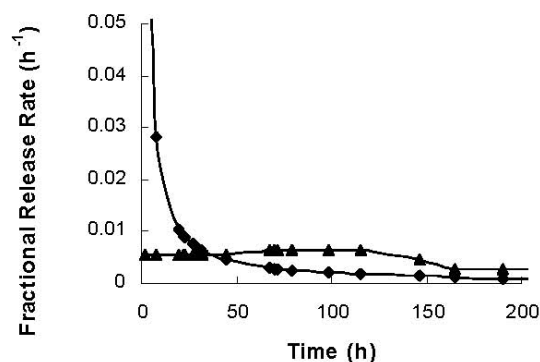
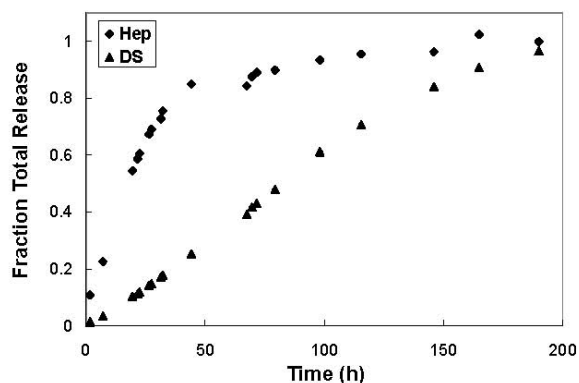
Figure 2.5 – Release of heparin from a PEM capped with a single crosslinked layer of PAH/PAA. Release of heparin-loaded films coated with a single layer of PAH/PAA crosslinked for 45 min at 215°C (filled diamond) is compared with untreated heparin-loaded films (open diamonds).

Remarkably, all of the noncovalent (noncrosslinked) barrier layers designed to physically separate the HEP and DS systems (Figure 2.3) resulted in simultaneous release of both components (see Figure 2.6). To further verify these findings, the above series of films was repeated at a range of fabrication conditions (pH, ionic strength, and number of deposited barrier layers), yet all resulted in simultaneous release in every case (data not shown).



(b)

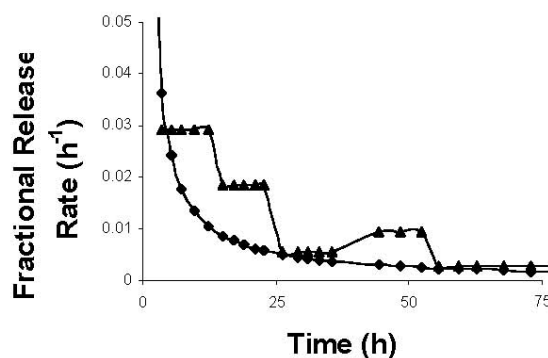
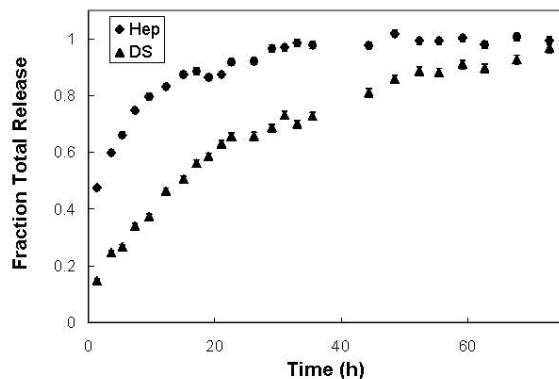
(i) - Heparin-loaded (base layer, diamond) and dextran-sulfate-loaded (surface layer, triangle) layers, separated by 20 polymer 1/SPS degradable dividing layers, sustain simultaneous release. (a) Fraction of mass release versus degradation time (error bars are small). (b) Fractional release rate versus time.



(a)

(b)

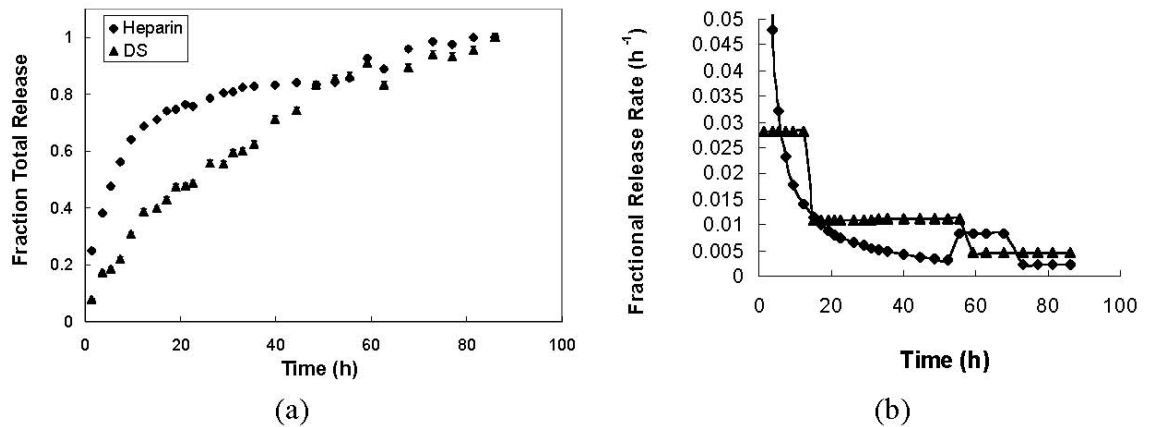
(ii) - Heparin-loaded (base layer, diamond) and dextran sulfate-loaded (surface layer, triangle) layers separated by 50 PDAC/SPS nondegradable dividing layers, sustain simultaneous release. (a) Fraction of mass release versus degradation time (error bars are small). (b) Fractional release rate versus time.



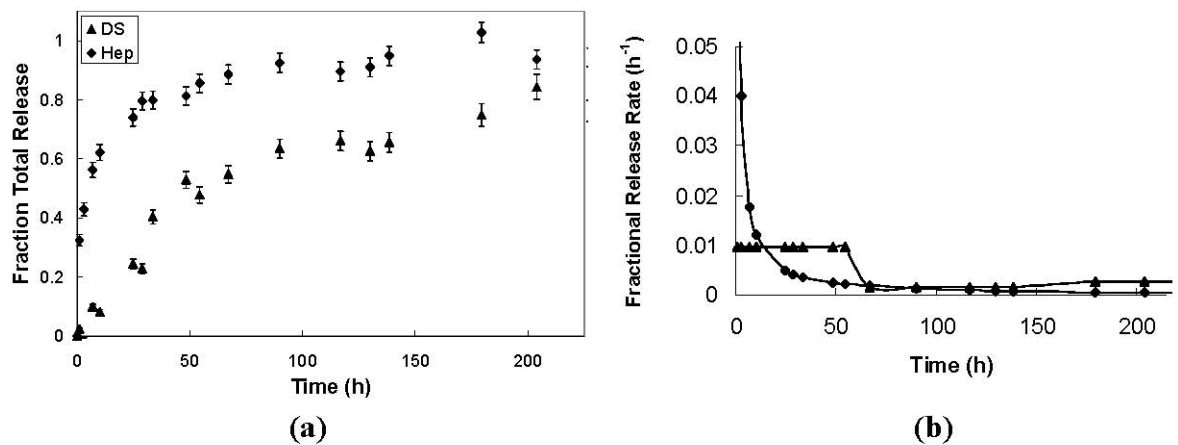
(a)

(b)

(iii) - Dextran-sulfate-loaded (base layer, triangle) and heparin-loaded (surface layer, diamond) layers without dividing layers sustain simultaneous release. (a) Fraction of mass release versus degradation time (error bars are small). (b) Fractional release rate versus time.



(iv) - Dextran-sulfate-loaded(base layer, triangle) and heparin-loaded (surface layer, diamond) layers separated by 50 polymer 1/SPS degradable dividing layers sustain simultaneous release. (a) Fraction of mass release versus degradation time (error bars are small). (b) Fractional release rate versus time.



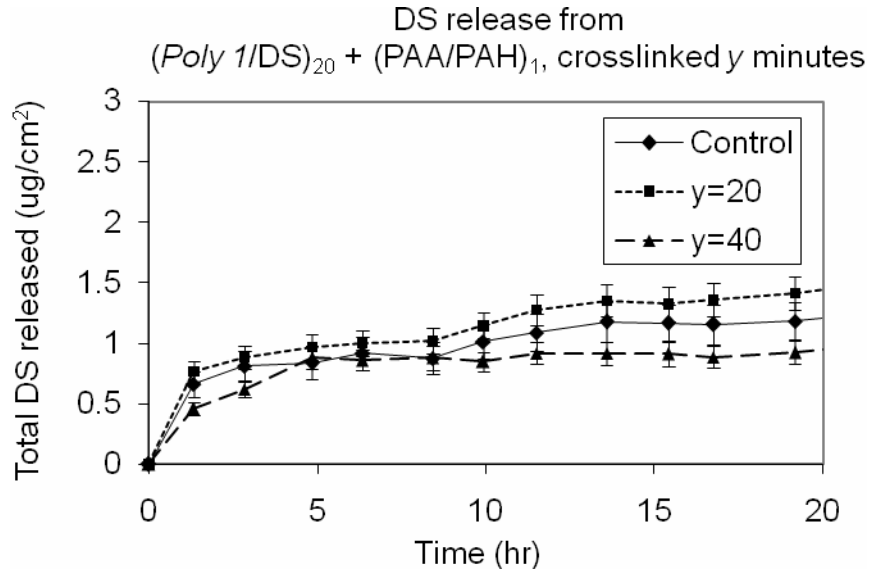
(v) - Dextran-sulfate-loaded (base layer, triangle) and heparin-loaded (surface layer, diamond) layers separated by 50 PDAC/SPS nondegradable dividing layers sustain simultaneous release. (a) Fraction of mass release versus degradation time. (b) Fractional release rate versus time.

Figure 2.6 – Heparin and dextran release from films formulated with various types of non-covalent barrier layers.

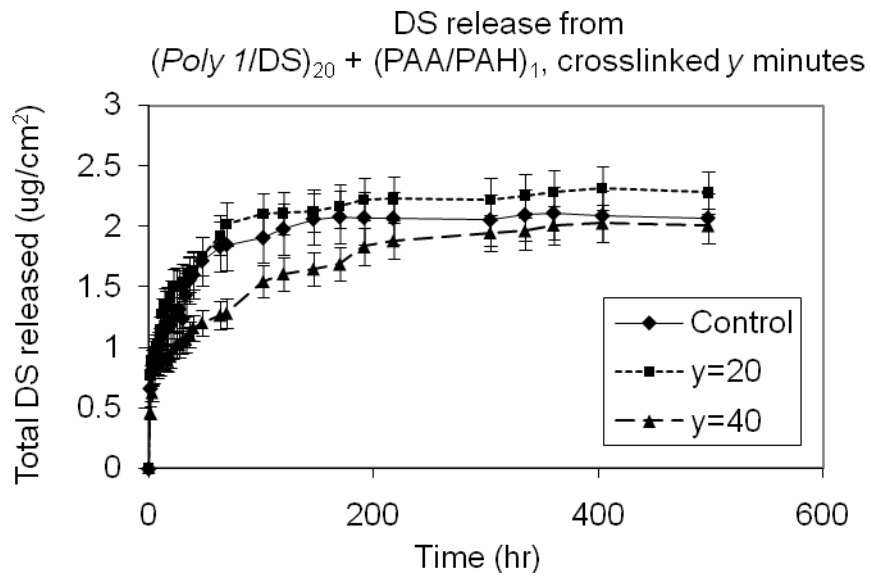
Data from Figure 2.6 suggest that noncovalent, electrostatically assembled barrier layers cannot block interlayer diffusion and, therefore, cannot be used to create compartmentalized structures involving diffusive polyelectrolytes. This finding is particularly interesting in light of another study that showed that compartmentalized films containing linearly and exponentially growing regions could be constructed

simply by depositing different films directly on top of one other¹⁵⁴. The incongruities between this study and ours could be a result of a number of factors, including different polymer systems, molecular weights, and deposition conditions; moreover, they suggest that factors outside of the nature of growth that a given system exhibits may powerfully influence the final film architecture.

Another finding that I made independently outside of the published PNAS work was that a $(Poly\ I/DS)_n$ film capped with crosslinked $(PAA/PAH)_1$ without any $(Poly\ I/HEP)_m$ on top did not result in a delayed release of dextran (see Figure 2.7). Combined with that observed in Figure 2.4, it appeared that the thermally crosslinked $(PAA/PAH)_1$ barrier layer alone could not delay dextran release. The heparin top layers might have served as additional diffusion control for the dextran underlayers.



(a)



(b)

Figure 2.7 – Release of dextran from PEMs capped with a single layer of (PAH/PAA) crosslinked for different amounts of time.

(a) zoomed into the first 20 hours to compare initial bursts among the three test groups, (b) complete release over 500 hours. No delayed release was observed for the number of barrier layers examined.

To more clearly demonstrate the effect of barrier layers on the average release rate from the aforementioned two-component systems, release rate is normalized and charted versus the type of barrier layer used in Figure 2.8. In Figure 2.8a, it is

apparent that the average release rate (taken as the average slope of the initial, linear portion of the release curve) of systems composed of an underlying layer of linearly growing DS can be broadly controlled by using both multiple layers of a nondegradable system PDAC/SPS or as little as a single layer of crosslinked PAH/PAA. Furthermore, by tuning any of the parameters affecting the degree of crosslinking (e.g., crosslinking time, temperature, or number of crosslinked layers), the release rate can be dramatically altered (crosslinking times of >1.5 h at 215°C and barriers containing more than five crosslinked layers, resulted in one- to two-order-of-magnitude decreases in release rate) (data not shown). Thus, milder crosslinking conditions (such as lower temperatures) may allow for a greater degree of flexibility in tailoring release profiles. Furthermore, aqueous, chemical crosslinking techniques using common biochemical reagents such as carbodiimides may represent a suitable alternative to thermal crosslinking when low temperature fabrication is required. Nevertheless, these proof-of-principle studies suggest that sampling a range of approaches to control the release of underlying species can yield effective results, particularly when the underlying species lacks the ability to diffuse throughout the film.

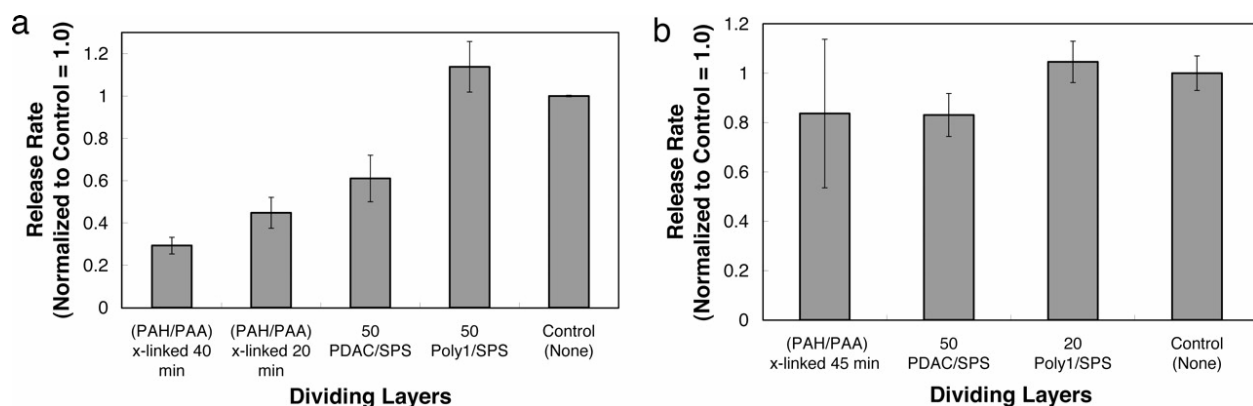


Figure 2.8 - Normalized initial average release rate ($\mu\text{g}/\text{hr}\cdot\text{cm}^2$) from base films containing DS (a) and HEP (b).

Films were capped with either no separation layers (control), or with a single layer of PAH/PAA crosslinked at 215°C for variable times, nondegradable PDAC/SPS, or degradable polymer 1/SPS. Initial average release rates were calculated from the average slope of the linear portion of the mass-released versus time curve during the first 50 h (DS) or 10 h (HEP) of degradation.

Taken together, the data in Figure 2.4 and Figure 2.8 yield a set of interesting hypotheses with respect to diffusion and release from multicomponent, hydrolytically degradable LbL films. First, when initially deposited layers contain a highly diffusible species, such as HEP, subsequent deposition of additional layers has little to no effect on its release because the diffusible species is likely able to migrate through tightly interacting networks within the film, effectively ensuring that it always resides near the film surface¹⁵³. However, when initially deposited layers contain a linearly growing species, such as DS, subsequent deposition of new species can have a significant impact on its release because the linearly growing system provides a structural substratum on which a tightly interacting network of barrier layers can be formed (which can then serve to hinder its release during degradation by physically separating it from subsequently adsorbed species). We demonstrate that a relatively simple understanding of the nature of build up and diffusion within a given system can allow one to engineer stratified,

multicompartment architectures with complex release profiles and that these profiles can be broadly controlled to suit the demands of a particular application.

2.1.4 **Conclusion.**

In this work, we systematically probed a series of strategies designed to physically separate multiple components within a LbL film by blocking interlayer diffusion. We measured the effect of each type of barrier by using an experimental system consisting of a hydrolytically degradable polymer alternately deposited with a series of radiolabeled polyelectrolytes. With this approach, we uncovered a set of strategies that allow for the production of compartmentalized, or stratified, films capable of releasing complex, tuned release profiles. In particular, we show that covalently crosslinked barriers can effectively block interlayer diffusion, leading to compartmentalized structures, although even very large numbers of ionically crosslinked (degradable or nondegradable) barrier layers cannot block interlayer diffusion. Perhaps most interestingly, we demonstrate that wide-ranging materials properties can be obtained from a single, relatively simple set of materials by judiciously applying strategies to control interlayer diffusion. Combining the attributes of the LbL processing technique, which allows for the rapid, all-aqueous, conformal fabrication of nanoscale coatings that are highly uniform and tunable, with the ability to spatially order active agents and control release kinetics for multiple species may yield significant opportunities in drug delivery, separations, electrooptical materials, and other fields.

2.2 *In vivo* assessment of heparin films

2.2.1 Introduction

Previous studies by Kris Wood, me, *et al.* established that polysaccharides such as heparin, dextran, and chondroitin sulfate can be encapsulated in layer-by-layer thin films with tunable dosage, sustained release, and even sequential release^{119, 120}. Among these model drugs, heparin is of especial interest because of its therapeutic action as an anti-coagulant. Sustained release of heparin could be especially useful on blood-contact device surfaces to prevent blood clots. Given our extensive studies on heparin release dosage and rate that demonstrated sustained, controllable release, we believed that the films should be assessed on *in vitro* activity.

Hence, the present study seeks to assess *in vitro* efficacy of layer-by-layer thin films encapsulating heparin, making use of an engineered mammalian cell line designed to respond to heparin supplementation through increased proliferation. Specifically, I used F32 cells, which are BaF3 cells (IL-3 dependent murine pro B cell line) transfected with fibroblast growth factor receptor c1 (FGFRc1) and can hence proliferate under a combined supplementation of basic fibroblast growth factor (bFGF or FGF-2) and heparin when maintained in a medium deficient of interleukin 3 (IL-3)¹⁵⁵. These cells were courtesy of David Berry in Professor Sasisekharan's lab. The *in vitro* response of F32 cells to heparin can be easily measured by cell density count.

2.2.2 Materials and Methods

NOTE: Materials and methods identical to those of 2.1 are not duplicated.

Materials. Recombinant human basic fibroblast growth factor (bGFG or FGF-2) and recombinant mouse interleukin-2 (IL-3) were purchased from R&D Systems (Minneapolis, MN). RPMI 1640 medium, fetal bovine serum (FBS), L-glutamine, and penicillin + streptomycin supplement were purchased from Invitrogen (Chicago, IL). All materials were used as supplied without further purification. F32, an engineered cell line derived from BaF-3 to proliferate in the presence of FGF-2 and heparin, transfected with FGF receptor c1 (FGFRc1) isoform¹⁵⁵, was a generous gift from Dr. David Berry of Harvard Medical School.

F32 Culture. F32 culture maintenance and proliferation assay were done following procedures of D. Berry *et al.*¹⁵⁶. Briefly, F32 cells were maintained as independent suspension cultures in propagation media composed of RPMI-1640 supplemented with 10% FBS, 100 µg/ml penicillin, 100 U/ml streptomycin, 500 µg/ml L-glutamine, and 1 ng/ml mouse recombinant IL-3. Cultures were grown in 75 cm² flasks at 37 °C in a 5% CO₂ humidified incubator and passaged 1:10 by dilution three times a week.

Unused FGF-2 was stored in sterile RPMI 1640 medium at 1 µg/mL in 1 mL aliquots at -80°C. Unused IL-2 were stored under identical conditions except at 0.5 µg/mL. Heparin supplements to the F32 assay cultures were prepared at 100 µg/mL in sterile RPMI 1640, sterile filtered, and stored in the refrigerator. *Poly I*

supplements were prepared right before each assay at 150 µg/mL in sterile RPMI 1640 and sterile filtered prior to use.

In a typical proliferation assay, F32 cells were seeded at a density of 10^5 cells/mL in IL-3 deficient RPMI-1640 after washing three times. Cell suspension was added to each well of 6-well plates, 2 mL/well. Cells were supplemented with various amounts of FGF-2, heparin, *Poly 1*, and or (*Poly 1/Hep*)_n thin films depending on the test protocol. The standard supplement conditions, denoted as the “1x” concentration for each component, were 50 ng/mL for FGF-2, 500 ng/mL for heparin, 750 ng/mL for *Poly 1*, and an amount of (*Poly 1/Hep*)_n film, tuned either by film size or number of bilayers, that would result in a total release of 500 ng/mL heparin into the culture. After defined periods of incubation under standard maintenance conditions, cell density was determined using a hemocytometer. Briefly, each well was gently resuspended, and three aliquots of 10 µL culture were withdrawn from each well. Each 10 µL culture was mixed with 10 µL of Trypan blue, and 10 µL of the mixture was used for hemocytometer counting.

2.2.3 Results and Discussion

Dosage and kinetics of heparin release from (*Poly 1/Hep*)_n films. Previous work reported by Kris Wood *et al.*¹²⁰ showed that (*Poly 1/Hep*)_n films release heparin over 20 hours in PBS at room temperature regardless of the film

thickness, with a dosage of approximate $5 \mu\text{g}/\text{cm}^2$ for a $(Poly\ I/Hep)_{20}$ film (see Figure 2.9 left panel).

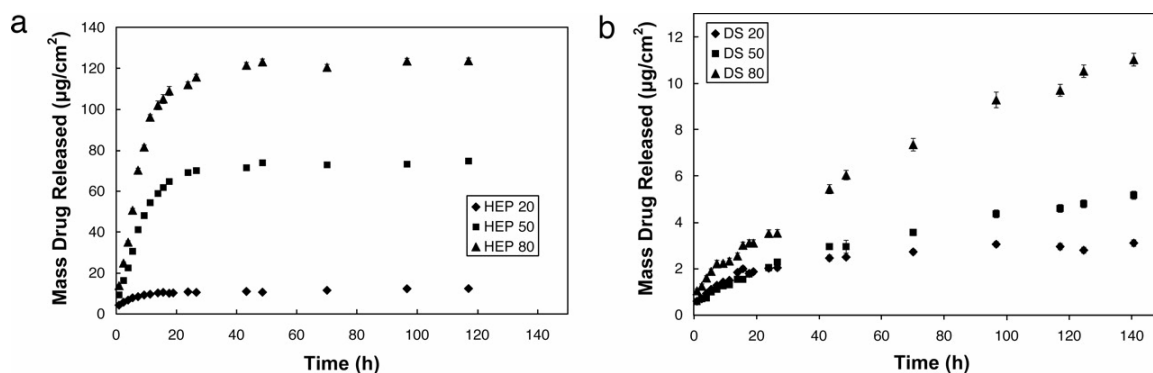


Figure 2.9 – Kinetics and dosage of heparin (left) and dextran (right) release from $(Poly\ I/heparin, dextran)_n$ films in PBS at 25°C .

From Wood *et al.*, PNAS 103(27): 10207-10212, 2006.

The present study also saw a 20-hour release of heparin from $(Poly\ I/Hep)_{20}$ films, but with a much higher dosage of around $45 \mu\text{g}/\text{cm}^2$ (see Figure 2.10). This dosage was reproducible over ten different samples, and the exact cause of discrepancy from previous data is yet unknown. It is worth noting that Kris also saw this high dosage on some of his trials (see Figure 2.11).

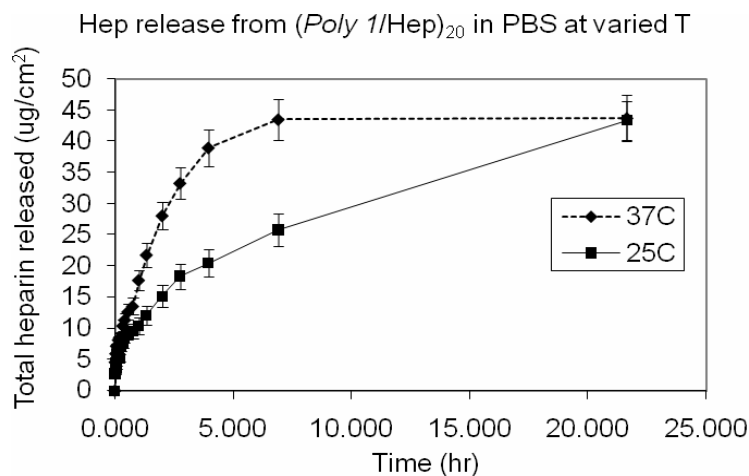


Figure 2.10 - Kinetics of heparin release from $(Poly\ I/Hep)_{40}$ films in PBS at various temperatures.

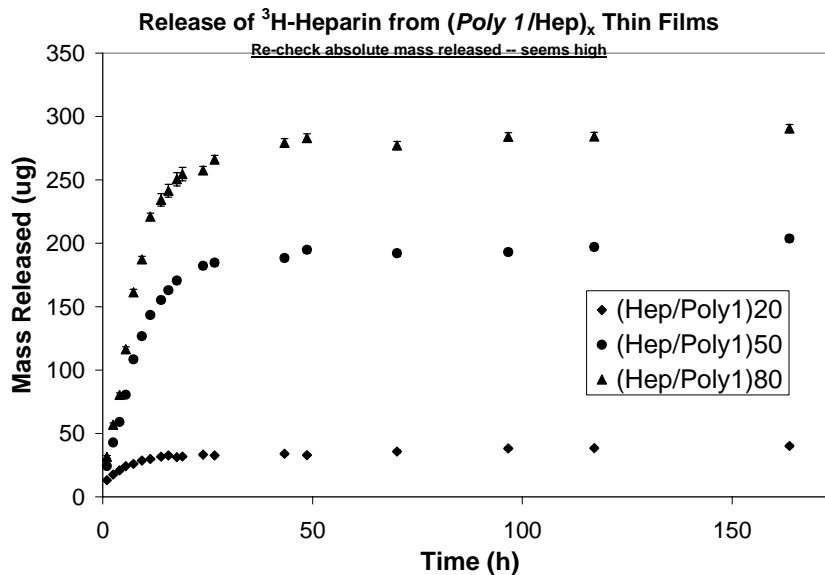


Figure 2.11 - Kris Wood's May 2005 data on heparin release from $(Poly\ 1/Hep)_n$ films.

Data in Figure 2.10 also compared release of heparin in PBS at room temperature (25°C) versus 37°C. Raising the temperature to body condition accelerated heparin release to completion within 7.5 hours. To further characterize heparin release under F32 culture conditions, $(Poly\ 1/Hep)_{20}$ films were eroded in F32 culture medium (composed of RPMI 1640 medium with various supplements – see Section 2.2.2) at 37°C. Interestingly, heparin release was found to be significantly accelerated in the F32 medium (see Figure 2.12). This was a surprising result as both PBS and F32 medium had similar ionic strength and pH (150 mM and 7.4, respectively), which were thought to be two of the most dominant factors inherent to a release medium that affect *Poly 1* degradation and polyelectrolyte multilayer dissolution rates. One potential explanation was that RPMI 1640 contains divalent ions, specifically calcium and magnesium, both around 0.4 mM, whereas PBS is composed entirely of monovalent ions. Even

though a total of 0.8 mM of divalent ions seems low, the divalency could result in strong electrostatic interactions that destabilizes the multilayers, so that heparin release could be driven by bulk deconstruction of the film rather than degradation of *Poly I* by water. Because of this finding, most subsequent experiments on *in vitro* release of any therapeutic were performed in modified simulated body fluid (m-SBF)¹⁵⁷, an ionic buffer that closely mimics human plasma including the divalent ions.

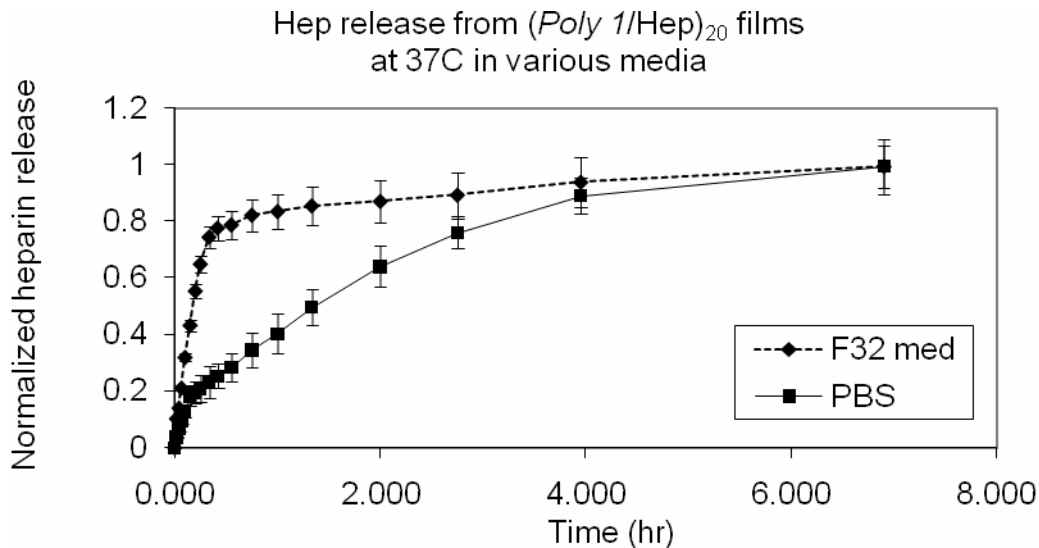


Figure 2.12 - Kinetics of heparin release from $(Poly\ I/Hep)_{20}$ films at 37°C in various media.

Since $45\ \mu\text{g}/\text{cm}^2$ is too large of a dosage for my need of $0.5\ \mu\text{g}$ per 1 mL culture, I also assessed heparin release from $(Poly\ I/Hep)_{10}$ films and found identical release rates under the various culture and temperature conditions, but with a dosage of $10\ \mu\text{g}/\text{cm}^2$ (data not shown).

Response of F32 cells to (Poly I/Hep)_n films. As specified under Section 2.2.2, typical supplementation to F32 cultures, as determined by Berry *et al.*¹⁵⁵, was 50 ng/mL of FGF-2 and 500 ng/mL of heparin. These will be denoted as “1x” concentrations in the following discussions, while “*n*x” will denote a concentration *n* times the 1x conditions. As an example, since F32 cultures were seeded at 2 mL per well, a “1x” amount of (*Poly I/Hep*)₁₀ film (10 μg/cm² of heparin) would be 0.1 cm² to release a total of 1 μg heparin, translating into 0.5 μg/mL or 500 ng/mL in a 2 mL culture. These 0.1 cm² films were obtained by splitting the coated 1.5 cm x 0.5 cm silicon substrates into four 0.4 cm x 0.25 cm pieces, discarding the bottom 0.7 cm section as this portion of the substrate. A 1x amount of direct *Poly I* supplementation is 750 ng/mL, or 1.5 times that of heparin, as this is the expected *Poly I*: heparin ratio within a (*Poly I/Hep*)_n film given 1:1 charge compensation.

The F32 cultures were treated with the specified test conditions immediately after seeding at 10⁵/mL. A small fraction of the each triplicated culture (30 μL per well or 1.5% of total initial volume) was withdrawn at each time point for triplicate counting of cell density. In all graphs presented in this section, the “normalized cell density” in the y-axis is relative to the seeding density of 10⁵/mL, *e.g.* a value of 10 on the y-axis represents cell density of 10 x 10⁵/mL. Note that the assays run on different days should not be compared on in a quantitative fashion, as F32 proliferative response was dependent on its passage number and other sources of culture variability. However, within each assay, the comparison between

different test groups should be reliable given the triplication in culture and counting, equivalent to nine total counts per data point.

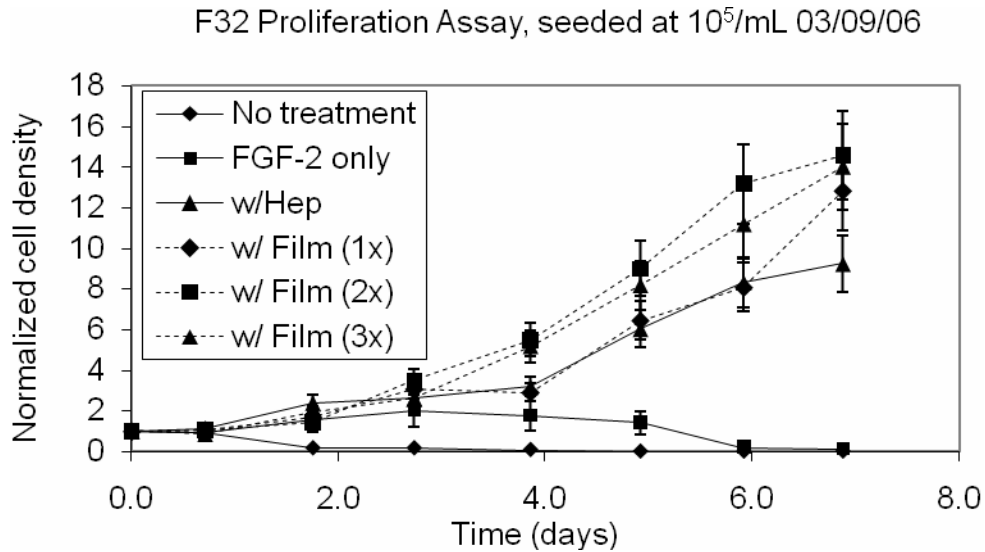


Figure 2.13 - F32 cell proliferation response to heparin administered via different means. All test groups except for “No Treatment” had 1x FGF-2 supplementation.

Three different test conditions were assessed along with the negative (‘no treatment’ and ‘FGF-2 only’) and positive (‘w/Hep’) controls, each involving direct co-incubation of F32 cultures with pieces of $(Poly\ I/Hep)_{10}$ films cut to the appropriate sizes to release the test amount of heparin in to the culture. A 1x film treatment was observed to result in a similar extent of F32 proliferation as the 1x positive control, suggesting that heparin was released from the $(Poly\ I/Hep)_{10}$ films in a therapeutically active form. Co-incubation with larger amounts of film at 2x and 3x amounts brought on additional proliferative response, although the contributions between heparin and other film components were not clear at this point, and were to be clarified by subsequent experiments.

As a follow-up to the previous assay, direct and film-released supplementations of heparin were compared at various concentrations. Heparin at 0.25x, 0.5x, 1x, and 2x, corresponding to 0.125, 0.25, 0.5 and 1.0 $\mu\text{g}/\text{mL}$ was administered either through direct supplementation or co-incubation with $(\text{Poly I}/\text{Hep})_{10}$ films. The resulting F32 response is shown in Figure 2.14. The data suggested that an equivalent amount of heparin released from a film could stimulate higher proliferation in comparison to direct heparin supplementation under the same concentration. Hence, co-released *Poly I* could actually affect cell proliferative response, either through a direct action on F32 or through secondary enhancement of heparin action. In fact, the secondary enhancement effect had already been reported by Berry *et al.*¹⁵⁸, who showed that *Poly I* enhanced murine melanoma cell uptake of heparin, resulting in the cancer cells' death.

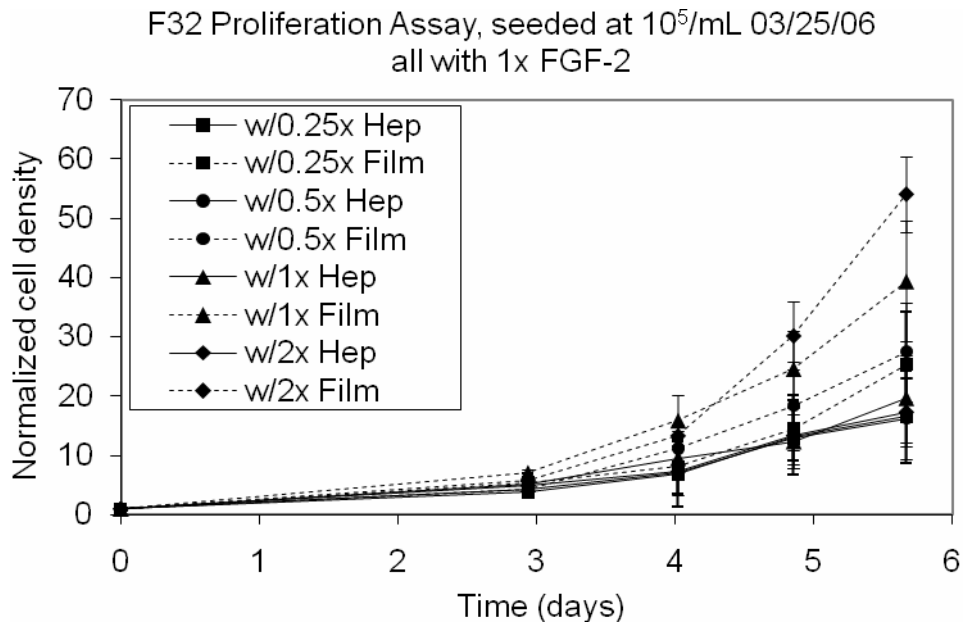


Figure 2.14 - F32 cell proliferation response to heparin administered via different means at various concentrations. All test groups had 1x FGF-2 supplementation.

At this stage, I believed that there was sufficient data to support the hypothesis that heparin was released from $(Poly\ I/heparin)_n$ films in therapeutically active forms, and wanted to direct further efforts on accessing *Poly I*'s enhancement effect. Additional assays were designed to involve direct supplementations of F32 cultures with heparin and various amounts of *Poly I*, the latter being freshly prepared right before each assay. Figure 2.15 presents one of the first sets of these assays, showing F32 cultures under 1x FGF-2 and heparin supplementations, but with different amounts of *Poly I*. Here, 1x *Poly I* corresponded to 750 ng/mL, 1.5 times that of 1x heparin, and this was based on 1:1 charge compensation between the two polyelectrolytes – the expected ratio of the two components within a $(Poly\ I/Hep)_n$ film. However, there was no guarantee that the 1:1 charge compensation was an exact mimic of film released conditions, only a close approximation.

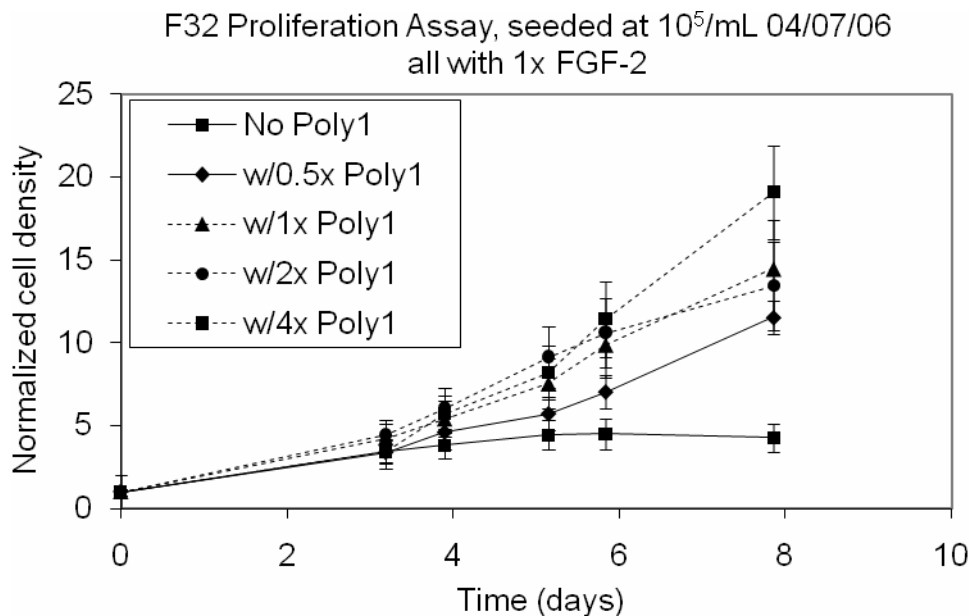


Figure 2.15 - F32 cell proliferation under various amounts of *Poly I* supplementation. All cultures received 1x FGF-2 and 1x heparin.

Data from Figure 2.15 supports the hypothesis that *Poly 1* enhances F32 proliferation in the presence of heparin, and the effect increases with increasing amount of *Poly 1* within the range of 0.5x to 4x concentrations. However, this set of data did not distinguish between independent proliferative action by *Poly 1* versus cooperative effect with heparin in stimulating proliferation. To further probe the mechanism, assays involving various combinations of heparin and/or *Poly X* supplementations were run, all with 1x FGF.

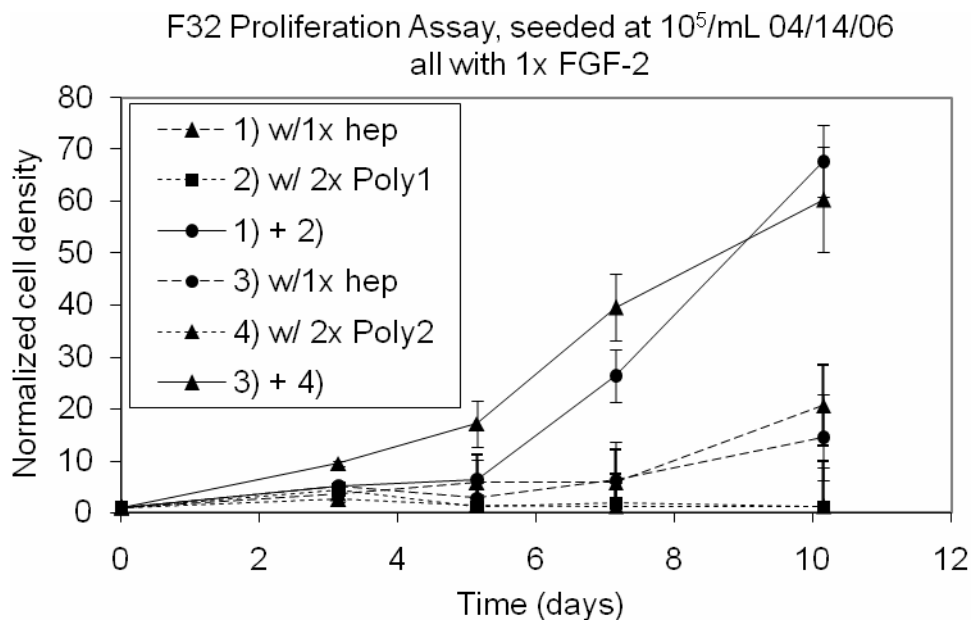


Figure 2.16 - F32 proliferation under various amounts of heparin and/or *Poly 1/2* supplementation.

All cultures received 1x FGF-2.

Data Figure 2.16 clearly demonstrated that cultures supplemented with *Poly X* but no heparin could not proliferate. Those supplemented with heparin alone (middle two curves) proliferated at a modest rate, while those with supplementations of both heparin and *Poly X*, whether *Poly 1* or *Poly 2*, proliferated noticeably faster

than those with heparin alone. The enhancement activities appeared similar between *Poly 1* and *Poly 2* as coupled with heparin administration. These observations confirmed the hypothesis that *Poly X* could not act alone on F32 cells but instead enhanced heparin action, possibly by increasing heparin uptake as observed by Berry *at al.*¹⁵⁸

Several variations of the study exemplified in Figure 2.16 were performed, continuing with *Poly 1* and *Poly 2* as model poly(β -amino esters). For example, in Figure 2.17 the *Poly X* supplementations were raised to 4x and 20x levels, and a combination of *Poly 1* and *Poly 2* was also examined. As was observed in Figure 2.16, *Poly 1* and *Poly 2* supplementations gave similar proliferative responses, and a combination of 2x *Poly 1* + 2x *Poly 2* gave a similar outcome as individual 4x *Poly 1* or 4x *Poly 2* treatments. Large doses of *Poly X* did not elicit significantly more proliferation. Most likely, all the available heparin had been taken up. Another possibility was that *Poly X* began exhibiting cytotoxicity at higher concentrations, and this inhibitory action canceled out additional proliferation enhancement.

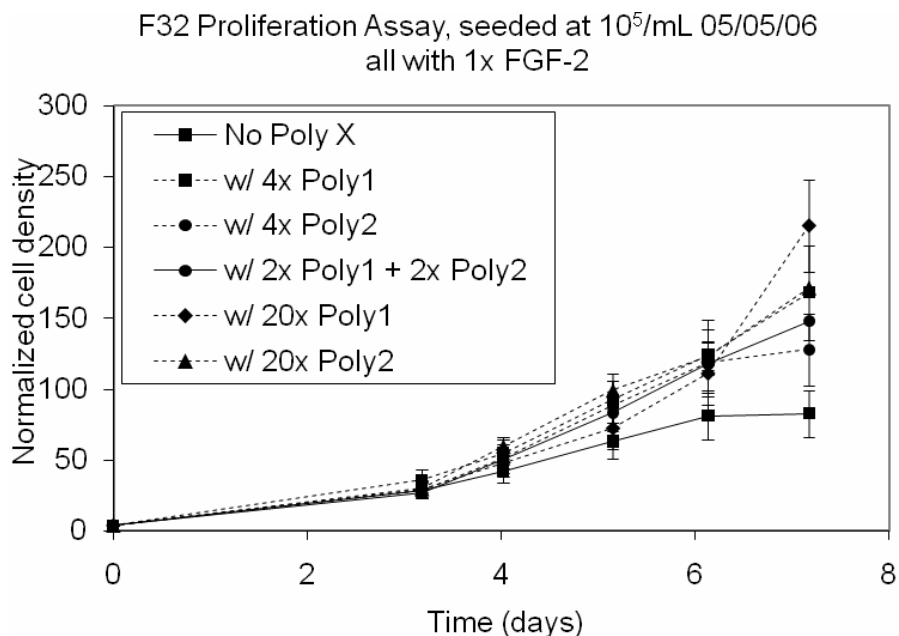


Figure 2.17 - F32 proliferation under various amounts of *Poly 1/2* supplementation. All cultures received 1x FGF-2 and 1x heparin.

2.2.4 Conclusion.

(*Poly 1/Heparin*)_n films were fabricated in a dosage-tunable fashion with high retention of *in vitro* activity. Additionally, poly(β -amino esters) were found to enhance F32 proliferation in the presence of heparin, likely through augmentation of heparin uptake. The effect appeared equivalent between the two different poly(β -amino esters) tested.

However, using the engineered F32 cell line was an indirect method of testing the *in vitro* efficacy of these heparin-releasing films. Ultimately we should demonstrate the film's *in vitro* and *in vivo* anti-coagulant action, through appropriate plasma models such as protein adsorption¹⁵⁹, plasma calcification

time¹⁶⁰, and platelet adhesion time^{160, 161}, and work towards a efficacious and biocompatible therapeutic film that can be applied on blood-contact devices.

Acknowledgements.

For the sequential release of polysaccharides, I would like to thank Kris Wood and his UROP Robert Batten for their close collaboration on this project, and Professor David Lynn and his students for their discussions in this area. I also wish to thank my UROP Yamicia Connor for performing some of the experiments described in this chapter. For the *in vitro* assessments, I would like to thank Kris Wood for providing the idea of using the F32 cells, and for training me on F32 culturing techniques. F32 cells and standard culture and assay protocols were courtesy of David Berry. Greg Zugates helped with the preparation of frozen F32 stocks at the conclusion of these experiments. Undergraduate assistant Jenny Yeh helped with many of the cell counting assays. Facilities in the Langer group were used for all F32 assays.

References.

- (1) Picart, C., Mutterer, J., Richert, L., Luo, Y., Prestwich, G. D., Schaaf, P., Voegel, J.-C. and Lavallo, P. *PNAS*, **2002**, *99*, 12531-12535
- (2) Lynn, D. M. and Langer, R. *J. Am. Chem. Soc.*, **2000**, *122*, 10761-10768
- (3) Decher, G. *Science*, **1997**, *277*, 1232-1237
- (4) Wood, K. C., Boedicker, J. Q., Lynn, D. M. and Hammond, P. T. *Langmuir*, **2005**, *21*, 1603-1609
- (5) Garza, J. M., Schaaf, P., Muller, S., Ball, V., Stoltz, J.-F., Voegel, J.-C. and Lavallo, P. *Langmuir*, **2004**, *20*, 7298-7302

(6) Wood, K. C., Chuang, H. F., Batten, R. D., Lynn, D. M. and Hammond, P. T. *PNAS*, **2006**, *103*, 10207-10212

(7) BERRY, D., KWAN, C.-P., SHRIVER, Z., VENKATARAMAN, G. and SASISEKHARAN, R. *FASEB J.*, **2001**, *15*, 1422-1424

(8) Berry, D., Shriver, Z., Venkataraman, G. and Sasisekharan, R. *Biochemical and Biophysical Research Communications*, **2004**, *314*, 994-1000

(9) Ayako Oyane, H.-M. K., Takuo Furuya, Tadashi Kokubo, Toshiki Miyazaki, Takashi Nakamura, . *Journal of Biomedical Materials Research Part A*, **2003**, *65A*, 188-195

(10) Berry, D., Lynn, D. M., Sasisekharan, R. and Langer, R. *Chemistry & Biology*, **2004**, *11*, 487-498

(11) Brynda, E., Houska, M., Jirouskova, M. and Dyr, J. E. *Journal of Biomedical Materials Research*, **2000**, *51*, 249-257

(12) Tana, Q., Ji, J., Barbosa, M. A., Fonseca, C. and Shen, J. *Biomaterials*, **2003**, *24*, 4699-4705

(13) Claudia Sperling, M. H. E. B. U. S. C. W. *Journal of Biomedical Materials Research Part A*, **2006**, *76A*, 681-689

Chapter 3. Biocompatibility assessment of *Poly X*'s

3.1 Introduction.

Given our intended biomedical application, assessment of biocompatibility of both individual film components and overall film system was essential. Most of the film components within my study, be the drug or a co-excipient, were expected to be biocompatible due to their endogenous origin and/or FDA-approved status. However, the *Poly X* component was a synthetic polymer that was rather novel, so little biocompatibility data was available even on an *in vitro* level.

Lynn *et al.* had demonstrated biocompatibility of *Poly I* towards the fibroblastic NIH3T3 cell line via the MTT assay²³ and indirectly showed its nontoxicity towards Cos-7 through the cell transfection assays in which no significant cell death was observed¹¹². Similar indirect inference of nontoxicity could be made from my data on F32 cell proliferation by (*Poly I*/heparin)_n films (see section 2.2). However, these constituted a very limited set of data, some of which involved only 5-hour treatments that were significantly shorter than our intended contact times between the film and the body. Questions remained as exactly how a direct exposure of mammalian cells to *Poly X* for an extended period of time could affect their viability. Hence, I conducted a series of assays to study the effect of *Poly X* treatment on two model mammalian cell lines, MC3T3 and Cos-7. These two cell lines were chosen because MC3T3, a murine pre-osteoblast, serve as a good model for our intended orthopedic application and was already in use for other LbL drug delivery studies, while Cos-7, a monkey kidney cell line, was sufficiently

different from MC3T3 to provide a more generalized survey of mammalian culture response. The popular but toxic gene delivery polymer, poly(ethylene imine) (PEI), was used as a positive control.

3.2 Materials and Methods.

Poly X's were synthesized as previously described²³. PEI was purchased from Sigma-Aldrich. MC3T3 source and culturing techniques, including alamarBlue® assays, were identical to those described under Chapter 5. Cos-7 cells were maintained and cultured in essentially identical procedures as those for MC3T3, except grown in Dulbecco's Modified Eagle's Medium (DMEM) supplemented with 10% FBS (fetal bovine serum) and antibiotics.

3.3 Results and Discussion.

Note that the assays run on different days should not be compared in a quantitative fashion, as cell metabolic activities were dependent on its passage number, and there was inherent biological variability of a live system. Hence, quantitative data of identical test conditions may vary from one assay to another. However, within each assay, the comparison between different test groups should be reliable given the identical passage number and incubation conditions. Most of the results below will focus on MC3T3 as it is the model mammalian cell line of interest, but a subset of equivalent data on Cos-7 will be discussed as well.

As-made vs. double-purified *Poly 1*. In the first series of experiments, MC3T3 cells were exposed to *Poly 1* solutions prepared freshly in a culture medium right before the administration. Both “as-made” *Poly 1* (*Poly 1* as obtained from standard synthesis procedure without further purification) and “double-purified” *Poly 1* (further re-crystallized twice) were examined. **Error! Reference source not found.** shows the result from one of these assays. Metabolic activities were normalized to that of negative control. A two-day treatment time was chosen for to maintain appropriate culture confluence throughout the assay period. Ideally the cells would be exposed for a longer period of time to emulate the multi-week exposure of the patient’s body to an implant coating. However, exposure times longer than 2-3 days were not feasible due to potential overgrowth of the cells leading to an inappropriate level of confluence.

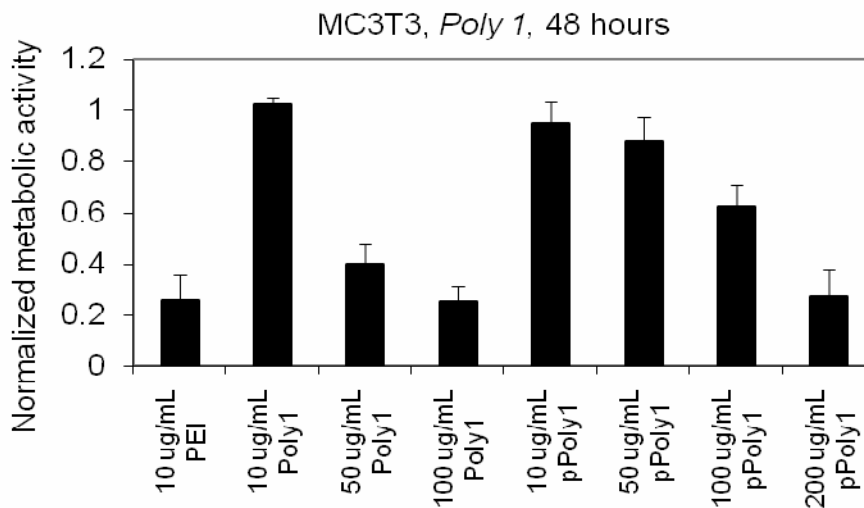


Figure 3.1 - Metabolic response of MC3T3 cells to *Poly 1* solutions after a 48-hour exposure. “p*Poly1*” denotes double-purified *Poly 1*.

As data from Figure 3.1 suggests, double-purified *Poly I* was less inhibitory on the metabolic activity of the MC3T3 cells. For the as-made *Poly I*, concentrations of 50 $\mu\text{g/mL}$ or above imposed noticeable inhibitory effect after a two-day exposure. This is a rather tight limit that may restrict the utility of *Poly I* (and possibly other *Poly X*) based films. However, *Poly I* that are incorporated within an LbL film may be purer than as-made *Poly I*, because the impurities are assumed to be monomeric or oligomeric species that would adsorb less readily when deposited from the same solution mixture as the polymeric *Poly I*.

Assessment of monomers. Given the suspicion that impurities in as-made *Poly I* would cause inhibitory effect on MC3T3s, the next step would be to characterize the degree of toxicity of the assumed impurity species. The impurities were hypothesized to be the diamine and diacrylate monomers, *i.e.* 4,4'-trimethylenedipiperidine and 1,4-butanediol diacrylate, that were used to synthesize *Poly I*. A small fraction might not have reacted and was not completely washed out at the end of the synthesis. Hence, a second series of assays were conducted to assess potential toxicity of these starting materials. MC3T3 cells were treated with various concentrations of either the diacrylate, the diamine, or the two monomers combined at a 1:1 molar ratio, as this is the expected molar balance between residuals of the two monomers. In addition, fully degraded (for at least 3 days) *Poly I* solutions were examined, as the monomers resulting from *Poly I* hydrolysis, 1,4-butanediol and β -amino acids, were different from the starting materials, and the toxicity effect of both types of monomer pairs should be examined. Treatments were conducted

over both 5 hrs and 2 days to match exposure times previously used by Lynn *et al.* and our first series of assays, respectively. The resulting metabolic activity data is shown in Figure 3.2. Each “combined” test group in the plot means a combination of the two monomers at concentrations indicated in the two test groups immediately to the left.

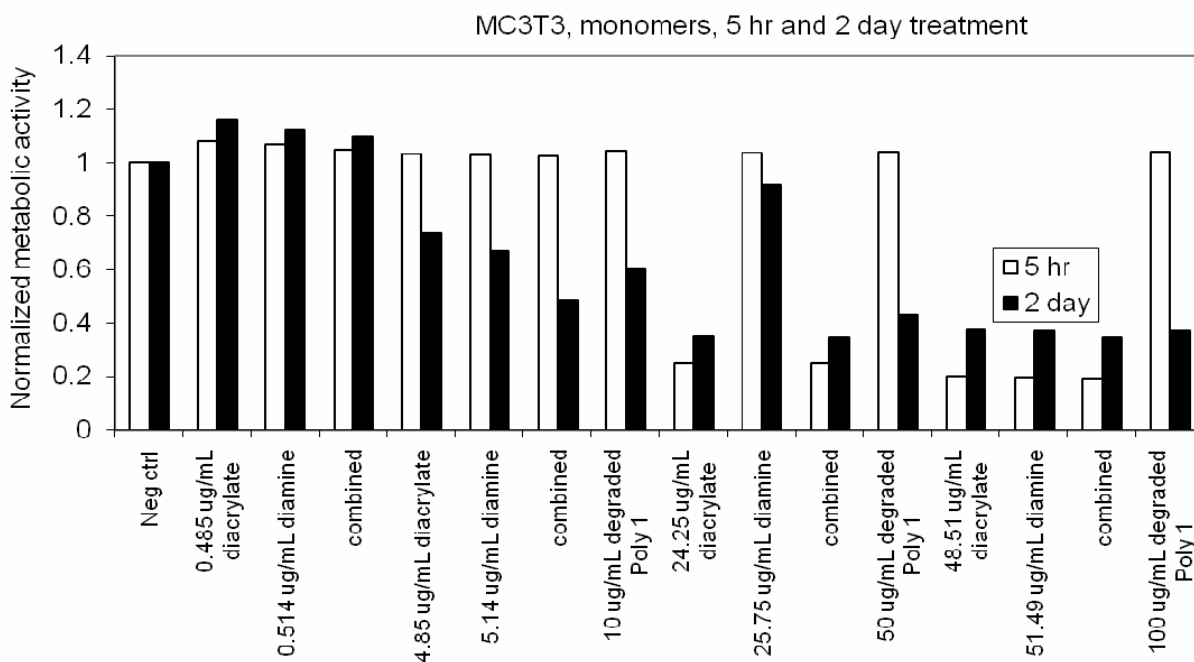


Figure 3.2 - Metabolic response of MC3T3 cells to various concentrations of diacrylate and diamine monomers of *Poly 1*.

Exposure times were 5 hrs or 2 days.

Figure 3.2 suggests several trends: (1) the monomers’ effect on MC3T3 could accumulate over days, (2) the diacrylate may be more toxic than the diamine, (3) a combined treatment of the two monomers tend to reflect the toxicity of the more toxic component, suggesting that there was no synergistic action between the two monomers, and (4) at equivalent concentrations, the starting monomers may be more toxic than the degradation products of *Poly 1*. Overall, the data support the hypothesis that residual monomers from

the synthesis could decrease observed biocompatibility of a *Poly I* sample. However, the residual amounts were not expected to be on the same order or magnitude as *Poly I* given the crystallization and wash procedures built into the synthesis process. Data from Figure 3.2 suggest that it would take almost a 1:1 molar ratio between the monomers and *Poly I* for the level of metabolic inhibition observed for the as-made *Poly I* in Figure 3.2. This seems somewhat unrealistic, so most likely there were other impurities within an as-made *Poly I* sample, possibly residual organic solvents. However, the identify and quantity of organic contaminants would be difficult to estimate, and hence no further assays were run to check on the identity and level of toxicity of these species.

“Fresh” vs. degraded *Poly I*. Given the findings thus far, double-purified *Poly I* was used for all subsequent assays to better clarify the toxicity of *Poly I* itself as opposed to other impurities. Also, as stated above, *Poly I* could be incorporated into an LbL film in a purer form due to its higher multivalency over oligomeric and monomeric contaminants. As a follow-up to the first series of assays represented in Figure 3.3, a new set was conducted at exposure times other than two days. A similar assay as Figure 3.3 was run, but with exposure times of 5 hours, 1 day, and 3 days. The results are shown in Figure 3.3. Note that not all concentrations were tested at all three exposure times. Due to material limitation at the time, the lower concentrations were administered for longer periods, while the higher range was administered for shorter periods.

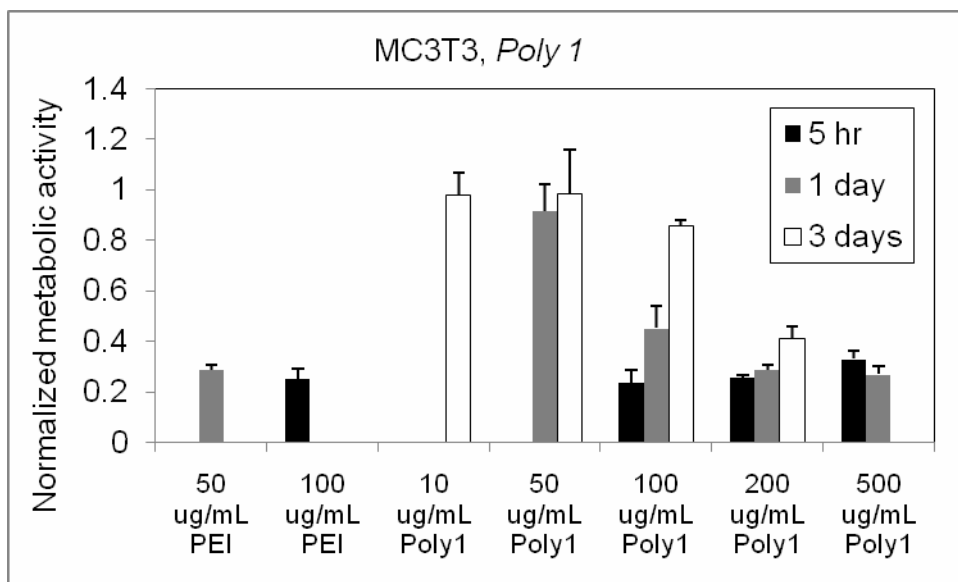


Figure 3.3 - Metabolic response of MC3T3 cells to *Poly 1* solutions after various exposure times.

Results in Figure 3.3 were rather puzzling – at several concentrations, *Poly 1* actually resulted in more metabolic arrest at shorter treatment times. 5-hr treatments were surprisingly toxic, with 100 $\mu\text{g/mL}$ *Poly 1* being essentially as toxic as an equivalent concentration of PEI. MC3T3 cells appeared to recover over the period of 1-3 days, suggesting that most of the detrimental impact of *Poly 1* was exerted within the first few hours. In addition, data in Figure 3.3 suggest that up to 100 $\mu\text{g/mL}$ of degraded *Poly 1* could be tolerated by MC3T3 over a 5-hr treatment. Hence, it appears that undegraded *Poly 1*, rather than the degradation products, accounted for most of the observed toxicity. The toxicity could arise from either the polycationic nature of undegraded *Poly 1* itself, or from the process of degradation. Many polycations have been found to be mildly toxic on mammalian cultures, so undegraded *Poly 1* could exert a similar polycation-derived toxicity effect. However, the toxicity could also arise from the chemistry of the degradation process. To further verify this observation, I treated MC3T3 with various

concentrations of either “fresh” or fully degraded *Poly 1*, for several exposure times.

Again, not all concentrations were represented under all exposure times due to

experimental constraints. The results are shown in Figure 3.4.

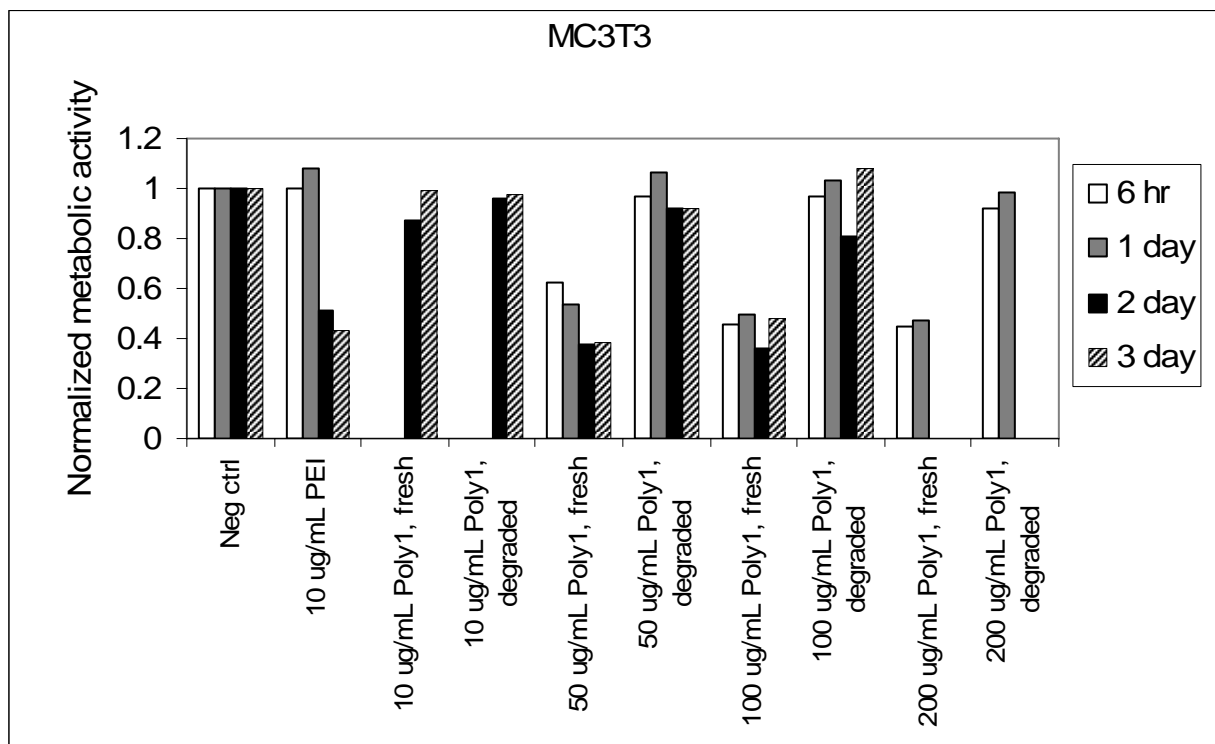


Figure 3.4 - Metabolic response of MC3T3 cells to "fresh" vs. "degraded" *Poly 1* solutions over various exposure times.

Poly 1 solutions were either freshly prepared right before exposure (“fresh”) or left to degrade overnight prior to use (“degraded”).

Data represented in Figure 3.4 very clearly show that fresh *Poly 1* was more toxic than degraded products when administered at equivalent concentrations. However, unlike previous observation made with Figure 3.3, the cells did not recover over time. Hence, while the hypothesis of higher toxicity of fresh *Poly 1* was well-supported, the ability of MC3T3 to “recover” was less certain.

Degradation process vs. polycationic effect. To additionally assess whether the degradation *process* or the polycationic nature of *Poly 1* that caused the toxicity, I examined treatment of MC3T3 by chitosan, a naturally occurring, non-degrading polycation, at several concentrations along with fresh and degraded *Poly 1*. Several degraded *Poly 6* solutions were run along with this assay to check for any differences in toxicity between the two sets of degradation products. Results are shown in Figure 3.5.

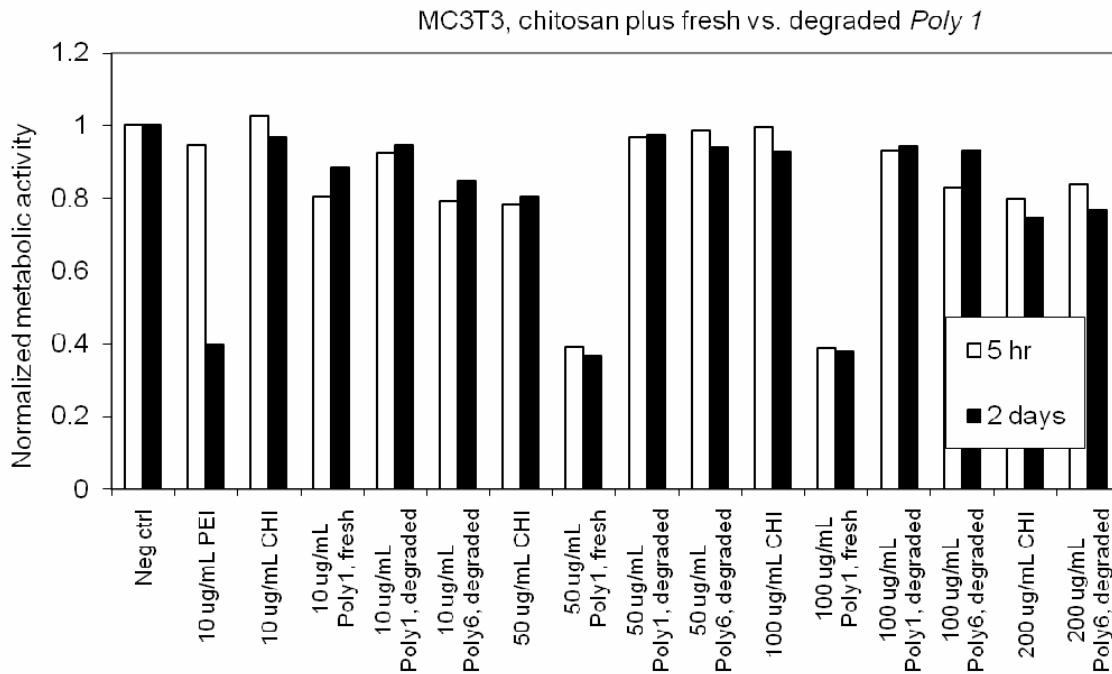


Figure 3.5 - Metabolic response of MC3T3 cells to chitosan solutions and fresh vs. degraded *Poly 1* solutions over various exposure times.

Chitosan treatments up to 200 µg/mL over 5 hours and 2 days appeared reasonably non-toxic, in stark contrast to fresh *Poly 1* solutions at equivalent concentrations and treatment times. Hence, it appears that the polycationicity alone did not account for the

level of toxicity observed. Degradation products of *Poly 1* and *Poly 6* appeared equal in their nontoxicity over the 5-hour to 2-day exposures.

The observation of fresh *Poly 1* being more toxic than its degraded counterpart was certainly intriguing, so additionally assays were run to examine very short exposures to fresh *Poly 1* to capture the more intense degradation activities within the initial hours of solution preparation. MC3T3 was exposed to fresh *Poly 1* (dissolved for 30 min prior to administration) at various concentrations for 15 min, 45 min, 1.5 hrs, and 3 hrs. The resulting “toxicity kinetics” are plotted in Figure 3.6. PEI at 100 $\mu\text{g}/\text{mL}$ was used as a positive control.

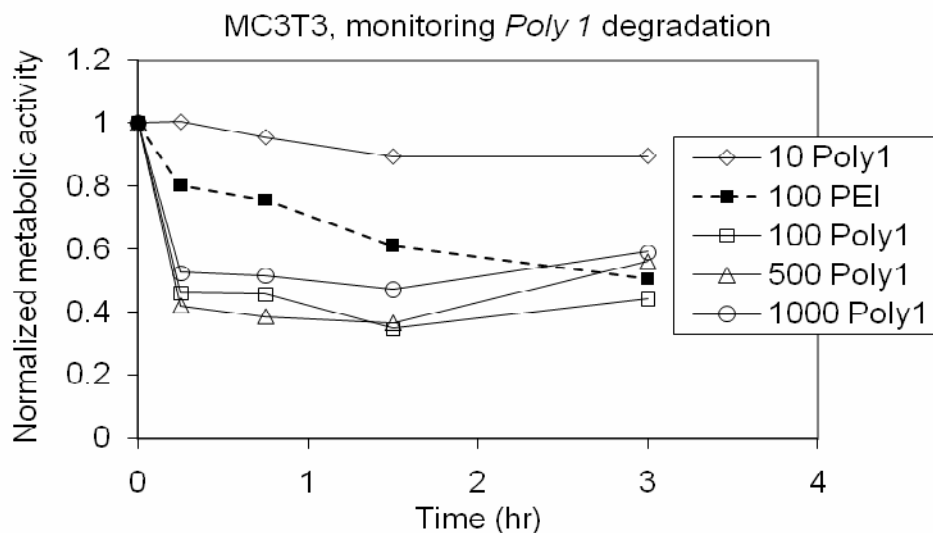


Figure 3.6 - Short-exposure monitoring of metabolic response of MC3T3 cells to freshly prepared *Poly 1* solutions.

Values indicated in the legend are in units of $\mu\text{g}/\text{mL}$.

Interestingly, a significant amount of the cytotoxic effect was found to occur within the first 15 min of fresh *Poly 1* treatment (but bearing in mind that the solution had been

stirred for 30 min prior to exposure). In some instances, MC3T3 appeared to begin recovering between 1.5 and 3 hours. PEI, on the other hand, had a more gradual and accumulating effect on the MC3T3 cultures. This set of data suggest that the degradation process, rather than the polycationicity, was detrimental to the MC3T3 cells.

Combing *Poly 1* with polysaccharides. After the degree and source of *Poly 1* toxicity were determined, a new set of assays were designed to examine the effect of combing fresh vs. degraded *Poly 1* with a polysaccharide in order to mimic the “cocktail” of polyelectrolyte components that a typical LbL drug delivery film would release. Heparin and dextran were chosen as the model polysaccharides. A fixed amount of 50 $\mu\text{g/mL}$ polysaccharide was administered to each culture, with variable concentrations of *Poly 1* in either fresh or degraded forms. The results are shown in Figure 3.7.

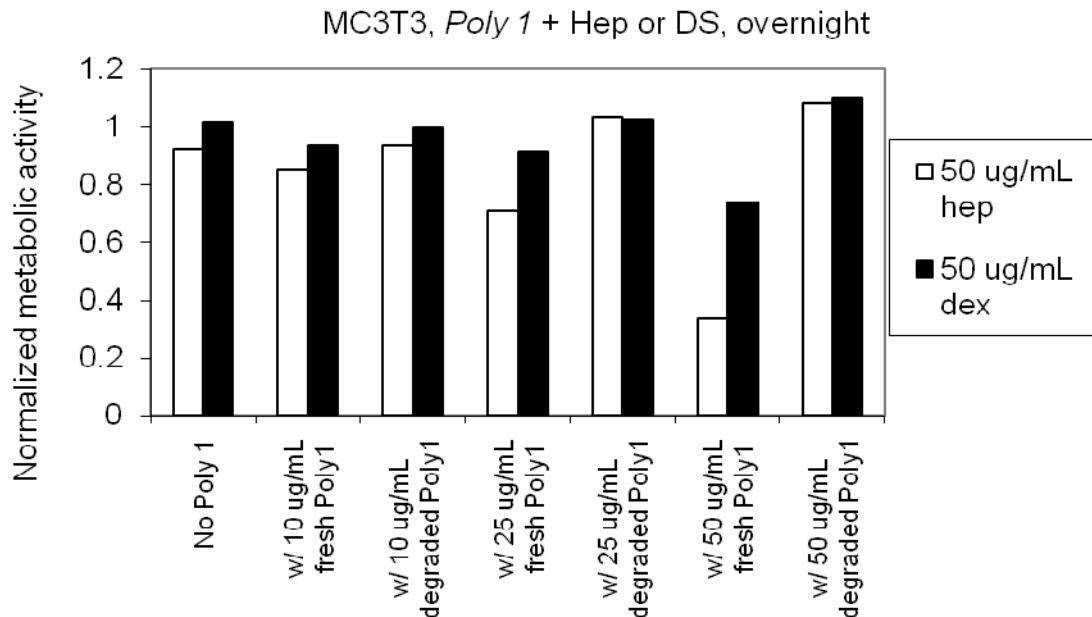


Figure 3.7 - Metabolic response of MC3T3 cells to various combinations of *Poly 1* with heparin or dextran, with overnight (18 hrs) exposure.

Not surprisingly, combination treatments involving fresh *Poly I* tended to be more toxic than those involving degraded *Poly I*. An additional observation was that combinations involving heparin were more toxic. This could be due to the higher toxicity of heparin itself, as demonstrated by the “No *Poly I*” test group. Whether the toxicity of fresh *Poly I* + heparin was accumulative or synergistic is unknown. Results from the 50 µg/mL test groups point out the fact that co-releases of *Poly I* with a polysaccharide at these concentrations or above may not be well-tolerated by mammalian cells. Although the results seen for MC3T3 may not generalize to other cell lines or *in vivo* environments, such findings should be taken into consideration when designing films that need to release a large amount of payload.

As subsequent thesis endeavors focused on $[(Poly\ I/HA)(GS/HA)]_n$ films (HA = hyaluronic acid and GS = gentamicin sulfate), one should consider how the biocompatibility assessments above would apply. Based on an assumed 1:1 charge ratio between *Poly I* and gentamicin within a $[(Poly\ I/HA)(GS/HA)]_n$ film, resulting in a 2.14:1.00 mass ratio between the two species, the observed 50 µg/mL toxicity limit for *Poly I* would mean that a gentamicin release above 23 µg/mL may result in some adverse side effect from *Poly I*. However, this is much higher than the MIC value for gentamicin against *Staphylococcus aureus* (0.1-1 µg/mL), so the gentamicin coatings do have a sufficient “operating margin”. Indeed, as to be seen in Chapter 5, up to at least 10 µg/mL release of gentamicin from $[(Poly\ I/HA)(GS/HA)]_n$ films was nontoxic towards MC3T3 and efficacious against *S. aureus* at the same time.

Cos-7 assessments. To assess the generality of the biocompatibility findings above, an identical series of assays was performed on Cos-7, a simian kidney cell line. The observed trends were very similar to those of MC3T3. For example, data in Figure 3.8 below suggest that Cos-7 was also more sensitive to fresh *Poly I* than to the fully degraded form. However, the normalized metabolic activities appeared lower than those of MC3T3 when compared at the same treatment concentrations and times.

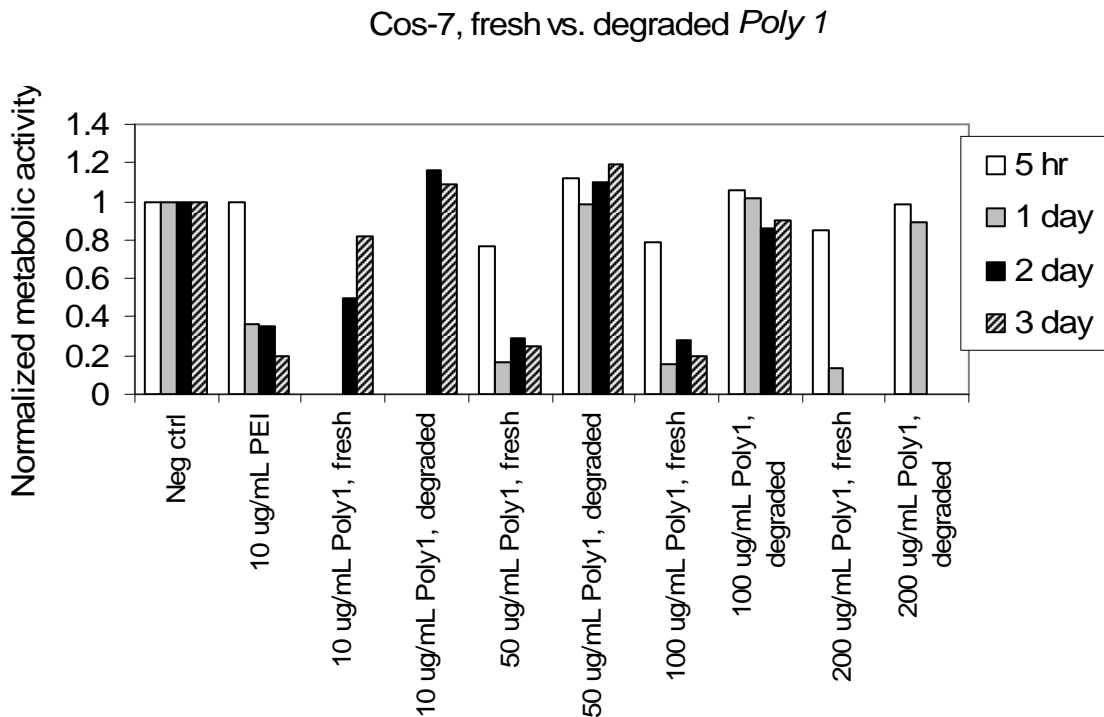
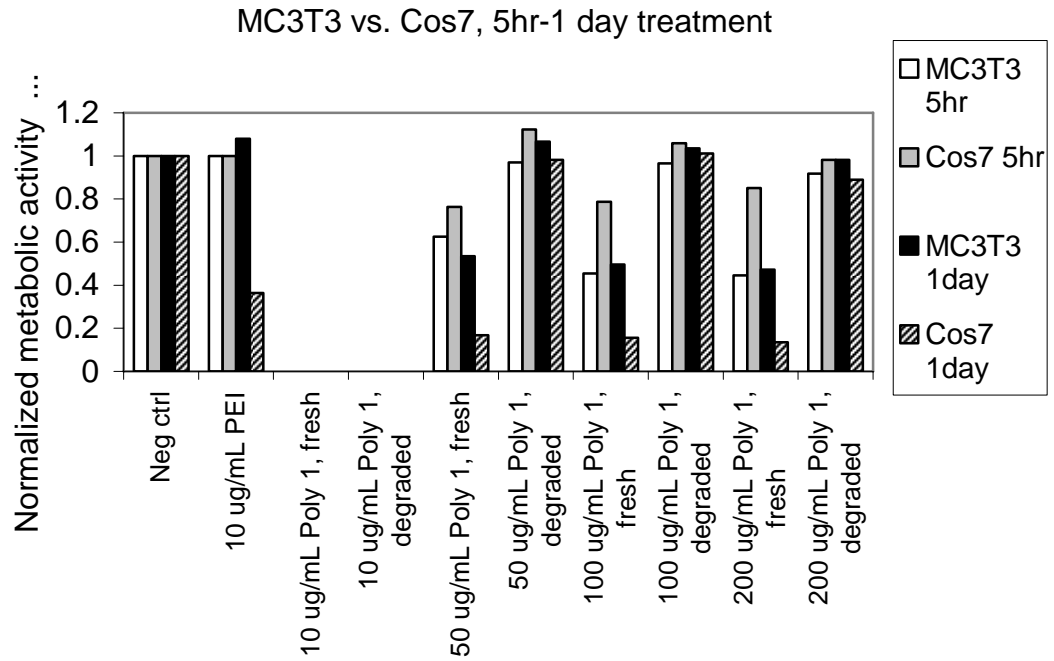


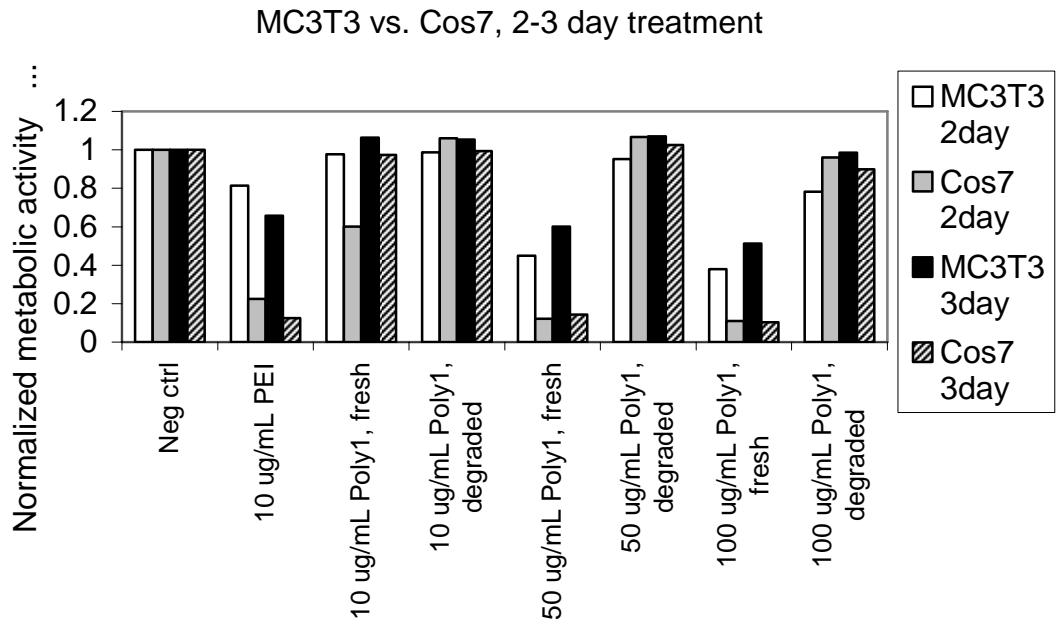
Figure 3.8 - Metabolic response of Cos-7 cells to fresh vs. degraded *Poly I* solutions over 5-hr to 3-day exposure times.

For better comparison of the differences in metabolic responses between MC3T3 vs. Cos-7, data from Figure 3.4 and Figure 3.8 are overlaid in Figure 3.9. For exposure times greater than 5 hours, Cos-7 had noticeably higher reduction in normalized metabolic activities under most treatment conditions, especially in the case of fresh *Poly I*.



(a)

Error!



(b)

Figure 3.9 - Comparison of metabolic responses of MC3T3 and Cos-7 cells to fresh vs. degraded *Poly 1*.

(a) 5hr and 1 day exposure times, (b) 2 and 3 day exposure times. Data taken from Figure 3.4 and Figure 3.8.

Cos-7's higher sensitivity to fresh *Poly I* was further revealed by the short-term response data as presented in Figure 3.10. Again, the largest drop in metabolic activity was observed within the first 15 min as was the case for MC3T3. However, Cos-7 was sensitive to fresh *Poly I* even at a low concentration of 10 $\mu\text{g/mL}$. For all *Poly I* concentrations, the normalized metabolic activities of Cos-7 cultures after 1-2 hours were approximately half of those of MC3T3. This finding could be explained by the fact that Cos-7 is a highly transfectable cell line, and in fact has been demonstrated by Lynn *et al.* to be efficiently transfected by a combination of *Poly X* and plasmids^{23, 111, 112, 162}. Cos-7's transfectability may very well be correlated to its sensitivity to *Poly I*. Assays with additional transfectable cell lines could further ascertain this hypothesis.

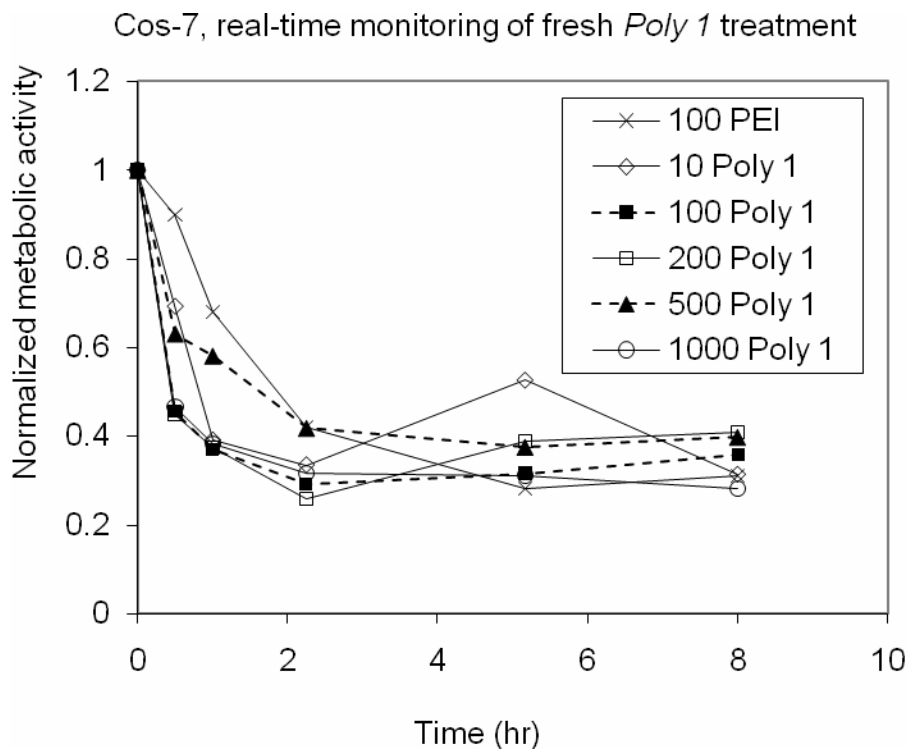


Figure 3.10 – Short-time monitoring of metabolic response of Cos-7 cells to freshly prepared *Poly 1* solutions.

3.4 Conclusion.

Biocompatibility of *Poly 1* towards MC3T3 and Cos-7 were assessed based on the cells' level of metabolic activity. Double-purified *Poly 1* was found to be less inhibitory than as-made *Poly 1*. While the identity of the impurities was not fully characterized, the two monomers used to synthesize *Poly 1*, especially the diacrylate, were found to be mildly toxic. However, monomers alone did not appear to account the observed level of toxicity, and other impurities such as residual organic solvent may be at play.

For a purified version of *Poly 1*, a freshly prepared solution was found to be much more toxic than a fully degraded one when administered at the same concentration. Further

assessments revealed that the degradation process, rather than the polycationicity of undegraded *Poly I*, was likely responsible for the observed toxicity. In fact, for both cell lines, most of the toxicity effect was observed within the initial 15 min of fresh *Poly I* exposure. The higher toxicity of fresh *Poly I* was observed when co-administered with polysaccharides as well. In particular, a combination with heparin was found to be more toxic than one with dextran.

Cos-7 was found to be more sensitive to *Poly I* treatments than MC3T3, especially in the cases of fresh *Poly I* exposures. This sensitivity may correlate with Cos-7's higher transfectability.

Acknowledgements.

I wish to thank my UROP Michelle Wilson for conducting some of the cell culture assays in this study. I would also like to thank Renee Smith and Mara Macdonald for providing *Poly X* in both as-made and double-purified forms. Many thanks also go to Naushad Hussein, a laboratory technician in the Langer group, for providing Cos-7 cells.

References.

- (1) Lynn, D. M. and Langer, R. *J. Am. Chem. Soc.*, **2000**, *122*, 10761-10768
- (2) Jewell, C. M., Zhang, J., Fredin, N. J. and Lynn, D. M. *Journal of Controlled Release*, **2005**, *106*, 214-223
- (3) Anderson, D. G., Lynn, D. M. and Langer, R. *Angewandte Chemie International Edition*, **2003**, *42*, 3153-3158
- (4) Zhang, J., Chua, L. S. and Lynn, D. M. *Langmuir*, **2004**, *20*, 8015-8021

Chapter 4. Incorporation of cyclodextrins for small molecule encapsulation

4.1 Introduction

Cyclodextrins are cyclic oligosaccharides that may include six (α), seven (β) (Figure 4.1), or eight (γ) glucose units. The ringed structure results in unique cup-like morphology with a polar exterior and a hydrophobic interior; this allows them to encapsulate small, hydrophobic molecules in an “inclusion complex” and allows for solubilization of these otherwise insoluble species. They have been used in pharmaceutical formulations since the 1950s because of their versatility and low toxicity¹⁶³.

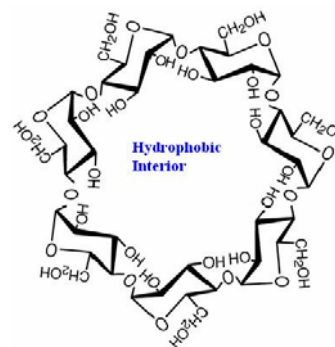


Figure 4.1 – Structure of unmodified β -cyclodextrin.

The exteriors of the cyclodextrin cups can be easily modified with various chemical groups for customized needs. Numerous chemical variants of cyclodextrins have been synthesized to optimize the complexation with small-molecule therapeutics such as the anti-inflammatories dexamethasone¹⁶⁴⁻¹⁶⁶ and piroxicam¹², several classes of antibiotics¹⁶⁷⁻¹⁷⁰, and anti-anxiety drug lorazepam¹⁷¹. In addition to functioning as a carrier, cyclodextrins may also enhance therapeutic effects^{168, 172} or reduce toxic side effects of drugs¹⁷³.

For layer-by-layer incorporation of drugs, the ability of cyclodextrins to convert a small, hydrophobic therapeutic into a charged or H-bonding species is a very promising feature. In fact, modified cyclodextrins have been used for multilayer incorporation of several drugs and model compounds^{12, 172, 174-178}, for both drug delivery and sensor applications. Two approaches were used: “pre-uptake” and “post-uptake” (Figure 4.2). The pre-uptake strategy involves formation of cyclodextrin-drug inclusion complexes followed by LbL deposition of the resulting complex, whereas the post-uptake strategy involves LbL buildup with empty cyclodextrins, followed by drug uptake by the cyclodextrin-loaded film. Benkirane-Jessel *et al.* used the pre-uptake method when they formed inclusion complexes of anti-inflammatory piroxicam with 6^A-toluenesulfonyl- β -cyclodextrin then bilayered the complex with poly(L-lysine) (PLL) either with or without poly(glutamic acid) (PGA)¹². The authors noted that uptake of the inclusion complex by a (PLL/PGA)_n film was not successful. On the other hand, Sato *et al.* reported uptake of methyl orange by a (PAH/sulfated α -cyclodextrin)_n film, but not by the sulfated β -cyclodextrin counterpart¹⁷⁸.

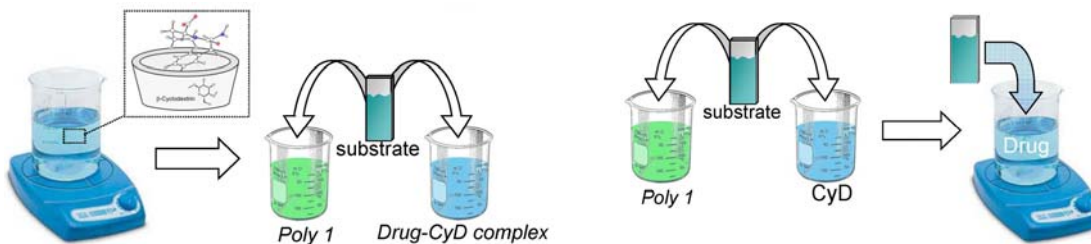


Figure 4.2 – Schematics of LbL drug incorporation methods via cyclodextrin inclusion complexes. (left) “pre-uptake” that involves LbL assembly of pre-formed inclusion complexes, (right) “post-uptake” which incorporates unloaded cyclodextrins into LbL films then uptakes drug with completed film.

As a proof-of-concept of drug incorporation via cyclodextrins, I sought anion-functionalized cyclodextrins that were available from commercial sources. Anion functionalization on the exterior would allow for direct deposition with *Poly X* as the complementary species. I decided to use sulfated versions of α - and β -cyclodextrins from Sigma, each with approximately 8 sulfate groups per cyclodextrin. As mentioned above, this sulfated variant of cyclodextrins has been successfully used by Sato *et al.* to incorporate dyes into LbL films.

In terms of drug candidates, I chose three small molecules of varying degrees of hydrophobicity (Figure 4.3): (1) dexamethasone, an anti-inflammatory that is hydrophobic, (2) gentamicin sulfate, an aminoglycosidic antibiotic that is hydrophilic and highly charged, and (3) ampicillin, a β -lactam antibiotic that is hydrophilic but less charged than gentamicin. These three variants should provide an initial understanding of how well sulfated cyclodextrins can facilitate small molecule incorporation with varying degrees of hydrophobic interaction and ionic cross-linking.

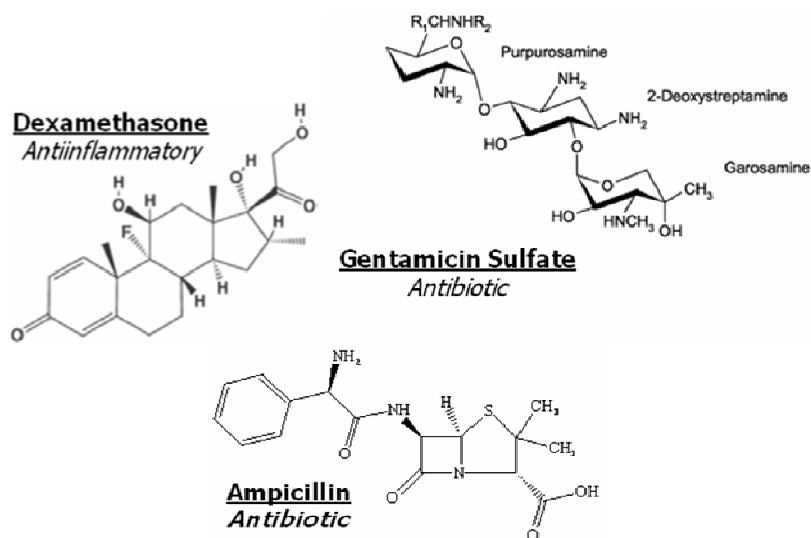


Figure 4.3 – Structures of the therapeutics used in this study.

While sulfated cyclodextrins were reported to form inclusion complexes with a dye like methyl orange (see Figure 4.4), other versions of cyclodextrins were used for the three proposed drugs. For example, 2-hydroxypropyl- β -cyclodextrin was most commonly used to include dexamethasone¹⁶⁴⁻¹⁶⁶. However, as proof-of-concept, I decided to use sulfated cyclodextrins for all three drug molecules to check on the degree of generality of this technique.

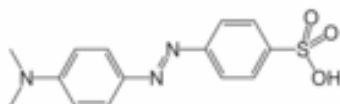


Figure 4.4 – Structure of methyl orange

4.2 Materials and Methods

Materials. Radiolabeled dexamethasone (3H-Dex) was ordered from American Radiolabeled Chemicals (St Louis, MO). Gentamicin sulfate and ampicillin were purchased from Mediatech (Manassas, VA). Sulfated α - and β -cyclodextrins were

purchased from Sigma Aldrich (St Louis, MO). IR-transparent silicon wafers were courtesy of Kevin Krogman. All other materials follow the same sources as outlined in Chapter 2.

Film construction. Standard layer-by-layer construction protocol was followed (see Chapter 2). Briefly, all dipping solutions were prepared in 0.1M sodium acetate at a concentration of 2 mg/mL unless otherwise noted. Each deposition cycle lasted for 10 min, with a cascade of three DI water rinses at 30, 45, and 60 seconds. All substrates were pre-deposited with a (LPEI/PSS)₁₀ base layer.

Pre-uptake method. Inclusion complexes were formed by stirring a solution of the 2 mg/mL cyclodextrin with molar balance of the drug in 0.1M sodium acetate buffer at room temperature. The stirring was allowed to proceed overnight or until the solution appeared completely clear. This solution was then used as the anion dipping solution the layer-by-layer assembly.

Post-uptake method. (Poly I/s-CyD)_n films were made using standard deposition conditions, in which the s-CyD species was deposited from a 0.1M sodium acetate solution at 2 mg/mL. For ampicillin and gentamicin, the cyclodextrin-loaded films were then soaked in a stirred solution of a drug at 10 mg/mL in 0.1M sodium acetate at pH 5.1 (natural pH of the acetate solution) and/or pH 3.5 under room temperature.

Dexamethasone uptake was performed in ethanol at 10 mg/mL and 0.1M sodium acetate without pH adjustment.

FTIR measurements. FTIR measurements of a thin film were performed by depositing the film on IR-transparent silicon, prepared in the same way as standard silicon substrates. Spectra were collected on a Nicolet Magna-IR® 550 Series II spectrophotometer, with accompanying OMNIC software version 6.1. All spectra were collected with at least 250 scans. A background of transparent silicon with (LPEI/PSS)₁₀ was subtracted from all images.

Drug release measurement. Standard scintillation protocol was used to measure the release of ³H-dexamethasone from thin films (see Chapters 2 and 5). Briefly, ³H-dex labeled films were immersed in 25 mL of pre-warmed PBS in a tightly-capped Falcon tube, maintained at 37°C in a water bath. A 1 mL sample was extracted at predetermined time points and analyzed by adding 5 mL of ScintiSafe Plus 50% (Fisher Scientific, Atlanta, GA) prior to measurement. The resulting mixtures were analyzed using a Tri-carb liquid scintillation counter (Model U2200). Raw data (disintegrations per minute, DPM) were converted to micrograms (μg) of dexamethasone using the conversion factor $2.2 \times 10^6 \text{ DPM} = 1 \text{ } \mu\text{Ci} = 1.0 \text{ } \mu\text{g } ^3\text{H-dex}$.

4.3 Results and Discussion

Growth of (*Poly I*/s-CyD)_n films. Direct bilayering between *Poly I* and both sulfated α- and β-cyclodextrins (denoted as s-α-CyD and s-β-CyD, respectively, or s-CyD for sulfated cyclodextrins in general) resulted in steady monotonic growths, as shown in Figure 4.5. Both cyclodextrins resulted in linear growths with *Poly I*, suggesting that the

cyclodextrins did not diffuse too freely. Interestingly, even though α - and β -cyclodextrins only differ by one glucose unit (six for α vs. seven for β), and both were reported by Sigma-Aldrich to have approximately 8 sulfate units per cyclodextrin, the growth rates between the two species were very different, with $(Poly\ I/s-\beta-CyD)_n$ growing about four times faster than the α counterpart. $S-\alpha-CyDs$ do have higher charge densities than $s-\beta-CyD$ given the same number of sulfate units at a lower molecular weight, and this could result in $(Poly\ I/s-\alpha-CyD)_n$ being more compact. It is also possible that $s-\alpha-CyD$'s smaller ring resulted in a more efficient “packing” into the multilayers.

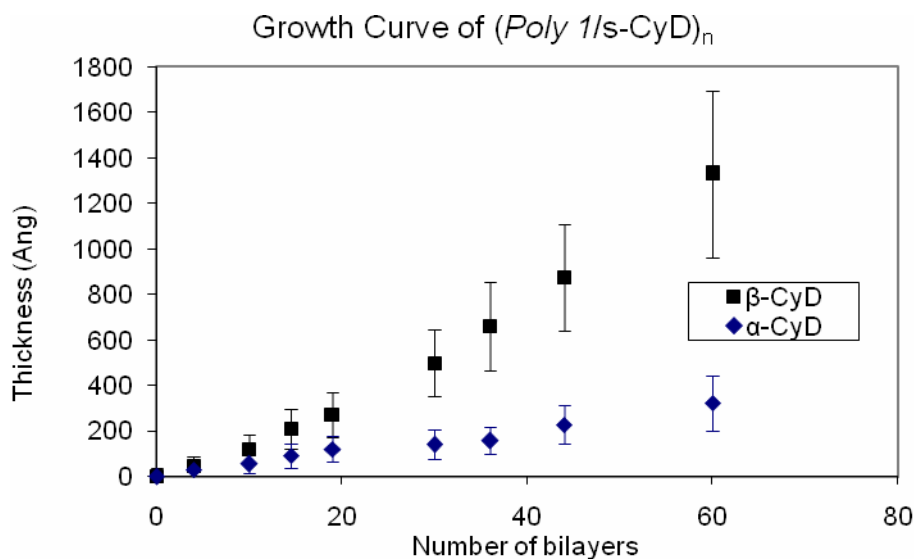


Figure 4.5 – Growth curve of $(Poly\ I/s-CyD)_n$ films.

Values represent averages of ellipsometer readings over multiple locations of a representative substrate, with error bars representing standard deviations from these readings. From SepOct05.

The growth curves suggest that the negatively functionalized cyclodextrins could be easily incorporated into an LbL film, despite their lack of polymeric structure.

The linearity of the growth curves was a promising suggestion that cyclodextrins

did not diffuse readily within these films, and hence could be useful for the design of multilayers for sequential release of small molecules. Erosion curves were not collected at this point, as I wanted to first verify the ability of these films to encapsulate and release small molecule drugs in a sustained fashion.

Since *(Poly I/s- α -CyD)_n* films were much thinner, their FTIR spectra also gave much weaker signals, making the results difficult to interpret. Coupled with the fact that β -CyD's were more commonly used in the reported literature, I decided to focus the data discussion on results from the *(Poly I/s- β -CyD)_n* films.

Ampicillin uptake. Figure 4.6 compares the FTIR spectra from a *(Poly I/s- β -CyD)₆₀* film (bottom spectrum) and a *(Poly I/[s- β -CyD.AmP])₆₀* films, where [s- β -CyD.drug] denotes the hypothetical inclusion complexes between s- β -CyD and a drug species that was assumed to have formed. While *(Poly I/[s- β -CyD.AmP])₆₀* gave a stronger signal, all the peaks match those of *(Poly I/s- β -CyD)₆₀* without any additional peaks indicative of ampicillin's presence. Hence, it appears that inclusion complexes did not form, but the presence of ampicillin in the s- β -CyD dipping solution altered the film construction in a way to promote thicker films.

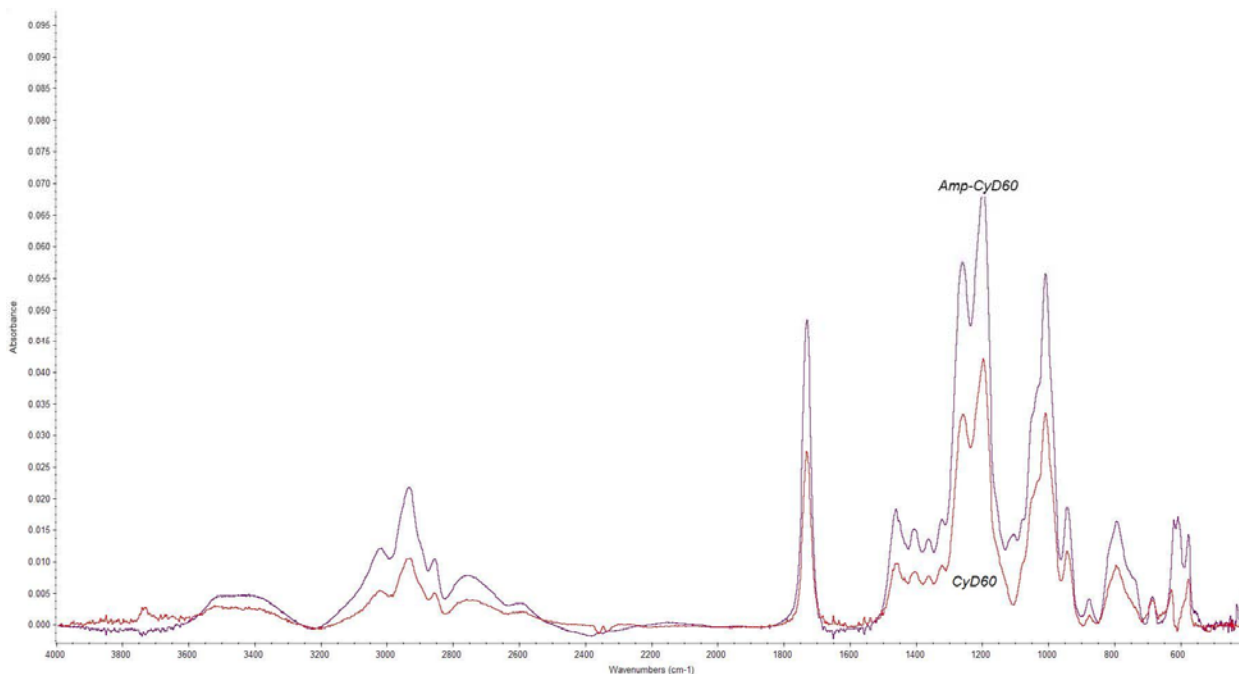
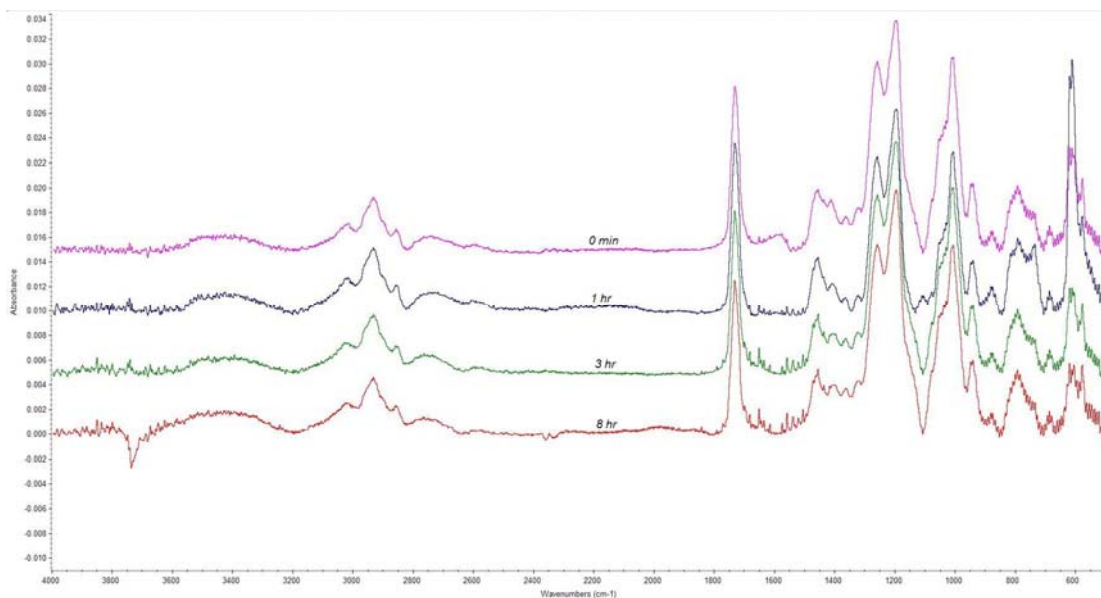


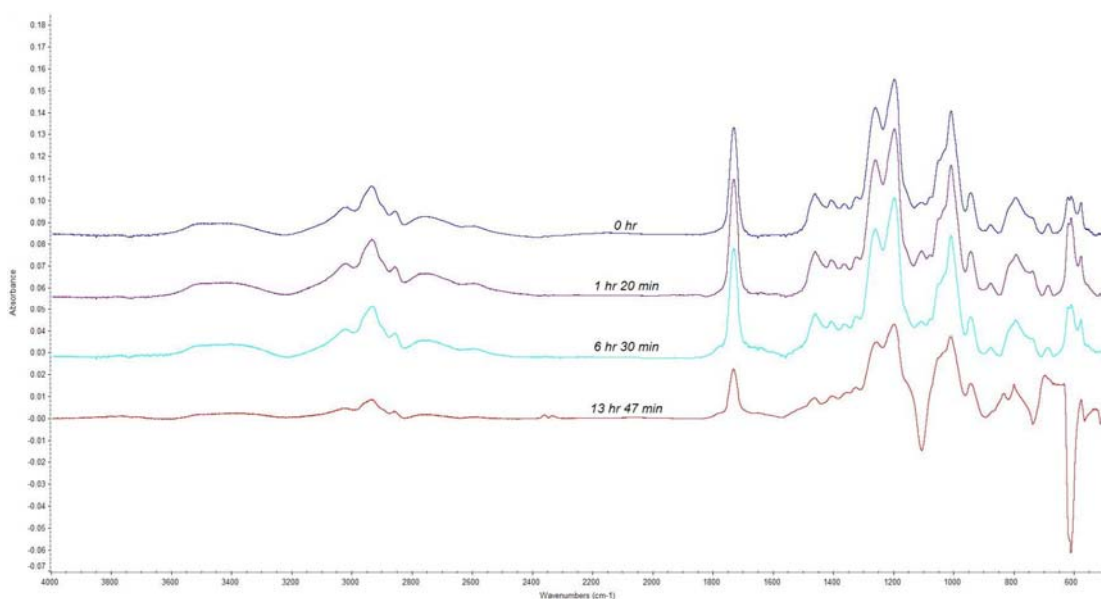
Figure 4.6 – Pre-uptake of AmP.

FTIR spectra of a $(Poly I/s-\beta-CyD)_{60}$ film (bottom spectrum) and a $(Poly I/[s-\beta-CyD.AmP])_{60}$ film (top spectrum).

Figure 4.7 shows uptake of ampicillin by $(Poly I/s-\beta-CyD)_{60}$ in 0.1M sodium acetate, either without pH adjustment (around 5.1, **a**), or pH adjusted to 3.5 by HCl (**b**). The experiments at the lower pH meant to check whether potential increase in protonation of ampicillin would aid its uptake.



(a)



(b)

Figure 4.7 –Post-uptake of ampicillin.

FTIR spectra of $(Poly I/s-\beta-CyD)_{60}$ film after noted amounts of immersion times in ampicillin solutions in 0.1M sodium acetate at (a) pH 5.1 (no adjustment), and (b) p 3.5 (adjusted by HCl).

At both pH 5.1 and 3.5 in the post uptake method, no noticeable spectra evolution occurred over the course of the multi-hour immersions. The consistency in the intensity of the peaks over time suggest that the $(Poly I/s-\beta-CyD)_{60}$ films did not

degrade appreciably over the examined time frame, except for the 14-hour immersion at pH 3.5. Overall, it appears that using s- β -CyD in an LbL film was not the best approach to encapsulating a polar uncharged species like ampicillin.

Dexamethasone uptake. Unlike ampicillin, dexamethasone (Dex, a non-steroidal anti-inflammatory drug, or NSAID) was hydrophobic and hence a more suitable candidate for cyclodextrin uptake. When dispersed in 0.1M sodium acetate, Dex created a cloudy solution that would not clear, suggesting its low solubility.

However, with 1:1 molar addition of s- β -CyD, the solution eventually cleared after 3-4 hours of stirring under room temperature. This was taken as a visual indication that Dex was solubilized by forming an inclusion complex with s- β -CyD, although the formation of these complexes was not verified by physicochemical means.

The hypothetical [s- β -CyD.Dex] solution was then bilayered with *Poly I*, and the resulting films were compared by FTIR with those made with pure s- β -CyD. The FTIR spectra of (*Poly I*/s- β -CyD)_n and (*Poly I*/[s- β -CyD.Dex])_n films are shown in Figure 4.8. A comparison between spectra of (*Poly I*/s- β -CyD)₁₀ and (*Poly I*/[s- β -CyD.Dex])₁₀ and those of (*Poly I*/s- β -CyD)₄₀ and (*Poly I*/[s- β -CyD.Dex])₃₆ did not reveal any significant difference, aside from an anomalous dip was seen around 600 cm⁻¹ and a small extra peak was seen for (*Poly I*/[s- β -CyD.Dex])₁₀ around 1100 cm⁻¹. Neither peak was characteristic of dexamethasone and could be instrumental artifacts. Despite visual observation that suggested inclusion complex formation, the resulting moiety did not appear to result in dexamethasone incorporation into

the film. Either empty α - β -CyD were favored over $[\alpha$ - β -CyD.Dex] complex during the deposition process, or dexamethasone might have “fallen out” of the cyclodextrin cups during deposition due to unknown competing forces. In either case, the pre-uptake strategy with the current methods did not assist with dexamethasone uptake.

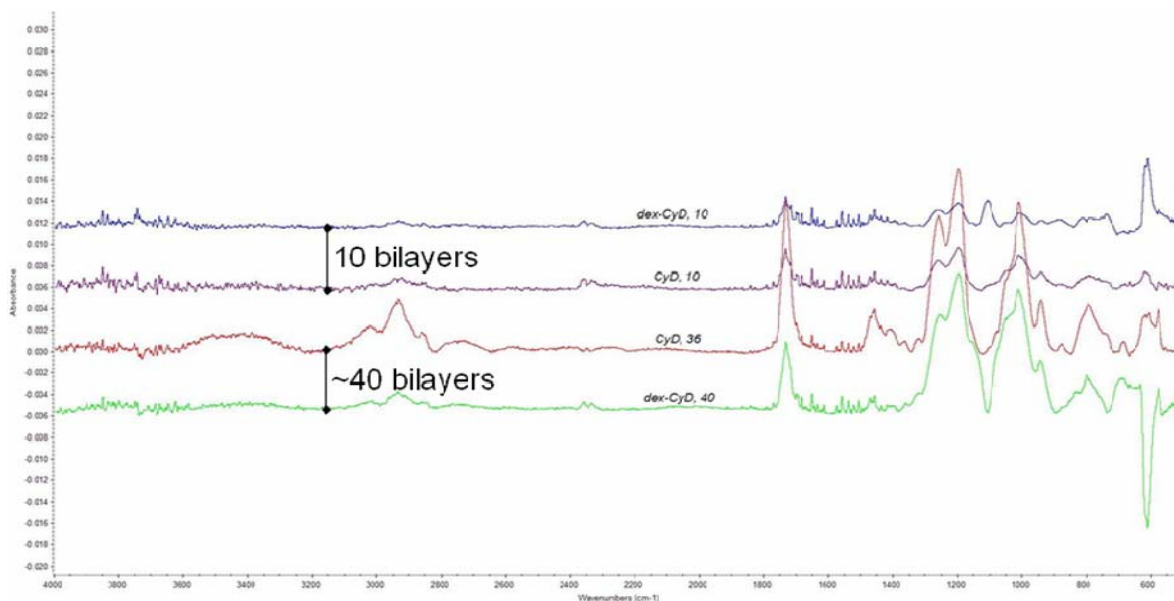


Figure 4.8 – Pre-uptake of Dexamethasone.

FTIR spectra of a $(Poly I/s-\beta-CyD)_{10,40}$ films and a $(Poly I/s-\beta-CyD.Dex)_{10,36}$ films. Each spectrum is identified on the graph itself.

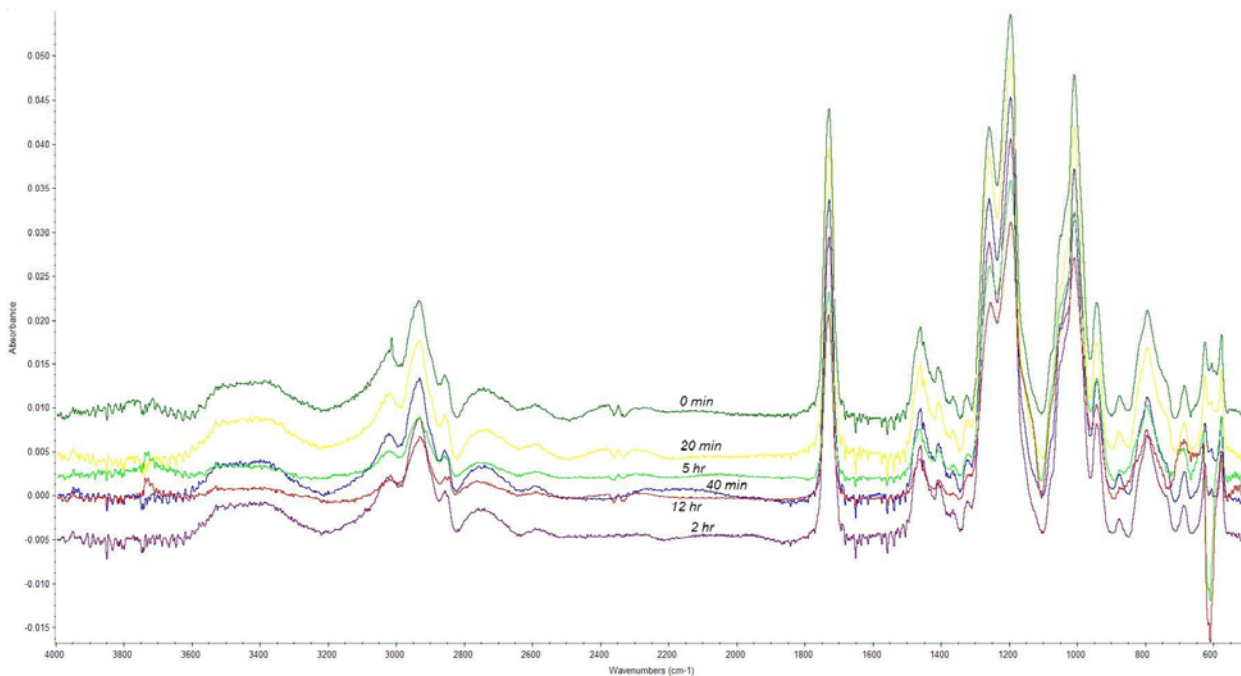
Similar to the pre-uptake method, the post-uptake strategy of immersing a $(Poly I/s-\beta-CyD)_{60}$ film in either ethanol or 0.1M sodium acetate did not yield definitive indication of dexamethasone uptake. (b)

Figure 4.9 (a) shows the FTIR spectra of a $(Poly I/s-\beta-CyD)_{60}$ film after various amounts of immersion time in an ethanol solution of dexamethasone at 10 mg/mL. Essentially no change in the spectra was observed over 12 hours of immersion.

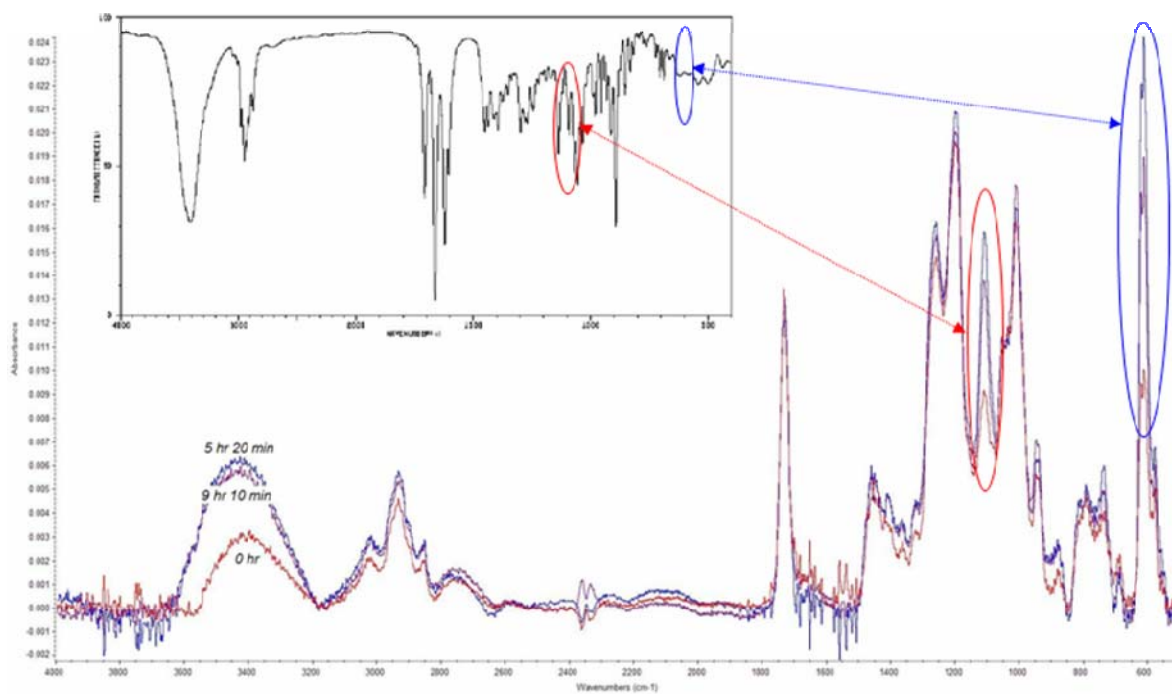
(b)

Figure 4.9 (b) shows the FTIR spectra of a $(Poly I/s-\beta-CyD)_{60}$ film after 0, 5 hr 20 min, and 9 hr 10 min immersions in a 0.1M sodium acetate solution of dexamethasone at 10

mg/mL. While dexamethasone was insoluble in 0.1M sodium acetate, the undissolved particles were continuously stirred to promote contact with film surface. Interestingly, I observed two distinct peak evolutions around 600 cm^{-1} and the other around 1100 cm^{-1} , corresponding to those found in the pre-uptake method that did not match any characteristic absorption of dexamethasone. This additional finding suggests that [s- β -CyD.Dex] might have signature bands at those wave numbers, but no verification of this hypothesis was done.



(a)



(b)

Figure 4.9 – Post-uptake of dexamethasone.

FTIR spectra of $(Poly\ 1/s-\beta-CyD)_{60}$ film after noted amounts of immersion times in dexamethasone solutions in (a) ethanol, (b) 0.1M sodium acetate, pH 5.1.

Since it was unclear whether dexamethasone was truly incorporated in the case of Figure 4.9 (b), I made $(Poly\ 1/s-\beta-CyD)_{60}$ with 6-hr uptake of 3H -Dex in 0.1M sodium acetate, then performed drug release assessment in PBS at 37°C. The resulting cumulative releases are shown in Figure 4.10. As suggested by the graphs, little to no dexamethasone was released over the time period investigated. The substrate appeared completely film-free after one day, but release was taken to as far as 5 days to verify the lack of dexamethasone release.

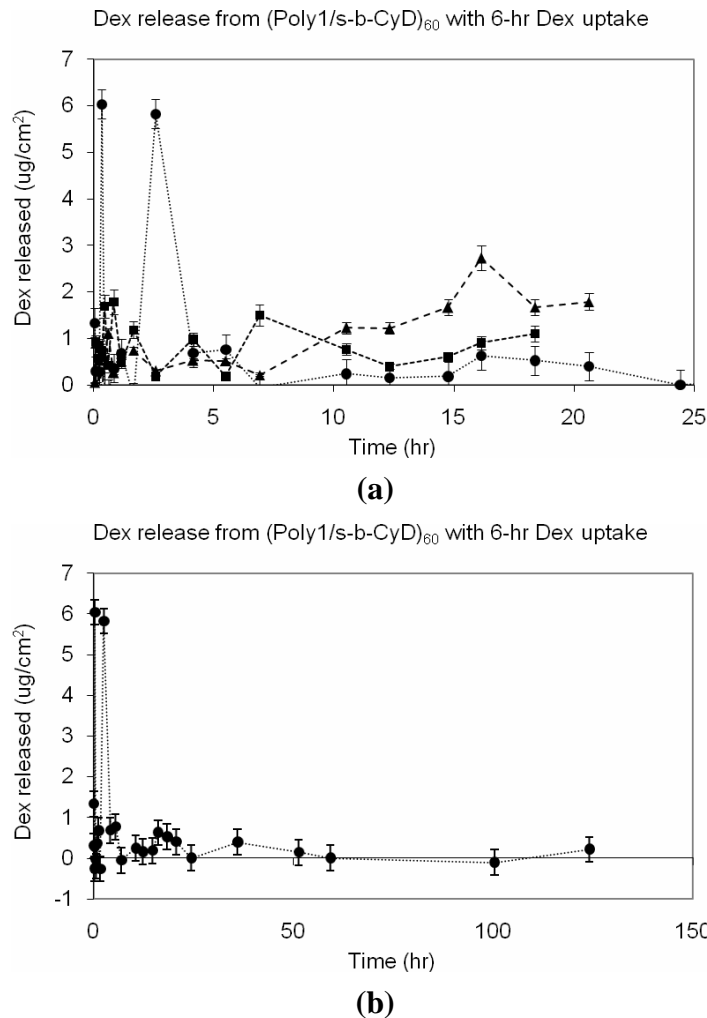


Figure 4.10 – Cumulative release of dexamethasone from $(Poly\ 1/s-\beta-CyD)_{60}$ after 9-hr uptake in ethanol. (a) data from three separate films over a release period of 25 hours, (b) one of the samples was extended to 120 hours to ascertain the lack of dexamethasone release. Error bars represent scintillation machine counting error.

Gentamicin uptake. In the case of gentamicin, no pre-uptake was attempted since gentamicin was highly charged and hence not expected to form inclusion complexes with cyclodextrins. However, it was tested in the post-uptake method as a comparison to ampicillin and dexamethasone. A $(Poly\ 1/s\text{-}\beta\text{-CyD})_{60}$ film was immersed in a 0.1M sodium acetate solution of gentamicin at 10 mg/mL with no pH adjustment (pH 5.1). FTIR spectra were collected at various amounts of time ranging from one to six hours (see Figure 4.11 (b)).

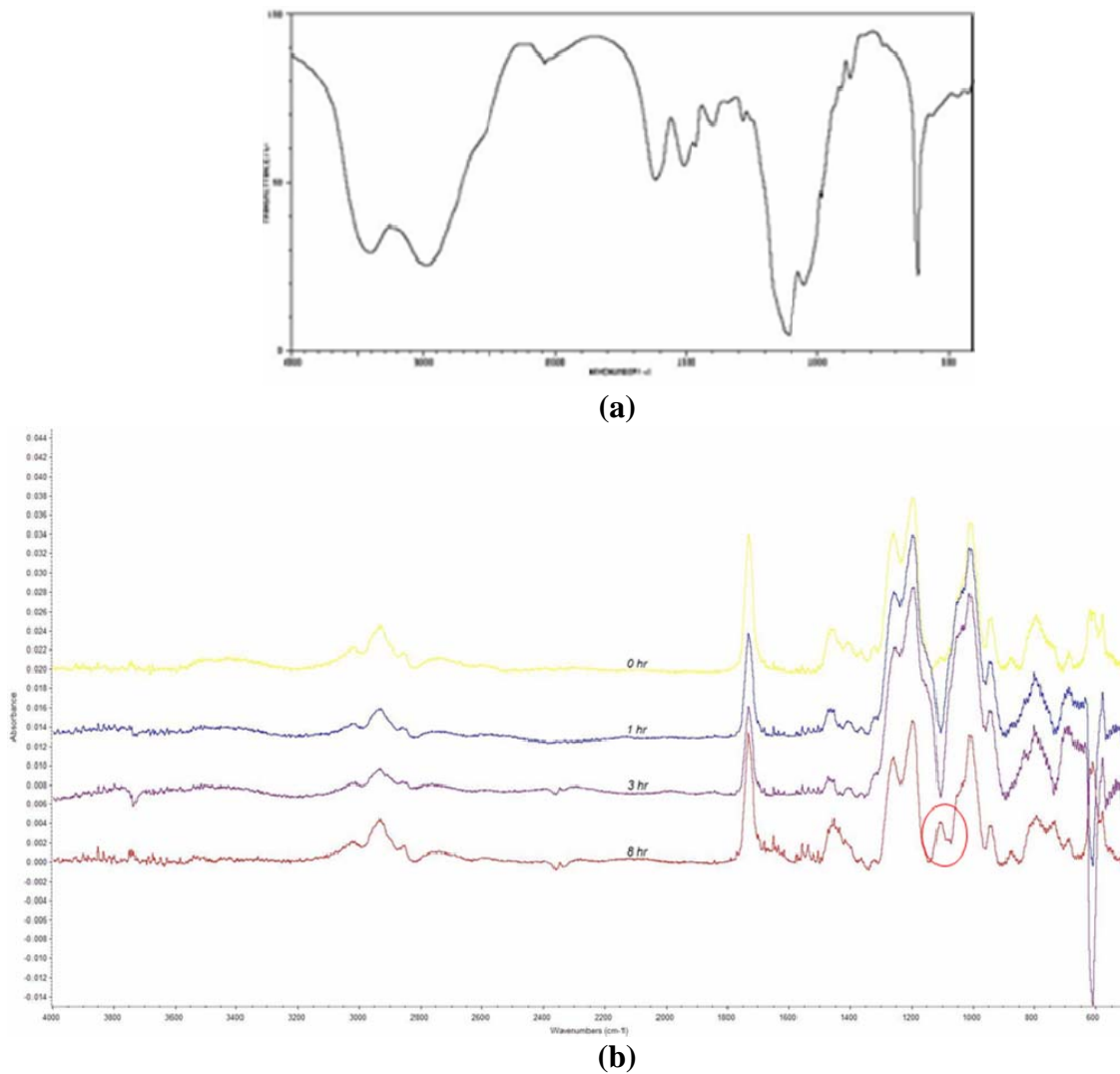


Figure 4.11 – Post-uptake of gentamicin. (a) FTIR spectrum of pure gentamicin, (b) FTIR spectra evolution for $(Poly\ 1/s\text{-}\beta\text{-CyD})_{60}$ immersed in 0.1M sodium acetate, pH 5.1 solution of gentamicin for different amounts of time.

A peak around 1100 cm^{-1} was seen to emerge after six hours of uptake. This absorption did correspond to a major peak in gentamicin's FTIR spectrum (see Figure 4.11 (a)) and suggested that gentamicin might have diffused into the film. Gentamicin uptake by the film was likely due to favorable electrostatic interactions with the sulfate groups of α - β -CyD. However, there was also the possibility that the peak was an artifact arising from a similar cause as that for dexamethasone's post-uptake. Gentamicin release was not assessed due to the unavailability of a labeled form at the time.

Subsequent experiments that directly incorporated gentamicin into an LbL assembly without any "helper" or pre-modification were successful. Gentamicin was deposited via the architecture $[(Poly\ X/PA)_a(gentamicin/PA)_b]_n$, where *Poly X* could be any member of the poly(β -amino ester) family, PA was a biocompatible polyanion, *e.g.* hyaluronic acid, alginic acid, or chondroitin sulfate, and (a, b, n) were independently adjustable parameters that could be used to tune film architecture. The construction and assessment of these LbL assemblies became a major portion of my thesis and will be elaborated in subsequent chapters.

4.4 Conclusion

Sulfated α - and β -cyclodextrins were successfully bilayered with *Poly I* with linear growth curves. However, under the conditions investigated, these molecules did not support incorporation of several small molecule drug candidates: dexamethasone, a hydrophobic anti-inflammatory drug, ampicillin, a polar but uncharged antibiotic, and gentamicin, a highly charged antibiotic.

The preliminary findings reported here do not necessarily discourage further experimentation with cyclodextrins, as there were many limitations to the present study: (1) the chemistry of the cyclodextrins, *i.e.* sulfation, was not necessarily optimized for the model drugs, (2) the uptake conditions, in both the pre- and post-uptake methods, were not necessarily optimized in terms of solvent choice, ionic strength, temperature, *etc.*, and (3) the detection method, *i.e.* FTIR, might not be sufficiently sensitive and might produce artifacts. Improvements to the above include (1) using cyclodextrins of a specific chemistry that has been reported to form inclusion complexes within a given drug or a close structural analog thereof, *e.g.* 2-hydroxypropyl- β -cyclodextrin for dexamethasone¹⁶⁴⁻¹⁶⁶, (2) optimizing solvents conditions, *e.g.* ones with less favorable interaction with the drug molecule to encourage its inclusion by cyclodextrins. This optimization should be done for both pre- and post-uptake methods, and (3) considering alternative detection methods such as UV-vis, fluorescence, *etc.* to complement FTIR measurements. In addition, polymerized cyclodextrins are promising alternatives to individual cyclodextrin molecules, as their polymeric character is expected to result in more stable film constructs. In fact, studies are underway by Renee Smith for the LbL incorporation of dexamethasone using Captisol® (sulfobutyl ether β -cyclodextrin) and other cyclodextrin-based polymers for ophthalmic drug delivery, and additional drug candidates such as paclitaxel are also under consideration.

Acknowledgements.

I would like to thank Nicole Zacharia for her consultation on the FTIR measurements, and Kevin Krogman for providing IR-transparent silicon wafers.

References.

- (1) Heidel, J. D. *Expert Opinion in Drug Delivery*, **2006**, *3*, 641-646
- (2) Gavrilin, M. V., Kompantseva, Y. V. and Ushakova, L. S. *Khimiko-Farmatsevticheskii Zhurnal*, **1994**, *28*, 44-46
- (3) Gavrilin, M. V., Kompantseva, E. V., Gusova, B. A., Ushakova, L. S., Makarov, V. A. and Karpenya, L. I. *Pharmaceutical Chemistry Journal*, **1999**, *33*, 45-48
- (4) Usayapant, A., Karara, A. H. and Narurkar, M. M. *Pharmaceutical Research*, **1991**, *8*, 1495-1499
- (5) Benkirane-Jessel, N., Schwinte, P., Falvey, P., Darcy, R., Haikel, Y., Schaaf, P., Voegel, J.-C. and Ogier, J. *Advanced Functional Materials*, **2004**, *14*, 174-182
- (6) Blanchemain, N., Haulon, S., Martel, B., Traisnel, M., Morcellet, M. and Hildebrand, H. F. *European Journal of Vascular and Endovascular Surgery*, **2005**, *29*, 628-632
- (7) Dhanaraju, M. D., Kumaran, K. S., Baskaran, T. and Moorthy, M. S. R. *Drug Development and Industrial Pharmacy*, **1998**, *24*, 583-587
- (8) G., A., S., M., E., L.-C., T., T. and E., A.-V. *Journal of Pharmacy and Pharmacology*, **2003**, *55*, 291-300
- (9) Domingues, Z. R., Cortes, M. E., Gomes, T. A., Diniz, H. F., Freitas, C. S., Gomes, J. B., Faria, A. M. C. and Sinisterra, R. D. *Biomaterials*, **2004**, *25*, 327-333
- (10) Sanghavi, N. M., Choudhari, K. B., Matharu, R. S. and Viswanathan, L. *Drug Development and Industrial Pharmacy*, **1993**, *19*, 701-712
- (11) Jessel, N., Oulad-Abdelghani, M., Meyer, F., Lavalle, P., Haikel, Y., Schaaf, P. and Voegel, J. C. *PNAS*, **2006**, *103*, 8618-8621
- (12) Uekama, K., Shiotami, K., Irie, T., Ishimaru, Y. and Pitha, J. *Journal of Pharmacy and Pharmacology*, **1993**, *45*, 745-747
- (13) Suzuki, I., Sato, K., Koga, M., Chen, Q. and Anzai, J.-i. *Materials Science and Engineering: C*, **2003**, *23*, 579-583
- (14) Yang, X., Johnson, S., Shi, J., Holesinger, T. and Swanson, B. *Sensors and Actuators B: Chemical*, **1997**, *45*, 87-92

- (15) Yang, X., Shi, J., Johnson, S. and Swanson, B. *Sensors and Actuators B: Chemical*, **1997**, *45*, 79-84
- (16) Yang, Y., Yang, X., Liu, Y.-L., Liu, Z.-M., Yang, H.-F., Shen, G.-L. and Yu, R.-Q. *Journal of Photochemistry and Photobiology A: Chemistry*, **2005**, *171*, 137-144
- (17) Sato, K., Suzuki, I. and Anzai, J.-i. *Langmuir*, **2003**, *19*, 7406-7412

Chapter 5. Polyelectrolyte multilayers for tunable release of antibiotics

5.1 Fabrication and characterization

Reproduced in part with permission from “Polyelectrolyte Multilayers for Tunable Release of Antibiotics” by Helen F. Chuang, Renee C. Smith, and Paula T. Hammod. *Biomacromolecules*, 9 (6), 1660–1668, 2008. 10.1021/bm800185h, © 2008 American Chemical Society.

5.1.1 Introduction

Many implanted biomedical devices suffer from infections that develop post-surgically on the device surface, which not only cause device failure but could also spread systemically¹²¹. This problem is critical and escalating, and it should be either prevented prophylactically or eradicated remedially. Of particular urgency are infections of orthopedic implants, which require that the patient undergo two or more additional surgeries with multi-week gaps in between, during which time the patient is left immobile¹⁷⁹. Such revisions are costly and inconvenient, and remedial implant products are yet to be developed.

Most of the antimicrobial orthopedic implant coatings under development, such as dip coating of hydroxyapatite¹²² or collagen¹²³, direct incorporation of antibiotics into glass implants¹²⁴, bone cement¹²⁵, PLGA-based coatings¹²⁶, or nitric oxide-releasing sol-gel coatings¹²⁷, cannot be easily tuned with regard to drug dosage or release rate. In some cases, residual foreign materials are left behind, which may induce long-term immunogenic responses. A biodegradable coating that can be

tuned to deliver the desired dosage of drugs over a specified amount of time, while leaving no residual material on the implant surface, would address both problems. Such an antimicrobial coating would also be applicable towards other implanted devices such as dental implants¹²⁸, catheters^{129, 130}, shunts¹³¹, and guide wires¹³².

As bacteria can be introduced either during the surgical process onto the implant surface or post-surgically from the patient's blood, an antimicrobial coating should both discourage bacteria attachment and impose antimicrobial action on the tissues and fluids immediately surrounding the implant. Such a dual action would effectively prevent biofilm formation, the major source of implant surface infection^{129, 130, 133-136}. Due to the widely differing timescales and severities in device infections that range from rapid acute infections to longer term chronic modes¹³⁶⁻¹³⁸, antimicrobial coatings with adjustable dosages and release rates are needed. Therefore, a coating with controls over both parameters would be highly desirable. Hence, we seek to develop an antimicrobial coating that can both discourage bacteria attachment to the implant surface and be able to release antibiotics into the surrounding tissues at a tunable dosage and rate. This can be achieved through a biodegradable coating that controllably sheds from its surface to release antibiotics. Specifically, we wish to construct a hydrolytically degradable thin film via the layer-by-layer (LbL) deposition technique encapsulating gentamicin, an antibiotic commonly used to treat device infections^{121, 139-141}.

LbL deposition is a nanoscale polymer thin film technique that can be applied to virtually any surface material of any size and geometry. The technique is based on the alternating deposition of polyelectrolytes or other multiply charged species⁵². LbL deposition results in multilayered films that are ultrathin, conformal, and highly tunable in both morphology and functionality. In addition, the fabrication process is simple, low-cost, scalable, and mild, as it only involves aqueous solutions at room temperature near physiological pH. In contrast to the harsh organic conditions often used in making polymeric drug depots¹⁸⁰, the mild aqueous environment of the LbL process is a distinct feature that proves especially beneficial for sensitive biologic drugs such as proteins, antibodies, nucleic acids, and peptides. Such coatings can be used to release a wide range of active substances including therapeutic agents. LbL coatings have been successfully applied to a variety of device surfaces, including stainless steel stents¹¹⁸, NiTi disks and wires for stent application¹⁰³, polyurethane vascular prostheses and polystyrene plates¹⁵⁹, silica capillary tubing¹⁸¹, and PMMA-based dental material¹⁸². Because of its numerous advantages, LbL-based films have been studied extensively as therapeutic coatings^{17, 25, 27, 73, 99, 101, 103, 110-112, 118-120, 172, 183-186}. Non-degradable LbL films can be used to improve device biocompatibility^{101, 103, 185} and impart surface bioactivity^{73, 103}, while decomposable LbL films, such as salt-induced degradation of LbL hollow capsules¹⁷, have been investigated for drug delivery. Other forms of LbL-based systems for drug release include pH-induced deconstruction of hydrogen-bonded LbL films²⁵, and pH-induced swelling of LbL films to release drugs^{27, 99}.

Despite the variety in mechanisms of therapeutic action, the controlled release of drugs under physiological conditions with tunable dosage remains a challenge. We have demonstrated controlled erosion¹¹⁰ and tunable drug release¹¹⁹ in physiological buffers from LbL films made with poly(β -amino esters)²³. These films are degraded via a hydrolytic mechanism that enables continuous elution of drugs without the need of enzymic or cellular interaction. Furthermore, we have demonstrated the sequential release of two model drugs, in which the release of the second agent was delayed by 20 hours¹²⁰. This approach has also been used to deliver DNA, with high transfection efficiency^{111, 112}.

While LbL systems incorporating antimicrobial agents, such as cetrimide and silver¹⁴²⁻¹⁴⁴, have been developed, there is significant concern over the toxicity of some of these agents¹⁴⁵. These agents may also be ineffective against bacterial colonization of orthopedic implants¹⁴⁶. In this paper we will demonstrate gentamicin-eluting coatings fabricated from LbL deposition that are efficacious against *S. aureus* and biocompatible towards osteoblasts. Gentamicin is an aminoglycoside antibiotic commonly used to treat osteomyelitis. Although most effective against gram-negative bacteria, gentamicin is also efficacious against certain gram-positive species such as *Staphylococcus aureus*, the most common source of osteomyelitis^{187, 188} and septic arthritis^{189, 190}. The efficacy of gentamicin against *S. aureus* has been demonstrated both *in vitro*^{191, 192} and *in vivo*^{141, 193, 194}, and antibacterial coatings on orthopedic implants based on

gentamicin have been reported ^{126, 139}. Gentamicin is also effective against methicillin-resistant *S. aureus* (MRSA)¹⁹⁵ and biofilms of several *staphylococci*¹⁹⁶. However, none of the previous gentamicin coatings allow for precise dosage or release rate tuning.

One potential difficulty in incorporating gentamicin into an LbL film is its non-polymeric character, since stable LbL film formation is generally favored by polymeric or nanoparticulate constituents with multiple sites for electrostatic interactions. Previously reported LbL films that incorporate small molecules needed pre-modifications such as prodrug formation ¹⁹⁷, pre-encapsulation ¹⁸³, and treatment with solubilizing compounds ¹⁹⁸. However, through proper film architecture design, we were able to incorporate gentamicin into LbL films without any pre-modification, rendering the film construction simple and efficient. Encapsulated dosage can be easily and precisely tuned by the number of deposited layers. These films can be applied to any biomedical device surface to impart tunable levels of antibacterial action. An added advantage is that the biodegradability of these coatings may offer further protection against bacterial adhesion, as the top-down erosion of the film naturally prevents bacterial attachment to the surface. This approach could represent a generalized strategy for incorporating charged small molecules into LbL films, expanding the range of functionality for these versatile thin films.

5.1.2 Materials and Methods

Materials. Poly(β -amino esters) (referred to as *Poly X*, $X = 1, 2$, and $6A$, see Figure 5.2) were synthesized as previously described²³. Silicon wafers (test grade n-type) were purchased from Silicon Quest (Santa Clara, CA). Linear poly(ethylenimine) (LPEI, $M_n = 25k$) was received from Polysciences, Inc. Poly(sodium 4-styrenesulfonate) (PSS, $M_n = 1M$) and sodium alginate (or alginic acid) were purchased from Sigma-Aldrich (St. Louis, MO). Sodium hyaluronate (or hyaluronic acid (HA), $M_n = 1.76$ MDa) was purchased from Lifecore Biomedical, Inc. (Chaska, MN). Nonradiolabeled gentamicin sulfate (GS) (in Cellgro® solution, 50 mg/mL in sterile filtered water) was purchased from Mediatech, Inc. (Herndon, VA). 3H -gentamicin sulfate was obtained from American Radiolabeled Chemicals, Inc (0.250 mCi total, 1 mCi/mL in ethanol, 0.200 mCi/mg). All materials and solvents were used as received without further purification. *Staphylococcus aureus*, strain 25923 with no antibiotic resistance, was provided by the Gregory Stephanopoulos group at MIT and ordered from ATCC (Manassas, VA). Cation-adjusted Mueller Hinton Broth II (CMHB) and BactoAgar™ were purchased from Difco™ (BD, Franklin Lakes, NJ). Gentamicin standard discs, 10 μ g loading, were purchased from BD Biosciences (Franklin Lake, NJ) as BBL™ Sensi-Disc™. MC3T3-E1 Subclone 4 CRL-2593 was obtained from ATCC (Manassas, VA). Minimum essential medium alpha medium, all media supplements, and alamarBlue™ (BioSource™) were obtained from Invitrogen (Carlsbad, CA).

Preparation of Polyelectrolyte Solutions. Dipping solutions containing *Poly X* and HA were made at a concentration of 10 mM with respect to the polymer repeat unit in 100 mM sodium acetate buffer (pH 5.1 by glacial acetic acid). GS dipping solutions were prepared by diluting the 50 mg/mL stock solution with sodium acetate buffer and glacial acetic acid to result in a solution of 10 mg/mL GS in 100 mM sodium acetate at pH 3.0. Nondegradable base layers were deposited from dipping solutions of LPEI and PSS in deionized water pH adjusted to 4.25 and 4.75, respectively. Deionized water used to prepare all solutions was obtained using a Milli-Q Plus (Bedford, MA) at 18.2 M Ω .

Polyelectrolyte Deposition. All polyelectrolyte LBL thin films were constructed as follows according to the alternate dipping method⁵³. Silicon wafers were cut into rectangular substrates approximately 2.0 cm \times 0.5cm each. The substrates were rinsed with methanol and deionized water, dried under nitrogen, and plasma etched in oxygen using a Harrick PDC-32G plasma cleaner at high RF power for 1 min. Layer-by-layer thin film deposition was performed using a Carl Zeiss HMS Series Programmable Slide Stainer. A nondegradable base film ((LPEI/PSS)₁₀) was deposited by submerging plasma treated silicon substrates in an LPEI dipping solution for 5 minutes, then a cascade rinse cycle consisting of three deionized water rinsing baths (15, 30, and 45 seconds, respectively). Substrates were then submerged in a PSS dipping solution for 5 minutes followed by the same cascade rinsing cycle, and the entire process was repeated ten times. Next, degradable films were deposited on the existing polyanion-terminated base

layer by repeating the above procedure with the $[(Poly\ X/HA)_a(GS/HA)_b]_n$ architecture, dipping for 10 min in each of the *Poly X*, HA, and GS solutions and repeating the $(Poly\ X/HA)_a(GS/HA)_b$ structure as many times (n) as desired. For films intended for drug release assessment, a 3H -labeled GS dipping solution was prepared by dissolving 0.060 mL of the stock (1 mCi/mL in ethanol, 0.200 mCi/mg) in 40 mL of a typical GS dipping solution (10 mg/mL in 100 mM sodium acetate buffer, pH 3.0 by glacial acetic acid), making a radiolabeled solution at 1.5 μ Ci/mL. An identical LBL deposition procedure was then performed.

Measurement of Film Thickness. Following deposition, films were immediately removed from the final rinsing bath and air dried. Film thickness was determined either by ellipsometry at ten different predetermined locations on the film surface or by profilometry at three different scratch sites. All measurements were performed in triplicate. Dry state ellipsometric measurements were conducted using a Gaertner Variable Angle Ellipsometer (6328 nm, 70° incident angle) and accompanying Gaertner Ellipsometer Measurement Program (GEMP) Version 1.2 software interface. *In situ* ellipsometric measurements were made on a J. A. Woollam Spectroscopic Ellipsometer XLS-100 (70° incident angle) with accompanying WVASE32 program Version 3.449, in a quartz cell with polished 70° windows for the incident and reflected beams. Profilometric measurements were taken on a KLA-Tencor P-10 Profilometer.

Measurement of Drug Release. Following deposition, ^3H -GS labeled films were immersed in 25 mL of pre-warmed modified simulated body fluid (m-SBF) ¹⁵⁷ in a tightly-capped Falcon tube, maintained at 37°C in a water bath. The degradation tubes were tightly capped between sample extractions to prevent evaporation of the buffer solution. A 1 mL sample was extracted at predetermined time points (every 1-5 minutes at the beginning, then gradually increasing the time intervals) and analyzed by adding 5 mL of ScintiSafe Plus 50% (Fisher Scientific, Atlanta, GA) prior to measurement. The resulting mixtures were analyzed using a Tri-carb liquid scintillation counter (Model U2200). The amount of radiolabel in each sample vial was measured using a ^3H counting protocol which was shown to be highly accurate over a broad concentration range (30-100,000 DPM/mL) in calibration experiments performed prior to drug release. Raw data (disintegrations per minute, DPM) were converted to micrograms (μg) of gentamicin using the conversion factor $2.2 \times 10^6 \text{ DPM} = 1 \mu\text{Ci} = 1.0 \mu\text{g } ^3\text{H-GS}$. Finally, the total gentamicin release from a single film was calculated according to the following equation:

$$M_i = \left((C_i \times V_i) + (1\text{mL}) \sum_{j=1}^{i-1} C_j \right) (1334)$$

where M_i (μg) is the total cumulative mass released from the film as of measurement i , C_i ($\mu\text{g/mL}$) is the concentration of sample i , V_i (mL) is the total volume of the degradation bath prior to measurement i , $(1\text{mL}) \sum_{j=1}^{i-1} C_j$ is the total

mass in previously extracted samples, and 1334 is equal to the mass ratio of total GS to ^3H -GS in the dipping solution (i.e., in the degradable film).

***Staphylococcus aureus* macrodilution assay.** All liquid assays were performed in cation-adjusted Mueller Hinton Broth II (CMHB). Qualitative assays were performed following standard macrodilution methods as outlined by the National Committee on Clinical Laboratory Standards (NCCLS M26-A, 1999) with a challenge of 10^5 CFU/mL. For assays involving co-incubation with films deposited on silicon, 24-well plates were used, with 0.5 mL of liquid culture per well. Briefly, each square-cut silicon substrate (1.0 cm x 1.0 cm), either bare or coated depending on the test group, was placed flat in the center of a well in a 24-well plate, polished side up. Each well was then filled with 0.50 mL of *S. aureus* in exponential growth phase at 10^5 CFU/mL in CMHB, completely immersing the substrate. For quantitative assays, an elution test with modified macrodilution assay was adopted to facilitate duplications of tests at various treatment levels. Briefly, $[(\text{Poly X/HA})_1(\text{GS/HA})_1]_{100}$ films with precisely cut film sizes were immersed in a set amount of culture medium at 37°C for 24+ hours for complete erosion of films. Estimated gentamicin concentration ([GS]) within this elution buffer can be computed based on the immersed film size and culture volume. The resulting elution medium was then serially diluted 1:2 with fresh medium 15 times, yielding 16 different concentrations, from the original elution medium strength down to a factor of 2^{-15} . Quantitative assays were done in 96-well plates with 150 μL of liquid culture per well, with 135 μL of test media and 15 μL of

inoculation culture at 10^5 CFU/mL in CMHB. All test media were sterile-filtered through 0.2 μ m membranes prior to use. Estimated test media conditions take the 9:10 dilution into account. For each set of assays, three wells were filled with culture fluid with no bacteria inoculated, while three negative controls were subject to the same bacterial challenge without any substrate. The plate was incubated at 37°C under gentle shaking for 16-18 hours. Cell density was read at OD 600 nm in a BioTek® PowerWave™ XS Microplate Spectrophotometer with accompanying Gen5 program Version 1.00.14. All treatments, whether direct infusion into culture or co-immersion of film substrates with the culture, were administered from the time of seeding to data observation. Cultures were incubated at 37°C for 16-18 hours under gentle shaking before observation.

***Staphylococcus aureus* Kirby-Bauer disc diffusion assay.** Kirby-Bauer disk diffusion assays were performed according to the NCCLS guidelines (M7-A4, 1997). Agar plates were formulated with CMHB and BactoAgar™. Each plate was inoculated with *S. aureus* culture in exponential growth phase at 10^8 CFU/mL in CMHB using a sterile cotton swab. The test substrate was immediately placed on the inoculated plate, coated side down, with gentle pressing by a pair of tweezers to ensure conformal contact, exercising particular care not to pierce the agar or move the substrate. All substrates were placed at least 5 cm apart from one substrate center to another and 2 cm from the edge of the dish. The plates were inverted and incubated at 37°C without shaking for 16-18 hours before observation.

Osteoblast toxicity assay through alamarBlue. MC3T3-E1 Subclone 4 was maintained in minimum essential medium alpha medium supplemented with 10% fetal bovine serum, 100 U/mL penicillin, and 100 mg/mL streptomycin. Cells were split 1:15 every 3-4 days, with the medium refreshed in between. Cells were examined under the microscope every 1-2 days to assess confluence and morphology. For the toxicity assays, cells were seeded at 10^4 /mL in a 96-well plate at 150 μ L per well. Three wells were filled with 150 μ L medium without cells as blank references. Cells were monitored daily until they reach 50% confluence, at which point the medium in each well was replaced with the test medium. All test media were sterile-filtered through 0.2 μ m membranes prior to use. Three wells were left untreated as negative controls. Cells were incubated with the test media for the defined test period. At the end of the test period, medium in each well was replaced with fresh untreated medium, and 15 μ L of alamarBlue was added to each well. Cells were incubated at 37°C for 4 hours, examined visually for color change then read at 570 nm and 600 nm by a microplate spectrophotometer. Cell metabolic activity was computed from the spectrophotometric readings based on manufacturer's specifications. ANOVA and other data analyses were performed by Analysis Toolpack in Microsoft Excel.

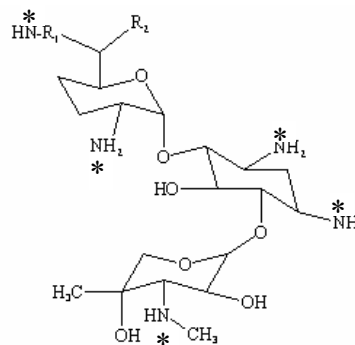
5.1.3 Results and Discussion

Incorporation of unmodified gentamicin through design of film architecture.

Initially we attempted to directly incorporate gentamicin (GS, see Figure 5.1) into an LbL thin film through a standard bilayer structure in which gentamicin was alternately deposited with a biologically compatible polyanion, alginic acid (Alg) or hyaluronic acid (HA). Such a bilayer deposition resulted in opaque, uneven films with little or no gentamicin incorporation, as inferred from drug release assessment through scintillation counting of release buffers from ($^3\text{H-GS/HA}$)₁₀₀ and ($^3\text{H-GS/Alg}$)₁₀₀ films. We hypothesize that gentamicin rapidly diffuses out of the polyelectrolyte layers during assembly, and hence was not able to function as a stable structural component in an LbL film. With a lack of polycationic species to form strong interactions with the polyanion in the LbL film, such a fabrication scheme did not result in stable film growth.

Figure 5.1 - Structure of gentamicin.

Sites that are protonated under deposition conditions are marked with an asterisk.



We also constructed films using a combined solution of *Poly X* and gentamicin as the polycation and a solution of HA as the polyanion. A film was constructed from this combination, but it exhibited no gentamicin release. In this case, the higher molecular weight species, which is the *Poly X*, was preferentially adsorbed

into the films over the low molar mass gentamicin molecules, leading to little or no gentamicin incorporation. Finally, direct complexation of gentamicin by HA in an HA/GS mixture with an excess of the polyanion did not result in the formation of stable colloidal structures that could be directly incorporated into multilayer thin films; resulting films generated from these systems did not lead to gentamicin incorporation either.

As an alternative, we designed a LbL heterostructure which incorporated an additional cationic species, specifically a degradable poly(β -amino ester)²³ (designated “*Poly X*”, where *X* is a number specifying the structure of the repeat unit). Films were assembled with the $[(Poly X/HA)_a(GS/HA)_b]_n$ architecture, where *a*, *b*, and *n* could be independently adjusted to tune film architecture. We will refer to films of this architecture, *i.e.* (*a*, *b*) = (1, 1), as *tetralayered* films, and each repeat of $(Poly X/HA)(GS/HA)$ constitutes a *tetralayer*. We chose to work with hyaluronic acid rather than alginic acid, as the former is an endogenous extracellular matrix component found in humans and hence a good candidate as a biocompatible inactive component of the film. Three degradable poly(β -amino esters) were studied: *Poly 1* (Mn = 15.5k), *Poly 2* (Mn = 9.7k), and *Poly 6A* (Mn = 16.7k). Their structures are shown in Figure 5.2. *Poly X*'s are hydrolyzed under physiological conditions²³, and hence films containing *Poly X*'s can erode and release encapsulated components when exposed to an aqueous physiological environment.

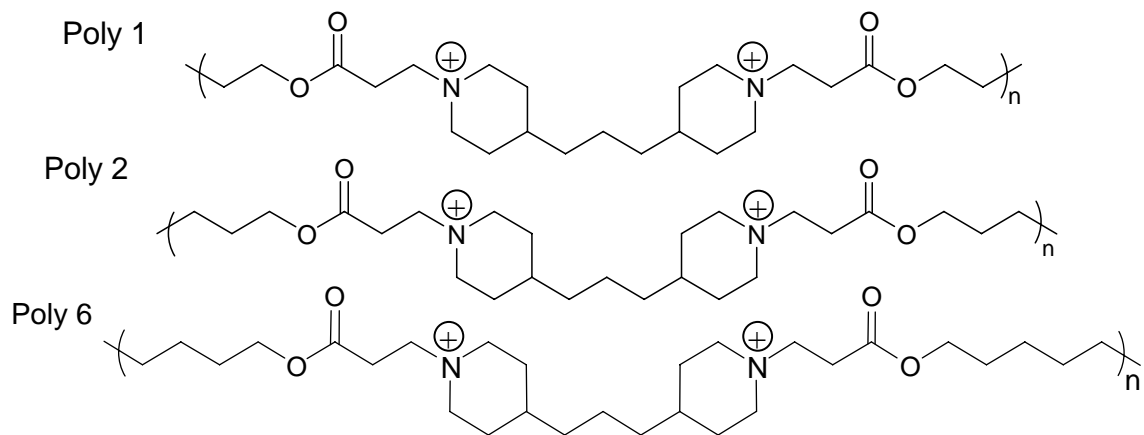


Figure 5.2 - Structures of *Poly X* used in this study.

Growth curve of $[(Poly X/HA)_a(GS/HA)_b]_n$ films. The $[(Poly X/HA)_a(GS/HA)_b]_n$ architecture resulted in reproducible film growth with tunable amounts of gentamicin incorporation. Figure 5.3 shows the growth curve of $[(Poly 1/HA)_1(GS/HA)_1]_n$ and $[(Poly 2/HA)_1(GS/HA)_1]_n$, namely a plot of film thickness versus n , the number of tetralayers. Thicknesses were measured by profilometry and averaged over triplicate trials, and error bars represent mean RMS roughness from triplicate samples. This growth curve indicates that $[(Poly X/HA)_a(GS/HA)_b]_n$ can grow reproducibly for at least 150 tetralayers, unlike the $(GS/Alg)_n$ and $(GS/HA)_n$ films. As we hypothesized above, the presence of *Poly X* likely helped to form a stable structural basis with HA and allowed for continued film growth.

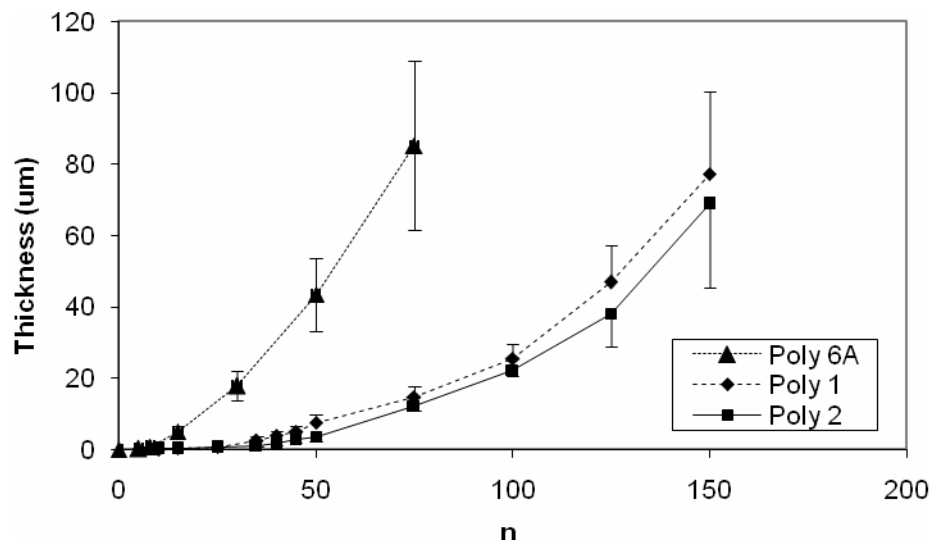


Figure 5.3 - Growth curves for $[(Poly X/HA)_1(GS/HA)_1]_n$.

Poly 6A film is only shown up to 75 tetralayers to keep y-axis within a reasonable scale range to inspect *Poly 1* and *Poly 2* growth curves.

One feature of these growth curves is their nonlinearity. This nonlinear growth trend, though not exponential, is likely caused by the same “in” and “out” diffusion mechanism proposed for exponentially growing LbL films¹⁵³. In particular, gentamicin is expected to diffuse within the film, since it is a small trisaccharide molecule with a molecular weight of 477Da. Similar nonlinear growth trends have been observed in our group for films made with LPEI (linear poly(ethylene imine))¹⁹⁹ and heparin^{119, 120}, and in other groups with HA^{153, 200-203}.

$[(Poly 6/HA)_1(GS/HA)_1]_n$ grew much faster than the *Poly 1* and *Poly 2* analogs.

These films are very thick compared to other hydrolytically degradable multilayers constructed with the poly(β -amino esters)^{110, 119, 120}. We suspect that

factors that drive exponential growth account for the high film thickness; both the interdiffusion of gentamicin during assembly and increasing surface roughness of the film as seen in Figure 5.3 could contribute to rapid film growth. We suspect that the higher hydrophobicity of *Poly 6A*, coupled with its lower charge density, resulted in decreased electrostatic interactions with HA; hence, “loopier”, less ionically crosslinked films were made with higher permeability to gentamicin interdiffusion and higher surface roughness, both of which contribute to faster growing films. *Poly 6A* films also had lower gentamicin loading per unit film thickness, further supporting the hypothesis on its loopier nature and lowered retention of GS within the film.

Tunability of gentamicin dosage. Figure 5.4 presents the dosage *vs.* layers correlation of $[(Poly\ X/HA)(GS/HA)]_n$ films. Error bars represent standard deviations on the dosage value over three samples. Gentamicin dosage were assessed by immersing $[(Poly\ X/HA)(^3H-GS/HA)]_n$ films in m-SBF at 37°C, allowing the released to complete as verified by collected release curve, and computing the total released amount based on scintillation counting of release buffer (see *Kinetics of gentamicin release from films*, next section). The total released amount was found to be monotonically increasing with the number of tetralayers, n . For $n = 0 - 150$, gentamicin dosage could be precisely tuned anywhere between 0 and $123\ \mu\text{g}/\text{cm}^2$. However, $123\ \mu\text{g}/\text{cm}^2$ is by no means an upper limit, as depositions of additional layers are expected to result in progressively higher dosages.

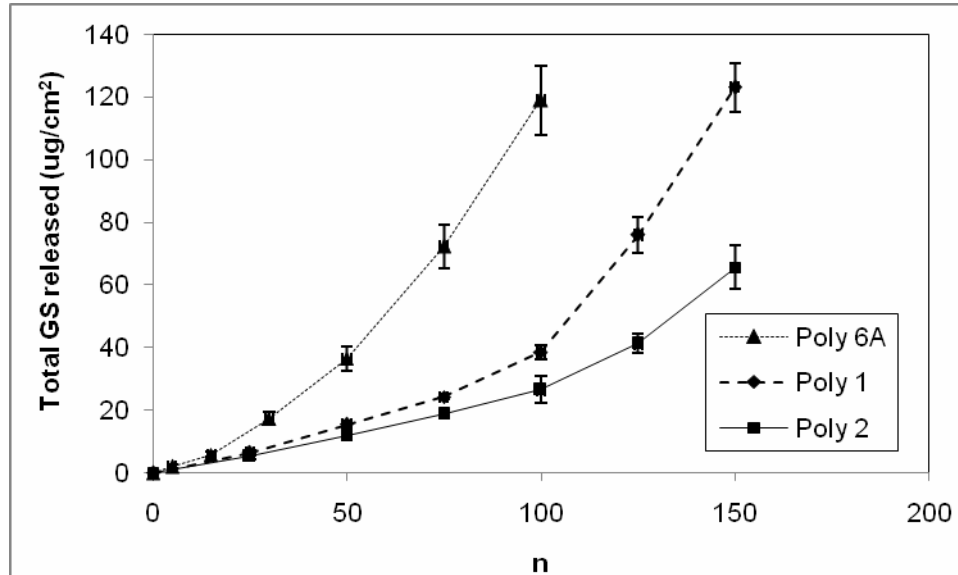


Figure 5.4 – Total gentamicin loading vs. number of tetralayers for $[(Poly X/HA)_i(GS/HA)_j]_n$.

Combining data from Figure 5.3 and Figure 5.4, we could compute the vertical loading density of gentamicin within the film, *i.e.* gentamicin per unit film area, divided by film thickness. The results are presented in Table 1. We found that each type of *Poly X* film, loading density is highest within the first 5 μm of growth, after which the density drops off to a steady-state value. This trend is consistent with a heterogeneous film loading model in which gentamicin is partitioned towards the top. This could be a result of its low molar mass, diffusivity, and hydrophilicity, yielding interdiffusion processes which favors GS accumulation at the top layers of the film. As layer thicknesses increase, the films become looper overall with a more pronounced partitioning effect, resulting in an overall decrease in gentamicin loading density. A steady-state loading density is reached when the decreasing film structural density balances with increasing permeability to gentamicin.

The steady-state loading densities are around 1.6, 1.1, and 0.82 $\mu\text{g}/\text{cm}^2/\mu\text{m}$ for *Poly 1*, *Poly 2*, and *Poly 6A* films respectively. Interestingly, film density ranked in order of hydrophilicity and charge density of the *Poly X*, suggesting that stronger electrostatic interactions within the film leads to higher gentamicin loading.

Table 1 - Thickness, gentamicin dosage, and vertical gentamicin loading density of $[(\text{PolyX}/\text{HA})(\text{GS}/\text{HA})]_n$ films, as a function of the number of tetralayers.

N	<i>Poly 1</i>			<i>Poly 2</i>			<i>Poly 6A</i>			
	Thick-ness (μm)	Dosage ($\mu\text{g}/\text{cm}^2$)	Loading density ($\mu\text{g}/\text{cm}^2\text{-}\mu\text{m}$)	Thick-ness (μm)	Dosage ($\mu\text{g}/\text{cm}^2$)	Loading density ($\mu\text{g}/\text{cm}^2\text{-}\mu\text{m}$)	n	Thick-ness (μm)	Dosage ($\mu\text{g}/\text{cm}^2$)	Loading density ($\mu\text{g}/\text{cm}^2\text{-}\mu\text{m}$)
0	0.00	0.00		0.00	0.00		0	0.00	0.00	
25	0.68	6.55	9.691	0.59	5.29	8.921	5	0.32	2.03	6.261
50	7.54	15.54	2.061	3.60	11.81	3.285	15	5.04	5.82	1.154
75	14.87	24.30	1.634	12.21	18.80	1.539	30	17.92	17.34	0.968
100	25.60	38.57	1.506	22.41	26.49	1.182	50	43.43	36.43	0.839
125	46.83	75.89	1.620	38.20	41.22	1.079	75	85.12	72.21	0.848
150	77.30	122.97	1.591	68.71	65.57	0.954	100	145.92	118.83	0.814

Kinetics of gentamicin release from films. Coupled with the released dosage studies were assessments on the kinetics of drug release from these films as exposed to a physiological environment. The films were immersed in modified simulated body fluid (m-SBF)¹⁵⁷, an ionic buffer that closely models conditions of the human blood without the biological components, maintained at 37°C in a water bath. Figure 5.5 shows typical gentamicin release curves from $[(\text{Poly X}/\text{HA})(\text{GS}/\text{HA})]_{50}$ with *Poly X* = *Poly 1*, *Poly 2*, and *Poly 6A*, with error bars representing standard deviations from scintillation counting protocol. These release curves are normalized to the total released dosage to allow for release rate

comparison. While films formulated with *Poly 6A* completed 95% of its release of gentamicin within 4 hours, those with *Poly 1* and *Poly 2* displayed more prolonged release of 10-15 hours for 95% release. Normalized release profiles at $n = 25$ and 100 gave similar quantitative results.

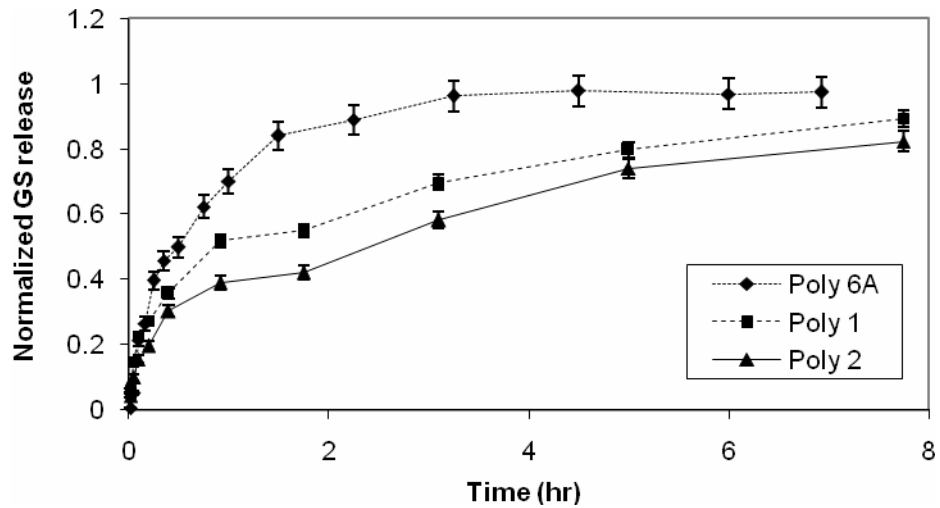


Figure 5.5 - Normalized cumulative gentamicin release from 50-tetralayer films made with different *Poly X*'s

As a comparison, Stigter *et al.*'s hydroxyapatite system¹²² released almost 100% of its gentamicin in PBS at 37°C in 30 min, with a total dosage of 28 μg released from a 45 μm coating on a 2x2 cm $\text{Ti}_6\text{Al}_4\text{V}$ plate, representing 3.5 $\mu\text{g}/\text{cm}^2$ encapsulation dosage (assuming coating on both sides of the plate). In contrast, a $[(\text{Poly } 1/\text{HA})_1(\text{GS}/\text{HA})_1]_{125}$ film, also 45 μm thick, could encapsulate 71 $\mu\text{g}/\text{cm}^2$ of gentamicin that was released over 15 hours under similar release conditions.

To further assess the gentamicin release mechanism, we tracked *in situ* film thickness (*i.e.* as immersed in the release buffer) during the erosion process. *In situ* thickness measurements were made with a spectroscopic ellipsometer; error bars represent uncertainty values computed by the software. In order to obtain consistent laser beam signal, we used thin $n = 10$ samples. Figure 5.6 shows the *in situ* thickness of a $[(Poly\ 2/HA)_1(GS/HA)_1]_{10}$ over 10 hours of incubation, normalized to the initial swollen film thickness (500 nm), and the corresponding normalized gentamicin release profile which was collected from a separate but identical set of films. Triplicates were run on both the erosion and drug release data, and all three trials yielded similar quantitative outcomes. Figure 5.6 shows data from a typical set, with error bars representing measurement uncertainties as computed by the equipment software.

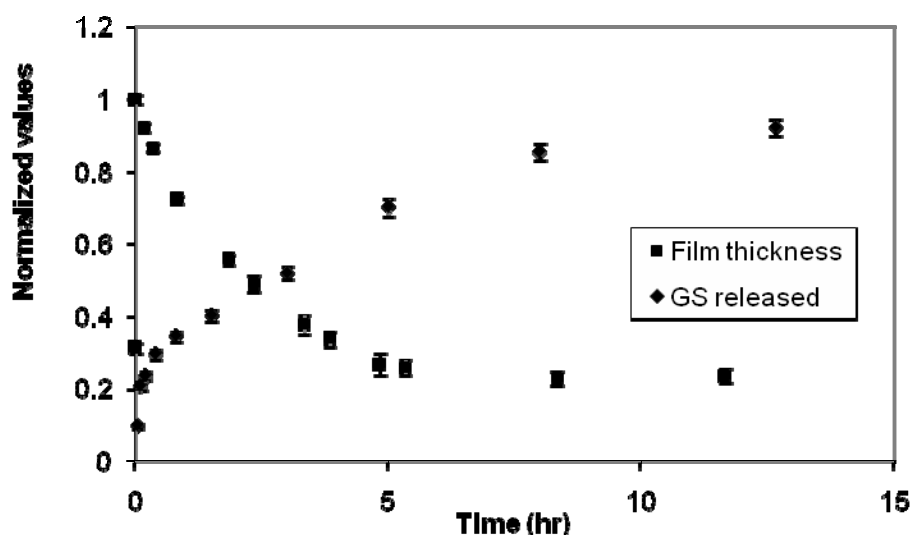


Figure 5.6 – Normalized *in situ* film erosion and gentamicin release from a *Poly 2* film.

In situ film thickness is normalized to initial swollen film thickness (500 nm), while cumulative gentamicin released is normalized to the final release amount ($4\ \mu\text{g}/\text{cm}^2$).

The film swelled to about three times its dry state thickness upon initial contact with the m-SBF buffer, from 160 nm in dry state to 500 nm in solution, possibly due to the HA content within the film. High degrees of swelling of multilayers made with HA have been observed for (PAH/HA)_n²⁰⁴, (PLL/HA)_n²⁰⁵, and (Chitosan/HA)_n²⁰⁶ films. The degree of film swelling can influence the diffusion flux of small molecules²⁰⁶ and hence has implications towards the release kinetics of gentamicin. Burke and Barrett found that many internal characteristics of the film, such as the extent of ionic cross-linking, affect the degree of swelling of HA-containing PEMs, and these characteristics can be tuned by a variety of factors such as film assembly pH^{204, 205}. Hence, tuning the assembly conditions for [(Poly X/HA)(GS/HA)]_n films could impart significant effect over gentamicin release, especially for the initial rapid release phase hypothesized to be driven in part by gentamicin diffusion.

Following the initial swelling, the film thickness steadily decreased over 8 hours, with corresponding drug release from the film. Beyond 8 hours, the remaining 20% of gentamicin was gradually released, while *in situ* film thickness remained steady around 115 nm over the next 48 hours (data not shown). Overall, approximately 80% of the film thickness was eroded away after extended time periods. The uneroded portion of the film was thought to be composed of a combination of HA and *Poly 2*. As discussed above, gentamicin is thought to partition towards the top of the film. Hence, as the film was deconstructed and eroded down to the polymer-rich and hence more stable bottom layers, the

degradation process slowed down. The apparent non-degradability of the film could be due to extensive ionic cross links that are formed between HA and *Poly 2* in the absence of gentamicin, resulting in a dense, stable film that hydrolyzes much more slowly.

The release of gentamicin appeared to undergo two phases. The first phase, represented by the first 8 hours, was driven predominantly by destabilization and deconstruction of the film, *i.e.* bulk polymers releasing from the film without complete hydrolysis due to loss of film stability as GS diffuses out of the film matrix, with a small contribution from hydrolysis of *Poly 2*. This phase accounted for about 80% of the gentamicin released, and Figure 5.6 shows that the release rate roughly scaled with film erosion rate during this phase. The second phase is driven by diffusion of gentamicin out of the uneroded HA residue, accounting for the remaining 20% drug release. During this phase, the *in situ* film thickness held constant while a small amount of gentamicin continued releasing at a low rate. Based on this set of film erosion data and our previous work on hydrolytically degradable LbL thin films^{119, 120}, we propose two mechanisms for erosion of the LbL delivery thin films: (1) direct deconstruction of the film without polymer degradation driven by a lowered film stability upon rapid diffusion of gentamicin out of the film matrix, and (2) hydrolytic degradation of the *Poly X* component. Each specific film construct experiences a different set of contributions from these mechanisms. For example, *Poly 6A* tetralayered films resulted in the fastest release, and we suspect that the

hydrophobicity and lower charge density of *Poly 6A* led to fewer electrostatic interactions. The decreased ionic cross linking had two effects: higher susceptibility to film deconstruction, and higher permeability for gentamicin to diffuse out of these films.

Release rate tuning through variation in film architecture. It has been shown that by “mixing and matching” several types of *Poly X* within a given film, one could obtain release rates intermediate between the individual polymers ¹¹⁷. Coupled with direct dosage tuning by the number of layers, we can potentially achieve any dosage and release timescale between 0-123 $\mu\text{g}/\text{cm}^2$ and 4-20 hours respectively. As mentioned above, these parameters do not signify the limit of the layer-by-layer system but merely the range examined under the present study.

In addition to the mix-and-match approach described above, we can maneuver release timescales without changing the *Poly X* species, through manipulation of the film architecture. In Figure 5.7, the release of gentamicin from our usual tetralayer, $[(\text{Poly I}/\text{HA})_1(\text{GS}/\text{HA})_1]_n$, was compared to that from a “hexalayer” structure, $[(\text{Poly I}/\text{HA})_2(\text{GS}/\text{HA})_1]_n$, in which the $(\text{Poly I}/\text{HA})$ bilayers were repeated twice for each bilayer of (GS/HA) . We saw variations in both the release timescale and encapsulation dosage, even though both films had 100 bilayers of gentamicin. The 100-hexalayer film (■) encapsulated 106 $\mu\text{g}/\text{cm}^2$ of gentamicin, approximately 2.5 times that of the tetralayer equivalent (◆).

However, the release timescale was much shorter – 3 hours for 95% release as

compared to 10 hours of the tetralayer. By tuning the number of hexalayers down from 100 to 70 (\blacktriangle), we brought the encapsulation dosage down to a similar level as a tetralayer at $n = 100$, around $40 \mu\text{g}/\text{cm}^2$, while maintaining the shorter release timescale. Hence, through architectural design within the same *Poly X* species, the release rate could be adjusted while preserving the total release dosage.

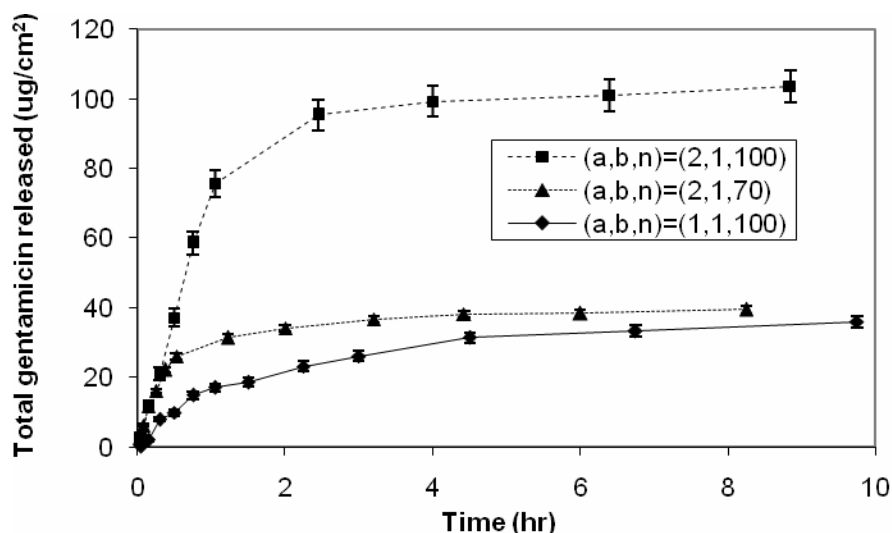


Figure 5.7 – Cumulative amount of gentamicin released from *Poly 1* films with variations in film architecture and number of deposited layers.

***In vitro* activity against *Staphylococcus aureus*.** *In vitro* assessments focused on films formulated with *Poly 1* and *Poly 2*, as these films exhibited more sustained released of gentamicin. Therapeutic activities of the films were assessed against proliferation of *Staphylococcus aureus* (ATCC 25923), a common source of biomedical implant infections. Three types of assays were conducted: a qualitative liquid culture, quantitative liquid culture, and quantitative agar cultures (Kirby-Bauer disk diffusion assay). The qualitative liquid assays gave a binary “yes” or “no” answer as to whether the specific test condition could inhibit the growth of *S. aureus* using standard macrodilution assays performed in accordance

to NCCLS M26-A guidelines. These qualitative assays provided a simple frontline assessment of the efficacy of gentamicin-loaded thin films. Table 2 summarizes results from these qualitative assays. In the table, “on silicon” denotes films left attached on the silicon substrates, while “free standing” films were those peeled off from the silicon substrate. The films remained intact and undistorted in dimensions after lift-off from the substrate, suggesting good mechanical stability.

Table 2 –Qualitative assessment of various film substrate in inhibiting growth of *S.aureus* in liquid culture.

Test Group	Film Type	Growth inhibition
1	Bare Si	No
2	(LPEI/PSS) ₁₀ on silicon	No
3	GS, 0.125 µg/mL	Yes
4	<i>Poly 1</i> , <i>Poly 2</i> , or HA, up to 512 µg/mL each	No
5	(<i>Poly X/HA</i>) _{50 or 100} on silicon	No
6	[(<i>Poly X/HA</i>) ₁ (GS/HA) ₁] _{50 or 100} on silicon	Yes
7	Free-standing [(<i>Poly X/HA</i>) ₁ (GS/HA) ₁] ₁₀₀	Yes

As expected, both a bare silicon chip and one with the non-degradable (LPEI/PSS)₁₀ base layer as a control resulted in no bacteria growth inhibition. Similarly, *Poly 1*, *Poly 2*, and HA solutions at concentrations up to 512 µg/mL, or released from multilayer thin films in combination from a 50- or 100-bilayer film, did not inhibit *S. aureus* growth. Direct administration of gentamicin at or above 0.125 µg/mL resulted in growth inhibition, as expected based on the literature-reported minimum inhibitory concentration (MIC) of 0.1-1.0 µg/mL against *S. aureus*²⁰⁷. Co-incubation of *S. aureus* with gentamicin-loaded tetralayered films, whether on silicon or free standing, resulted in growth inhibition, indicating that

sufficient gentamicin was released from the film in its therapeutically active form. These quick proof-of-concept assays affirmed that (1) blank substrates had no antimicrobial activity, (2) $[(Poly\ X/HA)_1(GS/HA)_1]_n$ films ($n = 50$ and 100) are active against *S. aureus*, and (3) the antibacterial action came from the released gentamicin and not the other film components or the underlying substrate.

Quantitative liquid assays were performed based on the optical density of the liquid cultures at 600 nm (OD_{600}). *S. aureus* cultures were exposed to elution buffers from $[(Poly\ X/HA)_1(GS/HA)_1]_{100}$ for 16 hours prior to measurement. A condensed set of data is shown in Figure 5.8, which plots the normalized bacteria density as a function of estimated gentamicin concentration contained in each dilution of the elution medium. Normalized bacteria density was computed as $(OD_{600, sample} - OD_{600, blank}) / (OD_{600, negative\ control} - OD_{600, blank})$. The horizontal axis is truncated to the lower concentration range to better display system behavior in this regime. Normalized bacteria density was statistically zero beyond estimated [GS] of 0.6 $\mu\text{g/mL}$.

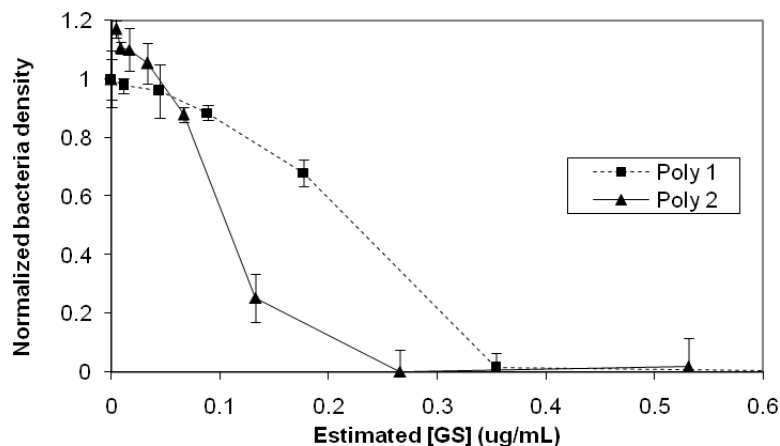


Figure 5.8 – Normalized density of *S. aureus* liquid cultures after treatment with elution buffers of $[(Poly X/HA)(GS/HA)]_{100}$.

Densities are based on OD_{600} after a 16-hr incubation with buffers eluted from $[(Poly X/HA)(GS/HA)]_{100}$ at various estimated gentamicin concentrations.

We saw that film elution media exhibited similar activity against *S. aureus* as direct addition of gentamicin into liquid cultures, with an observable minimum inhibitory concentration (MIC). However, the observed MICs from film elution media were higher than free gentamicin. MICs were about 0.3 and 0.2 $\mu\text{g/mL}$ for *Poly 1* and *Poly 2* tetralayers (with released [GS] estimated based on $n = 100$ film data), respectively, while MIC of free gentamicin was measured to be around 0.13 $\mu\text{g/mL}$. We verified through scintillation data that 20 hours was sufficient to elute all gentamicin in the CMHB medium. We initially suspected that some of the eluted materials, *i.e.* HA and *Poly X*, interacted with either gentamicin or the bacteria to reduce bacteria uptake of gentamicin. To assess this hypothesis, we administered various combinations of *Poly 1* and HA with serial dilutions of gentamicin to *S. aureus* cultures. Based on the assumption of 1:1 charge compensation between the film components, we expected a mass ratio of 2.14:1.00:4.06 for *Poly 1*:GS:HA within the film and further assumed that a

similar mass ratio was eluted. We therefore conducted three sets of gentamicin serial dilutions, with (1) 0.28 $\mu\text{g/mL}$ *Poly I* and 0.53 $\mu\text{g/mL}$ HA, (2) 10 \times of (1), and (3) 100 \times of (1). In all cases we observed inhibition of *S. aureus* proliferation between gentamicin dilutions of 0.125 and 0.0625 $\mu\text{g/mL}$, suggesting that MIC remains around 0.13 $\mu\text{g/mL}$ in the presence of various amounts of *Poly I* and HA. Thus, the eluted materials did not appear to interfere with gentamicin activity. Another possible explanation is that the estimated [GS] was not entirely accurate to the true [GS], due to small variability in film encapsulation dosage, and hence the true MIC from film-released gentamicin could be closer to free gentamicin than Figure 5.8 would suggest.

Several assays involving direct co-incubation of liquid *S. aureus* cultures with coated film substrates were also conducted, with estimated [GS] of 0.13, 0.25, and 0.5 $\mu\text{g/mL}$. Resulting bacteria densities were similar to those in Figure 5.8 and hence not presented. A wider concentration range was not tested for direct co-incubation due to difficulty in preparing silicon film substrates with small, precise film areas.

Kirby-Bauer assays. Additional quantitative assessment of the therapeutic activity of the antibacterial films was performed using Kirby-Bauer disk diffusion assays. Agar plates were inoculated with exponentially-growing *S. aureus* culture at 10^8 CFU/mL, with film substrates immediately placed on the plate with conformal contact. The entire assembly was incubated upside-down for 16-18

hours to results in a cultured plate covered with *S. aureus* colonies, except for a circular zone around gentamicin-eluting substrates inside which no colonies grew. The diameter of a ZOI provides a quantitative measure of the amount of *in vitro* active gentamicin released and diffused into the agar. Table 3 and Table 4 present a sampling of ZOI data for various film substrates. Note that the tabulated KB diameter represents overall ZOI *minus* the linear dimension of the film, *i.e.* 0.5 cm. Standard deviations were computed from triplicate trials of each test group.

Table 3 – Zone of inhibition (ZOI) of negative controls films and those estimated to contain 10 ug of gentamicin.

Films appeared to release most of its encapsulated gentamicin in a therapeutically active form.

Film Type	Gentamicin loading (ug)	KB diameter (cm)
Bare silicon or (LPEI/PSS) ₁₀ base layers	0	0.00
BD standard (round, diameter = 0.5cm)	10	1.71±0.05
[(<i>Poly 1</i> /HA) ₁ (GS/HA) ₁] ₁₀₀ , on silicon	10±0.5	1.66±0.11
[(<i>Poly 1</i> /HA) ₁ (GS/HA) ₁] ₁₀₀ , free-standing	10±0.5	1.65±0.13
[(<i>Poly 2</i> /HA) ₁ (GS/HA) ₁] ₁₂₅ , on silicon	10±0.7	1.67±0.09
[(<i>Poly 2</i> /HA) ₁ (GS/HA) ₁] ₁₂₅ , free-standing	10±0.7	1.68±0.11

Table 4 - ZOI of *Poly 2* tetralayer films on silicon with varying gentamicin dosages.

Films could release tunable amounts of gentamicin with corresponding levels of *in vitro* activity.

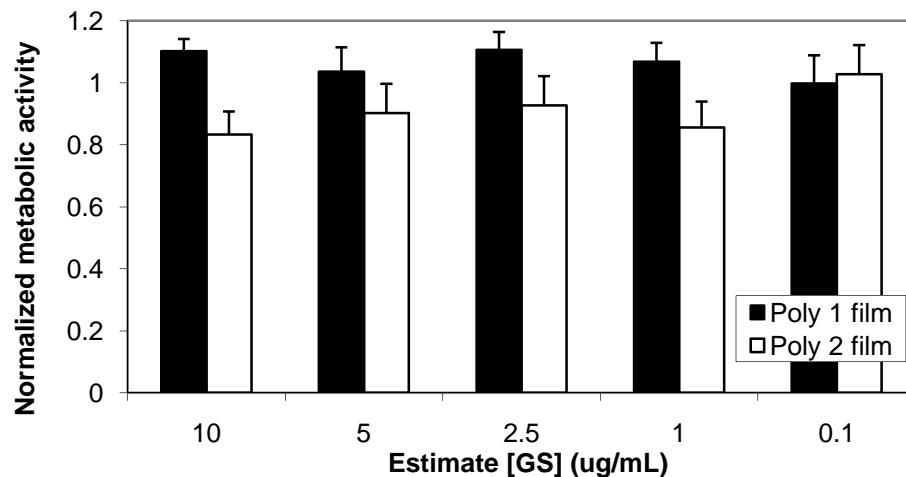
Film Type	Gentamicin loading (ug)	KB diameter (cm)
[(<i>Poly 2</i> /HA) ₁ (GS/HA) ₁] ₅₀	3.1±0.2	1.05±0.05
[(<i>Poly 2</i> /HA) ₁ (GS/HA) ₁] ₁₀₀	6.8±1.1	1.46±0.06
[(<i>Poly 2</i> /HA) ₁ (GS/HA) ₁] ₁₂₅	10±0.7	1.67±0.09
[(<i>Poly 2</i> /HA) ₁ (GS/HA) ₁] ₁₅₀	15±1.7	1.79±0.12

Table 3 presents data on a negative control and a series of films cut down to an appropriate size to release an estimated total of 10 µg of gentamicin. As expected, the bare silicon chip control resulted in no visible ZOI. Commercial BD Sensi-Disc™ specified by the manufacturer to release 10 µg of active gentamicin was used as a positive control. We observed that the tetralayered films had quantitatively comparable activities against *S. aureus* growth as positive controls. While Sensi-Disc™ produced a mean net diameter of 1.71 cm (consistent with manufacturer's specification of 1.4-2.2 cm), our films of similar dimensions, and estimated to contain the same total dosage of gentamicin, produced mean diameters of 1.65-1.68 cm, with standard deviations around 5-8% of mean values. There was no clear distinction between free standing films versus those remaining on silicon, suggesting that the antibacterial activity was independent of the underlying substrate, similar to findings in Table 2.

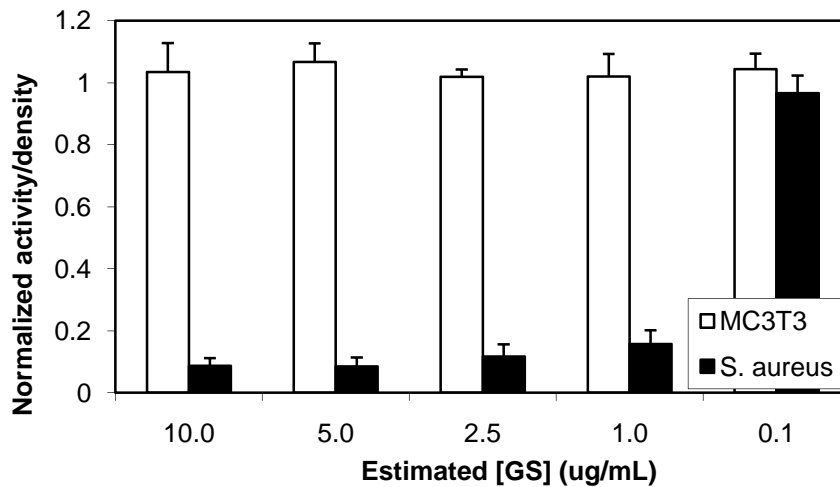
Table 4 shows the ZOI diameters of several *Poly 2* substrates with varying gentamicin dosage. The diameters steadily increased from a mean of 1.05 cm at 3.1 µg to 1.79 cm at 15 µg. *Poly 1* substrates resulted in a very similar set of data and hence were not duplicated in the table. Hence, we see that the precision in tuning released gentamicin dosage, as demonstrated in Figure 5.4, indeed translated into tunability of *in vitro* activity.

Nontoxicity towards MC3T3. While nontoxicity of several versions of *Poly X* has already been demonstrated towards NIH 3T3²³ and Cos-7^{111, 112} (the latter

indirectly through cell transfection protocols), we wanted to further confirm the nontoxicity of our specific film construct, specifically towards mammalian cells relevant to our orthopedic application. We chose MC3T3 (E1 subclone 4, ATCC CRL-2593) as the test cell line, a murine preosteoblast with high osteoblast differentiation and mineralization which serves as a model for human bone cells with which an orthopedic implant coating would come into contact. Degree of nontoxicity was quantified through the level of cellular metabolic activity, as assessed by the reduction of alamarBlue™. MC3T3 cells were pre-seeded to a 96-well plate and allowed to adhere and proliferate to 50% confluence prior to treatment by test substrate or media. Similar to the quantitative *S. aureus* liquid assays, we prepared culture media eluted from gentamicin films to facilitate replicated testing at various concentrations, but direct film-contact incubations were also run at 2.5, 5.0, and 10 µg/mL with similar results. Unlike the *S. aureus* assays, for which the incubation period was standardized to 16-18 hours, treatments of MC3T3 with film elution media were extended to 48 hours for additional compatibility challenge. Longer treatments were not possible due to the confluence level reached by the cells. We did, however, run a few assays with 16-hour treatments for consistency in comparison. Figure 5.9(A) plots the normalized metabolic activity of MC3T3 cultures treated with various dilutions of film elution buffers over 48 hours, relative to the activity of a culture under no treatment. Mean values over two sets of triplicate trials were plotted, with error bars representing standard deviations over the replicates.



(A)



(B)

Figure 5.9 - Combined data on *in vitro* efficacy and nontoxicity of $[(Poly\ 1,\ 2/HA)_1(GS/HA)_1]_{100}$. (A) metabolic activity of MC3T3 cells after a 48-hour treatment, normalized to negative control, (B) Combined results for nontoxicity towards MC3T3 and efficacy against *S. aureus* of $[(Poly\ 1/HA)_1(GS/HA)_1]_{100}$ over a 16-hour treatment period.

For these 48-hour treatments, MC3T3 retained similar levels of metabolic activity as negative controls for eluted gentamicin concentrations far above the MIC. 10 µg/mL is by no means an upper limit in nontoxicity, but merely the highest concentration tested under the present study. Two-factor ANOVA analysis indicates that the difference in MC3T3 response to *Poly 1* vs. *Poly 2* films is

statistically significant (p-value of 0.040 at $\alpha = 0.05$). The potential variation in biocompatibility is yet unexplained. A likely cause is the different chemistries of the oligomeric and monomeric degradation products from *Poly 1* and *Poly 2*, resulting in different interactions with cellular components.

Figure 5.9(b) presents combined data on efficacy against *S. aureus* and compatibility towards MC3T3 cells, both treated over a 16-hr period, with elution buffer from $[(Poly\ 1/HA)_1(GS/HA)_1]_{100}$. The open bars show normalized MC3T3 metabolic activity, while the filled bars represent normalized *S. aureus* density under identical treatments. As the chart indicates, at all strengths effective against *S. aureus* proliferation, the elution buffers remained nontoxic towards MC3T3. Between estimated gentamicin concentrations of 1.0 and 0.1 $\mu\text{g/mL}$, the gentamicin concentration fell below its MIC, and we hence observe *S. aureus* proliferation. The combination of data from Figure 5.9 suggests that film elution buffers were nontoxic towards MC3T3 over a contact period of 16 to 48 hours.

5.1.4 Conclusion

Antimicrobial thin films were fabricated through layer-by-layer deposition of gentamicin with two structural polyelectrolyte components, with precisely tunable dosage of released gentamicin. The films were deposited with a heterostructure alternating depositions between a hydrolytically-degradable poly(β -amino ester), a biocompatible polyanionic hyaluronic acid, and the antibiotic gentamicin, a design which allows for direct incorporation of gentamicin without having to pre-

modify it in any way. The films released gentamicin through a combination of hydrolytic degradation, film deconstruction, and gentamicin diffusion.

Encapsulation dosage could be easily modified by the number of deposited layers, while release rate may be modified by polymer chemistry and film architecture.

These films were demonstrated to have *in vitro* efficacy against *Staphylococcus aureus* proliferation and nontoxicity towards the murine preosteoblast MC3T3.

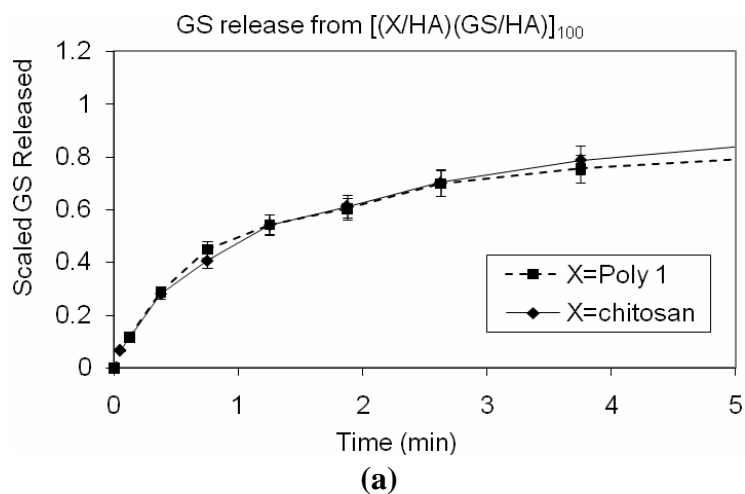
Efficacy level is comparable to positive controls of direct gentamicin administration. Even at dosage levels significantly above that necessary to inhibit *S. aureus* growth, the films did not appreciably affect the metabolic activity of MC3T3. Animal studies are currently under way, and will be coupled with assessment of the mechanical stability of these films.

In summary, we have designed *in vitro* active antibiotic-releasing films using the highly tunable layer-by-layer deposition technique and retained the ease. In particular, our level of antibiotic dosage and release rate control is significantly improved over previously reported antibiotic-eluting systems. This approach can be easily extended to encapsulation of other charged small molecules, resulting in a variety of single- and multi-release coatings for numerous biomedical applications.

5.2 Supplements to investigations on $[(\text{Poly } 1/\text{HA})(\text{GS}/\text{HA})]_n$

5.2.1 Chitosan substitution of *Poly 1* to probe release mechanism

As a further probe into the mechanism of gentamicin release from $[(\text{Poly } 1/\text{HA})(\text{GS}/\text{HA})]_{100}$ films, I constructed an analogous film using a non-degradable polycation as a substitute. A low-MW chitosan ($\sim 50\text{kDa}$) was ordered from Sigma-Aldrich for a closest match to the MW of *Poly 1* ($\sim 10\text{kDa}$; the five-fold difference was within the same order of magnitude and hence not expected to result in significant differences stemming from MW alone). $[(\text{Chitosan}/\text{HA})(^3\text{H-GS}/\text{HA})]_{100}$ films were constructed using an identical protocol as that used for *Poly 1* films, and the resulting films were assessed for *in vitro* release using identical buffer and counting protocols as well. The resulting release profile, along with those of $[(\text{Poly } 1/\text{HA})(\text{GS}/\text{HA})]_{100}$ for comparison, is shown in Figure 5.10.



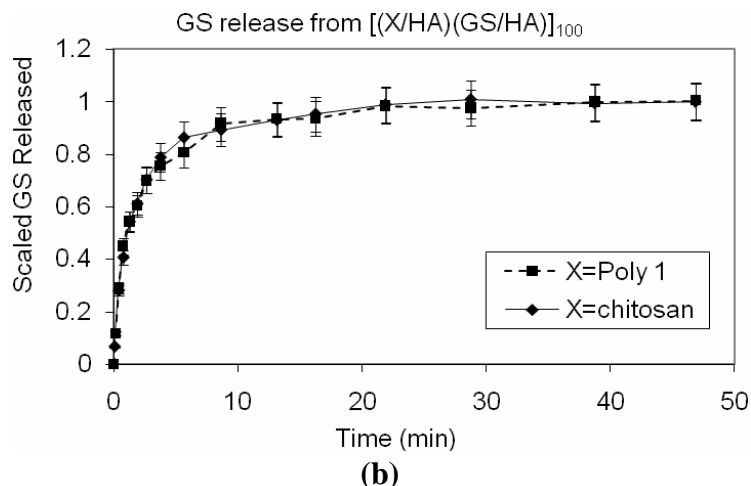


Figure 5.10 – Normalized release of gentamicin from $[(X/HA)(GS/HA)]_{100}$ in m-SBF at 37°C, with X being either *Poly 1* or chitosan.

(a) zoomed into the initial 5 hours, and (b) complete release over 50 hours. Note that X = Chitosan released a total of 20 $\mu\text{g}/\text{cm}^2$ gentamicin while X = *Poly 1* released 36 $\mu\text{g}/\text{cm}^2$. From *GS_fall06*.

Most intriguingly, the two type of films resulted in essentially identical release profiles when normalized to the final release amount. Even in the initial burst regime (see Figure 5.10(a)), the two curves overlap almost perfectly. This finding suggests that gentamicin release from both films could be driven predominantly by gentamicin diffusion and bulk film deconstruction, as opposed to hydrolytic degradation of *Poly 1*. Previous results showed that a *Poly 6* film released gentamicin faster than a *Poly 1* version, indicating that a *Poly 6* released more rapidly than the supposedly non-degradable $[(\text{Chitosan}/\text{HA})(\text{GS}/\text{HA})]_{100}$. This observation can again be explained by the hypothesis that gentamicin release was driven mostly by diffusion and film deconstruction, and hence the degree of ionic crosslinking within the film became a primary determinant of release rate. Growth and erosion curves of $[(\text{Chitosan}/\text{HA})(\text{GS}/\text{HA})]_{100}$ was not collected.

In terms of total released dosage, [(Chitosan/HA)(GS/HA)]₁₀₀ only encapsulated about 50% the amount of gentamicin of an analogous *Poly I* film. The dependence of gentamicin dosage on polymer chemistry was observed in other experiments as well (see section 5.2.2).

Conclusion. [(Chitosan/HA)(GS/HA)]₁₀₀ and [(*Poly I*/HA)(GS/HA)]₁₀₀ films had nearly identical normalized gentamicin release profiles, suggesting that [(*Poly I*/HA)(GS/HA)]₁₀₀ films released gentamicin predominantly via diffusion and film deconstruction, rather than hydrolytic degradation. Gentamicin encapsulation dosage was about 50% lower in the [(chitosan/HA)(GS/HA)]₁₀₀ films.

5.2.2 Alternative polyanion and influence of MW

Gentamicin releases from heterostructures formulated with polyanions other than HA were examined for various candidates including poly(styrene sulfonate) (PSS), poly(methacrylic acid) (PMA), and poly(acrylic acid) (PAA). Films made with PSS and PMA resulted in very little gentamicin encapsulation, while those of PAA gave somewhat promising results. In particular, PAA of molecular weights 5kDa and 1MDa were examined, and I found high dependence of release rates on the MW of the PAA (see Figure 5.11). The 200-fold increase in the MW of PAA significantly increased the release timescale of gentamicin. Interestingly, gentamicin dosage remained similar between the two films – around 60 $\mu\text{g}/\text{cm}^2$ for 100 tetralayers. This was higher than the dosage for equivalently-layered [(*Poly I*/HA)(GS/HA)]₁₀₀ films (MW of HA = 1.7 MDa), which was found to be around 36 $\mu\text{g}/\text{cm}^2$, suggesting a

chemistry-dependent loading of gentamicin. This finding was not surprising, as the loading was expected to correlate with the degree and nature of interaction between gentamicin and the polyanion.

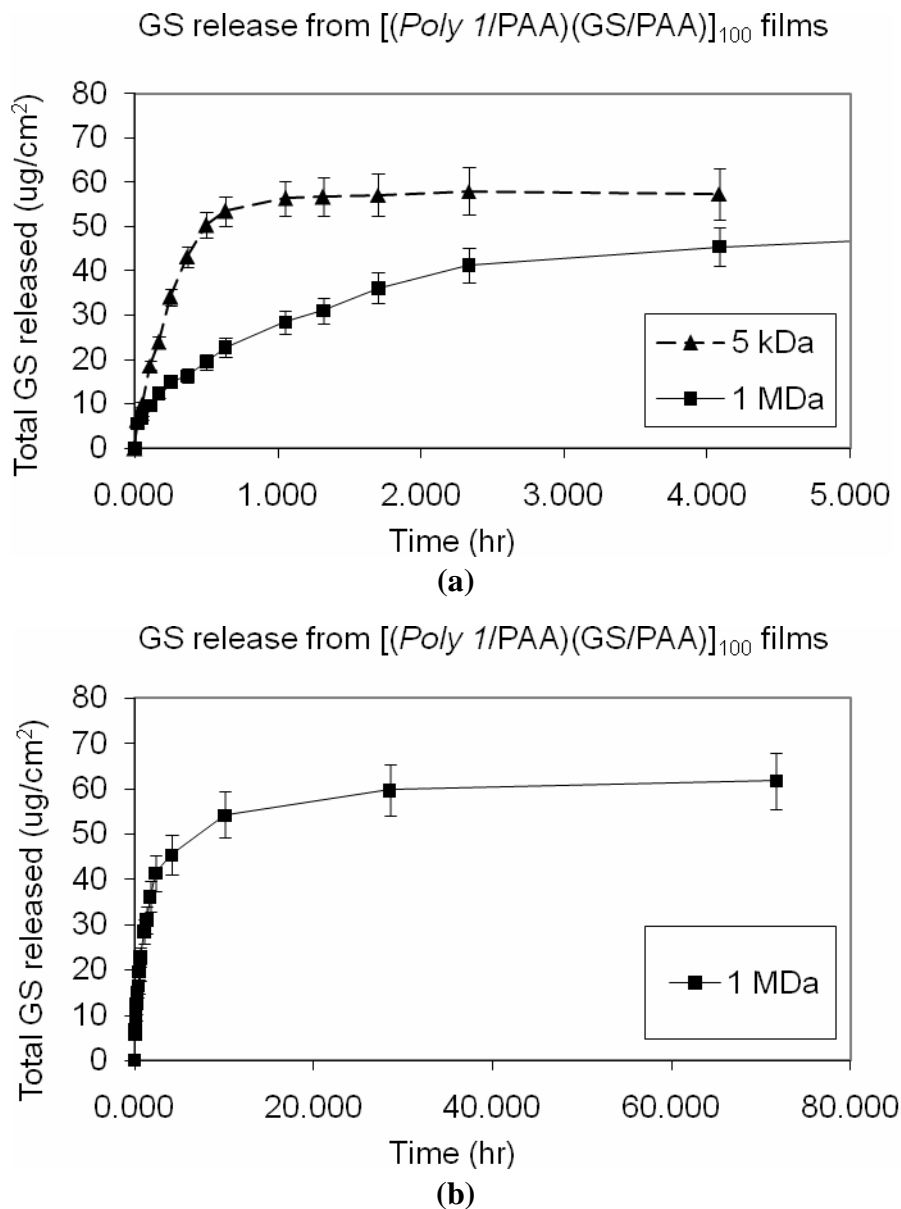


Figure 5.11 – Release of gentamicin from $[(Poly\ 1/PAA)(GS/PAA)]_{100}$ in m-SBF at 37°C, with PAA of different MWs.

(a) release curves from 5kDa and 1MDa PAA films in the initial 4 hours, and (b) complete release from 1MDa PAA film over 75 hours.

Interestingly, the $[(Poly\ I/PAA)(GS/PAA)]_{100}$ films made with MW_{1MDa} PAA had a similar release rate as the $[(Poly\ I/HA)(GS/HA)]_{100}$ films made with $MW_{1.7MDa}$ HA, suggesting that polyanion MW may be a much more influential factor than specific polyanion chemistry or charge density on the rate of gentamicin release. As a further verification on this hypothesis, $[(Poly\ I/HA)(GS/HA)]_{100}$ films with MW_{64kDa} HA were made, with resulting gentamicin release shown in Figure 5.12. Indeed, the release rate was much faster when the MW of HA was brought down by several orders of magnitude. Additionally, similar dosage correlation as that observed for PAA film was found, namely that given a particular polyanion, the MW did not appear to influence encapsulated gentamicin dosage very much. Both $MW_{1.7MDa}$ HA and MW_{64kDa} HA resulted in 100-tetralayered films that released around $36\ \mu\text{g}/\text{cm}^2$. Hence, drug loading was more dependent on polymer chemistry rather than MW.

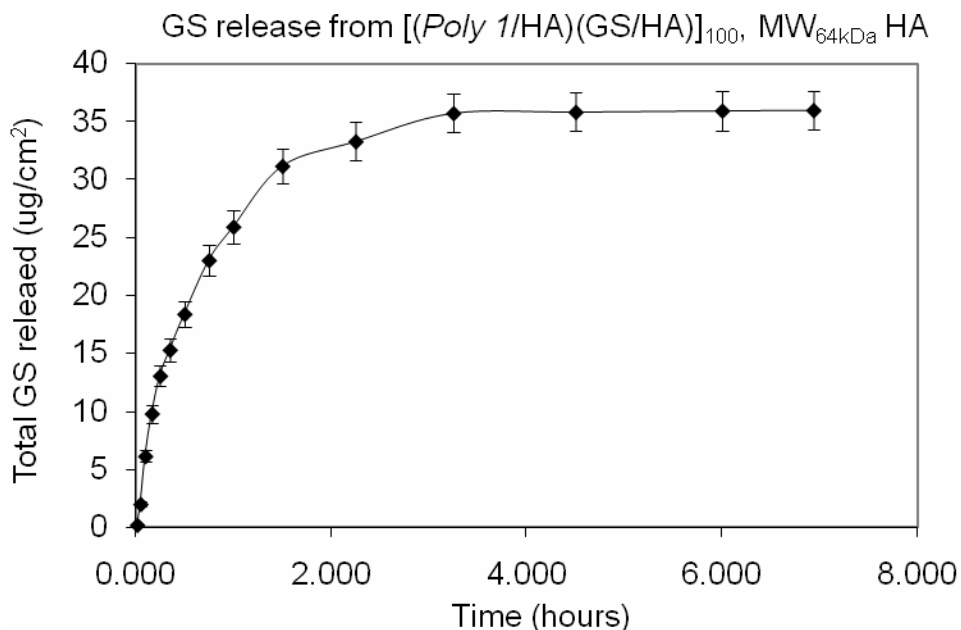


Figure 5.12 - Release of gentamicin from $[(Poly\ I/HA)(GS/HA)]_{100}$ in m-SBF at 37°C , with a MW_{64kDa} HA.

Although PAA appeared promising as an alternative polyanion, and both PAA and HA are FDA-approved for transdermal and topical applications, respectively, HA was favored due to its higher expected biocompatibility, as HA is an endogenous polysaccharide serving mostly as a structural component.

Conclusion. Molecular weight of the polyanion species, when varied over several orders of magnitude, has a significant impact on the release rate of gentamicin from a tetralayered film. However, the molecular weight has little impact on the encapsulation dosage. On the other hand, the polyanion chemistry does affect encapsulation dosage, although it does not appear to influence the release rate as much. The findings here may be specific to the release of small, hydrophilic drugs, and may not necessarily apply to tetralayers that encapsulate polysaccharides, proteins, or peptides. However, these observations suggest simple approaches to independently tuning the dosage and release rate within our film construct.

5.3 Physicochemical properties of [(Poly 1/HA)(GS/HA)]_n

5.3.1 Introduction.

In an effort to better understand the film properties, various physicochemical characterizations of the gentamicin films were carried out using microscopy, light scattering, and calorimetry. The goal was to identify any potential physicochemical trait, *e.g.* crystallinity, that could be used as control handles on drug release kinetics. Three different characterization methods were chosen: differential scanning calorimetry (DSC) to study the thermal transitions of the film and its individual components, scanning electron microscopy (SEM) to study the surface morphology of the film, and x-ray scattering, both small and wide angles (SAXS and WAXS), to study the crystallinity of the film and its individual components.

5.3.2 Materials and Methods.

Materials. All polymers, drugs, and chemicals used in dipping solutions, and methods of film sample preparation, were identical to those outlined under Section 5.1.2.

Film characterization. Differential scanning calorimetry (DSC) was done using a TA Instruments Q1000 differential scanning calorimeter with a scan range of -90 to 300°C at a rate of 10 °C/min. Scanning electron microscopy (SEM) studies were accomplished using a JEOL 6320FV scanning electron microscope at 10 kV. Small-angle X-ray scattering (SAXS) experiments were performed *in vacuo* with a Siemens

computer-controlled system with a rotating anode that produced Cu K α radiation ($\lambda = 1.54 \text{ \AA}$) at 40 kV and 30 mA on a free-standing film. Wide-angle X-ray scattering (WAXS) was done on a Bruker D8 Multipurpose Diffractometer. In the case of SAXS, film was scattered from a intact, free-standing film, while in the case of WAXS, the film had to be scraped into small pieces for loading into the cell. All the individual film components were scattered as a dense collection of solid powders.

5.3.3 Results and Discussion.

5.3.3.1 DSC.

An overlay of DSC spectra from the film and individual components is shown in Figure 5.13. *Poly I* had a distinct thermal transition around 70°C, which is mostly likely its melting temperature. HA and gentamicin had broad peaks around 120°C. Gentamicin has a reported melting point of 218-237°Cⁿ and is known to withstand steam sterilization^{208, 209} (121°C at 15 psi under saturated steam). Hence, the broad gentamicin heat absorption in the 100-220°C range likely induced gradual structural changes and only caused complete melting at the upper end. Hyaluronic acid does not have a reported melting point, but the DSC data suggest that a 1.74MDa sample may have a melting point around 120°C. The width of the peak may be a reflection of the polydispersity of the HA sample. Interesting, HA showed positive heat flow around 250°C, which could either be an experimental artifact or actual structural rearrangement of HA resulting in heat release. For each

ⁿ The Merck Index, 12th edition, entry 4398.

of the four samples, heat ramp back down did not result in any peak, suggesting that irreversible degradation or changes had occurred by 300°C, as one would expect due to extremity of this high temperature. Most importantly, the DSC data revealed that the major thermal transition of the film (black) very closely matched that of HA, suggesting HA might constitute a majority of the film mass.

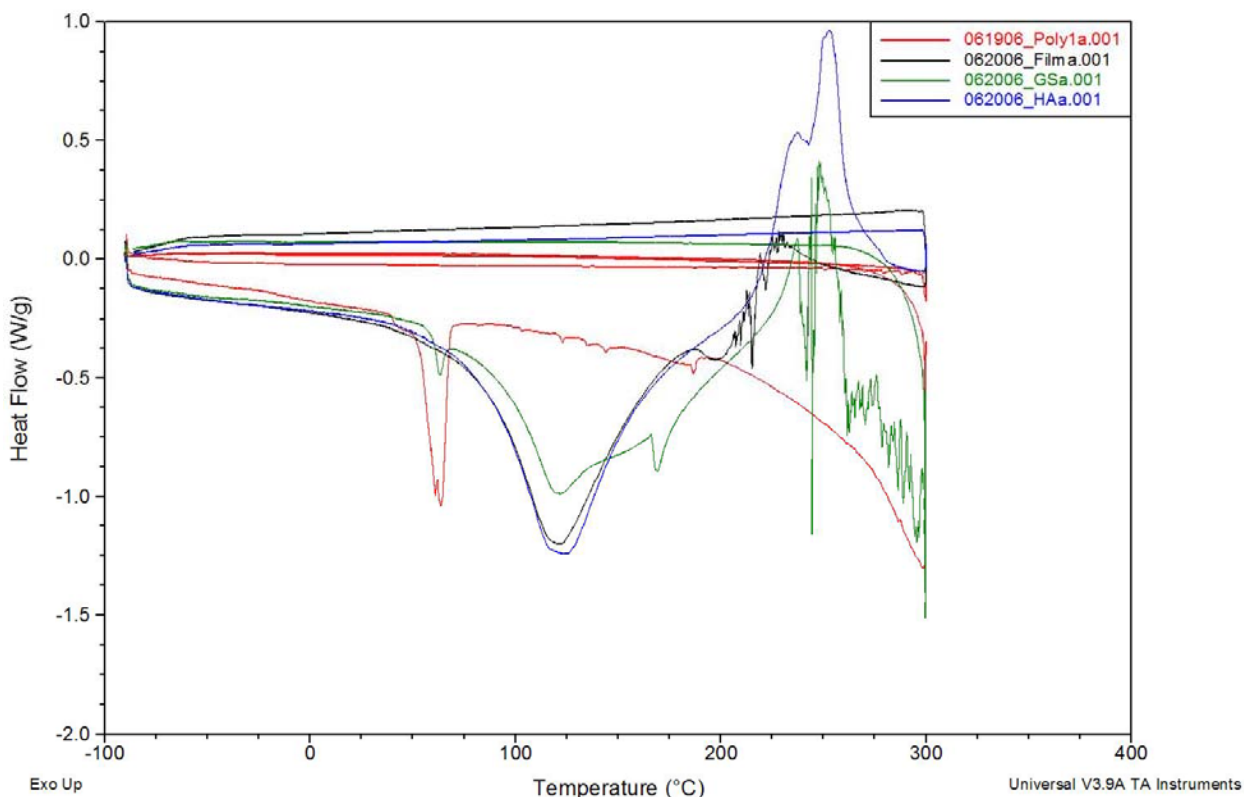


Figure 5.13 – Overlay of DSC spectra of $[(Poly I/HA)(GS/HA)]_{100}$ and individual film components. [red = *Poly I*, blue = hyaluronic acid, green = gentamicin, and black = film.]

5.3.3.2 SEM.

Figure 5.14 shows representative images from the SEM of the surface of a $[(Poly I/HA)(GS/HA)]_{100}$ film. No unusual morphological features were observed. Films were generally smooth with small specks of dust or other particulate attachments.

The “top” of the film, which would be on the bottom during the dipping process, tended to be thicker and rougher as revealed in the image of the bottom right corner. An intentional scratch revealed jagged scratch lines that suggested that the film had fairly good tensile strength.

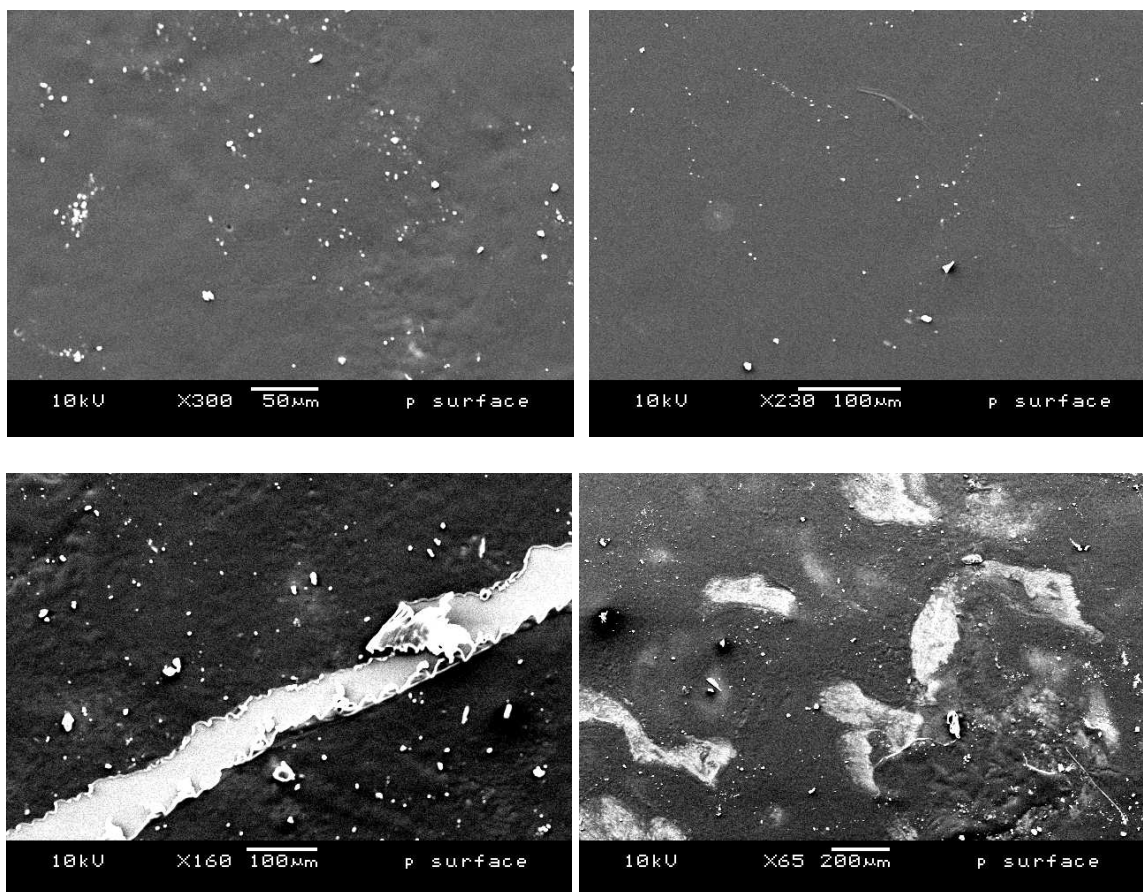


Figure 5.14 – SEM images of the surface of a [(*Poly I*/HA)(GS/HA)]₁₀₀ film.

Clockwise from top left: (1) 300x zoom, (2) 230x zoom, (3) 65x zoom on the “rough” top portion of the film, and (4) 160x zoom with an intentional scratch to reveal film thickness.

5.3.3.3 X-ray scattering.

Data from SAXS and WAXS of [(*Poly I*/HA)(GS/HA)]₁₀₀ films and individual film components are shown in Figure 5.15 and Figure 5.16. Images from SAXS reveal that both *Poly I* and HA had crystalline structures with several spacings as

suggested by the distinct rings on the scattering plot. Gentamicin solid was less crystalline, with only one distinct peak, while the intact free-standing film appeared more amorphous overall, with two less-defined rings. Hence, the crystallinity of individual polymers appeared to not be preserved within the film, and these polymers did not establish new crystalline structures within the film.

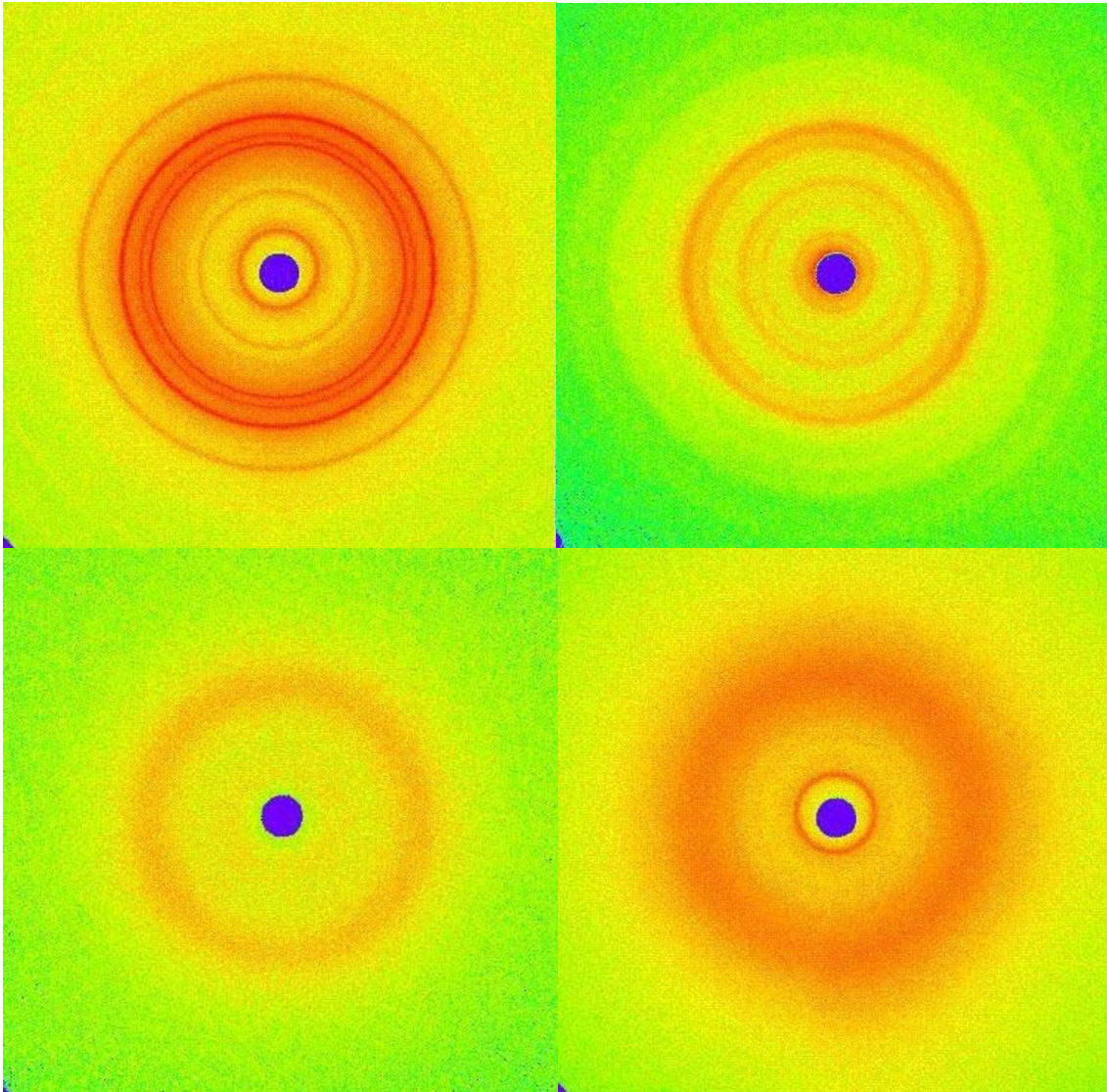
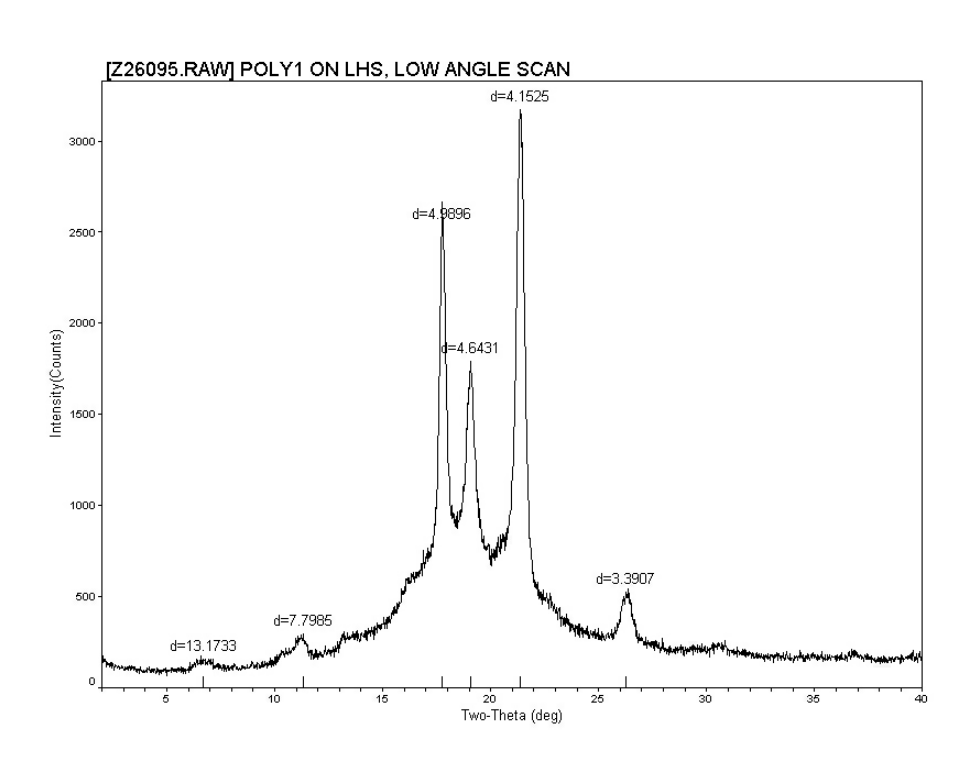
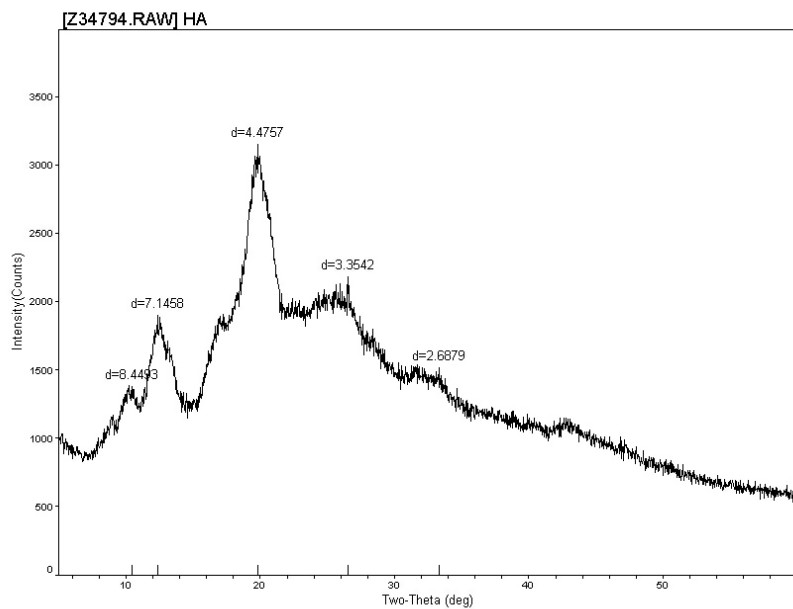


Figure 5.15 – SAXS images of $[(Poly\ I/HA)(GS/HA)]_{100}$ and its individual film components. Clockwise from top left: (1) *Poly I* (~10 kDa), (2) hyaluronic acid (1.74 MDa), (3) gentamicin sulfate, and (4) $[(Poly\ I/HA)(GS/HA)]_{100}$.

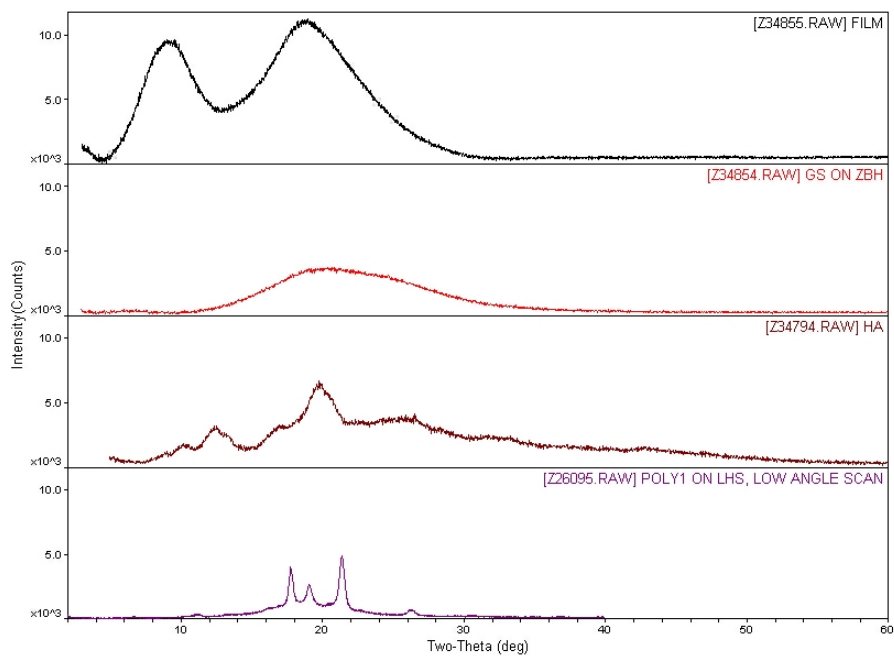
Data from WAXS support observations made from SAXS. In Figure 5.16 (a) and (b), *Poly 1* and HA were again observed to have very distinct scattering peaks, with d-spacings marked on the plots. WAXS data on gentamicin and scraped film are shown in the composite plot in Figure 5.16 (c), which suggests that the film had a dominant contribution from either gentamicin or HA. Interestingly, the WAXS overlay also clearly revealed a unique peak from the film sample not present in any of the individual film components, with a d-spacing of approximately 8.5. This could be a unique structural feature of the film, though it is not clear which film components interacted in what manner to result in this feature.



(a) *Poly 1*



(b) HA



(c) Composite of film, gentamicin, HA, and Poly I

Figure 5.16 – WAXS data on [(Poly I/HA)(GS/HA)]₁₀₀ and individual film components.

(a) Poly I, (b) hyaluronic acid, and (c) film.

5.3.4 **Conclusion.**

Physicochemical characterizations on [(Poly 1/HA)(GS/HA)]₁₀₀ and its individual components suggested that the film was generally smooth on the surface, amorphous in matrix structure, and large composed of HA. Most of the observations were within our expectations, although the unique d-spacing exhibited by the film under WAXS may be linked to a distinctive structural feature that can be further probed.

5.4 PLGA Encapsulation of Gentamicin

5.4.1 Introduction

In seeking methods for extending release timescale and allowing for additional degrees of control over release rate, I ran proof-of-concept experiments examining PLGA (poly(lactic-*co*-glycolic acid)) nanoencapsulation of gentamicin. PLGA nano- and micro-encapsulation has been well characterized for the delivery of a variety of drugs ranging from small molecules to proteins or even cells^{20, 126, 180, 210-216}. In fact, PLGA has been used for encapsulation and release of gentamicin^{126, 215-217} and one of the systems was found to be sterilizable by irradiation²¹⁷. PLGA spheres are naturally negatively charged on their surface, making them suitable for layer-by-layer deposition. With the assistance of Dr. Yoon Yeo, a postdoctoral fellow in the Langer group, I constructed PLGA nanospheres encapsulating radiolabeled gentamicin, then directly bilayered the nanospheres with *Poly I* and characterized the resulting release dosage and kinetics.

5.4.2 Materials and Methods

Materials. PLGA with 50/50 lactic:glycolic ratio, inherent viscosity (IV) of 0.67 (corresponding to MW ~ 44kDa, see Figure 5.18), and carboxylate end functionalization was kindly supplied by Dr. Frank Gu of the Langer group and originally ordered from LACTEL Absorbable Polymers (Cupertino, CA). Methylene chloride and poly(vinyl alcohol) (PVA) were supplied by Dr. Yoon Yeo.

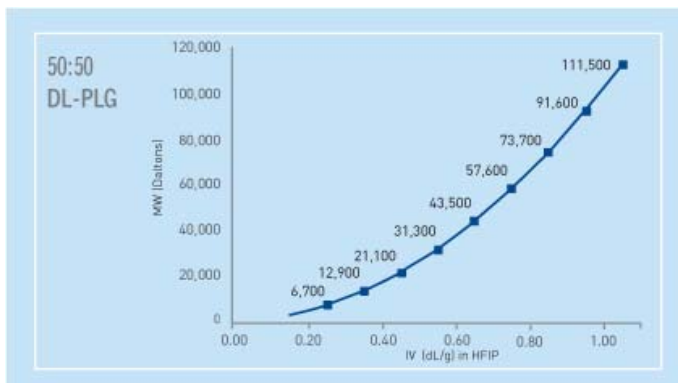
Figure 5.17 - MW versus IV correlation for a 50:50 PLGA copolymer.

© DUREC 2007, <http://www.absorbables.com/inherentviscosity.htm>

Nanoparticle formation. The encapsulation protocol was adopted from Dr. Yeo's procedure and modified by her for optimal gentamicin loading. 100 mg of PLGA was dissolved in 2.5 mL methylene chloride (A). 25 mg of gentamicin, which includes 18.7 ug of ³H-labeled form, was dissolved in 0.1 mL of 0.5% PVA solution at pH 6.0 (B). Solution B was then added to solution A, with resulting mixture sonicated for 1 min using a Vibracell VC-250 sonicating probe (Sonics & Materials Inc., Dunbury, CT) to generate a w/o emulsion. The emulsion was then directly added to 10 mL of 1% PVA solution, with resulting mixture sonicated for 3 min to generate a w/o/w emulsion. The w/o/w emulsion was then poured into 10 mL of distilled water and stirred for 3 hours at room temperature. Particle sizes were measured by ZetaPALS (Phase Analysis Light Scattering, by Brookhaven Instruments Corporation, Holtsville, NY). The resulting solution was directly used for layer-by-layer construction without lyophilization or further purification. As a comparison between standard versus adopted protocol for PLGA nanoencapsulation, Table 5 summarizes experimental parameters for these different protocols.

Table 5 - PLGA nanoencapsulation procedure parameters.

Comparing between standard Langer lab protocol (JAC), Dr. Yoon Yeo's protocol, and the one modified for gentamicin encapsulation.



	JAC	Yeo	Gentamicin
PLGA*	200 mg	500 mg	100 mg
PLGA solvent*	5 ml ethyl acetate	10 ml MC	2.5 ml MC
Drug	5-50 mg gentamicin	50 mg albumin	25 mg gentamicin
Drug solvent	0.2 ml 0.5% PVA (pH 6.0)	2 ml DW	0.1 ml 0.5% PVA (pH 6.0)
W/O	Sonication for 1 min	Sonication for 1 min	Sonication for 1 min
W/O/W	2 ml 1% PVA	50 ml 1% PVA	10 ml 1% PVA
W/O/W method*	Sonication	Sonication	Sonication for 3 min
W/O/W/W	50 ml 0.2% PVA	250 ml DW	15 ml DW
Purification	12,000 rpm x 30 min	16,000 rpm x 20 min	No purification

Multilayer buildup with nanospheres. Standard layer-by-layer deposition cycles were employed, using 2 mg/mL of *Poly I* in 0.1M sodium acetate as the polycation solution and the as-made PLGA nanosphere solution as the polyanion solution. Typical deposition times (10 min in each polyion bath) and rising cycle (15, 30, and 45 seconds in three separate baths of MilliQ water for each polyion) were used, and films were deposited on cleaned silicon chips with (LPEI/PSS)₁₀ base layers.

Measurement of gentamicin release. Standard gentamicin release measurement via scintillation counting was conducted. Briefly, film substrates were immersed in 25 mL of m-SBF (modified simulated body fluid) at 37°C, and 1 mL aliquots were taken at pre-determined time points. Each aliquot was then analyzed by adding 5 mL of ScintiSafe Plus 50% (Fisher Scientific, Atlanta, GA) prior to reading by Tri-carb liquid scintillation counter (Model U2200).

5.4.3 Results and Discussion.

Nanoparticle size and surface charge. The size and surface charge of the PLGA-gentamicin nanoparticles were measured by ZetaPALS. For a fresh suspension taken right after the last step of the synthesis procedure, triplicate readings yielded mean diameter of 417.3 ± 10.8 nm, with a polydispersity of 0.214 ± 0.012 . ξ -potential was -7.25 ± 1.21 mV, consistent with our expectation of a negatively-charged surface that would arise from the carboxylate groups of PLGA.

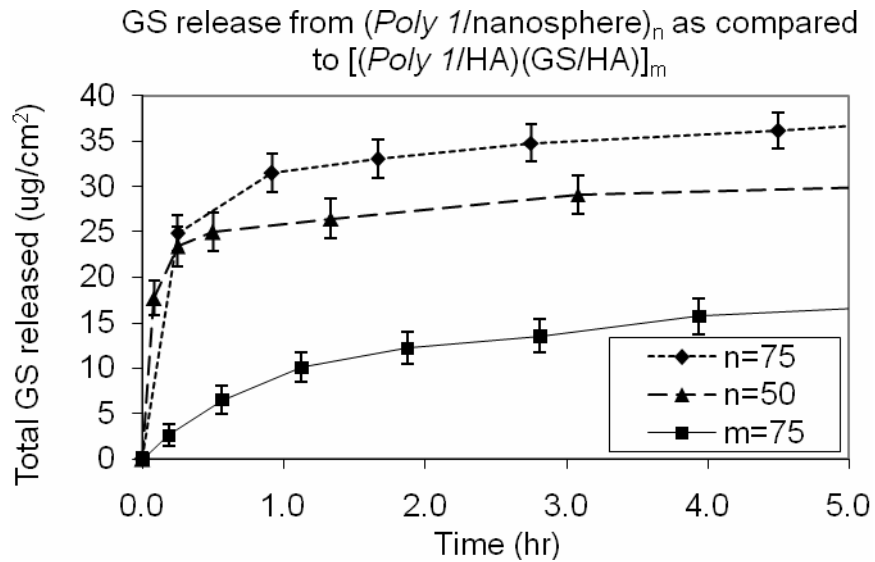
As an assessment on the stability of these particles, a fraction of the suspension was left at room temperature overnight. The resulting suspension had a mean diameter of 348.8 ± 21.7 nm, with polydispersity of 0.0775 ± 0.075 . ξ -potential had reduced to -4.52 ± 1.20 mV. Overall there was a 16.4% reduction in diameter accompanied by a 63.8% reduction in polydispersity, suggesting particle degradation at a modest rate, with larger particles degrading faster relative to their sizes. The concomitant reduction in ξ -potential could be due to physical or chemical modification of the surface carboxylate groups. For example, the additionally released gentamicin could adsorb to the carboxylate groups to neutralize particle surface charge. Further ZetaPALS assessment of particle suspension at 4°C or -20°C conditions would help to better define a storage protocol. Nevertheless, the stability of the PLGA nanoparticles at room temperature appeared sufficient for LbL deposition purposes. Hence, a fresh solution was prepared for LbL assembly of $(Poly\ I/PLGA\ particle)_{50, 75}$, a process which occurred over a period of 24-26 hours.

Fabrication of and release from nanoparticle LbL assembly. The as-made PLGA-gentamicin suspension was directly used as the dipping solution in the LbL assembly process. One caveat of directly using the PLGA nanosphere emulsion without further purification is that it contains a mixture of nanoparticles, free PLGA, free gentamicin, and other inactive ingredients such as PVA. The solution was not under the standard 0.1M sodium acetate buffer condition that was usually used for our multilayer construction. However, for this proof-of-concept experiment, I believed that using the unmodified emulsion was acceptable because: (1) *Poly X* was still fairly stable at pH 6.0, (2) methylene chloride, PVA, and gentamicin would not readily adsorb during the LbL deposition process due to their lack of polymeric nature or negative charge, and (3) though some free PLGA remained, the concentration was assumed to be sufficiently low to not compete with adsorption of the nanospheres.

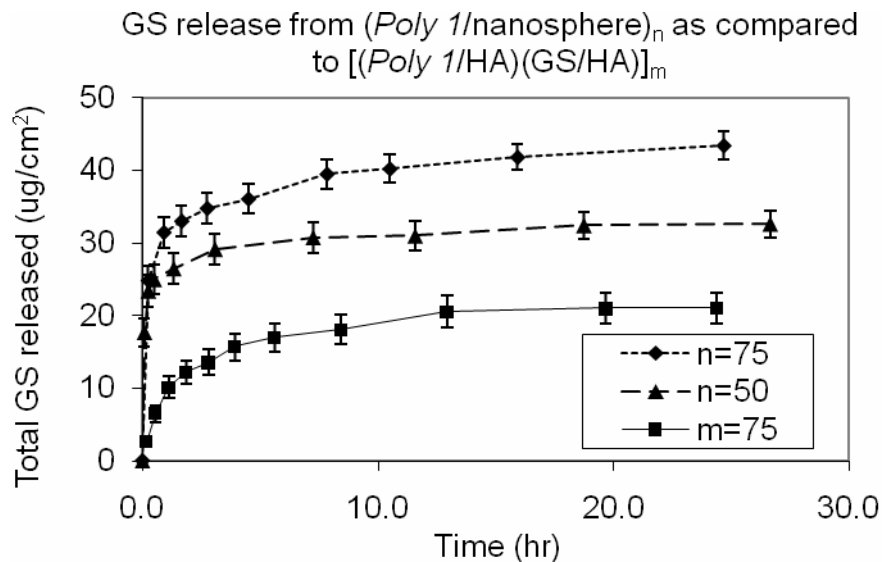
(*Poly I*/nanosphere)_n films were made with n = 50 and 75. The resulting films underwent gentamicin release assessment using the standard scintillation counting protocol. One concern was that the current release protocol would not distinguish between released versus PLGA-encapsulated gentamicin in the release buffer.

However, Dr. Yeo believed that the PLGA nanospheres would easily deconstruct within minutes, as hydrophilic molecules like gentamicin are not favorable for this encapsulation process. Hence, most of the gentamicin in the release buffer should be in its free solution form, so that the scintillation reading would be a reasonably accurate measurement of *in vitro* available gentamicin.

Figure 5.18 shows the release curves of $(Poly\ I/nanosphere)_n$ for $n = 50$ and 75 , vs. a traditional tetralayered film with 75 tetralayers. While nanosphere films exhibited good drug loading, the associated gentamicin releases were actually faster than a $[(Poly\ I/HA)(GS/HA)]_m$ film, with a more notable burst release at the beginning. Hence, pre-encapsulation of gentamicin by PLGA did not result in more sustained release. Again, some of the scintillation-counted gentamicin could be encapsulated within PLGA nanospheres that were released from the film but had not degraded to release its gentamicin content, and thus the release of *free-solution* gentamicin could be more sustained than observed. However, this scenario was not likely based on Dr. Yeo's input on the stability of PLGA nanospheres incorporating small hydrophilic molecules.



(a)



(b)

Figure 5.18 - Gentamicin release from films made with free or pre-encapsulated gentamicin, in comparison to tetralayers incorporating non-modified gentamicin.

(a) zoomed into the first 5 hours to display initial burst, and (b) complete release over 25 hours.

One method to further probe the release mechanism would be to measure the erosion curve of $(Poly\ 1/nanosphere)_n$ films and correlate film erosion rate to that of gentamicin release. Similarly, establishing the growth curve of $(Poly\ 1/nanosphere)_n$ films could also further elucidate mechanisms of release, as the shape of the growth

curve may suggest degree of diffusivity of the nanoparticles within the film.

Additionally, ZetaPALS could be run in fresh release fractions to detect the presence of undegraded PLGA particles.

5.4.4 Conclusion.

Proof-of-concept experiments of LbL incorporation of PLGA-gentamicin nanoparticles were conducted with intended goal of achieving more sustained gentamicin release. However, the $(Poly\ I/nanosphere)_n$ films were found to release gentamicin more rapidly than $[(Poly\ I/HA)(GS/HA)]_m$ films based on scintillation counting of radiolabeled species. Nevertheless, this approach could still be promising because (1) the protocol for PLGA encapsulation of gentamicin could likely be optimized further, *e.g.* through PLGA MW, copolymer ratio, solvent choice, and sonication parameters, (2) the dipping condition for the PLGA-gentamicin nanoparticles was not optimized, and (3) the observed gentamicin release from scintillation counting may reflect gentamicin still encapsulated within PLGA particles. Additional experiments in growth curve, erosion curve, and light scattering on release fractions could further elucidate the release mechanism and aid with optimization of the protocol.

Even if optimized PLGA encapsulation does not result in more sustained and controllable release of gentamicin, it may still be a promising approach for LbL incorporation of other small molecule therapeutics, especially hydrophobic ones. In general, encapsulation approaches involving particles, vesicles, or micelles are all

promising methods for more tunable incorporation of small molecule drugs into LbL film, and active efforts are under way in our laboratory.

Acknowledgements.

Many thanks go to Dr. Yoon Yeo, who helped me with researching literature, designing the encapsulation protocol, and running the experiments with me. I also would like to thank Dr. Daniel Kohane for his initial consultation with this research, and Dr. Jordan Green for training and assistance on ZetaPALS.

References.

- (1) Anderson, J. M. and Shive, M. S. *Advanced Drug Delivery Reviews*, **1997**, 28, 5-24
- (2) Burton, K. W., Shameem, M., Thanoo, B. C. and Deluca, P. P. *Journal of Biomaterials Science, Polymer Edition*, **2000**, 11, 715-729
- (3) Cohen, S., Yoshioka, T., Lucarelli, M., Hwang, L. H. and Langer, R. *Pharmaceutical Research*, **1991**, 8, 713-720
- (4) Jackanicz, T. M., Nash, H. A., Wise, D. L. and Gregory, J. B. *Contraception*, **1973**, 8, 227-234
- (5) Lu, W. and Park, T. G. *PDA Journal of Pharmaceutical Science and Technology*, **1995**, 49, 13-19
- (6) Ogawa, Y., Okada, H., Yamamoto, M. and Shimamoto, T. *Chemical & Pharmaceutical Bulletin*, **1988**, 36, 2576-2581
- (7) Okumu, F. W., Cleland, J. L. and Borchardt, R. T. *Journal of Controlled Release*, **1997**, 49, 133-140
- (8) Monika Schlapp, W. F. *Journal of Pharmaceutical Sciences*, **2003**, 92, 2145-2151
- (9) Narahariseti, P. K., Lee, H. C. G., Fu, Y.-C., Lee, D.-J. and Wang, C.-H. *Journal of Biomedical Materials Research Part B: Applied Biomaterials*, **2006**, 77B, 329-337
- (10) Price, J. S., Tencer, A. F., Arm, D. M. and Bohach, G. A. *Journal of Biomedical Materials Research*, **1996**, 30, 281-286
- (11) Friess, W. and Schlapp, M. *European Journal of Pharmaceutics and Biopharmaceutics*, **2005**, 63, 176-187

5.5 Methods for Film Sterilization

5.5.1 Introduction

Since the designed drug delivery coatings were to be applied onto medical implants, assessment of film robustness under FDA approved methods of sterilization would eventually be needed. Approved methods include autoclave (steam sterilization), ethylene oxide, irradiation, dry heat, and gas plasma²¹⁸, with the former three being the most commonly practiced and accepted methods²¹⁹. Each sterilization method is described further below:

Steam sterilization, or autoclaving, is the most commonly practiced sterilization technique for *in vitro*, *in vivo*, and clinical settings. It is fast, effective, simple, and leaves no toxic residues. Through exposure of the substrate to saturated steam at an elevated temperature, microorganisms are killed due to denaturation of proteins and lipids²¹⁸. However, the same temperature and humidity conditions are also expected to degrade numerous biopolymers.

As an alternative to steam sterilization, dry heat is also an accepted method for sterilizing certain medical devices^o. To make up for the lack of high pressure and humidity necessary to ensure complete killing of microorganisms, dry heat treatment requires high temperatures for longer exposure times.

Ethylene oxide (EtO) is a popular alternative to steam sterilization for materials that cannot withstand the high temperature. Processing typically occurs at 30-50°C with

^o From CDC website, http://www.cdc.gov/ncidod/dhqp/bp_sterilization_medDevices.html.

40-90% humidity, with EtO gas concentration of 0.6-1.2 g/L, from several hours to 2 days²¹⁸. EtO is a reactive molecule that alkylates sulfhydryl, amino, carboxyl, phenolic and hydroxyl groups in nucleic acids, causing cell injury or death. Hence, a principal disadvantage of EtO sterilization is the residual toxic gas, and all EtO-treated materials require hours or even weeks of aeration before use²²⁰. In addition, EtO may not thoroughly penetrate some materials. While certain subclasses of polyethylene, polycarbonate, and poly(L-lactic acid) were found to withstand EtO treatment without changes in molecular weight or materials properties^{221, 222}, others were found to be significantly modified by EtO, especially polyurethanes²²³. Not as much has been reported on polyesters or polysaccharides, but given the variety of functional groups available on these polymers, it is conceivable that EtO treatment would affect film properties through modifying polyelectrolyte backbone structures and hence disrupting electrostatic and van der Waals interactions.

In terms of irradiation sterilization, two types of treatments are available: gamma rays from ⁶⁰Co, or accelerated electron beams. It is an alternative to materials that cannot withstand steam sterilization, with several advantages over ethylene oxide including excellent penetration, dose uniformity, and lack of toxic residues. The process generates free radicals and causes oxidation to biomolecules. However, it has drawbacks of its own. Aside from its high capital cost, gamma irradiation is also known to degrade many biomaterials. A broad survey of the literature reveals that many natural and synthetic polymers experience a decrease in molecular weight and/or viscosity after irradiation²²⁴. The free radicals generated by irradiation could modify polymers through such mechanisms as chain scission or cross-linking²¹⁸. Sintzel *et al.* gives an excellent review of the effect of irradiation on many types of polymers including polyesters, polyurethanes, polysaccharides, polypeptides, *etc.*²²⁴.

As an example, hyaluronic acid is sensitive to gamma irradiation due to the resulting glycosidic cleavage²²⁵. Several classes of polyesters and poly(ortho esters), such as PLGA, were found to have a decrease in M_w of 30-60% after standard irradiation treatment (2.5 million rads for 2 hours). As a further example of polymer sensitivity to sterilization, PLGA (poly(lactic-*co*-glycolic acid)) microparticles containing gentamicin were found to burst release the drug after ethylene oxide or gamma irradiation treatments²¹⁷. Hence, there was a high probability that [(*Poly* X/HA)(GS/HA)]_n films would not survive irradiation sterilization, but as a proof-of-concept, it would still be investigated.

A 70% v/v ethanol/water solution is commonly used in cell culture studies for sterilization. Ethanol kills bacteria by denaturing their proteins and dissolving their lipids and is in fact effective against many fungi and viruses as well²²⁶. A 70% mixture with water is found to be optimal in the denaturing action against hydrophilic proteins. Due to low penetrability and potentially non-uniform coverage, surface treatment with 70% ethanol is not an accepted method for sterilizing medical implants and instruments for human patients. However, it is accepted for sterilizing implanted materials used in small animal studies, and hence would be a viable method for *in vivo* experiments involving rabbits. Due to its mechanism of action, ethanol treatment is not suitable for films that contain proteins. However, ethanol should be safe on synthetic and natural polymers without tertiary structures.

Gentamicin and aminoglycosides in general are known to withstand harsh sterilization conditions such as autoclaving and dry heat^{208, 209}. Aside from its primary and secondary amine groups, gentamicin does not contain reactive functionalities that can

be easily modified by chemical methods such as ethylene oxide. However, the polyelectrolyte components of the film, *i.e.* poly(β -amino ester) and hyaluronic acid, may be highly susceptible to heat, humidity, irradiation, and chemical treatments, especially given the reported results summarized above. In fact, differential scanning calorimetry (see Section 5.3.3.1) data suggested that *Poly I* had a melting temperature around 70°C, implying that any sterilization that imposes a temperature above that may not be suitable for *Poly I*-based films. In addition, biologic drugs such as polysaccharides, peptides, and proteins may also be sensitive to standard sterilization techniques and will need to be examined on a drug-by-drug case.

As a proof-of-concept assessment of the stability of hydrolytically degradable coatings under various sterilization methods, [(*Poly I*/HA)(GS/HA)]₁₀₀ films were subject to several treatment methods and evaluated on release dosage and kinetics. The rate of drug release, in comparison to an untreated film, was used as a rough indicator of the degree of degradation of the coating. In defining a final sterilization protocol, additional parameters such as film morphology, thermal properties, and surface bioactivity will also need to be examined.

5.5.2 Materials and Methods

Materials. All polymers, drugs, fluids, and substrates used for making multilayer thin film samples under this study were from the same sources as other studies under this thesis. Simax glass rods (group 3.3 of clear hard borosilicate glasses) with outer diameter of 3 ± 0.10 mm were ordered from Friedrich & Dimmock (Millville, NJ).

Preparation of film samples. $[(Poly\ I/HA)(GS/HA)]_n$ film samples on either silicon or glass rods were deposited via the layer-by-layer technique by a slide stainer using the standard protocols on dipping solution preparations and dipping cycles. Glass rods were cut into 1" long samples using a diamond scribe, and plasma-etched for 5 min (in contrast to the 1 min treatment for silicon substrates) prior to $(LPEI/PSS)_{10}$ base layer deposition. After complete film deposition, the top 1-cm portion of the rod was cut off as the actual coated sample. Teflon holders for glass rods for mounting onto the slide stainer were custom made by the MIT Central Machine Shop.

General consideration for sterilization. Film samples were always placed in appropriate closed secondary containers to avoid contamination to the equipment. For example, in the case of steam sterilization, film substrates were placed in autoclavable metal boxes. After sterilization, a wipe test was performed on the interior and exterior of the container and surfaces of the equipment around the container.

Steam Sterilization (Autoclave). Autoclaving of samples were performed in the autoclave in the tissue culture area of the ISN on the 4th floor. Samples were placed in

an autoclave-safe box and autoclaved at 121°C at 15 psi under saturated steam for 30 min with 15 min of drying.

Dry Heat. Dry heat sterilization of samples was performed by placing samples in a 160°C oven for 2 hours. Samples were placed inside a pre-heated closed glass Petri dish.

Ethylene oxide. Ethylene oxide (EtO) sterilization of samples was performed in an Anprolene AN74ix system by Andersen Sterilizers (Haw River, NC) using the 12-hour cycle. The equipment is located in the E25 animal facility in the basement, and sterilization was performed by the veterinary technicians. Samples were placed in a Seal and Peel® waterproof bag. Sterilized samples were left to degas under ambient conditions for at least 24 hours before retrieval for analysis.

Gamma irradiation. Gamma irradiation of samples was performed in Gammacell 220 located in 6-107, with assistance and supervision from Chris Tavares of the MIT Radiation Protection Office. Irradiation was administered at 2.5 million rads for 2 hours to achieve FDA-approved level of sterilization. Samples were sealed in a water-tight container and placed in a cup with ice to avoid over-heating by the irradiation process. Dry ice was not used as the irradiation cell could be sealed airtight, and the sublimed carbon dioxide could build up dangerous pressure.

Ethanol treatment. Ethanol sterilization of samples was performed by immersing samples in 70% v/v ethanol/water mixture for define periods of time. After treatment, samples were air-dried prior to drug release assessment.

5.5.3 Results and Discussion.

Steam Sterilization (Autoclave). Poly(β -amino esters) were not expected to survive steam sterilization due to their water-labile nature. Nevertheless, a quick test of autoclaving on $[(Poly\ I/HA)(GS/HA)]_{100}$ films was performed to assess the degree of degradation to these films. The autoclaved films were visually much smoother than the untreated films, suggesting that the films had “melted” and reannealed during the sterilization process. The resulting gentamicin release profiles are shown in Figure 5.19, which presents cumulative amount of gentamicin released from autoclaved and unautoclaved films as a function of time.

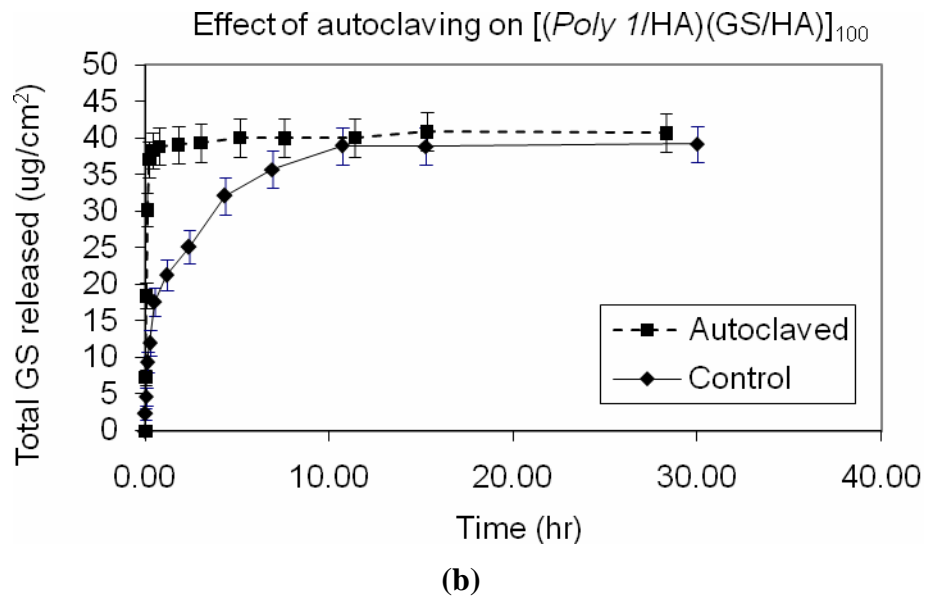
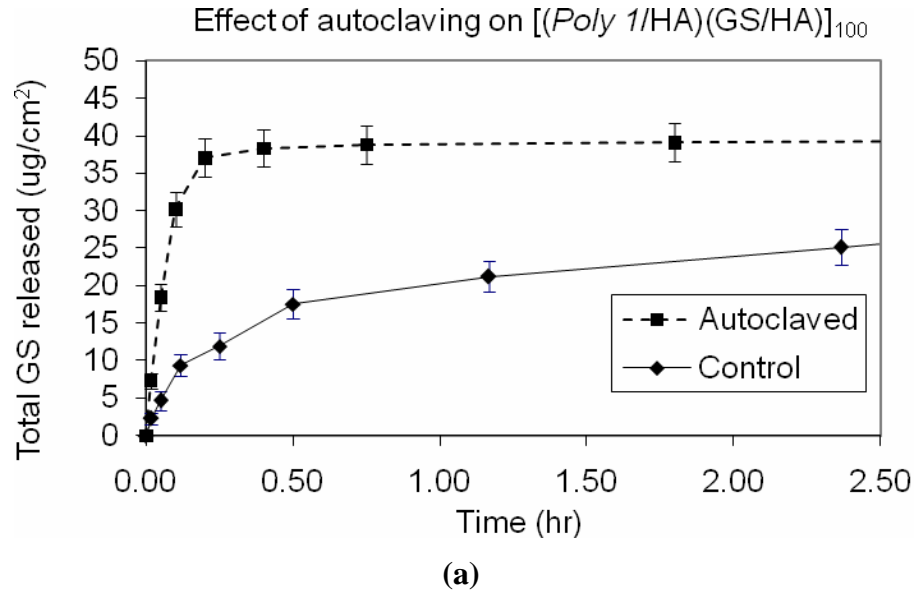


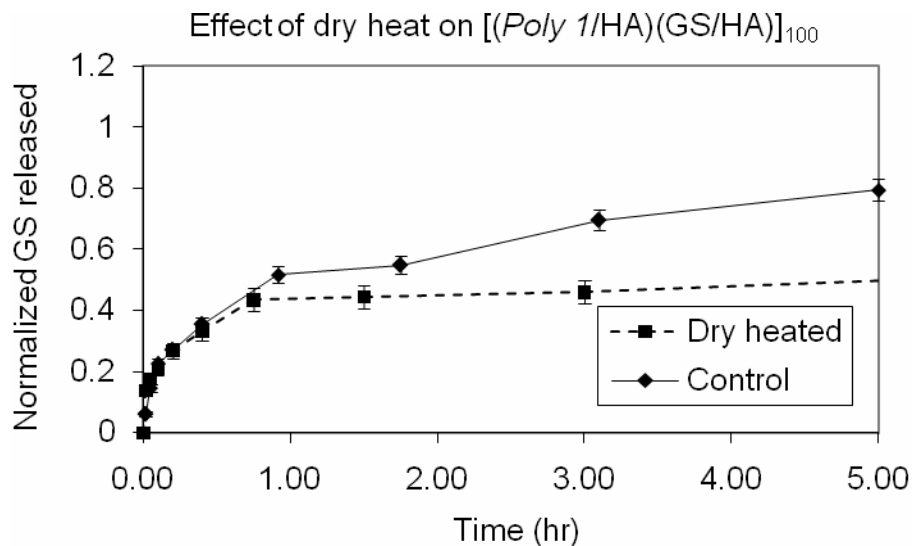
Figure 5.19 - Comparing gentamicin release from untreated versus autoclaved $[(Poly\ 1/HA)(GS/HA)]_{100}$.

(a) zoomed into the first 2.5 hrs, (b) complete release over 30 hrs.

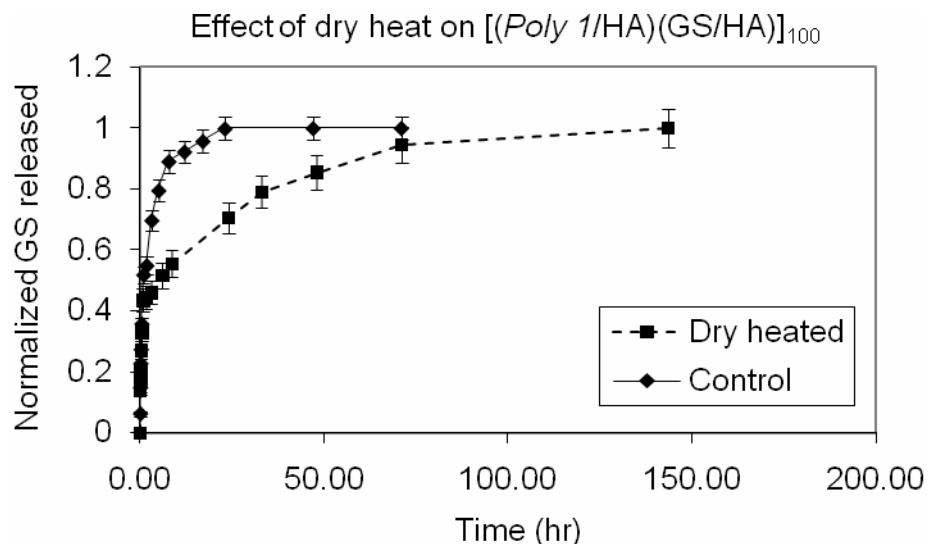
It is apparent autoclaving significantly degraded the films so that gentamicin was burst released. This result was as expected – that steam sterilization imposed more heat and

humidity than the amount that can be tolerated by hydrolytically degrade poly(β -amino esters).

Dry Heat. For dry heat sterilization, CDC guidelines specify 160°C for 2 hours in the case of a non-circulating oven²²⁷, and this is the condition used to dry heat the samples under this study. After dry heat treatment, the three film samples were visibly charred and burnt onto the silicon substrate. While this sterilization method was obviously not viable, I assessed gentamicin release from these burnt films out of curiosity. A representative release profile is shown in Figure 5.20, along with comparison to an unheated film.



(a)



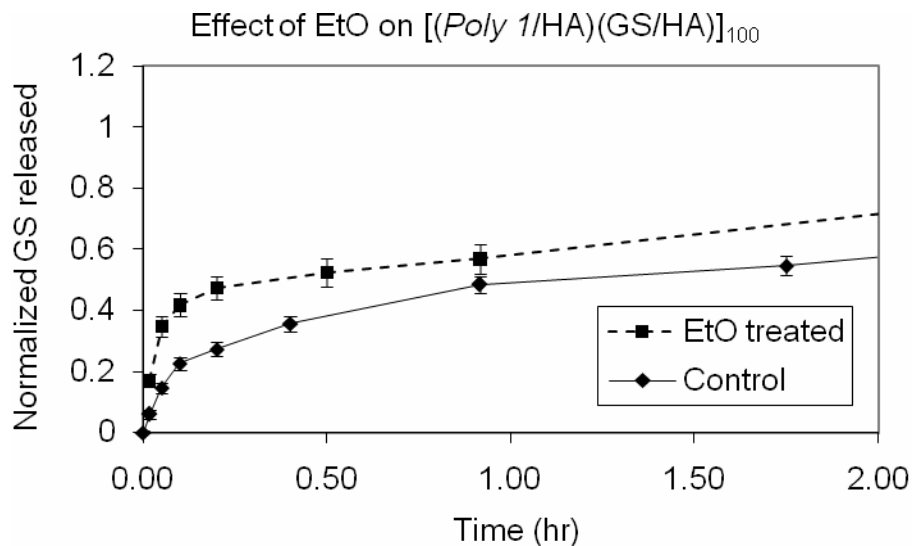
(b)

Figure 5.20 - Normalized gentamicin release from untreated vs. dry heated $[(Poly1/HA)(GS/HA)]_{100}$. Data were scaled to the final cumulative released amount from each film. Dry heat treated film released a total of 13 $\mu\text{g}/\text{cm}^2$ gentamicin, while the control released a total of 36 $\mu\text{g}/\text{cm}^2$: (a) zoomed into the first 5 hrs, (b) complete release over 150 hours.

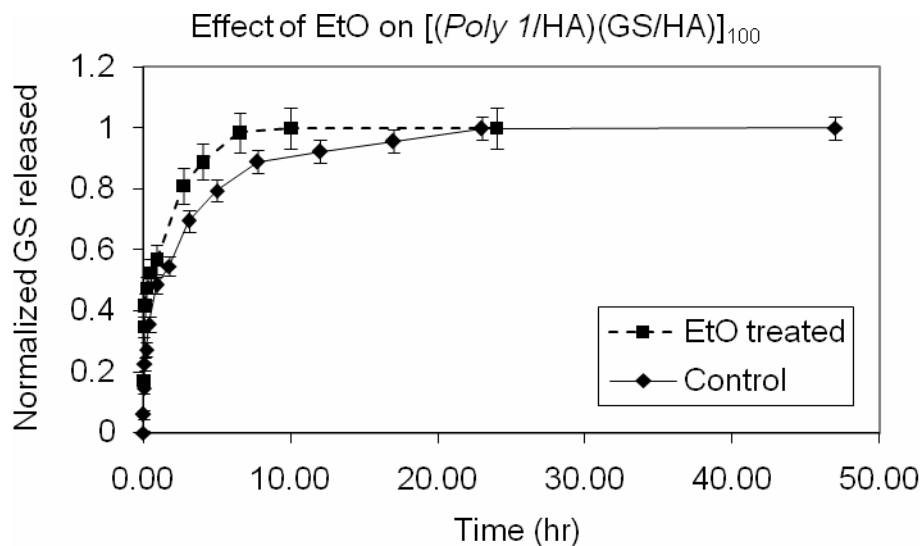
As Figure 5.20 (b) suggests, dry heat did indeed “fix” the film and resulted slower release of gentamicin, either through retardation of gentamicin diffusion through the film matrix, or through slower erosion of the charred film mass. However, the heat fixation did not eliminate the rapid burst release that occurred within the first hour.

Another interesting finding was that there was only an average of 13 $\mu\text{g}/\text{cm}^2$ of gentamicin released from the dry heat treated film, as compared to 36 $\mu\text{g}/\text{cm}^2$ of an untreated film. Either some gentamicin was “burnt off” during the treatment process, or permanently fixed into chunks of charred film which fell off from the silicon substrate but did not release the entrapped gentamicin. It is also possible, though less likely, that the dry heat treatment affected the ^3H label either by knocking it off its host gentamicin, so the low observed gentamicin release may not necessarily correspond to actual decrease in gentamicin delivery. However, a wipe test throughout the secondary container (glass Petri dish) did not reveal an appreciable amount of radioactivity, suggesting that gentamicin remained inside the charred film and was likely trapped within non-degrading pieces of films.

Ethylene Oxide. EtO treatments were performed by the E25 animal facility personnel in their Anprolene AN74ix system under a 12-hour cycle. Figure 5.21 presents results from EtO-treated versus untreated films in normalized gentamicin release.



(a)



(b)

Figure 5.21 - Normalized gentamicin release from EtO-treated vs. untreated [(Poly1/HA)(GS/HA)]₁₀₀. Data were scaled to the final cumulative released amount from each film. The EtO-treated version released a total of 20 $\mu\text{g}/\text{cm}^2$ of gentamicin, while untreated version released 36 $\mu\text{g}/\text{cm}^2$: (a) zoomed into the first 2 hrs, (b) complete release over 50 hours.

Figure 5.21 (b) suggests that on a longer timescale of 50 hours, the EtO treatment actually did not significantly impact the release kinetics of gentamicin. However, when we examine release first 2 hours (Figure 5.21 (a)), we see that an EtO-treated

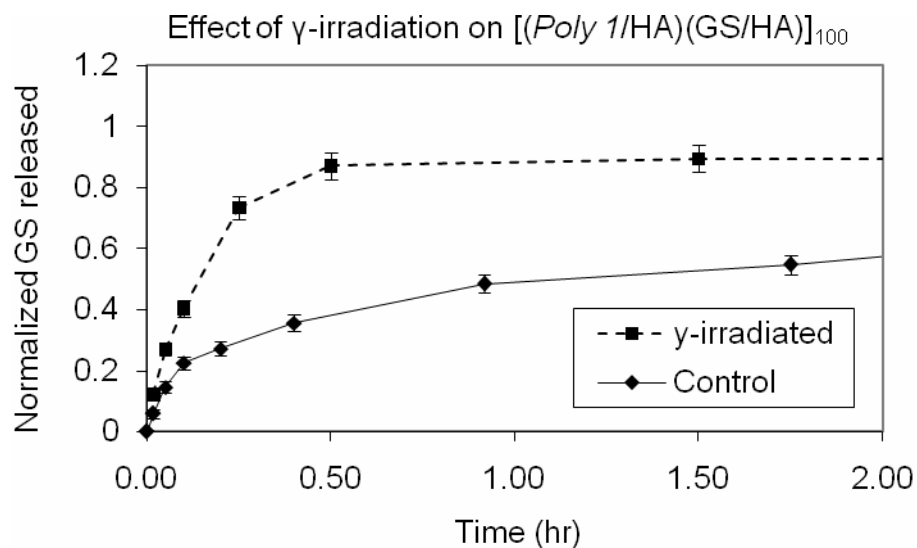
film burst released a bit more within the first 30 min. Hence, the EtO treatment did affect drug release properties of the film, though the effect was less pronounced than most other methods.

Since EtO only affected drug release kinetics within the first hour and preserved most of the multi-hour release afterwards, one possibility is that EtO did not penetrate all the way through the film, and instead only alkylated film components near the surface. Hence, only the release of gentamicin from the top layers was affected. By exponential growth theory, the top layers would contain most of the gentamicin, as seen with the 60% release within the first hour. Another theory is that EtO alkylation “loosened up” the film without affecting the polymer degradation rate, and hence the hypothesized early-phase diffusion-driven release of gentamicin was accelerated, while the late-phase degradation-driven release remained at a similar rate.

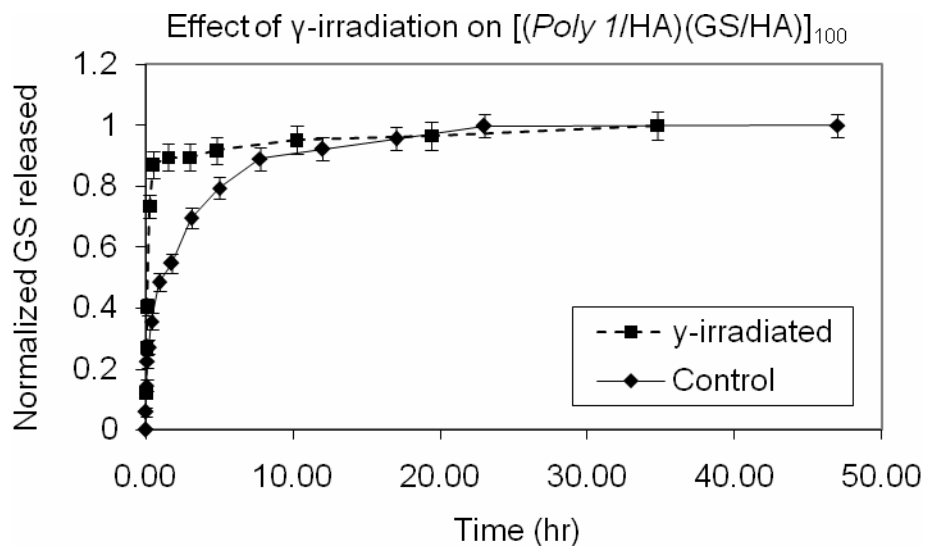
One puzzling observation was the decrease in observed gentamicin dosage after EtO treatment. Unlike films treated with dry heat, EtO-treated films were observed to degrade completely into the solution without leaving residual film pieces behind, and hence we would not expect film-trapped gentamicin. Even if the gentamicin was somehow conjugated to or packaged by either *Poly I* or HA, the released polymer-gentamicin composites should still give off scintillation signal. Therefore, the most likely scenario was the loss of gentamicin during the EtO treatment process. Perhaps the alkylation of polyelectrolytes caused reduction in electrostatic interaction with gentamicin, and some film was rubbed off in the sterilization bag.

Overall, EtO treatment is a potentially viable sterilization technique with less disruption to the drug release properties than most other methods. With proper optimization on operating parameters such as temperature, humidity, EtO concentration, and time, we may minimize any undesirable effect such as drug loss and initial burst.

Gamma Irradiation. As discussed in the introduction, γ -irradiation is known to cause degradation of many synthetic polymers. However, as a proof of concept, I proceeded to investigate the effect of this treatment on $[(Poly\ I/HA)(GS/HA)]_{100}$ films. The resulting gentamicin release is shown in Figure 5.22.



(a)



(b)

Figure 5.22 - Comparing gentamicin release from γ -irradiated vs. untreated $[(Poly 1/HA)(GS/HA)]_{100}$. Data were scaled to the final cumulative released amount from each film. The gamma irradiated version released a total of $16 \mu\text{g}/\text{cm}^2$ of gentamicin, while untreated version released $36 \mu\text{g}/\text{cm}^2$: (a) zoomed into the first 2 hrs, (b) complete release over 50 hours.

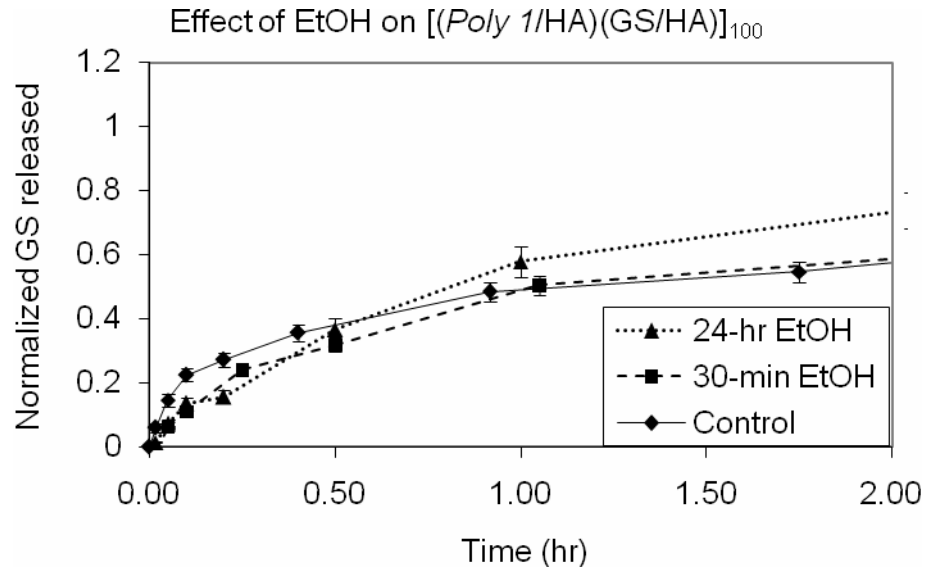
Similar to steam sterilization, gamma irradiation degraded the film components to the extent that all gentamicin was burst released within 30 min. Interestingly, a decrease in gentamicin dosage after irradiation was also observed. Unlike the case of dry heat

treatment, no fragments of film were observed in release buffer that would entrap gentamicin. It is possible that gamma rays interfered with the ability of the ^3H labels to scintillate. Having a protocol to quantify gentamicin without the use of radioactive labels would help clarify the cause of lower observed gentamicin dosage.

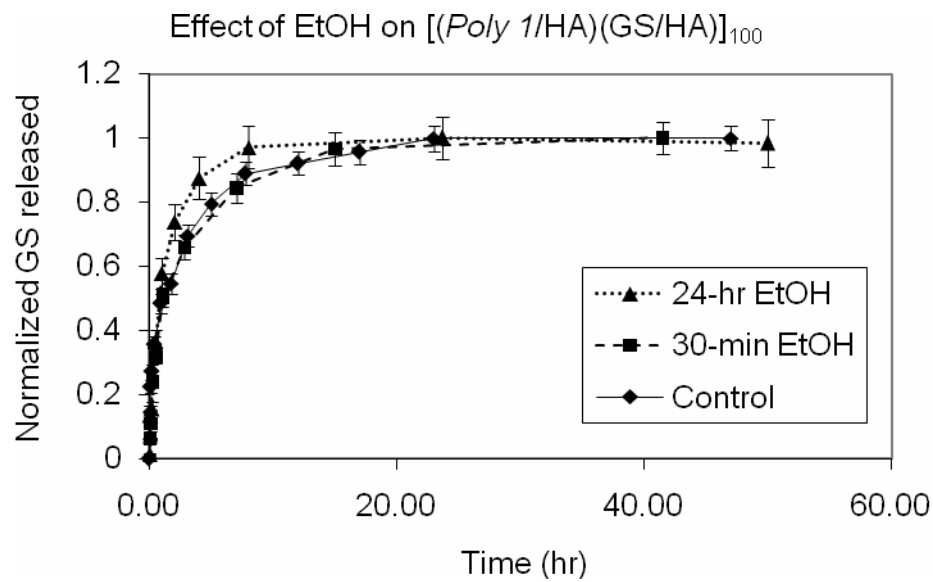
Regardless of the cause of gentamicin loss, gamma irradiation appears to significantly damage the film matrix to result in burst release. Hence, it is not a suitable method for sterilization of *Poly X*-based films.

Ethanol. Standard ethanol sterilization makes use of a 70% ethanol solution, and the 30% water content was concerning due to *Poly X*'s hydrolyzability. Deionized water generally exhibits pH around 5.0-5.5, in which *Poly I* has a half-life of 7-8 hours in free solution²³. However, *Poly X* deposited into a film should have a longer "film half-life" due to its less direct contact with the external aqueous environment.

Coupled with the 70% ethanol content, ethanol sterilization could be sufficiently non-degrading to a *Poly X*-based film. To assess the actual effect, a set of [(*Poly I*/HA)(GS/HA)]₁₀₀ films were immersed in 5 mL of 70% ethanol for either 30 min or 24 hours at room temperature. The used ethanol solutions were saved for assessing potential gentamicin leaching from the film. Figure 5.23 plots gentamicin release data from ethanol treatment.



(a)



(b)

Figure 5.23 - Comparing gentamicin release from $[(Poly\ 1/HA)(GS/HA)]_{100}$ films that are either untreated, or immersed in 70% ethanol for 30 min or 24 hrs.

Data were scaled to the final cumulative released amount from each film. The 30-min and 24-hr films released a total of $25\ \mu\text{g}/\text{cm}^2$ and $16\ \mu\text{g}/\text{cm}^2$ of gentamicin, while untreated version released $36\ \mu\text{g}/\text{cm}^2$: (a) zoomed into the first 2 hrs, (b) complete release over 50 hours.

Similar to the result observed under ethylene oxide treatment, the overall release rate was not significantly affected by the treatment. Interestingly, within the initial 30 min

(see Figure 5.23(a)), ethanol-treated films actually released gentamicin in a slightly more sustained fashion as compared to the untreated ones. The films might have rearranged or re-annealed during the ethanol immersion to result in more stable surface layers. However, over the course of a 24-hour immersion, the 70% ethanol treatment appeared to slightly destabilize the bulk and resulted in a faster release over a 20-hour timescale (see Figure 5.23(b)).

Another negative effect of the ethanol treatment was leaching of gentamicin during the treatment process. Thickness measurements were not taken before and after the treatment to compare overall film mass, though the immersion fluids were scintillation counted to assess amount of leached gentamicin. For the 30-min films, the scintillation readings of the three samples gave a mean of 1.9 $\mu\text{g/mL}$, or 9.5 $\mu\text{g/cm}^2$ released from each film given film sizes of 1 cm^2 . For the 24-hour films, the release solutions gave a mean of 3.5 $\mu\text{g/mL}$, translating to 17.5 $\mu\text{g/cm}^2$ loss. These numbers match well with those from the drug release assessments, which yielded an average of 10 $\mu\text{g/cm}^2$ and 20 $\mu\text{g/cm}^2$ for the 30-min and 24-hr treatments, respectively. This gentamicin loss should be taken into account for *in vivo* assessments of $[(\text{PolyI}/\text{HA})(\text{GS}/\text{HA})]_{100}$ film efficacy. Despite the confirmed leaching of gentamicin, the 70% ethanol treatment was chosen as the sterilization method for *in vivo* studies because it had the least impact on gentamicin release properties, and had less loss of gentamicin than EtO treatment. In addition, the loss of gentamicin was confirmed as being leached into the treatment solution, whereas in the case of many other techniques, the exact cause of loss is still unknown.

5.5.4 Conclusion.

Several sterilization methods were performed on [(*PolyI*/HA)(GS/HA)]₁₀₀ films to assess their effects on gentamicin release from these films. Among the FDA-approved methods of sterilizing medical devices, only ethylene oxide was found to not significantly degrade the films into a rapid burst release. However, the EtO treatment parameters, such as temperature, pressure, EtO concentration, humidity, and treatment time, should be optimized for minimal interference to film integrity. However, EtO may ultimately not be the ideal sterilization method, as it can easily damage biomolecules and hence is unsuitable for films delivery proteins, peptide, and nucleic acids. Other sterilization methods were found to either result in burst release within an hour, as in the case of autoclaving and gamma irradiation, or in complete alteration of film's physical properties, as in the case of dry heat. Immersion in 70% ethanol was found to be sufficiently gentle on the film, though some gentamicin loss was observed, and this method can only be used for small animal experiments.

Several other emerging sterilization methods could be considered for evaluation, including electron beam irradiation, H₂O₂ plasma, UV light²²⁸, or pulsed white light²²⁹⁻²³¹. In addition, the effect of sterilization on the mechanical or morphological properties of the films, as well as the activity and biocompatibility of the resulting film, should all be examined. For example, various sterilization methods have been found to affect surface properties of titanium and result in altered bone cell expression²³². We hope that as sterilization techniques evolve over time, more options

will emerge that provide equivalent antimicrobial action without the negative impact on biomaterials.

Acknowledgements.

S. aureus and MC3T3 assays were conducted with assistance from Christopher Loose and Mara Macdonald respectively. Taras Gorishnyy helped with *in situ* ellipsometry set-up. Kris Wood provided general laboratory training. Eric Verploegen and Scott Speakman helped with SAXS and WAXS, respectively. Eric additionally helped me with SEM images, and Steve Kooi provided counsel on SEM. Shawna Liff trained me on the use of DSC. For PLGA encapsulation of gentamicin, many thanks go to Dr. Yoon Yeo, who helped me with researching literature, designing the encapsulation protocol, and running the experiments with me. Dr. Daniel Kohane consulted with the PLGA encapsulation approach, and Jordan Green trained and assisted me on ZetaPALS. For film sterilization, I would like to thank Chris Travares at the MIT RPO for assisting with the γ -irradiation and Chris Autieri at the E25 animal facility for performing the EtO sterilization.

References

- (1) Schmidmaier, G., Lucke, M., Wildemann, B., Haas, N. P. and Raschke, M. *Injury*, **2006**, 37, S105-S112
- (2) Bauer, T. W. and Schils, J. *Skeletal Radiology*, **1999**, 28, 483-497
- (3) Stigter, M., Bezemer, J., de Groot, K. and Layrolle, P. *Journal of Controlled Release*, **2004**, 99, 127-137

- (4) Humphrey, J. S., Mehta, S., Seaber, A. V. and Vail, T. P. *Clinical Orthopaedics And Related Research*, **1998**, 218-224
- (5) L. Meseguer-Olmo, M. J. R.-N., M. Clavel-Sainz, V. Vicente-Ortega, M. Alcaraz-Baños, A. Lax-Pérez, D. Arcos, C. V. Ragel, M. Vallet-Regí,. *Journal of Biomedical Materials Research*, **2002**, 61, 458-465
- (6) Johannes G.E. Hendriks, D. N., Jim R. van Horn, Henny C. van der Mei, Henk J. Busscher,. *Journal of Biomedical Materials Research Part B: Applied Biomaterials*, **2003**, 64B, 1-5
- (7) Price, J. S., Tencer, A. F., Arm, D. M. and Bohach, G. A. *Journal of Biomedical Materials Research*, **1996**, 30, 281-286
- (8) Nablo, B. J., Rothrock, A. R. and Schoenfisch, M. H. *Biomaterials*, **2004**, 26, 917-924
- (9) Chung, R.-J., Hsieh, M.-F., Huang, C.-W., Perng, L.-H., Wen, H.-W. and Chin, T.-S. *Journal of Biomedical Materials Research Part B: Applied Biomaterials*, **2006**, 76B, 169-178
- (10) Balaban, N., Gov, Y., Bitler, A. and Boelaert, J. R. *Kidney International*, **2003**, 63, 340-345
- (11) Danese, P. N. *Chemistry & Biology*, **2002**, 9, 873-880
- (12) Bayston, R., Ashraf, W. and Bhundia, C. *J. Antimicrob. Chemother.*, **2004**, 53, 778-782
- (13) Camiel C. L. Peerlings, H. H. L. H., Raymond T. J. Bevers, Erik J. H. Boelen, Bram J. Stelt, Eva J. M. Korthagen, Leo H. Koole,. *Journal of Biomedical Materials Research*, **2002**, 63, 692-698
- (14) Belt, H. v. d., Neut, D., Schenk, W., Horn, J. R. v., Mei, H. C. v. d. and Busscher, H. J. *Acta Orthopaedica Scandinavica*, **2001**, 72, 557-571
- (15) Ramage, G., Tunney, M. M., Patrick, S., Gorman, S. P. and Nixon, J. R. *Biomaterials*, **2003**, 24, 3221-3227
- (16) Harris, L. G. and Richards, R. G. *Injury*, **2006**, 37, S3-S14
- (17) Lynch, A. S. and Robertson, G. T. *Annual Review of Medicine*, **2008**, 59, 415-428
- (18) Costerton, J. W., Khoury, A. E., Ward, K. H. and Anwar, H. *The International Journal of Artificial Organs*, **1993**, 16, 765-770

- (19) Esposito, S. and Leone, S. *International Journal of Antimicrobial Agents*, **2007**, *29*, 494-500
- (20) Lucke, M., Schmidmaier, G., Sadoni, S., Wildemann, B., Schiller, R., Haas, N. P. and Raschke, M. *Bone*, **2003**, *32*, 521-531
- (21) Hanssen, A. D. and Spangehl, M. J. *Clinical Orthopaedics And Related Research*, **2004**, 79-85
- (22) Alt, V., Bitschnau, A., Osterling, J., Sewing, A., Meyer, C., Kraus, R., Meissner, S. A., Wenisch, S., Domann, E. and Schnettler, R. *Biomaterials*, **2006**, *27*, 4627-4634
- (23) Decher, G. and Hong, J. D. *Berichte der Bunsen-Gesellschaft*, **1991**, *95*, 1430-1434
- (24) Lu, W. and Park, T. G. *PDA Journal of Pharmaceutical Science and Technology*, **1995**, *49*, 13-19
- (25) Jewell, C. M., Zhang, J., Fredin, N. J., Wolff, M. R., Hacker, T. A. and Lynn, D. M. *Biomacromolecules*, **2006**, *7*, 2483-2491
- (26) Thierry, B., Winnik, F. M., Merhi, Y., Silver, J. and Tabrizian, M. *Biomacromolecules*, **2003**, *4*, 1564-1571
- (27) Brynda, E., Houska, M., Jirouskova, M. and Dyr, J. E. *Journal of Biomedical Materials Research*, **2000**, *51*, 249-257
- (28) Graul, T. W. and Schlenoff, J. B. *Anal. Chem.*, **1999**, *71*, 4007-4013
- (29) Etienne, O., Gasnier, C., Taddei, C., Voegel, J.-C., Aunis, D., Schaaf, P., Metz-Boutigue, M.-H., Bolcato-Bellemin, A.-L. and Egles, C. *Biomaterials*, **2005**, *26*, 6704-6712
- (30) Jewell, C. M., Zhang, J., Fredin, N. J. and Lynn, D. M. *Journal of Controlled Release*, **2005**, *106*, 214-223
- (31) Zhang, J., Chua, L. S. and Lynn, D. M. *Langmuir*, **2004**, *20*, 8015-8021
- (32) Vazquez, E., Dewitt, D. M., Hammond, P. T. and Lynn, D. M. *J. Am. Chem. Soc.*, **2002**, *124*, 13992-13993
- (33) Wood, K. C., Boedicker, J. Q., Lynn, D. M. and Hammond, P. T. *Langmuir*, **2005**, *21*, 1603-1609
- (34) Wood, K. C., Chuang, H. F., Batten, R. D., Lynn, D. M. and Hammond, P. T. *PNAS*, **2006**, *103*, 10207-10212

- (35) Hiller, J. A. and Rubner, M. F. *Macromolecules*, **2003**, *36*, 4078-4083
- (36) Chung, A. J. and Rubner, M. F. *Langmuir*, **2002**, *18*, 1176-1183
- (37) Sukhishvili, S. A. and Granick, S. *Macromolecules*, **2002**, *35*, 301-310
- (38) Schuler, C. and Caruso, F. *Biomacromolecules*, **2001**, *2*, 921-926
- (39) Berg, M. C., Yang, S. Y., Hammond, P. T. and Rubner, M. F. *Langmuir*, **2004**, *20*, 1362-1368
- (40) Hahn, S. K. and Hoffman, A. S. *Biotechnology and Bioprocess Engineering*, **2004**, *9*, 179-183
- (41) Ai, H., Jones, S. A. and Lvov, Y. M. *Cell Biochemistry and Biophysics*, **2003**, *39*, 23-43
- (42) Jessel, N., Oulad-Abdelghani, M., Meyer, F., Lavallo, P., Haikel, Y., Schaaf, P. and Voegel, J. C. *PNAS*, **2006**, *103*, 8618-8621
- (43) Schneider, A., Vodouhe, C., Richert, L., Francius, G., LeGuen, E., Schaaf, P., Voegel, J. C., Frisch, B. and Picart, C. *Biomacromolecules*, **2007**, *8*, 139-145
- (44) Zhu, H., Ji, J. and Shen, J. *Journal of Biomaterials Science. Polymer Edition*, **2005**, *16*, 761-774
- (45) Prouty, M., Lu, Z., Leuschner, C. and Lvov, Y. *Journal of Biomedical Nanotechnology*, **2007**, *3*, 184-189
- (46) Lynn, D. M. and Langer, R. *J. Am. Chem. Soc.*, **2000**, *122*, 10761-10768
- (47) Cook, G., Costerton, J. W. and Darouiche, R. O. *International Journal of Antimicrobial Agents*, **2000**, *13*, 169-173
- (48) Gosheger, G., Harges, J., Ahrens, H., Streitburger, A., Buerger, H., Erren, M., Gonsel, A., Kemper, F. H., Winkelmann, W. and von Eiff, C. *Biomaterials*, **2004**, *25*, 5547-5556
- (49) Grunlan, J. C., Choi, J. K. and Lin, A. *Biomacromolecules*, **2005**, *6*, 1149-1153
- (50) Hollinger, M. A. *Critical Reviews in Toxicology*, **1996**, *26*, 255-260
- (51) Sheehan, E., McKenna, J., Mulhall, K. J., Marks, P. and McCormack, D. *Journal of Orthopaedic Research*, **2004**, *22*, 39-43
- (52) Sax, H. and Lew, D. *Current Infectious Disease Reports*, **1999**, *1*, 261-266

- (53) Waldvogel, F. A. and Papageorgiou, P. S. *New England Journal of Medicine*, **1980**, 303, 360-370
- (54) Goldenberg, D. L. *Lancet*, **1998**, 351, 197-202
- (55) Hamed, K. A., Tam, J. Y. and Prober, C. G. *Clinical Pharmacokinetics*, **1996**, 31, 156-163
- (56) Tam, V. H., Kabbara, S., Vo, G., Schilling, A. N. and Coyle, E. A. *Antimicrob. Agents Chemother.*, **2006**, 50, 2626-2631
- (57) Schafer, J. A., Hovde, L. B. and Rotschafer, J. C. *J. Antimicrob. Chemother.*, **2006**, 58, 108-111
- (58) Stallmann, H. P., Faber, C., Bronckers, A. L. J. J., Nieuw Amerongen, A. V. and Wuisman, P. I. J. M. *J. Antimicrob. Chemother.*, **2004**, 54, 472-476
- (59) Schultheis, K. H., Rehm, K. E., Voelkel, W., Schiefer, H. G., Schulz, A. and Kahl, M. *Chirurgisches Forum fuer Experimentelle und Klinische Forschung*, **1983**, 127-131
- (60) Kotlus, B. S., Wymbs, R. A., Vellozzi, E. M. and Udell, I. J. *American Journal of Ophthalmology*, **2006**, 142, 721-726
- (61) Edmiston, C. E., Goheen, M. P., Seabrook, G. R., Johnson, C. P., Lewis, B. D., Brown, K. R. and Towne, J. B. *American Journal of Surgery*, **2006**, 192, 344-354
- (62) Thierry, B., Kujawa, P., Tkaczyk, C., Winnik, F. M., Bilodeau, L. and Tabrizian, M. *J. Am. Chem. Soc.*, **2005**, 127, 1626-1627
- (63) Caruso, F., Yang, W., Trau, D. and Renneberg, R. *Langmuir*, **2000**, 16, 8932-8936
- (64) Decher, G. *Science*, **1997**, 277, 1232-1237
- (65) Ayako Oyane, H.-M. K., Takuo Furuya, Tadashi Kokubo, Toshiki Miyazaki, Takashi Nakamura., *Journal of Biomedical Materials Research Part A*, **2003**, 65A, 188-195
- (66) Picart, C., Mutterer, J., Richert, L., Luo, Y., Prestwich, G. D., Schaaf, P., Voegel, J.-C. and Lavallo, P. *PNAS*, **2002**, 99, 12531-12535
- (67) Zacharia, N. S., DeLongchamp, D. M., Modestino, M. and Hammond, P. T. *Macromolecules*, **2007**, 40, 1598-1603
- (68) Kujawa, P., Moraille, P., Sanchez, J., Badia, A. and Winnik, F. M. *J. Am. Chem. Soc.*, **2005**, 127, 9224-9234

- (69) Porcel, C., Lavallo, P., Ball, V., Decher, G., Senger, B., Voegel, J. C. and Schaaf, P. *Langmuir*, **2006**, 22, 4376-4383
- (70) Porcel, C., Lavallo, P., Decher, G., Senger, B., Voegel, J. C. and Schaaf, P. *Langmuir*, **2007**, 23, 1898-1904
- (71) Richert, L., Lavallo, P., Payan, E., Shu, X. Z., Prestwich, G. D., Stoltz, J.-F., Schaaf, P., Voegel, J.-C. and Picart, C. *Langmuir*, **2004**, 20, 448-458
- (72) Burke, S. E. and Barrett, C. J. *Biomacromolecules*, **2005**, 6, 1419-1428
- (73) Burke, S. E. and Barrett, C. J. *Biomacromolecules*, **2003**, 4, 1773-1783
- (74) Miller, M. D. and Bruening, M. L. *Chem. Mater.*, **2005**, 17, 5375-5381
- (75) Zhang, J. and Lynn, D. M. *Macromolecules*, **2006**, 39, 8928-8935
- (76) Standards, N. C. f. C. L. Journal, **1997**, *Approved standard M7-A4*,
- (77) Traub, W. H. and Leonhard, B. *J. Antimicrob. Chemother.* %R 10.1093/jac/35.1.149, **1995**, 35, 149-154
- (78) Mingeot-Leclercq, M.-P., Glupczynski, Y. and Tulkens, P. M. *Antimicrob. Agents Chemother.*, **1999**, 43, 727-737
- (79) Anderson, J. M. and Shive, M. S. *Advanced Drug Delivery Reviews*, **1997**, 28, 5-24
- (80) Burton, K. W., Shameem, M., Thanoo, B. C. and Deluca, P. P. *Journal of Biomaterials Science, Polymer Edition*, **2000**, 11, 715-729
- (3) Cohen, S., Yoshioka, T., Lucarelli, M., Hwang, L. H. and Langer, R. *Pharmaceutical Research*, **1991**, 8, 713-720
- (4) Jackanicz, T. M., Nash, H. A., Wise, D. L. and Gregory, J. B. *Contraception*, **1973**, 8, 227-234
- (5) Lu, W. and Park, T. G. *PDA Journal of Pharmaceutical Science and Technology*, **1995**, 49, 13-19
- (6) Ogawa, Y., Okada, H., Yamamoto, M. and Shimamoto, T. *Chemical & Pharmaceutical Bulletin*, **1988**, 36, 2576-2581
- (7) Okumu, F. W., Cleland, J. L. and Borchardt, R. T. *Journal of Controlled Release*, **1997**, 49, 133-140

- (8) Monika Schlapp, W. F. *Journal of Pharmaceutical Sciences*, **2003**, 92, 2145-2151
- (9) Narahariseti, P. K., Lee, H. C. G., Fu, Y.-C., Lee, D.-J. and Wang, C.-H. *Journal of Biomedical Materials Research Part B: Applied Biomaterials*, **2006**, 77B, 329-337
- (10) Price, J. S., Tencer, A. F., Arm, D. M. and Bohach, G. A. *Journal of Biomedical Materials Research*, **1996**, 30, 281-286
- (11) Friess, W. and Schlapp, M. *European Journal of Pharmaceutics and Biopharmaceutics*, **2005**, 63, 176-187
- (1) Schmidmaier, G., Lucke, M., Wildemann, B., Haas, N. P. and Raschke, M. *Injury Infection in Fracture Fixation. From basic research, to diagnosis, to evidence-based treatment*, **2006**, 37, S105-S112
- (2) Bauer, T. W. and Schils, J. *Skeletal Radiology*, **1999**, 28, 483-497
- (3) Stigter, M., Bezemer, J., de Groot, K. and Layrolle, P. *Journal of Controlled Release*, **2004**, 99, 127-137
- (4) Humphrey, J. S., Mehta, S., Seaber, A. V. and Vail, T. P. *Clinical Orthopaedics And Related Research*, **1998**, 218-224
- (5) L. Meseguer-Olmo, M. J. R.-N., M. Clavel-Sainz, V. Vicente-Ortega, M. Alcaraz-Baños, A. Lax-Pérez, D. Arcos, C. V. Ragel, M. Vallet-Regí,. *Journal of Biomedical Materials Research*, **2002**, 61, 458-465
- (6) Johannes G.E. Hendriks, D. N., Jim R. van Horn, Henny C. van der Mei, Henk J. Busscher,. *Journal of Biomedical Materials Research Part B: Applied Biomaterials*, **2003**, 64B, 1-5
- (7) Price, J. S., Tencer, A. F., Arm, D. M. and Bohach, G. A. *Journal of Biomedical Materials Research*, **1996**, 30, 281-286
- (8) Nablo, B. J., Rothrock, A. R. and Schoenfisch, M. H. *Biomaterials*, **2004**, 26, 917-924
- (9) Chung, R.-J., Hsieh, M.-F., Huang, C.-W., Perng, L.-H., Wen, H.-W. and Chin, T.-S. *Journal of Biomedical Materials Research Part B: Applied Biomaterials*, **2006**, 76B, 169-178
- (10) Balaban, N., Gov, Y., Bitler, A. and Boelaert, J. R. *Kidney International*, **2003**, 63, 340-345
- (11) Danese, P. N. *Chemistry & Biology*, **2002**, 9, 873-880

- (12) Bayston, R., Ashraf, W. and Bhundia, C. *J. Antimicrob. Chemother.*, **2004**, *53*, 778-782
- (13) Camiel C. L. Peerlings, H. H. L. H., Raymond T. J. Bevers, Erik J. H. Boelen, Bram J. Stelt, Eva J. M. Korthagen, Leo H. Koole., *Journal of Biomedical Materials Research*, **2002**, *63*, 692-698
- (14) Belt, H. v. d., Neut, D., Schenk, W., Horn, J. R. v., Mei, H. C. v. d. and Busscher, H. J. *Acta Orthopaedica Scandinavica*, **2001**, *72*, 557-571
- (15) Ramage, G., Tunney, M. M., Patrick, S., Gorman, S. P. and Nixon, J. R. *Biomaterials*, **2003**, *24*, 3221-3227
- (16) Harris, L. G. and Richards, R. G. *Injury Infection in Fracture Fixation. From basic research, to diagnosis, to evidence-based treatment*, **2006**, *37*, S3-S14
- (17) Lynch, A. S. and Robertson, G. T. *Annual Review of Medicine*, **2008**, *59*, 415-428
- (18) Costerton, J. W., Khoury, A. E., Ward, K. H. and Anwar, H. *The International Journal of Artificial Organs*, **1993**, *16*, 765-770
- (19) Esposito, S. and Leone, S. *International Journal of Antimicrobial Agents*, **2007**, *29*, 494-500
- (20) Lucke, M., Schmidmaier, G., Sadoni, S., Wildemann, B., Schiller, R., Haas, N. P. and Raschke, M. *Bone*, **2003**, *32*, 521-531
- (21) Hanssen, A. D. and Spangehl, M. J. *Clinical Orthopaedics And Related Research*, **2004**, 79-85
- (22) Alt, V., Bitschnau, A., Osterling, J., Sewing, A., Meyer, C., Kraus, R., Meissner, S. A., Wenisch, S., Domann, E. and Schnettler, R. *Biomaterials*, **2006**, *27*, 4627-4634
- (23) Decher, G. and Hong, J. D. *Berichte der Bunsen-Gesellschaft*, **1991**, *95*, 1430-1434
- (24) Lu, W. and Park, T. G. *PDA Journal of Pharmaceutical Science and Technology*, **1995**, *49*, 13-19
- (25) Jewell, C. M., Zhang, J., Fredin, N. J., Wolff, M. R., Hacker, T. A. and Lynn, D. M. *Biomacromolecules*, **2006**, *7*, 2483-2491
- (26) Thierry, B., Winnik, F. M., Merhi, Y., Silver, J. and Tabrizian, M. *Biomacromolecules*, **2003**, *4*, 1564-1571

- (27) Brynda, E., Houska, M., Jirouskova, M. and Dyr, J. E. *Journal of Biomedical Materials Research*, **2000**, *51*, 249-257
- (28) Graul, T. W. and Schlenoff, J. B. *Anal. Chem.*, **1999**, *71*, 4007-4013
- (29) Etienne, O., Gasnier, C., Taddei, C., Voegel, J.-C., Aunis, D., Schaaf, P., Metz-Boutigue, M.-H., Bolcato-Bellemin, A.-L. and Egles, C. *Biomaterials*, **2005**, *26*, 6704-6712
- (30) Jewell, C. M., Zhang, J., Fredin, N. J. and Lynn, D. M. *Journal of Controlled Release*, **2005**, *106*, 214-223
- (31) Zhang, J., Chua, L. S. and Lynn, D. M. *Langmuir*, **2004**, *20*, 8015-8021
- (32) Vazquez, E., Dewitt, D. M., Hammond, P. T. and Lynn, D. M. *J. Am. Chem. Soc.*, **2002**, *124*, 13992-13993
- (33) Wood, K. C., Boedicker, J. Q., Lynn, D. M. and Hammond, P. T. *Langmuir*, **2005**, *21*, 1603-1609
- (34) Wood, K. C., Chuang, H. F., Batten, R. D., Lynn, D. M. and Hammond, P. T. *PNAS*, **2006**, *103*, 10207-10212
- (35) Hiller, J. A. and Rubner, M. F. *Macromolecules*, **2003**, *36*, 4078-4083
- (36) Chung, A. J. and Rubner, M. F. *Langmuir*, **2002**, *18*, 1176-1183
- (37) Sukhishvili, S. A. and Granick, S. *Macromolecules*, **2002**, *35*, 301-310
- (38) Schuler, C. and Caruso, F. *Biomacromolecules*, **2001**, *2*, 921-926
- (39) Berg, M. C., Yang, S. Y., Hammond, P. T. and Rubner, M. F. *Langmuir*, **2004**, *20*, 1362-1368
- (40) Hahn, S. K. and Hoffman, A. S. *Biotechnology and Bioprocess Engineering*, **2004**, *9*, 179-183
- (41) Ai, H., Jones, S. A. and Lvov, Y. M. *Cell Biochemistry and Biophysics*, **2003**, *39*, 23-43
- (42) Jessel, N., Oulad-Abdelghani, M., Meyer, F., Lavallo, P., Haikel, Y., Schaaf, P. and Voegel, J. C. *PNAS*, **2006**, *103*, 8618-8621
- (43) Schneider, A., Vodouhe, C., Richert, L., Francius, G., LeGuen, E., Schaaf, P., Voegel, J. C., Frisch, B. and Picart, C. *Biomacromolecules*, **2007**, *8*, 139-145

- (44) Zhu, H., Ji, J. and Shen, J. *Journal of Biomaterials Science. Polymer Edition*, **2005**, *16*, 761-774
- (45) Prouty, M., Lu, Z., Leuschner, C. and Lvov, Y. *Journal of Biomedical Nanotechnology*, **2007**, *3*, 184-189
- (46) Lynn, D. M. and Langer, R. *J. Am. Chem. Soc.*, **2000**, *122*, 10761-10768
- (47) Cook, G., Costerton, J. W. and Darouiche, R. O. *International Journal of Antimicrobial Agents*, **2000**, *13*, 169-173
- (48) Gosheger, G., Harges, J., Ahrens, H., Streitburger, A., Buerger, H., Erren, M., Gonsel, A., Kemper, F. H., Winkelmann, W. and von Eiff, C. *Biomaterials*, **2004**, *25*, 5547-5556
- (49) Grunlan, J. C., Choi, J. K. and Lin, A. *Biomacromolecules*, **2005**, *6*, 1149-1153
- (50) Hollinger, M. A. *Critical Reviews in Toxicology*, **1996**, *26*, 255-260
- (51) Sheehan, E., McKenna, J., Mulhall, K. J., Marks, P. and McCormack, D. *Journal of Orthopaedic Research*, **2004**, *22*, 39-43
- (52) Sax, H. and Lew, D. *Current Infectious Disease Reports*, **1999**, *1*, 261-266
- (53) Waldvogel, F. A. and Papageorgiou, P. S. *New England Journal of Medicine*, **1980**, *303*, 360-370
- (54) Goldenberg, D. L. *Lancet*, **1998**, *351*, 197-202
- (55) Hamed, K. A., Tam, J. Y. and Prober, C. G. *Clinical Pharmacokinetics*, **1996**, *31*, 156-163
- (56) Tam, V. H., Kabbara, S., Vo, G., Schilling, A. N. and Coyle, E. A. *Antimicrob. Agents Chemother.*, **2006**, *50*, 2626-2631
- (57) Schafer, J. A., Hovde, L. B. and Rotschafer, J. C. *J. Antimicrob. Chemother.*, **2006**, *58*, 108-111
- (58) Stallmann, H. P., Faber, C., Bronckers, A. L. J. J., Nieuw Amerongen, A. V. and Wuisman, P. I. J. M. *J. Antimicrob. Chemother.*, **2004**, *54*, 472-476
- (59) Schultheis, K. H., Rehm, K. E., Voelkel, W., Schiefer, H. G., Schulz, A. and Kahl, M. *Chirurgisches Forum fuer Experimentelle und Klinische Forschung*, **1983**, 127-131
- (60) Kotlus, B. S., Wymbs, R. A., Vellozzi, E. M. and Udell, I. J. *American Journal of Ophthalmology*, **2006**, *142*, 721-726

- (61) Edmiston, C. E., Goheen, M. P., Seabrook, G. R., Johnson, C. P., Lewis, B. D., Brown, K. R. and Towne, J. B. *American Journal of Surgery*, **2006**, *192*, 344-354
- (62) Thierry, B., Kujawa, P., Tkaczyk, C., Winnik, F. M., Bilodeau, L. and Tabrizian, M. *J. Am. Chem. Soc.*, **2005**, *127*, 1626-1627
- (63) Caruso, F., Yang, W., Trau, D. and Renneberg, R. *Langmuir*, **2000**, *16*, 8932-8936
- (64) Decher, G. *Science*, **1997**, *277*, 1232-1237
- (65) Ayako Oyane, H.-M. K., Takuo Furuya, Tadashi Kokubo, Toshiki Miyazaki, Takashi Nakamura, *Journal of Biomedical Materials Research Part A*, **2003**, *65A*, 188-195
- (66) Picart, C., Mutterer, J., Richert, L., Luo, Y., Prestwich, G. D., Schaaf, P., Voegel, J.-C. and Lavallo, P. *PNAS*, **2002**, *99*, 12531-12535
- (67) Zacharia, N. S., DeLongchamp, D. M., Modestino, M. and Hammond, P. T. *Macromolecules*, **2007**, *40*, 1598-1603
- (68) Kujawa, P., Moraille, P., Sanchez, J., Badia, A. and Winnik, F. M. *J. Am. Chem. Soc.*, **2005**, *ASAP article*,
- (69) Porcel, C., Lavallo, P., Ball, V., Decher, G., Senger, B., Voegel, J. C. and Schaaf, P. *Langmuir*, **2006**, *22*, 4376-4383
- (70) Porcel, C., Lavallo, P., Decher, G., Senger, B., Voegel, J. C. and Schaaf, P. *Langmuir*, **2007**, *23*, 1898-1904
- (71) Richert, L., Lavallo, P., Payan, E., Shu, X. Z., Prestwich, G. D., Stoltz, J.-F., Schaaf, P., Voegel, J.-C. and Picart, C. *Langmuir*, **2004**, *20*, 448-458
- (72) Burke, S. E. and Barrett, C. J. *Biomacromolecules*, **2005**, *6*, 1419-1428
- (73) Burke, S. E. and Barrett, C. J. *Biomacromolecules*, **2003**, *4*, 1773-1783
- (74) Miller, M. D. and Bruening, M. L. *Chem. Mater.*, **2005**, *17*, 5375-5381
- (75) Zhang, J. and Lynn, D. M. *Macromolecules*, **2006**, *39*, 8928-8935
- (76) Standards, N. C. f. C. L. *Journal*, **1997**, *Approved standard M7-A4*,
- (77) Traub, W. H. and Leonhard, B. *J. Antimicrob. Chemother. %R* *10.1093/jac/35.1.149*, **1995**, *35*, 149-154

- (78) Mingeot-Leclercq, M.-P., Glupczynski, Y. and Tulkens, P. M. *Antimicrob. Agents Chemother.*, **1999**, *43*, 727-737
- (79) Anderson, J. M. and Shive, M. S. *Advanced Drug Delivery Reviews*, **1997**, *28*, 5-24
- (80) Burton, K. W., Shameem, M., Thanoo, B. C. and Deluca, P. P. *Journal of Biomaterials Science, Polymer Edition*, **2000**, *11*, 715-729
- (81) Cohen, S., Yoshioka, T., Lucarelli, M., Hwang, L. H. and Langer, R. *Pharmaceutical Research*, **1991**, *8*, 713-720
- (82) Jackanicz, T. M., Nash, H. A., Wise, D. L. and Gregory, J. B. *Contraception*, **1973**, *8*, 227-234
- (83) Ogawa, Y., Okada, H., Yamamoto, M. and Shimamoto, T. *Chemical & Pharmaceutical Bulletin*, **1988**, *36*, 2576-2581
- (84) Okumu, F. W., Cleland, J. L. and Borchardt, R. T. *Journal of Controlled Release*, **1997**, *49*, 133-140
- (85) Monika Schlapp, W. F. *Journal of Pharmaceutical Sciences*, **2003**, *92*, 2145-2151
- (86) Pavan Kumar Naraharisetti, H. C. G. L., Yin-Chih Fu, Duu-Jong Lee, Chi-Hwa Wang, . *Journal of Biomedical Materials Research Part B: Applied Biomaterials*, **2006**, *77B*, 329-337
- (87) Friess, W. and Schlapp, M. *European Journal of Pharmaceutics and Biopharmaceutics*, **2005**, *63*, 176-187
- (88) Simmons, A. *Journal*, **2004**,
- (89) Health, F. C. f. D. a. R. *Guidance for Industry*, **1994**,
- (90) Anderson, J. M., Bavacqua, B., Cranin, A. N. and al., e. *Journal*, **1996**, 415-420
- (91) Hooper, K. A., Cox, J. D. and Kohn, J. *Journal of Applied Polymer Science*, **1997**, *63*, 1499-1510
- (92) Goldman, M., Gronsky, R. and Pruitt, L. *Journal of Materials Science - Materials in Medicine*, **1998**, *9*, 207-212
- (93) Zhang, Y. Z., Bjursten, L. M., Freij-Larsson, C., Kober, M. and Wesslen, B. *Biomaterials*, **1996**, *17*, 2265-2272
- (94) Sintzel, M. B., Merkli, A., Tabatabay, C. and Gurny, R. *Drug Development and Industrial Pharmacy*, **1997**, *23*, 857-878

- (95) Balazs, E. A., Davies, J. V., Phillips, G. O. and Young, M. D. *Radiation Research*, **1967**, 31, 243
- (96) McDonnell, G. and Russell, A. D. *Clinical Microbiology Review*, **1999**, 12, 147-179
- (97) CDC. *MMWR*, **2003**, 52, 1-66
- (98) Riley, D. J., Bavastrello, V., Covani, U., Barone, A. and Nicolini, C. *Dental Materials*, **2005**, 21, 756-760
- (99) McDonald, K. F., Curry, R. D., Clevenger, T. E., Unklesbay, K. A. U. K., Eisenstark, A. A. E. A., Golden, J. A. G. J. and Morgan, R. D. A. M. R. D. *Plasma Science, IEEE Transactions on*, **2000**, 28, 1581-1587
- (100) RD, W., R, M., K, R., JM, H. and WH, C. *Biomed. Instrum. Technol.*, **2001**, 35, 323-330
- (101) Krishnamurthy, K., Demirci, A. and Irudayaraj, J. *Journal of Food Protection*, **2004**, 67, 1027-1030
- (102) Stanford, C. M., Keller, J. C. and Solursh, M. *J Dent Res*, **1994**, 73, 1061-1071

Chapter 6. Gentamicin-Protein Combination Films

6.1 Introduction

Total joint replacement (TJR), particularly of the hip and knee, has become one of the most frequent prosthetic surgeries due to its success in restoring mobility to patients suffering from various forms of bone degeneration. An estimated one million joint placements are performed worldwide each year³², with half being performed in the U.S.. Unfortunately, due to surgical and implant-derived complications, about 10% such joint replacements eventually fail and require a *revision arthroplasty*³³, in which the patient may undergo more than two additional surgeries – a costly and debilitating process. Therefore, reductions to primary failures and improvements revision success are of utmost importance.

There are many sources to implant failures, the most serious of which is infection at the implant site^{32, 33, 36, 37}. Bacteria could flourish within the microscopic crevices of the implant, rendering systemic administration of antibiotics futile. Thus, an implant that not only resists bacterial adhesion but also elutes antibiotics from all accessible surfaces would be invaluable. Other complications include the common aseptic loosening³³, thromboembolism³⁸⁻⁴⁰, ischemia to the lower extremities⁴¹, and tumor^{42, 43} or cyst⁴⁴ formations. On top of these more immediate complications, implant rejection may also occur on the longer term, caused by a lack of tissue growth onto the implant to promote its integration into the body.

Gentamicin is a common choice for osteomyelitis treatment. Its efficacy against *Staphylococcus aureus*, the most common source of osteomyelitis^{187, 188} and septic arthritis^{189, 190}, has been demonstrated both *in vitro*^{191, 192} and *in vivo*^{141, 193, 194}. Gentamicin is also effective against methicillin-resistant *S. aureus* (MRSA)¹⁹⁵ and biofilms of several *staphylococci*¹⁹⁶. On top of reducing implant-associated illnesses, we can incorporate growth factors into our multilayers to promote bone regeneration and implant integration. Both the osteoinductive agent BMP-2 (bone morphogenetic protein-2)⁷⁶⁻⁸¹ and the angiogenetic agent VEGF (vascular endothelial growth factor)⁸²⁻⁸⁵ have been well-studied *in vitro* and *in vivo* to have positive therapeutic impact on bone regeneration. The incorporation of large biomolecules such as proteins into PEMs is well-documented in the literature^{58, 70, 86}.

Layer-by-layer (LbL) assembly is a thin film fabrication technique based on the alternating deposition of polyelectrolytes or other multiply charged species⁵². The resulting *polyelectrolyte multilayers*, or PEMS, are ultrathin, conformal, and highly tunable in functionality and morphology. Since the deposition is frequently performed in aqueous solutions under ambient conditions, the process is simple, low-cost, scalable, and mild – a sharp contrast to the harsh organic conditions often employed in other drug encapsulation techniques¹⁸⁰. This feature will prove especially beneficial for the delivery of biologic drugs such as proteins, antibodies, nucleic acids, and peptides.

As the technique is based on non-specific interactions, LbL coatings can be deposited on virtually any surface material. In fact, they have been successfully applied onto a variety

of implant surfaces, including stainless steel¹¹⁸, NiTi¹⁰³, polyurethane and polystyrene¹⁵⁹, silica¹⁸¹, and PMMA¹⁸². LbL coatings are also flexible in its functionality, and have been demonstrated as coatings on implants that are antimicrobial^{144, 147, 233, 234}, anti-coagulant¹⁵⁹, anti-restenotic¹⁹⁷, tissue growth promoting²³⁵, and wear-resist⁷⁴. While gentamicin-incorporated coatings for orthopedic implants have been reported^{121, 122, 126, 139, 141, 236, 237}, none of these had precise dosage and rate tunability, high surface conformality, or ease and low cost of process. These necessary features can be addressed by LbL coatings because of their process advantages.

We have previously demonstrated controlled erosion¹¹⁰, tunable drug release^{119, 147}, and sequential drug release¹²⁰ under physiological conditions from LbL films made with poly(β -amino esters)²³. Specifically, tunable releases of gentamicin¹⁴⁷ and bFGF been achieved. In the preset study, we examined the build-up, erosion, and drug release kinetics of an LbL construct that incorporated both gentamicin and bFGF. We demonstrated co-release of both therapeutics in a dosage-tunable fashion, with excellent *in vitro* activity of the released gentamicin.

6.2 Materials and Methods

Materials. Poly(β -amino esters) (referred to as *Poly X*, $X = 1, 2$, see Figure 5.2) were synthesized as previously described²³. Silicon wafers (test grade n-type) were purchased from Silicon Quest (Santa Clara, CA). Linear poly(ethylenimine) (LPEI, $M_n = 25k$) was received from Polysciences, Inc. Poly (sodium 4-styrenesulfonate) (PSS, $M_n = 1M$) and sodium alginate (or alginic acid) were purchased from Sigma-Aldrich (St. Louis, MO).

Sodium hyaluronate (or hyaluronic acid (HA), $M_n = 1.76$ MDa) was purchased from Lifecore Biomedical, Inc. (Chaska, MN). Nonradiolabeled gentamicin sulfate (GS) (in Cellgro® solution, 50 mg/mL in sterile filtered water) was purchased from Mediatech, Inc. (Herndon, VA). ^3H -gentamicin sulfate was obtained from American Radiolabeled Chemicals, Inc (0.250 mCi total, 1 mCi/mL in ethanol, 0.200 mCi/mg). Heparin sodium salt was obtained from Celsus Laboratories (Cincinnati, OH), and bFGF was obtained from Peprotech (Rocky Hill, NJ). All materials and solvents were used as received without further purification.

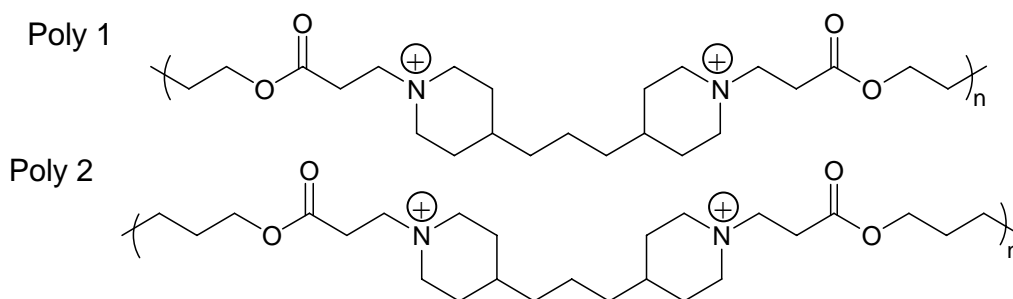


Figure 6.1 - Structures of *Poly X* used in this study.

Staphylococcus aureus, strain 25923 with no antibiotic resistance, was provided by the Gregory Stephanopoulos group at MIT and ordered from ATCC (Manassas, VA).

Cation-adjusted Mueller Hinton Broth II (CMHB) and BactoAgar™ were purchased from Difco™ (BD, Franklin Lakes, NJ). Gentamicin standard discs, 10 µg loading, were purchased from BD Biosciences (Franklin Lake, NJ) as BBL™ Sensi-Disc™. MC3T3-E1 Subclone 4 CRL-2593 was obtained from ATCC (Manassas, VA). Alpha Minimum essential medium (α -MEM), FBS, Penicillin, Streptomycin, and alamarBlue™ (BioSource™) were obtained from Invitrogen (Carlsbad, CA).

Preparation of Polyelectrolyte Solutions. Dipping solutions containing *Poly X* and HA were made at a concentration of 10 mM with respect to the polymer repeat unit in 100 mM sodium acetate buffer (pH 5.1 by glacial acetic acid). Heparin was used at a concentration of 2 mg/mL while bFGF was used at a concentration of 1 ug/mL, both in 100 mM sodium acetate buffer at pH 5.1 GS dipping solutions were prepared by diluting the 50 mg/mL stock solution with sodium acetate buffer and glacial acetic acid to result in a solution of 10 mg/mL GS in 100 mM sodium acetate. Nondegradable base layers were deposited from dipping solutions of LPEI and PSS in deionized water pH adjusted to 4.25 and 4.75, respectively. Deionized water used to prepare all solutions was obtained using a Milli-Q Plus (Bedford, MA) at 18.2 M Ω .

Polyelectrolyte Deposition. All polyelectrolyte LBL thin films were constructed as follows according to the alternate dipping method⁵³. Silicon wafers were cut into rectangular substrates approximately 2.0 cm \times 0.5cm each. The substrates were rinsed with methanol and deionized water, dried under nitrogen, and plasma etched in oxygen using a Harrick PDC-32G plasma cleaner at high RF power for 1 min. Layer-by-layer thin film deposition was performed using a Carl Zeiss HMS Series Programmable Slide Stainer. A nondegradable base film ((LPEI/PSS)₁₀) was deposited by submerging plasma treated silicon substrates in an LPEI dipping solution for 5 minutes, then a cascade rinse cycle consisting of three deionized water rinsing baths (15, 30, and 45 seconds, respectively). Substrates were then submerged in a PSS dipping solution for 5 minutes followed by the same cascade rinsing cycle, and the entire process was repeated ten

times. Next, degradable films were deposited on the existing polyanion-terminated base layer by repeating the above procedure with $[(Poly\ I/Hep)(bFGF/Hep)]_n$ and $[(Poly\ I/HA)(GS/HA)]_n$ architectures, dipping for 10 min in each of the *Poly X*, bFGF, HA, and GS solutions and 7.5 min for heparin solutions with cascading rinses between each step and repeating the bracketed structures as many times (n) as desired.

For films intended for drug release assessment, a ^3H -labeled GS dipping solution was prepared by dissolving 0.060 mL of the stock (1 mCi/mL in ethanol, 0.200 mCi/mg) in 40 mL of a typical GS dipping solution (10 mg/mL in 100 mM sodium acetate buffer, pH 3.0 by glacial acetic acid), making a radiolabeled solution at 1.5 $\mu\text{Ci/mL}$. An identical LBL deposition procedure was then performed.

Measurement of Film Thickness. Following deposition, films were immediately removed from the final rinsing bath and air dried. Film thickness was determined by profilometry at three or more different scratch sites on a KLA-Tencor P-10 Profilometer. All measurements were performed in triplicate.

Measurement of FGF release. Sample substrates were immersed in 1 mL of filtered medium (henceforth called release medium) consisting of 1% FBS, 1% penicillin/streptomycin in alpha essential medium. Samples were placed in an incubator at 37°C, and at several timepoints, 0.5 mL samples were obtained and replaced with 0.5 mL of fresh medium. Samples were frozen at -70°C until analysis using an ELISA

development kit (Peprotech, Rocky Hill NJ) and with proliferation assays described below.

Measurement of Gentamicin Release. Gentamicin release was assessed via incorporation of ^3H -labeled drug in the film. Two different types of release assays were conducted: (1) films were immersed in 25 mL of pre-warmed modified simulated body fluid (m-SBF) ¹⁵⁷ in a tightly-capped Falcon tube, maintained at 37°C in a water bath. The degradation tubes were tightly capped between sample extractions to prevent evaporation of the buffer solution. A 1 mL sample was extracted at predetermined time points, (2) films underwent identical release protocol as that for FGF release as outlined above, with each 0.5 mL aliquot diluted with 0.5 mL of m-SBF. For both release assays, the resulting 1-mL aliquots were analyzed by adding 5 mL of ScintiSafe Plus 50% (Fisher Scientific, Atlanta, GA) prior to measurement. The resulting mixtures were analyzed using a Tri-carb liquid scintillation counter (Model U2200). The amount of radiolabel in each sample vial was measured using a ^3H counting protocol which was shown to be highly accurate over a broad concentration range (30-100,000 DPM/mL) in calibration experiments performed prior to drug release. Raw data (disintegrations per minute, DPM) were converted to micrograms (μg) of gentamicin using the conversion factor $2.2 \times 10^6 \text{ DPM} = 1 \mu\text{Ci} = 1.0 \mu\text{g } ^3\text{H-GS}$. Finally, the total gentamicin release from a single film was calculated according to the following equation:

$$M_i = \left((C_i \times V_i) + (1\text{mL}) \sum_{j=1}^{i-1} C_j \right) (1334)$$

where M_i (μg) is the total cumulative mass released from the film as of measurement i , C_i ($\mu\text{g/mL}$) is the concentration of sample i , V_i (mL) is the total volume of the degradation bath prior to measurement i , $(1\text{mL})\sum_{j=1}^{i-1} C_j$ is the total mass in previously extracted samples, and 1334 is equal to the mass ratio of total GS to ^3H -GS in the dipping solution (i.e., in the degradable film).

***Staphylococcus aureus* macrodilution assay.** All liquid assays were performed in cation-adjusted Mueller Hinton Broth II (CMHB). Qualitative assays were performed following standard macrodilution methods as outlined by the National Committee on Clinical Laboratory Standards (NCCLS M26-A, 1999) with a challenge of 10^5 CFU/mL. An elution test with modified macrodilution assay was adopted to facilitate duplications of tests at various treatment levels. Briefly, films with precisely cut sizes were immersed in a set amount of culture medium at 37°C for 72+ hours for complete erosion of films. Estimated gentamicin concentration ([GS]) within this elution buffer can be computed based on the immersed film size and culture volume. The resulting elution medium was then serially diluted 1:2 with fresh medium 15 times, yielding 16 different concentrations, from the original elution medium strength down to a factor of 2^{-15} . Quantitative assays were done in 96-well plates with 150 μL of liquid culture per well, with 135 μL of test media and 15 μL of inoculation culture at 10^5 CFU/mL in CMHB. All test media were sterile-filtered through 0.2 μm membranes prior to use. Estimated test media conditions take the 9:10 dilution into account. For each set of assays, three wells were filled with culture fluid with no bacteria inoculated, while three negative controls were subject to the

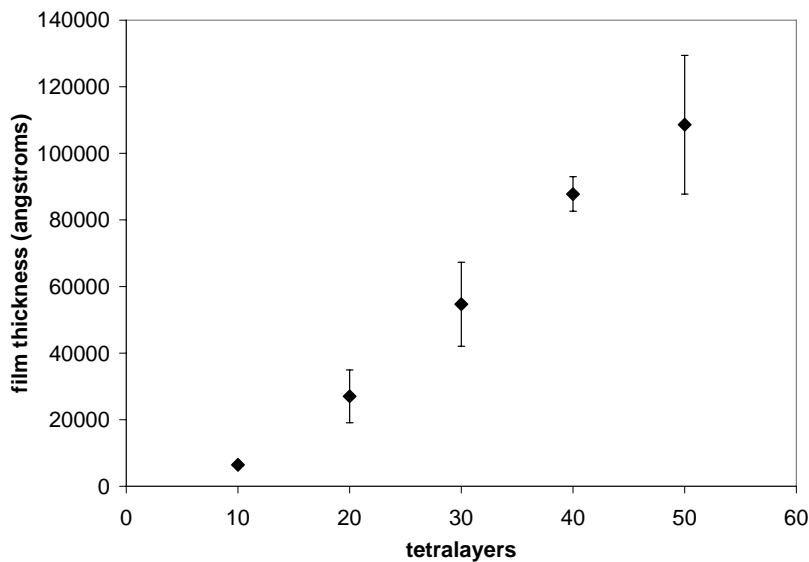
same bacterial challenge without any substrate. The plate was incubated at 37°C under gentle shaking for 16-18 hours. Cell density was read at OD 600 nm in a BioTek® PowerWave™ XS Microplate Spectrophotometer with accompanying Gen5 program Version 1.00.14. All treatments, whether direct infusion into culture or co-immersion of film substrates with the culture, were administered from the time of seeding to data observation. Cultures were incubated at 37°C for 16-18 hours under gentle shaking before observation.

***Staphylococcus aureus* Kirby-Bauer disc diffusion assay.** Kirby-Bauer disk diffusion assays were performed according to the NCCLS guidelines (M7-A4, 1997). Agar plates were formulated with CMHB and BactoAgar™. Each plate was inoculated with *S. aureus* culture in exponential growth phase at 10⁸ CFU/mL in CMHB using a sterile cotton swab. The test substrate was immediately placed on the inoculated plate, coated side down, with gentle pressing by a pair of tweezers to ensure conformal contact, exercising particular care not to pierce the agar or move the substrate. All substrates were placed at least 5 cm apart from one substrate center to another and 2 cm from the edge of the dish. The plates were inverted and incubated at 37°C without shaking for 16-18 hours before observation.

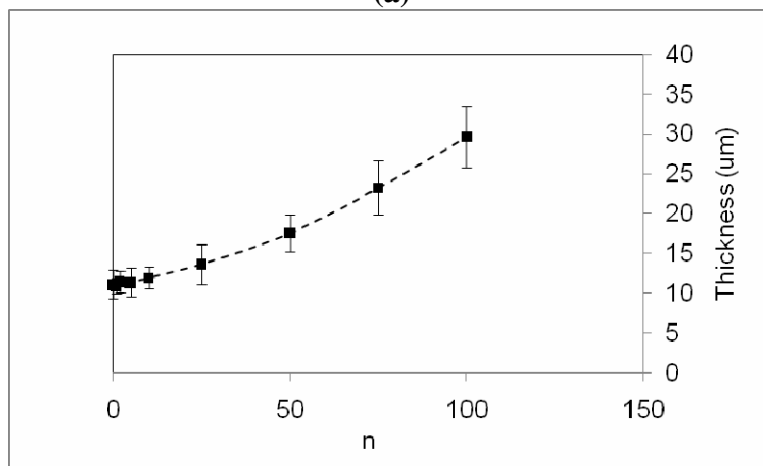
6.3 Results and Discussion

Growth curve of combination films. [(*Poly I*/HA)(GS/HA)] tetralayers were deposited on top of a [(*Poly I*/Hep)(FGF/Hep)]₅₀ film. Figure 6.2 shows the growth curves of both

the bFGF bottom layers and the subsequent GS layers. Within the first ten [(Poly I/HA)(GS/HA)] tetralayers, very little growth was observed. However, significant amounts of gentamicin were loaded within the first ten tetralayer deposition, suggesting that gentamicin was diffusing into the film during these deposition cycles. At 25 tetralayers and above, noticeable film growth was observed, with increasing surface roughness. The overall trend of this growth curve is non-linear, suggesting that gentamicin was diffusing throughout the film per the “in and out” mechanism as proposed by Picart *et al.*¹⁵³. A similar trend was observed by the authors for a [(Poly I/HA)(GS/HA)]_n-only film¹⁴⁷ and was attributed to the size of the gentamicin molecule.



(a)



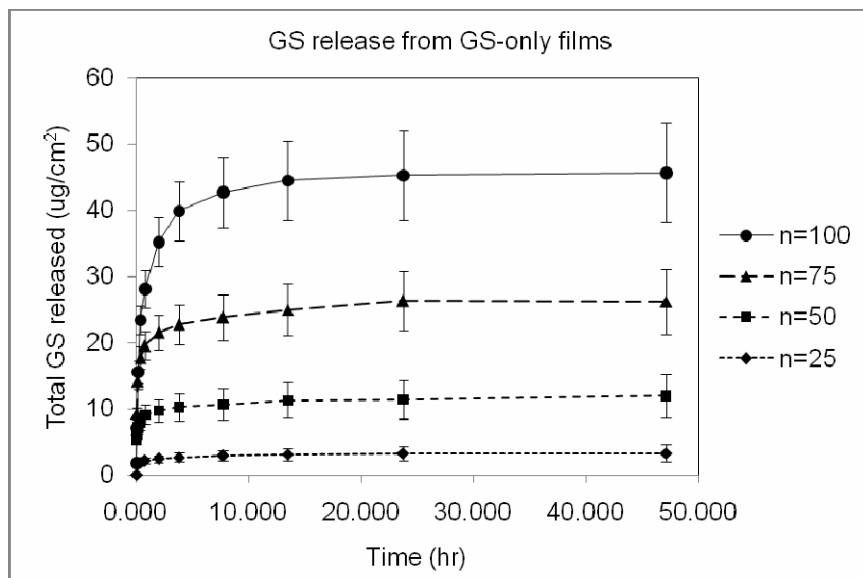
(b)

Figure 6.2 – Growth curve (a) $[(Poly\ I/Hep)(FGF/Hep)]_n$, and (b) $[(Poly\ I/Hep)(FGF/Hep)]_{50} + [(Poly\ I/HA)(GS/HA)]_n$.

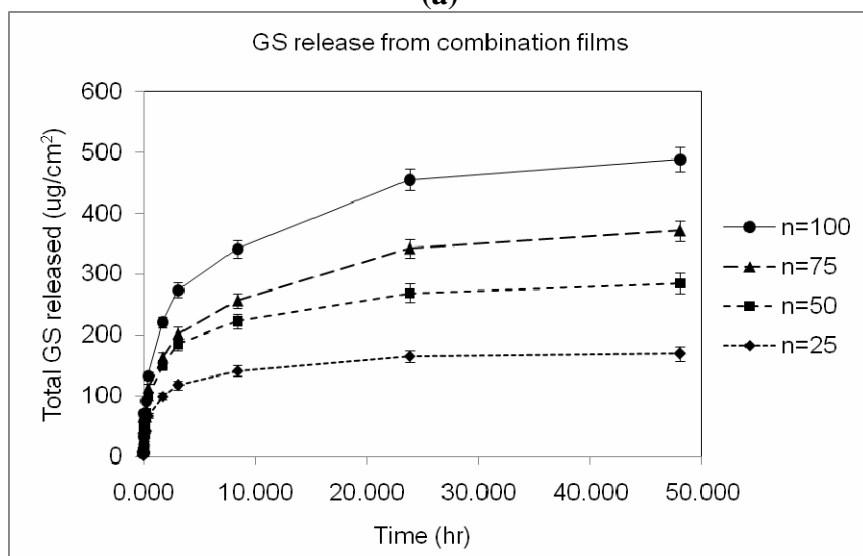
Figure (a) is courtesy of Mara Macdonald.

Gentamicin release dosage and kinetics. The dosage and kinetics of gentamicin release were compared between $[(Poly\ I/HA)(GS/HA)]_n$ (“GS only”) films and $[(Poly\ I/Hep)(FGF/Hep)]_{50} + [(Poly\ I/HA)(GS/HA)]_n$ (“combination”) films (see Figure 6.3). In this set of release assessments, films were immersed in m-SBF (modified simulated body fluid) at 37°C with a total initial volume of 25 mL. As the figure suggests,

gentamicin was released at a higher dosage and a slower rate from a combination film when compared to a GS-only film with the same number of $[(Poly\ I/HA)(GS/HA)]_n$ tetralayers. For example, at $n = 100$, a GS-only film released a total of $45\ \mu\text{g}/\text{cm}^2$ of gentamicin with 95% completion around 10 hours, while the combination counterpart released a total of $510\ \mu\text{g}/\text{cm}^2$ of gentamicin with 95% completion around 48 hours. The remarkable increase in gentamicin dosage may be attributed to gentamicin's diffusion into the $[(Poly\ I/Hep)(FGF/Hep)]_{50}$ underlayers, which served as a flexible reservoir for gentamicin.



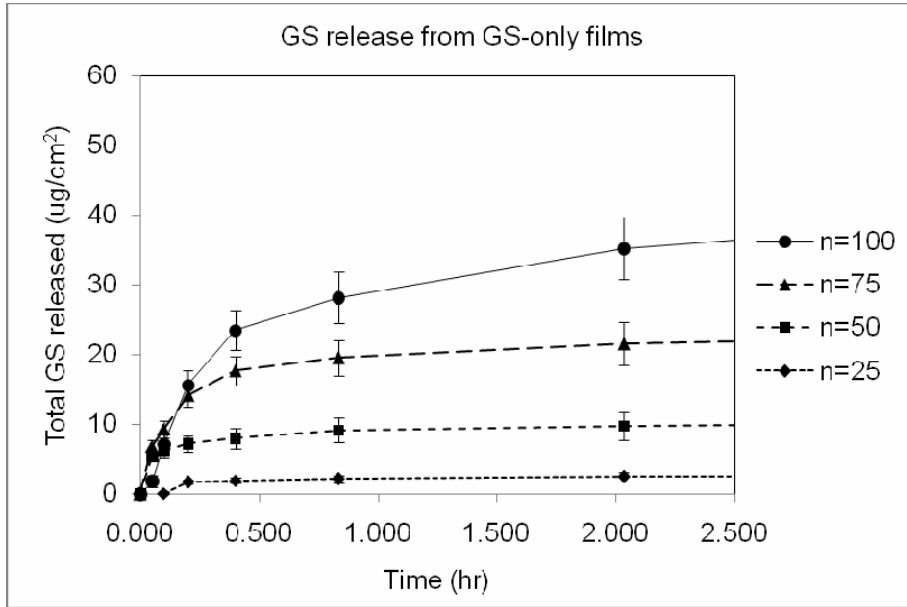
(a)



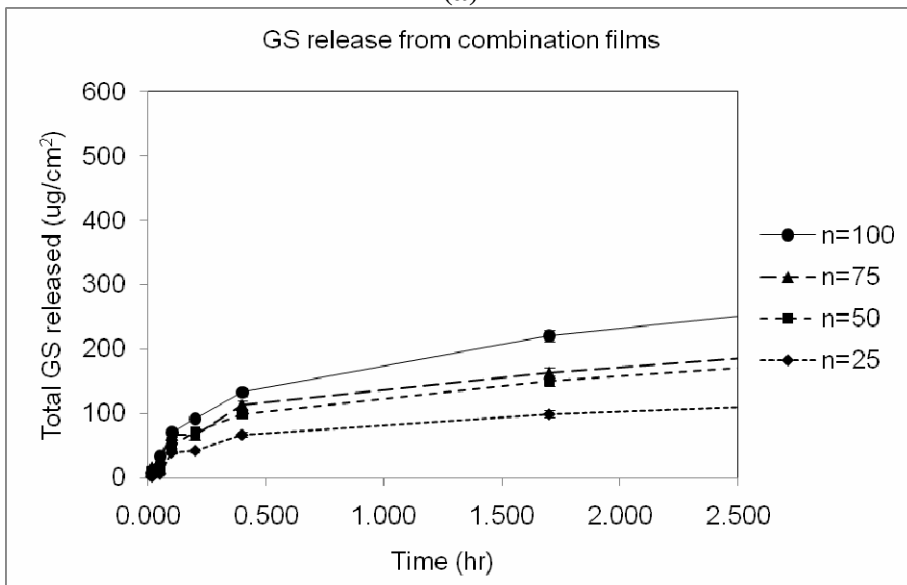
(b)

Figure 6.3 – Cumulative release of gentamicin in m-SBF, 37°C from (a) $[(Poly\ I/HA)(GS/HA)]_n$ films, and (b) $[(Poly\ I/Hep)(FGF/Hep)]_{50} + [(Poly\ I/HA)(GS/HA)]_n$ films.

Figure 6.4 replicates data from Figure 6.3, but displayed on a different x-axis scale to provide further release rate comparison within the first 2.5 hours. A combined look at both figures show that a combination film not only has a longer overall release, but also a more attenuated initial burst. GS-only films released 50% of its total gentamicin within the first 0.5 hour, whereas combination films reached 50% release only beyond 2.5 hours.



(a)



(b)

Figure 6.4 – Cumulative release of gentamicin in m-SBF, 37°C, zoomed into the initial 2.5 hours, from (a) $[(Poly\ I/HA)(GS/HA)]_n$ films, and (b) $[(Poly\ I/Hep)(FGF/Hep)]_{50} + [(Poly\ I/HA)(GS/HA)]_n$ films.

Additional release assessments were performed in “release medium” (1% FBS, 1% penicillin/streptomycin in alpha essential medium) at 37°C under identical sampling protocol and frequency as those used for FGF release assessment. The resulting gentamicin release from combination films is shown in Figure 6.5. Gentamicin release observed under this sampling protocol was more sustained than the previous method in 25 mL m-SBF (see Figure 6.3(b)), with 50% release in 6 hours and 95% release in 70 hours, as compared to 2.5 hours and 45 hours respectively for an identical film released in m-SBF. It was not clear which sampling method was a better mimic for *in vivo* conditions, but this set of data highlights the importance in the selection of *in vitro* release protocol when the release kinetics is a primary concern. In our case, we are most concerned with the *comparison* of gentamicin releases between GS-only and combination films (as in Figure 6.3 and Figure 6.4) and between gentamicin and FGF releases from identical combination films (see Figure 6.7, to be discussed later). Hence, as long as we maintain an identical sampling protocol within each set of comparison, the qualitative assessments should remain valid.

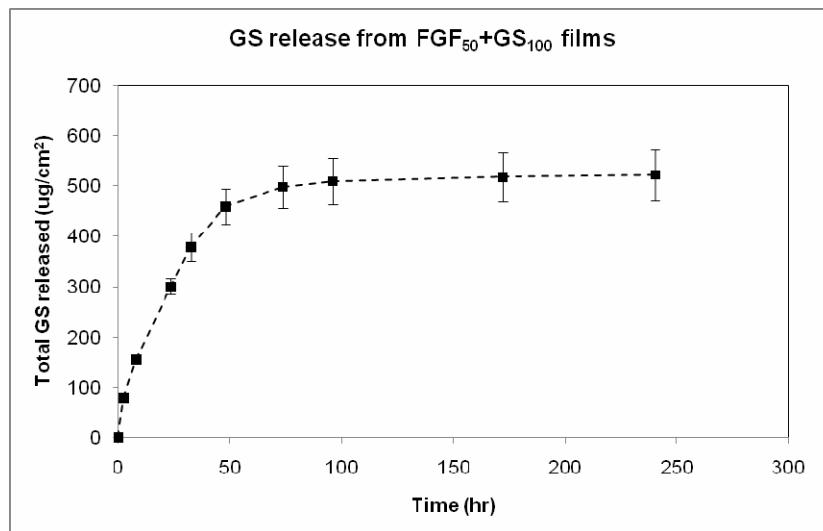
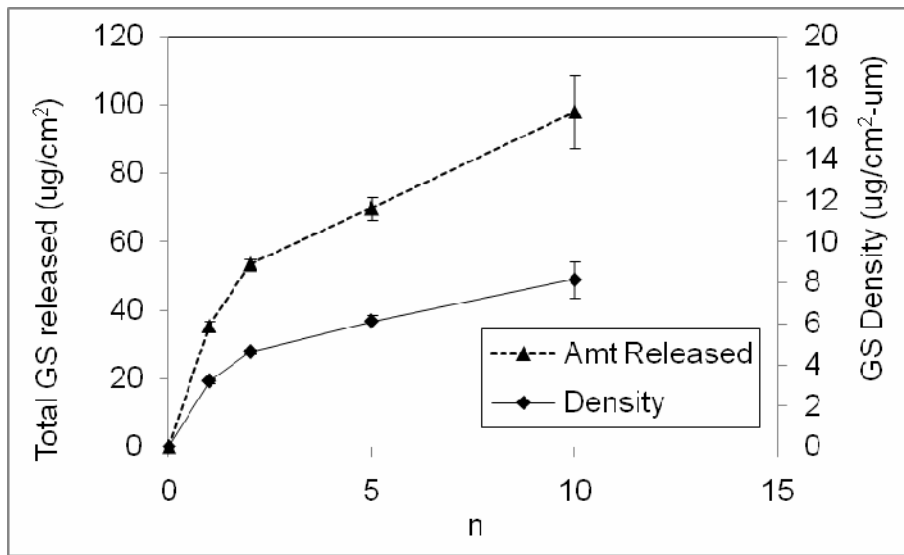
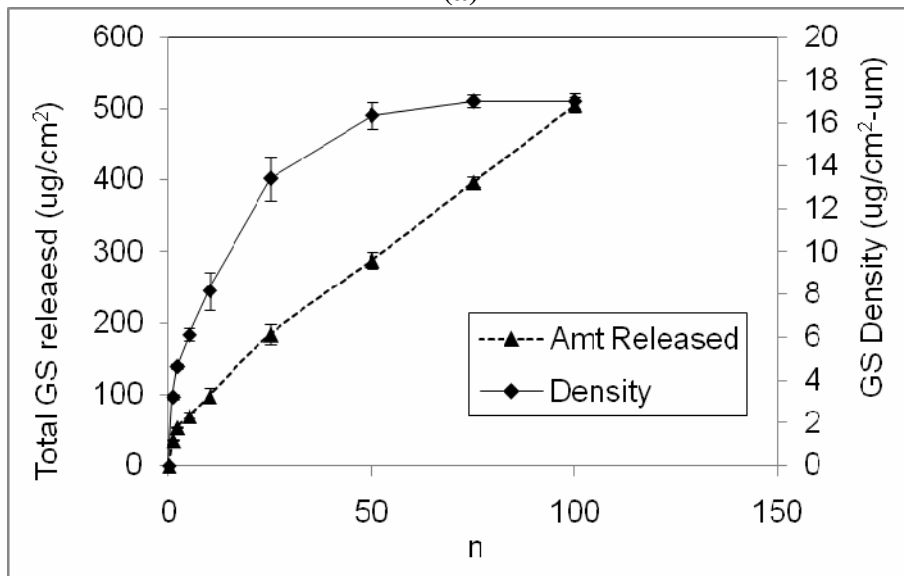


Figure 6.5 - Cumulative release of gentamicin in release medium from $[(Poly\ I/Hep)(FGF/Hep)]_{50} + [(Poly\ I/HA)(GS/HA)]_n$ films.

Gentamicin loading and density within combination films. Through release assessments described above, the total amounts of gentamicin released from each set of combination films could be tabulated. In addition, these release amounts could be divided by the mean thicknesses of the films to yield a “density” of gentamicin within the film. Both of these parameters are displayed as a function of n in Figure 6.6. The two figures are from identical sets of data, with (a) displaying data zoomed into the $n = 1$ to 10 region.



(a)

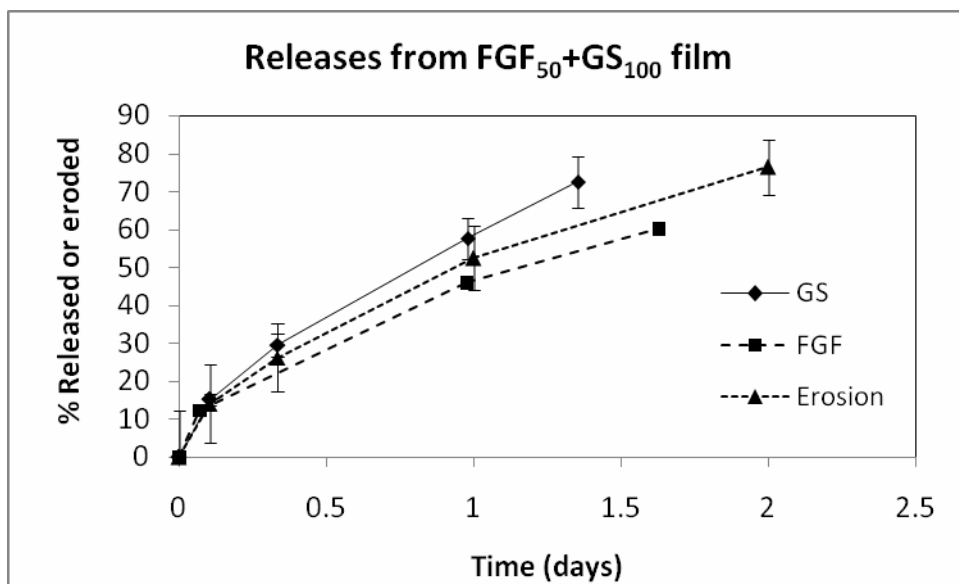


(b)

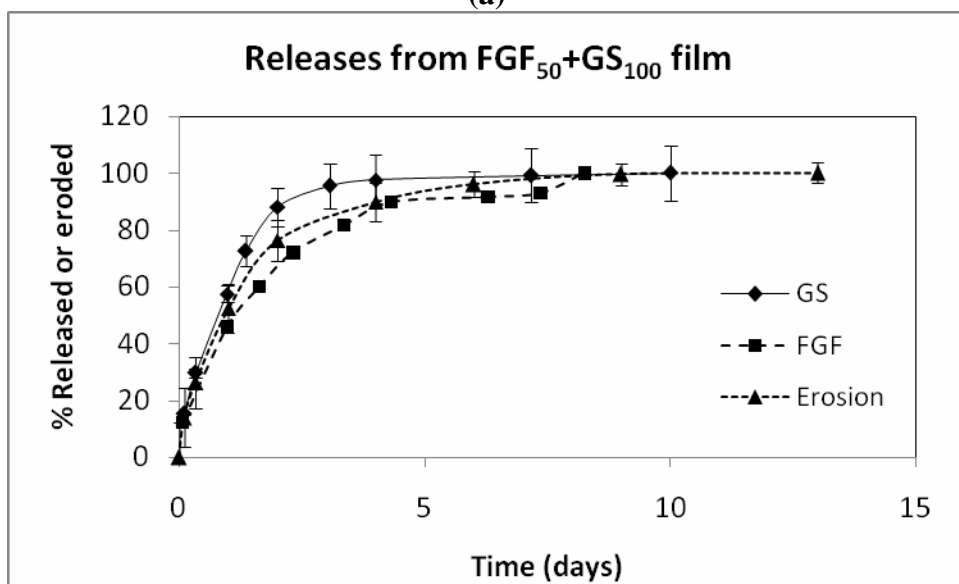
Figure 6.6 – Total loading and loading density of gentamicin into combination films as a function of number of [(*Poly I*/HA)(GS/HA)] tetralayers deposited on top of [(*Poly I*/Hep)(FGF/Hep)]₅₀. (a) zoomed into the lower regime of n = 0 to 10, (b) overall representation from n = 0 to 100.

As the data suggests, there was a steady, monotonic increase in gentamicin loading (assumed to be identical in amounts as what was released) as more number of tetralayers were deposited. However, as the combination film had very little growth in thickness within the first ten gentamicin tetralayers, the density of gentamicin was increasing at a faster pace. Again, this may be attributed to the diffusion of gentamicin into the [(*Poly I*/Hep)(FGF/Hep)]₅₀ underlayers during the initial depositions. The density appeared to reach a maximum of 17 $\mu\text{g}/\text{cm}^2\text{-}\mu\text{m}$ after 50 tetralayers, suggesting that gentamicin might have completely penetrated the [(*Poly I*/Hep)(FGF/Hep)]₅₀ underlayers after 50 deposition cycles, so that additional gentamicin incorporation at $n \geq 50$ could be attributed mostly to extra film build-up. This hypothesis is consistent with the observation that the [(*Poly I*/Hep)(FGF/Hep)]₅₀ + [(*Poly I*/HA)(GS/HA)]_n films were growing at a faster rate for $n \geq 50$ (see Figure 6.2).

Comparison of drug release and film erosion. Figure 6.7 presents three sets of data from a [(*Poly I*/Hep)(FGF/Hep)]₅₀ + [(*Poly I*/HA)(GS/HA)]₁₀₀ film – gentamicin release (from Figure 6.5), FGF release (data courtesy of Mara Macdonald), and thickness erosion of the film – all conducted under an identical release protocol. For ease of comparison, the release and erosion data are all displayed as % total completion. The two plots in Figure 6.7 are from identical sets of data, with plot (a) zoomed into the initial 2 days for a clearer display in this regime.



(a)



(b)

Figure 6.7 - Normalized cumulative releases of gentamicin (GS) and FGF from a [(Poly I/Hep)(FGF/Hep)]₅₀ + [(Poly I/HA)(GS/HA)]₁₀₀ film, with accompanying film erosion curve.

(a) zoomed into the first 2 days, and (b) overall data gathered up to 13 days.

The data suggest that gentamicin release, FGF release, and film erosion all occurred at similar rates from the combination film, with FGF release being slightly more sustained than that of gentamicin. Film erosion correlated closely with FGF release, suggesting that FGF release was driven primarily by the erosion process, while gentamicin release

could be partially driven by diffusion. Overall, the film behaved more as a “co-release” system than a sequential release one.

Activity of [(Poly I/Hep)(FGF/Hep)]₅₀ films towards *S. aureus*. To assess whether the [(Poly I/Hep)(FGF/Hep)]₅₀ underlayers could affect *S. aureus* proliferation, CMHB elution buffers of [(Poly I/Hep)(FGF/Hep)]₅₀ films were prepared with an estimated [FGF] = 50 µg/mL. The buffers were serially diluted 1:2 down to 0.20 µg/mL and administered to *S. aureus* cultures under standard macrodilution protocol. The *S. aureus* cultures were observed to proliferate to the same extent as negative controls under all dilutions of the FGF film buffer, suggesting that none of the components eluted from the FGF underlayers exhibited noticeable activity towards *S. aureus*. A similar assay on Poly I, HA, and combinations of the two was previously performed¹⁴⁷ (see Chapter 5) and neither proliferative nor inhibitive effect was observed.

Activity of combination films against *S. aureus*. CMHB Elution buffers of [(Poly I/Hep)(FGF/Hep)]₅₀ + [(Poly I/HA)(GS/HA)]₁₀₀ films were prepared to assess their activity against *S. aureus* proliferation. *S. aureus* cultures were treated with several dilutions of these elution buffers under standard macrodilution protocol. The resulting culture densities were quantified by OD₆₀₀ measurement and shown in Figure 6.8. Each of the three film samples were split into triplicate assessments, with error bars representing standard deviations of the triplicate trials. As the data suggest, all three films samples were effective against *S. aureus* proliferation at estimated gentamicin concentrations of ~0.15 µg/mL and higher, consistent with reported free-solution

gentamicin MIC of 0.125-0.25 $\mu\text{g/mL}$. Hence, all of the film-released gentamicin appeared to remain *in vitro* active, with little inhibitory effect experienced from the co-excipients of the film.

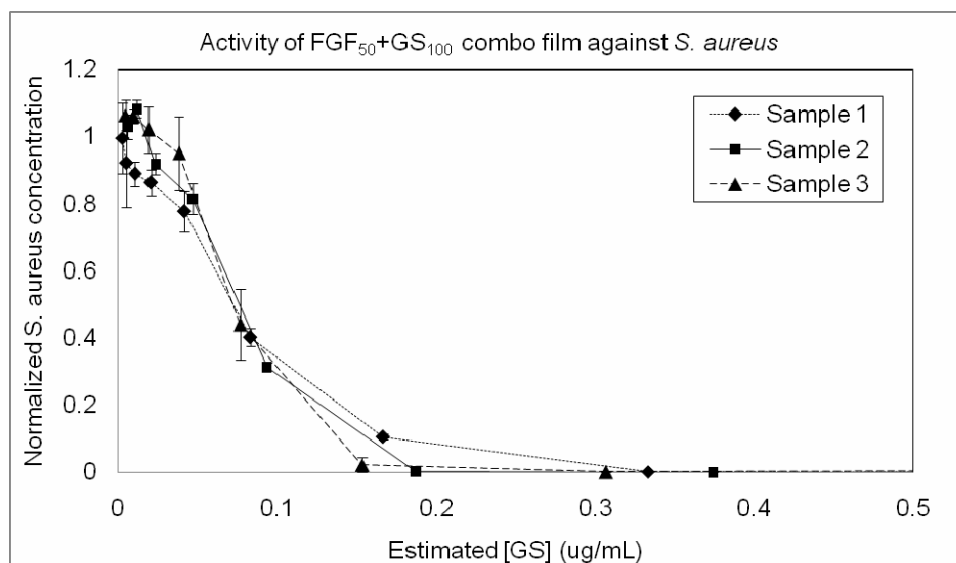


Figure 6.8 – Macrodilution assay of $[(Poly\ I/Hep)(FGF/Hep)]_{50} + [(Poly\ I/HA)(GS/HA)]_{100}$ film against *S. aureus*.

Additional antibacterial activity assessments were performed using the Kirby-Bauer (KB) disc diffusion assay, in which the film samples were directly incubated on the surface of an inoculated agar plate to assess the activity of the antibiotic as released and diffused into the agar. The first set of KB assays was performed using $[(Poly\ I/Hep)(FGF/Hep)]_{50} + [(Poly\ I/HA)(GS/HA)]_{25}$ films trimmed down to sufficiently small squares to result in a total release of $\sim 10\ \mu\text{g}$ gentamicin per square sample. This facilitates comparisons to positive controls, which were BD Sensi-Discs[®] specified to release $10\ \mu\text{g}$ of gentamicin. Table 6 reports data from this set of assays. As the data indicate, the film samples

produced very similar diameters as those of positive controls, again suggesting that gentamicin was released in its active form with little inhibition from co-excipients.

Table 6 – Kirby-Bauer diameters of $[(Poly\ I/Hep)(FGF/Hep)]_{50} + [(Poly\ I/HA)(GS/HA)]_{25}$ substrates and 10 μg BD Sensi-Disc® controls. Substrate sizes were chosen to yield GS loadings of ~ 10 μg per sample.

	Area [†] (cm ²)	Estimated GS dosage [‡] (μg)	Net KB diameter (cm)	Diameter/dosage (cm/ μg)
Control 1	0.785	10	1.72	0.172
Control 2	0.785	10	1.73	0.173
Control 3	0.785	10	1.72	0.172
Average			1.72	0.172
% Std Dev			0.34%	0.34%
Sample 1	0.053	9.74	1.71	0.176
Sample 2	0.058	10.6	1.74	0.164
Sample 3	0.053	9.74	1.73	0.178
Average				0.172
% Std Dev				4.24%

[†] Controls are BD Sensi-Discs® standardized as 0.5-cm diameter circles; samples were square-shaped.

[‡] Controls are specified by BD as containing 10 μg gentamicin; sample gentamicin dosage were estimated by multiplying the sample area by the average loading for the 25-gentamicin-layered film (184 $\mu\text{g}/\text{cm}^2$)

Additional $[(Poly\ I/Hep)(FGF/Hep)]_{50} + [(Poly\ I/HA)(GS/HA)]_n$ film samples of various gentamicin dosages were assessed by KB, with resulting data displayed in Figure 6.9.

Two sets of samples were run with films made in different batches. The data had good consistency between different batches, and overlapped well with those of BD Sensi-Disc® controls. A saturation in KB diameter was observed at high gentamicin dosages, most likely due to the steady state diffusion limits of gentamicin within the CMHB agar. An analytical model that couples the mass transport of gentamicin within the agar with the growth kinetic of *S. aureus* could further ascertain this diffusion limit, but is beyond the scope of the current study.

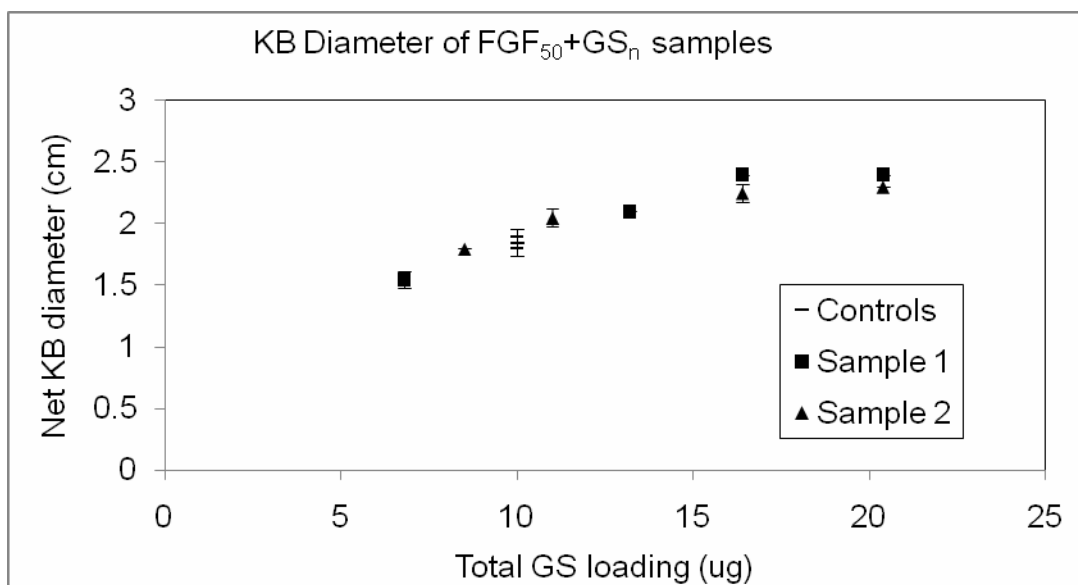


Figure 6.9 –Net Kirby-Bauer diameters of various combination film samples in correlation to the estimated total gentamicin within the sample. Controls were BD Sensi-Disc®.

6.4 Conclusion

A dual-therapy coating was constructed using layer-by-layer deposition, resulting in a biodegradable coating that can release both the antibiotic gentamicin and the growth factor bFGF in a concurrent fashion. The combination coating allowed for a 5x enhancement in the sustainability of gentamicin release, and a 10x increase in gentamicin dosage, as compared to an analogous layer-by-layer coating of only gentamicin without the bFGF co-encapsulant. Release rates of gentamicin and FGF correlated well with that of film erosion. The resulting film exhibited excellent *in vitro* antimicrobial activity with no inhibitory effect from the film co-excipients. Further assessments on FGF release and activity from these combinations films are currently under way to fully characterize the therapeutic potential of these films.

Acknowledgements.

Many thanks go to Mara Macdonald for her close collaboration on this project, Jeff Easley for contributing to a significant extent of the experimental work, Natalia Rodriguez for assisting with the FGF portion of this study, and Josh Moskowitz for participating in some of the initial experiments on film growth.

References.

- (1) Bernard, L., Hoffmeyer, P., Assal, M., Vaudaux, P., Schrenzel, J. and Lew, D. J. *Antimicrob. Chemother.*, **2004**, 53, 127-129
- (2) Bauer, T. W. and Schils, J. *Skeletal Radiology*, **1999**, 28, 483-497
- (3) Bourne, R. B. *The Journal of Arthroplasty*, **2004**, 19, 69-72
- (4) Fluckiger, U. and Zimmerli, W. *Der Orthopade*, **2004**, 33, 416-423
- (5) Bottner, F., Sculco, T. P., Sharrock, N. E., Westrich, G. H. and Steinbeck, J. *Der Orthopade*, **2001**, 30, 890-896
- (6) Heisel, C., Clarius, M., Schneider, U. and Breusch, S. J. *Zeitschrift fur Orthopadie und ihre Grenzgebiete*, **2001**, 139, 221-228
- (7) Dahl, O. E. *Drugs*, **2004**, 64, 17-25
- (8) Patil, S., Allan, D. B. and Quin, R. *The Journal of Arthroplasty*, **2002**, 17, 882-886
- (9) Cole, B. J., Schultz, E., Smilari, T. F., Hajdu, S. I. and Krauss, E. S. *Skeletal Radiology*, **1997**, 26, 559-563
- (10) Ganapathi, M., Lake, D. N. W. and Griffiths, A. P. *The Journal of Arthroplasty*, **2001**, 16, 229-232
- (11) Korkala, O. and Syrj nen, K. J. *Archives of Orthopaedic and Trauma Surgery*, **1998**, 118, 113-115
- (12) Sax, H. and Lew, D. *Current Infectious Disease Reports*, **1999**, 1, 261-266

- (13) Waldvogel, F. A. and Papageorgiou, P. S. *New England Journal of Medicine*, **1980**, 303, 360-370
- (14) Goldenberg, D. L. *Lancet*, **1998**, 351, 197-202
- (15) Hamed, K. A., Tam, J. Y. and Prober, C. G. *Clinical Pharmacokinetics*, **1996**, 31, 156-163
- (16) Tam, V. H., Kabbara, S., Vo, G., Schilling, A. N. and Coyle, E. A. *Antimicrob. Agents Chemother.*, **2006**, 50, 2626-2631
- (17) Schafer, J. A., Hovde, L. B. and Rotschafer, J. C. *J. Antimicrob. Chemother.*, **2006**, 58, 108-111
- (18) Stallmann, H. P., Faber, C., Bronckers, A. L. J. J., Nieuw Amerongen, A. V. and Wuisman, P. I. J. M. *J. Antimicrob. Chemother.*, **2004**, 54, 472-476
- (19) Schultheis, K. H., Rehm, K. E., Voelkel, W., Schiefer, H. G., Schulz, A. and Kahl, M. *Chirurgisches Forum fuer Experimentelle und Klinische Forschung*, **1983**, 127-131
- (20) Alt, V., Bitschnau, A., Osterling, J., Sewing, A., Meyer, C., Kraus, R., Meissner, S. A., Wenisch, S., Domann, E. and Schnettler, R. *Biomaterials*, **2006**, 27, 4627-4634
- (21) Kotlus, B. S., Wymbs, R. A., Vellozzi, E. M. and Udell, I. J. *American Journal of Ophthalmology*, **2006**, 142, 721-726
- (22) Edmiston, C. E., Goheen, M. P., Seabrook, G. R., Johnson, C. P., Lewis, B. D., Brown, K. R. and Towne, J. B. *American Journal of Surgery*, **2006**, 192, 344-354
- (23) Ono, I., Tateshita, T., Inoue, M. and Kuboki, Y. *Journal of Bone and Mineral Metabolism*, **1998**, 16, 81-87
- (24) Li, R. H., Bouxsein, M. L., Blake, C. A., D'Augusta, D., Kim, H., Li, X. J., Wozney, J. M. and Seeherman, H. J. *Journal of Orthopaedic Research*, **2003**, 21, 997-1004
- (25) Geiger, M., Li, R. H. and Friess, W. *Advanced Drug Delivery Reviews*, **2003**, 55, 1613-1629
- (26) Keskin, D. S., Tezcaner, A., Korkusuz, P., Korkusuz, F. and Hasirci, V. *Biomaterials*, **2005**, 26, 4023-4034
- (27) Kroese-Deutman, H. C., Ruhe, P. Q., Spauwen, P. H. M. and Jansen, J. A. *Biomaterials*, **2005**, 26, 1131-1138
- (28) Kaito, T., Myoui, A., Takaoka, K., Saito, N., Nishikawa, M., Tamai, N., Ohgushi, H. and Yoshikawa, H. *Biomaterials*, **2005**, 26, 73-79

- (29) Tabata, Y., Miyao, M., Ozeki, M. and Ikada, Y. *Journal of Biomaterials Science, Polymer Edition*, **2000**, *11*, 915-930
- (30) Yamamoto, M., Ikada, Y. and Tabata, Y. *Journal of Biomaterials Science, Polymer Edition*, **2001**, *12*, 77-88
- (31) Carano, R. A. D. and Filvaroff, E. H. *Drug Discovery Today*, **2003**, *8*, 980-989
- (32) Gu, F., Amsden, B. and Neufeld, R. *Journal of Controlled Release*, **2004**, *96*, 463-472
- (33) Caruso, F., Niikura, K., Furlong, D. N. and Okahata, Y. *Langmuir*, **1997**, *13*, 3427-3433
- (34) Kotov, N. A. *Nanostructured Materials*, **1999**, *12*, 789-796
- (35) Lvov, Y. M. and Sukhorukov, G. B. *Membrane Cell Biology*, **1997**, *11*, 277-303
- (36) Decher, G. and Hong, J. D. *Berichte der Bunsen-Gesellschaft*, **1991**, *95*, 1430-1434
- (37) Lu, W. and Park, T. G. *PDA Journal of Pharmaceutical Science and Technology*, **1995**, *49*, 13-19
- (38) Jewell, C. M., Zhang, J., Fredin, N. J., Wolff, M. R., Hacker, T. A. and Lynn, D. M. *Biomacromolecules*, **2006**, *7*, 2483-2491
- (39) Thierry, B., Winnik, F. M., Merhi, Y., Silver, J. and Tabrizian, M. *Biomacromolecules*, **2003**, *4*, 1564-1571
- (40) Brynda, E., Houska, M., Jirouskova, M. and Dyr, J. E. *Journal of Biomedical Materials Research*, **2000**, *51*, 249-257
- (41) Graul, T. W. and Schlenoff, J. B. *Anal. Chem.*, **1999**, *71*, 4007-4013
- (42) Etienne, O., Gasnier, C., Taddei, C., Voegel, J.-C., Aunis, D., Schaaf, P., Metz-Boutigue, M.-H., Bolcato-Bellemin, A.-L. and Egles, C. *Biomaterials*, **2005**, *26*, 6704-6712
- (43) Chuang, H. F., Smith, R., xe, C and Hammond, P. T. *Biomacromolecules*, **2008**, *ASAP Article*,
- (44) Grunlan, J. C., Choi, J. K. and Lin, A. *Biomacromolecules*, **2005**, *6*, 1149-1153
- (45) Etienne, O., Picart, C., Taddei, C., Haikel, Y., Dimarcq, J. L., Schaaf, P., Voegel, J. C., Ogier, J. A. and Egles, C. *Antimicrob. Agents Chemother.*, **2004**, *48*, 3662-3669

- (46) Boulmedais, F., Frisch, B., Etienne, O., Lavalle, P., Picart, C., Ogier, J., Voegel, J.-C., Schaaf, P. and Egles, C. *Biomaterials*, **2004**, *25*, 2003-2011
- (47) Thierry, B., Kujawa, P., Tkaczyk, C., Winnik, F. M., Bilodeau, L. and Tabrizian, M. *J. Am. Chem. Soc.*, **2005**, *127*, 1626-1627
- (48) A. Dierich, E. Le G. N. M. J. F. S. P. N. P. S. J. C. V. N. B.-J. *Advanced Materials*, **2007**, *19*, 693-697
- (49) Pavoor, P. V., Gearing, B. P., Bellare, A. and Cohen, R. E. *Wear*, **2004**, *256*, 1196-1207
- (50) Lucke, M., Schmidmaier, G., Sadoni, S., Wildemann, B., Schiller, R., Haas, N. P. and Raschke, M. *Bone*, **2003**, *32*, 521-531
- (51) Price, J. S., Tencer, A. F., Arm, D. M. and Bohach, G. A. *Journal of Biomedical Materials Research*, **1996**, *30*, 281-286
- (52) Diefenbeck, M., Muckley, T. and Hofmann, G. O. *Injury Infection in Fracture Fixation. From basic research, to diagnosis, to evidence-based treatment*, **2006**, *37*, S95-S104
- (53) Lucke, M., Wildemann, B., Sadoni, S., Surke, C., Schiller, R., Stemberger, A., Raschke, M., Haas, N. P. and Schmidmaier, G. *Bone*, **2005**, *36*, 770-778
- (54) Schmidmaier, G., Lucke, M., Wildemann, B., Haas, N. P. and Raschke, M. *Injury*, **2006**, *37*, S105-S112
- (55) Stigter, M., Bezemer, J., de Groot, K. and Layrolle, P. *Journal of Controlled Release*, **2004**, *99*, 127-137
- (56) Vazquez, E., Dewitt, D. M., Hammond, P. T. and Lynn, D. M. *J. Am. Chem. Soc.*, **2002**, *124*, 13992-13993
- (57) Wood, K. C., Boedicker, J. Q., Lynn, D. M. and Hammond, P. T. *Langmuir*, **2005**, *21*, 1603-1609
- (58) Wood, K. C., Chuang, H. F., Batten, R. D., Lynn, D. M. and Hammond, P. T. *PNAS*, **2006**, *103*, 10207-10212
- (59) Lynn, D. M. and Langer, R. *J. Am. Chem. Soc.*, **2000**, *122*, 10761-10768
- (60) Decher, G. *Science*, **1997**, *277*, 1232-1237

(61) Ayako Oyane, H.-M. K., Takuo Furuya, Tadashi Kokubo, Toshiki Miyazaki, Takashi Nakamura, *Journal of Biomedical Materials Research Part A*, **2003**, 65A, 188-195

(62) Eda, H., Aoki, K., Marumo, K., Fujii, K. and Ohkawa, K. *Biochemical and Biophysical Research Communications*, **2008**, 366, 471-475

(63) Li, C. F. and Hughes-Fulford, M. *Journal of Bone and Mineral Research*, **2006**, 21, 946-955

(64) Picart, C., Mutterer, J., Richert, L., Luo, Y., Prestwich, G. D., Schaaf, P., Voegel, J.-C. and Lavallo, P. *PNAS*, **2002**, 99, 12531-12535

Chapter 7. Antimicrobial Peptide (AmP) Delivery

7.1 Introduction.

Antimicrobial peptides (AmPs) are a novel class of antibiotics that are 12-35 amino acids in length, typically isolated from mammalian cells²³⁸. They are active against a broad spectrum of bacteria, including strains resistant to traditional antibiotics such as vancomycin and tetracycline²³⁹. They are also robust against the development of antibiotic resistance due to their mechanism of action, which involves their insertion into the bacterial membrane that results in poration and disruption, leading to cell death.

Christopher Loose from the Gregory Stephaopoulos group, who worked on the rational design of AmP sequences^{240, 241}, proposed a research collaboration for the incorporation of AmPs into LbL films for tunable, sustained release.

A few AmP-incorporating LbL films have been reported in the literature. Etienne *et al.* incorporated defensin in a non-degradable PEI-(PSS-PAH)₂-PGA-PLL-(PGA-defensin-PLL)_n architecture with either a PLL or PGA top layer²³³. When co-incubated with *M. luteus* or *E. coli* cultures, only films capped with a PLL top layer were found to inhibit *E. coli* growths, suggesting that attachment of bacteria onto a positively-charged outer surface was necessary for these films' efficacy. The authors also reported in a separate study that (PLL/PGA)_n(PLL/PGA-g-PEG)_n films inhibit *E. coli* adhesion²³⁴, supporting their hypothesis above. The authors subsequently incorporated an anti-fungal AmP chromofungin (Chf) in LbL films of architectures PEI-(PSS/PAH)₂-(PGA/Chf/PLL)₂₄ or PEI-(PSS/PAH)₂-((PGA*Chf)/PLL)₂₄, where PGA*Chf denotes a solution mixture of

PGA and Chf (“peptidized polyanion”)¹⁸². The films were found to inhibit growth of the yeast *C. albicans*. However, the authors noted that no solid evidence was available to support actual incorporation of chromofungin into these films, and that the anti-fungal activity could conceivably arise from the other components of the film. In addition, neither of the studies above allowed for tunable release of the AmP, and instead the films relied upon bacteria attachment onto the surface to exert their antimicrobial actions.

While the aforementioned studies made use of positively charged AmPs that could be directly incorporated into electrostatic LbL assemblies, Guyamard *et al.* reported the incorporation of a hydrophobic AmP, gramicidin A, into a multilayer through complexation with an anionic amphiphilic polysaccharide²⁴² (a hydrophobically modified carboxymethylpullulan). The negatively charged complex was bilayered with PLL with tunable amounts of AmP incorporation. The film was active against *E. faecalis* through both surface contact and release of gramicidin A into the culture. However, the release was inferred strictly from bacteria culture and not assessed rigorously through a quantitative *in vitro* release assay.

Given the lack of rigorous, quantitative data on AmP dosage and release kinetics from LbL films, Chris and I sought to establish such a set of data using several naturally-occurring AmPs. There is a wide variety of natural AmPs available with variable lengths, conformations, and hence antimicrobial activities. AmPs Dermasetin, Melittin, Cecropin-A-Melittin hybrid, and Ponericin were investigated under this study to demonstrate the generality of AmP encapsulation and release using the LbL deposition

method. The eventual focus will be on Ponericins due to their high activity against *S. aureus* and low hemolytic activity. Ponericins are natural AmPs isolated from the venom of an arboreal ponerine ant. They were discovered and extensively characterized by Orivel *et al.*²⁴³ Ponericins are classified into three families – G, W, and L – based on their sequences and structures. The G family is structurally similar to another natural AmP, Cecropin, and is further divided into subtypes G1, G3, G4, and G6. Ponericin G1 was found to be particularly active against a broad spectrum of gram-positive and gram-negative organisms. They were also found to have insecticidal activity, yet exhibited little hemolytic activity towards sheep or horse erythrocytes, suggesting a certain degree of specificity towards eukaryotic cells.

7.2 Materials and Methods.

Materials. Poly(β -amino esters) (referred to as *Poly X*, $X = 1$ and 6A, see Figure 5.2) were synthesized as previously described²³. Silicon wafers (test grade n-type) were purchased from Silicon Quest (Santa Clara, CA). Linear poly(ethylenimine) (LPEI, $M_n = 25k$) was received from Polysciences, Inc. Poly (sodium 4-styrenesulfonate) (PSS, $M_n = 1M$) was purchased from Sigma-Aldrich (St. Louis, MO). Sodium hyaluronate (or hyaluronic acid (HA), $M_n = 1.76$ MDa) was purchased from Lifecore Biomedical, Inc. (Chaska, MN). Nonradiolabeled gentamicin sulfate (GS) (in Cellgro® solution, 50 mg/mL in sterile filtered water) was purchased from Mediatech, Inc. (Herndon, VA). ³H-gentamicin sulfate was obtained from American Radiolabeled Chemicals, Inc (0.250 mCi total, 1 mCi/mL in ethanol, 0.200 mCi/mg). All antimicrobial peptides (AmPs), both fluorescently labeled (denoted as AmP*) and native versions, were courtesy of the Greg

Stephanopoulos group and synthesized by the MIT Biopolymers Lab. Please see Table 7 for the list of AmPs considered under this study. All materials and solvents were used as received without further purification.

Table 7 - List of antimicrobial peptides used in this study.

Name	Sequence
Dermaseptin (Derm)	ALWKTLLKKVLKA
Melittin (Mel)	GIGAVLKVLTTGLPALISWIKRKRQQ
Cecropin A Melittin (CM)	KWKLFFKKIGAVLKVL
Ponericin G1 (“Pon”)	GWKDWAKKAGGWLKKKGPGMAKAALKAAMQ

Staphylococcus aureus (ATCC 25923, no antibiotic resistance) and methicillin-resistant *S. aureus* (MRSA, ATCC 700698) were purchased from American Type Culture Collection (ATCC, Manassas, VA). Cation-adjusted Mueller Hinton Broth II (CMHB) was purchased from Difco™ (BD, Franklin Lakes, NJ). Bacto Agar™ was also purchased from Difco™. Gentamicin standard discs, 10 µg loading, were purchased from BD Biosciences (Franklin Lake, NJ) as BBL™ Sensi-Disc™. Alamar Blue (BioSource™) was obtained from Invitrogen (Carlsbad, CA). Micro BCA Protein Assay Kit was obtained from Pierce (Rockford, IL).

Preparation of Polyelectrolyte Solutions. Dipping solutions containing *Poly X*, HA, and heparin were made at a concentration of 10 mM with respect to the polymer repeat unit in 100 mM sodium acetate buffer (pH 5.1 by glacial acetic acid). AmP dipping solutions were prepared by dissolving lyophilized samples or diluting liquid stock with sodium acetate buffer and glacial acetic acid to result in a solution of 0.5-1 mg/mL AmP

in 100 mM sodium acetate at either pH 5.5 or pH 3.0. Nondegradable base layers were deposited from dipping solutions of LPEI and PSS in deionized water pH adjusted to 4.25 and 4.75, respectively. Deionized water used to prepare all solutions was obtained using a Milli-Q Plus (Bedford, MA) at 18.2 M Ω .

Polyelectrolyte Deposition. All polyelectrolyte LBL thin films were constructed as follows according to the alternate dipping method⁵³. Silicon wafers were cut into rectangular substrates approximately 2.0 cm \times 0.5cm each. The substrates were rinsed with methanol and deionized water, dried under nitrogen, and plasma etched in oxygen using a Harrick PDC-32G plasma cleaner at high RF power for 1 min. Layer-by-layer thin film deposition was performed using a Carl Zeiss HMS Series Programmable Slide Stainer. A ten-bilayer nondegradable base film ((LPEI/PSS)₁₀) was deposited by submerging plasma treated silicon substrates in an LPEI dipping solution for 5 minutes, then a cascade rinse cycle consisting of three deionized water rinsing baths (15, 30, and 45 seconds, respectively). Substrates were then submerged in a PSS dipping solution for 5 minutes followed by the same cascade rinsing cycle, and the entire process was repeated ten times. Next, degradable films were deposited on the existing polyanion-terminated base layer by repeating the above procedure with the [(*Poly X*/HA)_a(AmP/HA)_b]_n architecture, dipping for 10 min in each of the *Poly X*, HA, and GS solutions and repeating the (*Poly X*/HA)_a(AmP/HA)_b structure as many times (n) as desired. *Poly X* and HA dipping solutions were re-made every 24 hours.

Measurement of Film Thickness. Following deposition, films were immediately removed from the final rinsing bath and air dried. Film thickness was determined either by ellipsometry at ten different predetermined locations on the film surface or by profilometry at three different scratch sites. All measurements were performed in triplicate. Dry state ellipsometric measurements were conducted using a Gaertner Variable Angle Ellipsometer (6328 nm, 70° incident angle) and accompanying Gaertner Ellipsometer Measurement Program (GEMP) Version 1.2 software interface. Profilometric measurements were taken on a KLA-Tencor P-10 Profilometer.

Measurement of Drug Release. For release assessments by either fluorescence or BCA, calibration curves were established for each specific type of AmP by running a set of standards at known concentrations within a range relevant to my observed release concentrations, and performing linear regression on the concentration vs. fluorescent/colorimetric signal to establish a calibration curve. For drug release assessment by fluorescence measurement, $[(Poly\ X/HA)_a(AmP^*/HA)_b]_n$ films were immersed in 1 mL of pre-warmed 37C phosphate buffered saline (PBS) in a tightly capped vial wrapped with aluminum foil to block out light. Vials were kept in cell incubators to maintain 37C. At pre-determined time periods, three samples of 0.100 mL release buffer would be withdrawn from the vial and transferred each into the well of a black 96-well plate and read in a fluorescence microplate reader (fmax, Molecular Devices, Sunnyvale, CA). After reading, all buffer samples would be returned to the vial to maintain 1 mL of total release buffer. For drug release assessment by BCA assay, a $[(Poly\ X/HA)_a(AmP/HA)_b]_n$ film was trimmed into smaller pieces and immersed in 0.5

mL of PBS ¹⁵⁷ in an Eppendorf tube maintained at 37°C in a water bath. A 0.150 mL sample was extracted at predetermined time points (every 1-5 minutes at the beginning, then gradually increasing the time intervals) and replaced with fresh 0.150 mL pre-warmed PBS. Aliquots of 0.150 mL release samples were stored at -20C until all samples were ready for BCA. Each 0.150 mL sample was then diluted to 0.300 mL total, allowing for triplicate assessment at 0.100 mL each. BCA assay was run according to manufacturer's product insert, using the microplate method.

***Staphylococcus aureus* macrodilution assays.** All liquid assays were performed in cation-adjusted Mueller Hinton Broth II (CMHB). Qualitative assays were performed following standard macrodilution methods as outlined by the National Committee on Clinical Laboratory Standards (NCCLS M26-A, 1999)²⁴⁴ with a challenge of 10⁵ CFU/mL. For assays involving co-incubation with films deposited on silicon, 24-well plates were used, with 0.5 mL of liquid culture per well. Briefly, each square-cut silicon substrate (1.0 cm x 1.0 cm), either bare or coated depending on the test group, was placed flat in the center of a well in a 24-well plate, polished side up. Each well was then filled with 0.50 mL of *S. aureus* in exponential growth phase at 10⁵ CFU/mL in CMHB, completely immersing the substrate. Quantitative assays were done in 96-well plates with 150 µL of liquid culture per well, with 135 µL of test media and 15 µL of inoculation culture at 10⁶ CFU/mL in CMHB. All test media were sterile-filtered through 0.2 µm membranes prior to use. Estimated test media conditions take the 9:10 dilution into account. For each set of assays, three wells were filled with culture fluid with no bacteria inoculated, while three negative controls were subject to the same bacterial

challenge without any substrate. The plate was incubated at 37°C under gentle shaking for 16-18 hours. Cell density was read at OD 600 nm in a BioTek® PowerWave™ XS Microplate Spectrophotometer with accompanying Gen5 program Version 1.00.14. All treatments, whether direct infusion into culture or co-immersion of film substrates with the culture, were administered from the time of seeding to data observation. Cultures were incubated at 37°C for 16-18 hours under gentle shaking before observation.

MC3T3 toxicity assay through alamarBlue. MC3T3-E1 Subclone 4 was maintained in minimum essential medium alpha medium supplemented with 10% fetal bovine serum, 100 U/mL penicillin, and 100 mg/mL streptomycin. Cells were split 1:15 every 3-4 days, with the medium refreshed in between. Cells were examined under the microscope every 1-2 days to assess confluence and morphology. For the toxicity assays, cells were seeded at 10^4 /mL in a 96-well plate at 150 μ L per well. Three wells were filled with 150 μ L medium without cells as blank references. Cells were monitored daily until they reach 50% confluence, at which point the medium in each well was replaced with the test medium. All test media were sterile-filtered through 0.2 μ m membranes prior to use. Three wells were left untreated as negative controls. Cells were incubated with the test media for the defined test period. At the end of the test period, medium in each well was replaced with fresh untreated medium, and 15 μ L of alamarBlue was added to each well. Cells were incubated at 37°C for 4 hours, examined visually for color change then read at 570 nm and 600 nm by a microplate spectrophotometer. Cell metabolic activity was computed from the spectrophotometric readings based on manufacturer's specifications.

7.3 Results and Discussion.

Based on my previous work on the incorporation of positively-charged antibiotic gentamicin into polyelectrolyte multilayers²⁴⁵ (see Chapter 5), AmPs were incorporated through a similar multilayer heterostructure with specific architecture [(Poly X/HA)(AmP/HA)]_n, in which *Poly X* is a degradable poly(β-amino ester) and HA is hyaluronic acid. Each repeat of (Poly X/HA)(GS/HA) constitutes a *tetralayer*. Two degradable poly(β-amino esters) were studied: *Poly 1* (Mn = 15.5k) and *Poly 6* (Mn = 16.7k), with structures shown in Figure 5.2.

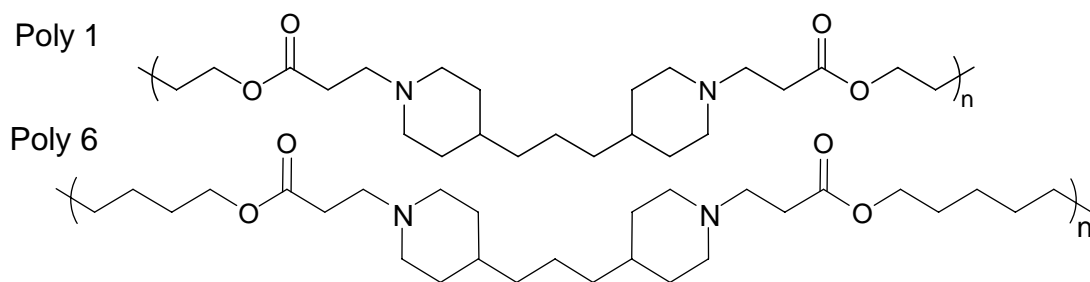
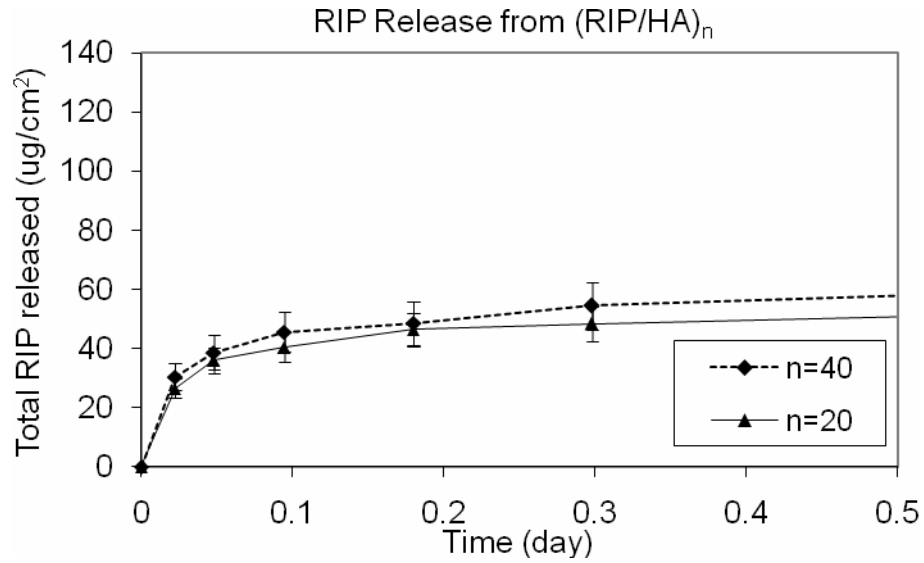


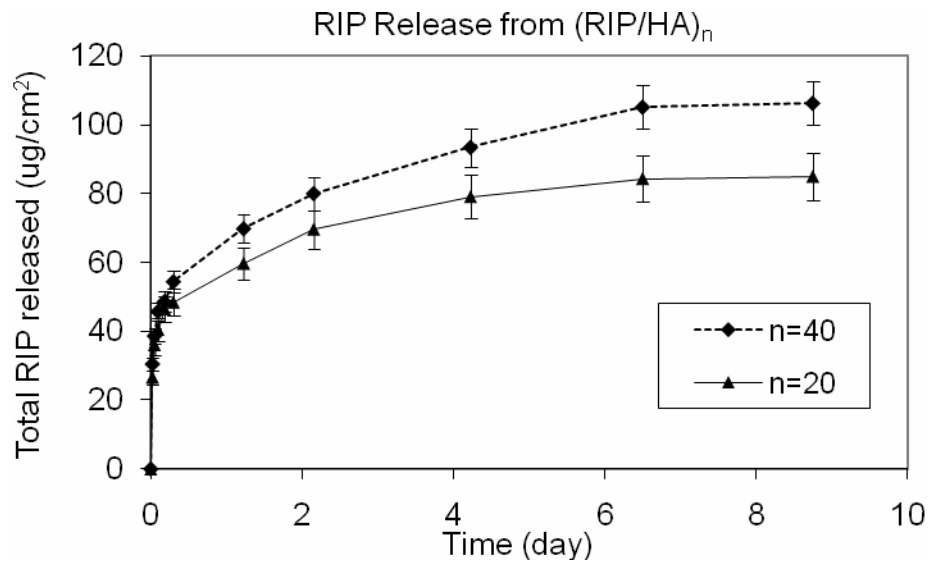
Figure 7.1 - Structures of *Poly X* used in this study.

Choice of film architecture. Proof-of-concept LbL films incorporating AmPs were constructed either with or without *Poly X*, with sodium alginate and hyaluronic acid as the polyanionic component. RNAIII-inhibiting peptide (RIP) and Dermaseptin (Derm) were chosen as the AmP candidates as they were found to be synergistic in the killing of *S. aureus* and MRSA²⁴⁶. I first verified the ability of AmPs to participate in a layer-by-layer process by bilayering them with a polyanion. LbL deposition was performed manually in small wells due to the small quantities of available AmPs. Visual inspections based on yellow hues of the fluorescently-labeled AmPs suggested that a smooth film

was building up over many deposition cycles, although no thickness or absorbance data were gathered for confirmation. The films were subsequently exposed to 1x PBS at 37°C for release assessment, with measurement through fluorescent signal from the peptides' FITC tags. Despite the lack of hydrolytically degradable components within the film, releases of both RIP and Derm from the bilayer constructs were observed (see Figure 7.2 and Figure 7.3). The observed release likely resulted from the oligomeric character of the AmPs, which resulted in LbL films less stable than those constructed solely with polyelectrolytes. Release dosage and rate were tunable based on number of deposited layers and choice of polyanion.



(a)



(b)

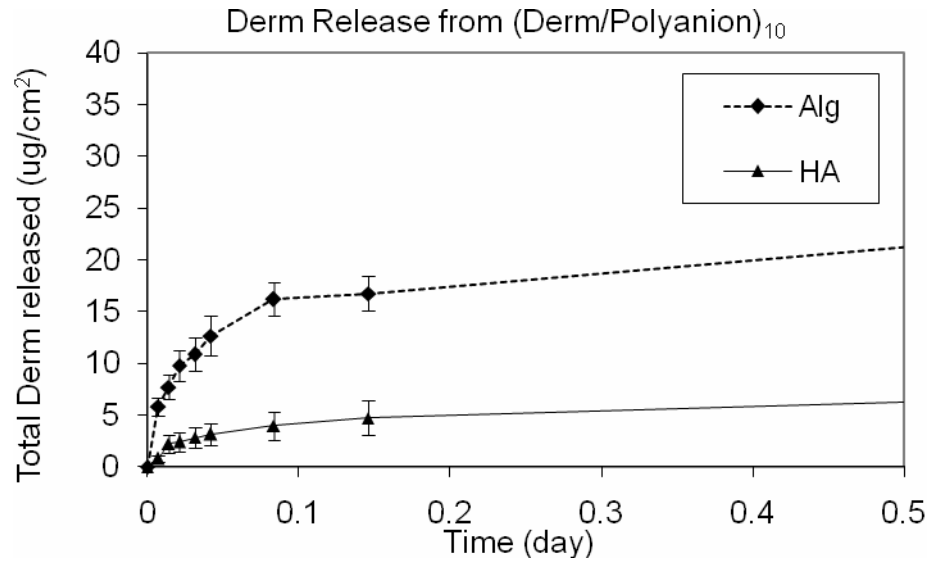
Figure 7.2 – Release of RNAIII-inhibiting peptide (RIP) from a bilayer construct with hyaluronic acid: (a) release curves zoomed in to the initial 0.5 day to compare the burst release profiles between the two types of films, and (b) overall release curves as assessed over 9 days.

As Figure 7.2 shows, RIP release from a (RIP/HA)_n construct can be sustained over 8 days, with approximately 50% burst released within the first 1-2 hours. Based on calibration from FITC-RIP standards, a total of 80 and 100 ug/cm² of RIP was released

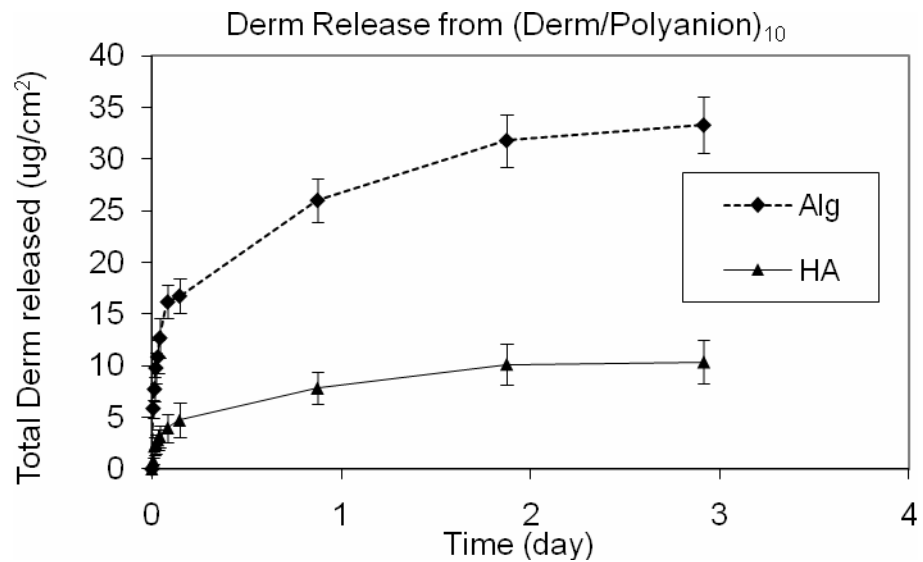
from $n=20$ and 40 , respectively. While this trend was not linear with the number of layers, it did indicate dosage tunability.

A note of caution here is that I eventually found the FITC quantification method to be unreliable due to batch-to-batch variability in the FITC labeling density and general sensitivity of RF signals to experimental conditions. Hence, all the release dosages reported under fluorescence detection should be taken with a grain of salt. This will be further discussed later in this chapter.

For Dermaseptin, I examined the effect of polyanion choice on film release properties. (Derm/Polyanion)₁₀ films were constructed using alginic acid (Alg) and hyaluronic acid (HA) as the polyanions. As Figure 7.3 indicates, a (Derm/Alg)₁₀ film was able to incorporate significantly more Dermaseptin than a (Derm/HA)₁₀ film (35 vs. 10 $\mu\text{g}/\text{cm}^2$), though a more pronounced burst behavior was observed for the former. Both types of films were able to sustain the release of Dermaseptin over 3 days, with (Derm/Alg)₁₀ displaying a two-phase release curve characterized by a rapid 50% release within the first 2.5 hours followed by a slow-release regime over the subsequent 3 days.



(a)



(b)

Figure 7.3 - Release of Dermaseptin (Derm) from a bilayer construct with alginate and hyaluronic acid/

(left) release curves zoomed in to the first day to compare the burst release profiles between the two types of films, and (right) overall release curves as assessed over 3 days.

Hyaluronic acid (HA) was subsequently chosen as the polyanion due to separate experiments demonstrating that alginic acid in combination with *Poly X* could have

independent antimicrobial activities. Additional experiments focused on Dermaseptin due to its ready availability from the Stephanopoulos group.

While the bilayered films gave sustained, dosage-tunable release of RIP and Derm, I wanted to examine films incorporating *Poly X* to allow for an additional degree of release control based on *Poly X* chemistry. Hence, $[(Poly\ X/HA)(AmP/HA)]_n$ were constructed, similar to those for gentamicin incorporation. Releases of Dermaseptin from $(Derm/HA)_{50}$ and $[(Poly\ I/HA)(Derm/HA)]_{50}$ are shown in Figure 7.4.

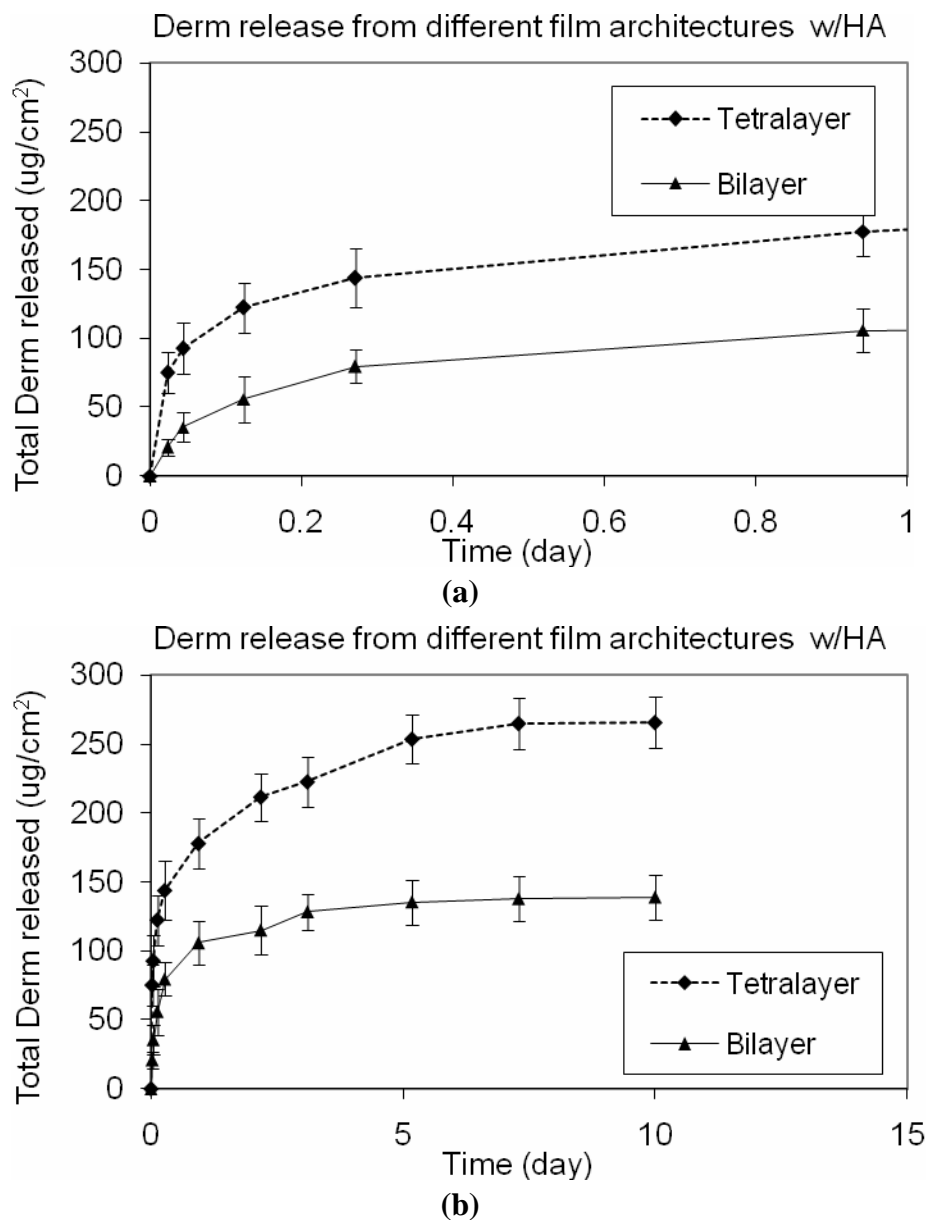


Figure 7.4 - Release of Dermaseptin (Derm) from a 50-bilayer versus 50-tetralayer constructs with *Poly I* and hyaluronic acid.

(a) release curves zoomed in to the first day to compare the burst release profiles between the two types of films, and (b) overall release curves as assessed over 10 days.

The tetralayer construct resulted in more sustained release of Dermaseptin. While 50% total release of Dermaseptin was achieved within 2-4 hours for both types of films, the

tetralayers were able to sustain the slow regime for 8 days as compared to 3 days of the bilayers. Overall, the tetralayered architecture displayed more desirable release properties, and given its additional degree of control through choice of *Poly X*, it was a more appropriate construct to pursue further.

Evaluation of different *Poly X*'s in tetralayer structure. To demonstrate control over AmP release rate through the choice of *Poly X*, tetralayered films formulated with different *Poly 1* vs. *Poly 6* (see Figure 5.2) were compared. Dermaseptin was used in this study, along with Melittin which had a higher activity against *S. aureus*. Figure 5.3 shows the growth curves of $[(Poly\ 1/HA)(Mel/HA)]_n$, $[(Poly\ 1/HA)(Derm/HA)]_n$, and $[(Poly\ 6/HA)(Derm/HA)]_n$. Thicknesses were measured by ellipsometry, and error bars represent standard deviations among multiple sampling locations on each substrate. Data range was limited to the early regime at lower *n*, where films were sufficiently thin and transparent for measurement by ellipsometry.

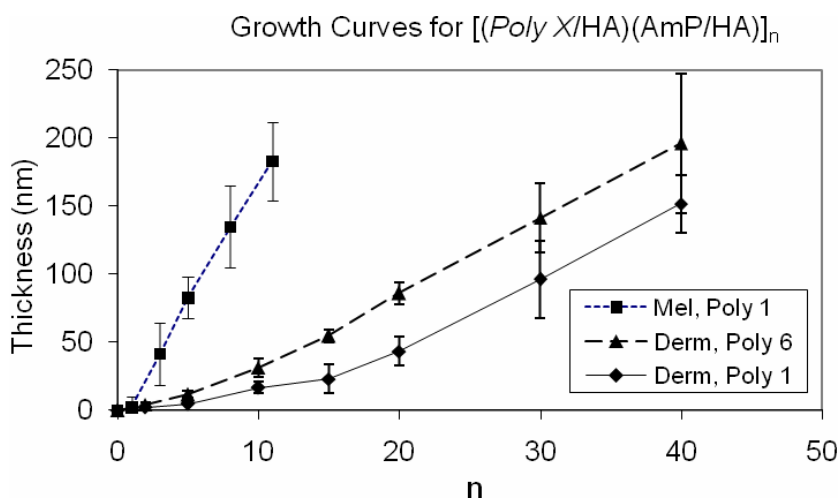


Figure 7.5 - Growth Curves for $[(Poly\ X/HA)(AmP/HA)]_n$ at the early regime with various *Poly X*s and AmPs.

The growth curves suggest that $[(Poly\ X/HA)(AmP/HA)]_n$ generally grew in a linear fashion. This indicates that there was not as much “in and out” diffusion of film components as compared to gentamicin films (see Chapter 5). The higher linearity of $[(Poly\ X/HA)(AmP/HA)]_n$ in comparison to $[(Poly\ X/HA)(GS/HA)]_n$ was expected, as AmPs are much larger than gentamicin and hence less likely to diffuse.

For Dermaseptin, a *Poly 6* film was found to grow faster than a *Poly 1* counterpart, which might arise from *Poly 6*'s higher hydrophobicity that resulted in thicker and loopier films.

For *Poly 1*-based films, a Melittin construct grew faster than the Dermaseptin counterpart. This could be due to Melittin's higher MW and lower charge density:

Melittin was double the length of Dermaseptin (27 amino acids as compared to Dermaseptin's 13) and at the same time only has 5 positively charged residues (counting Lysine (K) and Arginine (R)) as compared to 4 for Dermaseptin, yielding a sequence charge density of 18% for Melittin as compared to Dermaseptin's 31%. Hence, higher hydrophobicity on either the *Poly X* or AmP component was found to result in thicker films.

Release of Dermaseptin from $[(Poly\ X/HA)(Derm/HA)]_{20}$ films was assessed at both 25°C and 37°C. The resulting release profiles are plotted in Figure 7.6. For both types of films, releases at 37°C were expectedly faster than those at 25°C, although the difference was much more pronounced for *Poly 6* films. For *Poly 1*, there was essentially no difference between the two temperatures especially in consideration of the error bars. A possible explanation for the observed differences in temperature dependence was that

Poly 6's hydrophobicity effectively discouraged approach by water molecules to attack its ester bonds, whereas *Poly 1* was not hydrophobic enough to deter rapid seepage of water molecules into its films. Hence, the kinetic enhancement by temperature elevation would be more noticeable for a *Poly 6* film. The hydrophobic effect could also explain the more sustained releases seen from *Poly 6* films.

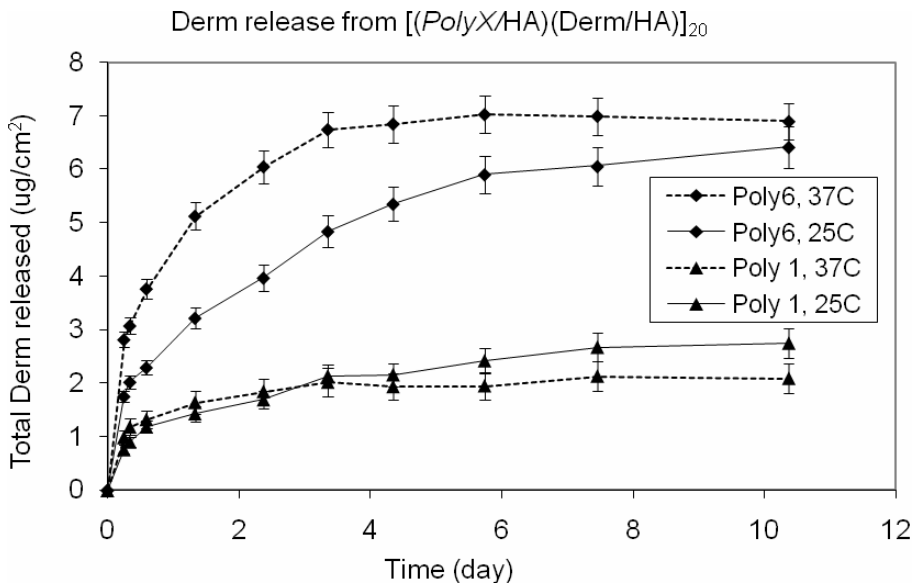


Figure 7.6 – Cumulative release of Dermaseptin from [(*Poly X*/HA)(Derm/HA)]_n films formulated with various *Poly X*s, each assessed at both room temperature (25°C) and physiological temperature (37°C).

Strangely, subsequent experiments could not reproduce the release profiles of [(*Poly 6*/HA)(Derm/HA)]₂₀ films as those in Figure 7.6. Instead, release from a *Poly 6* film was repeatedly found to follow that of Figure 5.5, with a much more pronounced burst. Consequently, subsequent studies were focused on films formulated with *Poly 1*, which were found to yield more reproducible results.

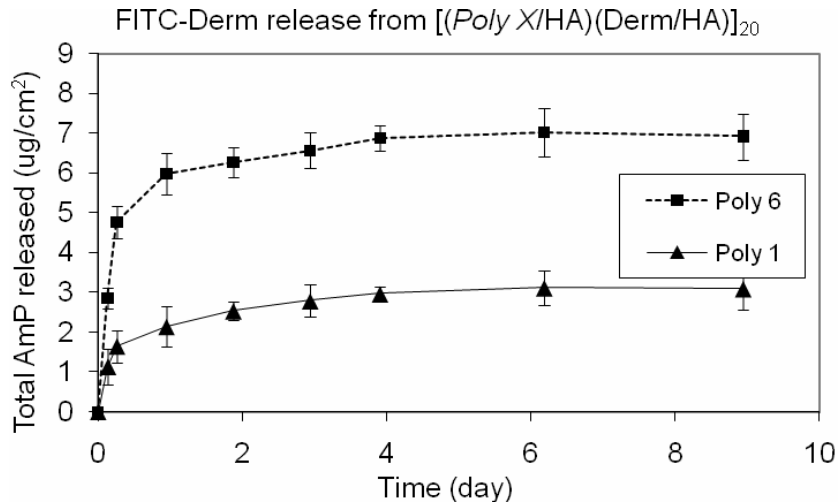


Figure 7.7 – Cumulative Dermaseptin release from 20-tetralayer films made with different *Poly X*'s.

AmP quantification by BCA. All experiments up to this point were performed with fluorescence assessment of AmP quantity. However, significant deviations in release quantities from identical films made with different batches of FITC-Dermaseptin (as made by the MIT Biopolymers Lab) were observed. In addition, the RF signals could fluctuate from one measurement to another due to their sensitivity to ambient light (despite careful controls in foil wrapping and keeping the room dark) and possible decay over time. I suspected that the FTIC labeling density varied from batch to batch, and made a simultaneous comparison of calibration curves constructed from different batches of FTIC-Dermaseptin. As Figure 7.8 suggests, the labeling density varied by as much as 50% between three randomly chosen batches, and could vary by a higher percentage between the two most disparate batches on hand.

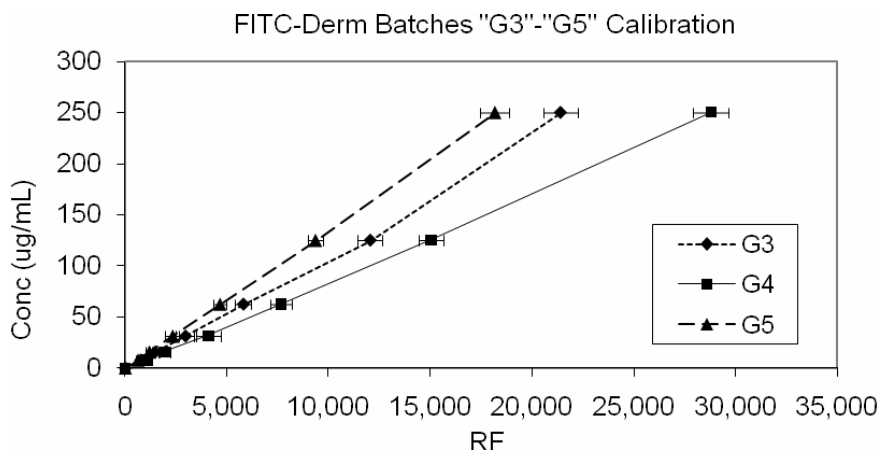


Figure 7.8 – Calibration of RF signals from FITC-Derm samples synthesized in different batches.

The high variability in FITC labeling density would require that a new calibration be constructed for every batch of Dermaseptin received, involving significant time and money expenditure, especially given the fact that only 1-2 g could be made per batch. In addition, I found that the FITC labels were not very stable over time (see Figure 7.9), despite several attempts at improved tag selection by the synthesis lab. Hence, I decided that a new AmP quantification protocol needed to be defined.

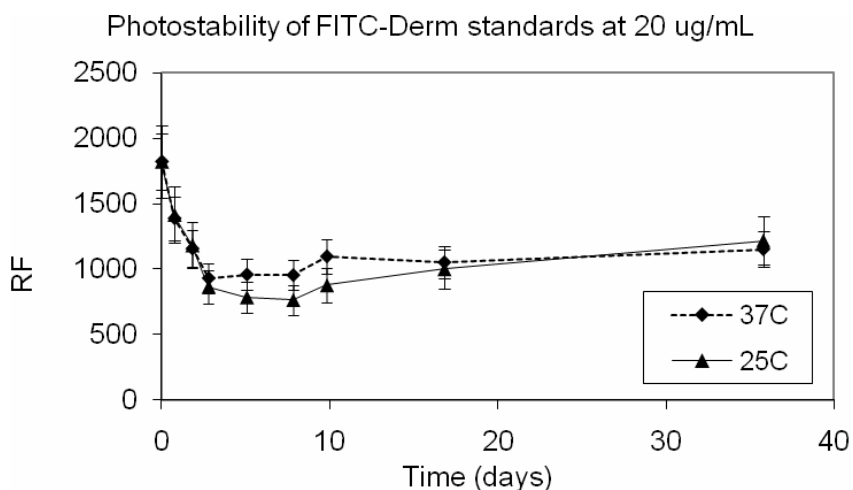


Figure 7.9 – Evolution of RF signal from FITC-Derm standards at 20 ug/mL.

A promising method was the BCA (bicinchoninic acid) protein assay, an assay based on the reduction of Cu^{2+} to Cu^{1+} by protein in an alkaline medium followed by colorimetric detection of Cu^{1+} by bicinchoninic acid. It is a common method for quantifying proteins and peptides, and was already used extensively by Mara Macdonald. To verify the feasibility of using the BCA assay to measure AmP concentrations, I constructed a calibration curve using the fluorescently labeled Dermasetin on hand, and found a decent linear trend (see Figure 7.10).

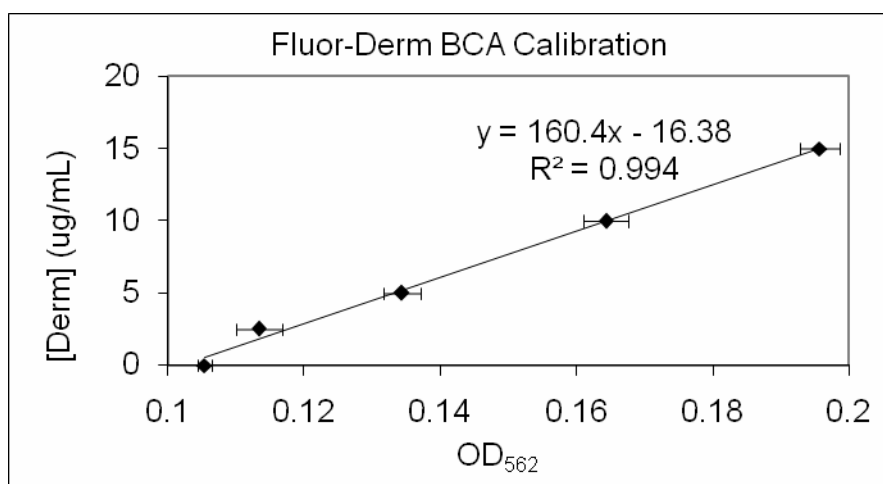


Figure 7.10 – BCA calibration curve for FITC-Derm.

BCA calibrations for both Dermaeptin and Melittin were then constructed, and releases of both AmPs from $[(Poly\ I/HA)(AmP/HA)]_{100}$ films were assessed by BCA. Thicker films were used to ensure adequate BCA signal for accuracy. As Figure 7.11 shows, BCA assessment yielded similar release profiles as those produced through fluorescence quantification. However, the dosages were markedly lower under BCA measurements. For example, $[(Poly\ I/HA)(Dermasetin/HA)]_{50}$ under fluorescence assessment gave $250\ \text{ug}/\text{cm}^2$ (see Figure 7.4), whereas a 100-tetralayer film assessed by BCA gave 150

ug/cm². The fluorescence data was thought to be less accurate due to its batch-to-batch variability and lack of stability. As seen in Figure 7.6 and Figure 5.5, a 20-tetralayer film only released 2.5 ug/cm² of Dermaseptin under fluorescence detection, which again might be an inaccurate figure due to the method of quantification.

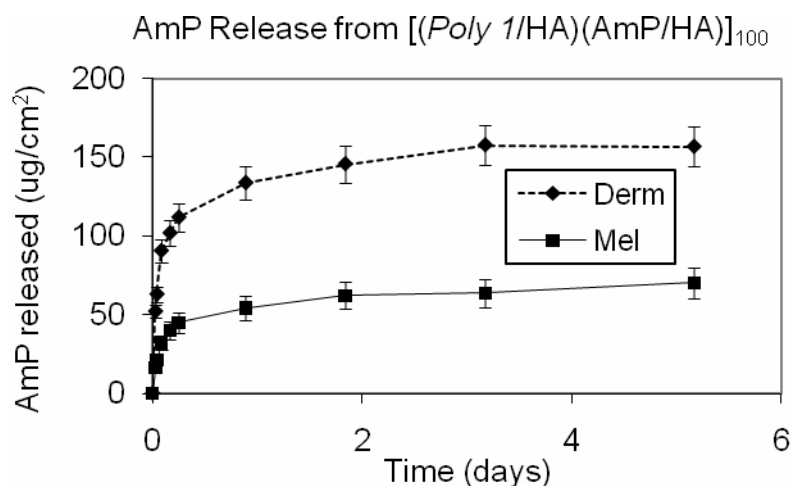


Figure 7.11 - Cumulative Dermaseptin and Melittin releases from $[(Poly\ I/HA)(AmP/HA)]_{100}$. Release assessment was based on BCA rather than FITC signal.

Construction at a milder pH. All experiments thus far were conducted on films made with AmP dipping solution at pH 3.0; the low pH was meant to maximize protonation of the AmPs to facilitate LbL deposition. However, such low pH values may both disrupt AmP activity and cause acid hydrolysis of *Poly X*. Hence, the dipping condition was modified to straight 0.1M sodium acetate without any pH adjustment (~pH 5.1). Growth curves for $[(Poly\ I/HA)(Derm/HA)]_n$ under the both pH conditions are compared in Figure 7.12.

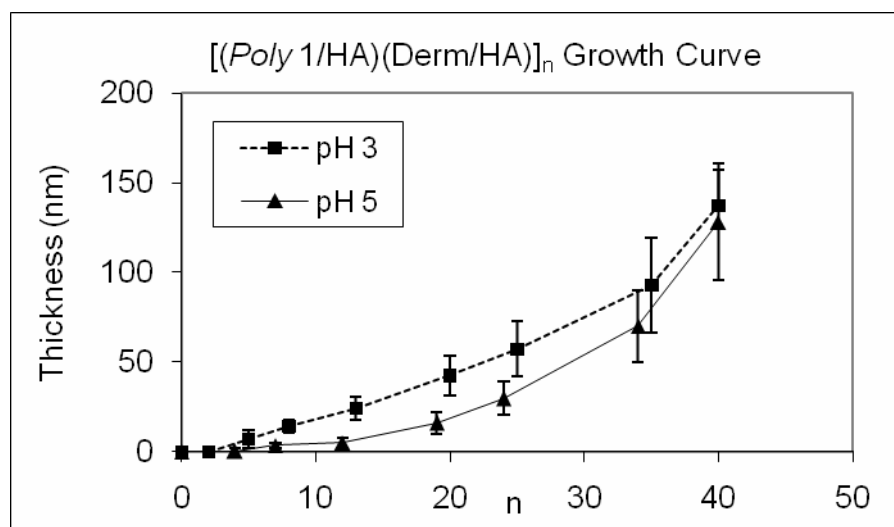


Figure 7.12 - Growth curves of $[(Poly\ 1/HA)(Derm/HA)]_n$ at different pHs.

$[(Poly\ 1/HA)(Derm/HA)]_n$ constructed at pH 5.1 gave similar thicknesses as one at pH 3 in the range examined. However, deposition at pH 5.1 gave somewhat thinner films with a less linear growth trend, suggesting that Dermaseptin may diffuse more easily when it was less protonated. The decreased charge density at pH 5.1 may result in less ionic crosslinking that led to greater freedom of AmP interdiffusion within the film matrix. Overall, deposition at the milder pH appeared feasible, so additional experiments were performed with AmP dipping solutions in 0.1M sodium acetate without pH adjustment.

Co-release with bFGF. It was previously found that a film composed of $[(Poly\ X/heparin)(protein/heparin)]_n$ (where “protein” can be any positively-charged protein, *e.g.* lysozyme, bFGF) followed by $[(Poly\ X/HA)(gentamicin/HA)]_m$ on top can release gentamicin in a much more sustained fashion than a stand-alone $[(Poly\ X/HA)(gentamicin/HA)]_m$ film (see Chapter 6). A similar effect could occur for AmP film constructs. Hence, in collaboration with Mara Macdonald, I constructed combination drug films composed of $[(Poly\ 2/heparin)(bFGF/heparin)]_n + [(Poly$

$X/HA)(Dermaseptin/HA)]_m$. The resulting Dermaseptin release is shown in Figure 7.13, in which the (a) and (b) parts exhibit the same set of data displayed on different time scales. As plots show, the $[(Poly\ 2/heparin)(bFGF/heparin)]_n$ underlayers could indeed extend the release of Dermaseptin from 4 days (see Figure 7.11) to about 2 weeks. In addition, the dosage of Dermaseptin was noticeably increased from $150\ \mu\text{g}/\text{cm}^2$ to $325\ \mu\text{g}/\text{cm}^2$. This increase was most likely due to the diffusion of Dermaseptin into the bFGF underlayer, a similar effect as that observed for gentamicin films (see Chapter 6).

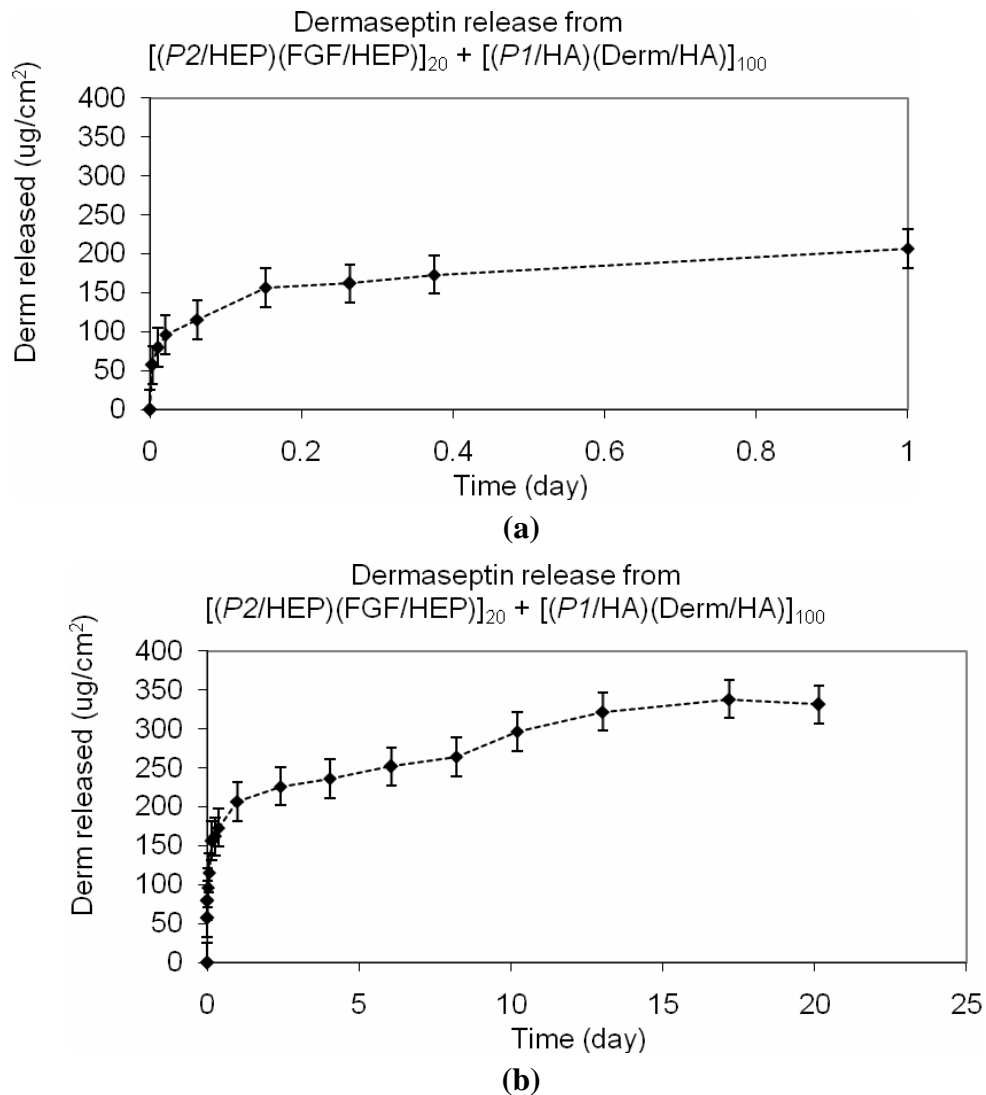


Figure 7.13 – Release of Dermaseptin from $[(Poly\ 2/Hep)(FGF/Hep)]_{20} + [(Poly\ 1/HA)(Derm/HA)]_{100}$. (a) release curve zoomed in to the first day, and (b) overall release curve as assessed over 20 days.

A significant amount of burst release was observed in the first hour. As part (a) shows, about 50% of the total release ($325 \mu\text{g}/\text{cm}^2$ total) occurred within the first 2.5 hours. However, the remaining 50% was released in a steady, pseudo-linear fashion over the subsequent 2 weeks. This release profile may be particularly suitable for remedial treatment of device infections. These complications generally need an immediate burst release of a large dose of antibiotics to kill the infection in place, followed by a sustained, lower dose release to ensure complete eradication. Hence, the profile achieved a protein co-release film would be appropriate for such needs.

Ponericin encapsulation and release. Recent efforts on AmP encapsulation shifted towards the AmP Ponericin G1, which as stated in the Introduction is particularly active against *S. aureus* and a variety of other gram-positive and gram-negative microorganisms, with potentially higher biocompatibility given its low hemolytic activity. Preliminary assessments on Ponericin release are shown in Figure 7.15.

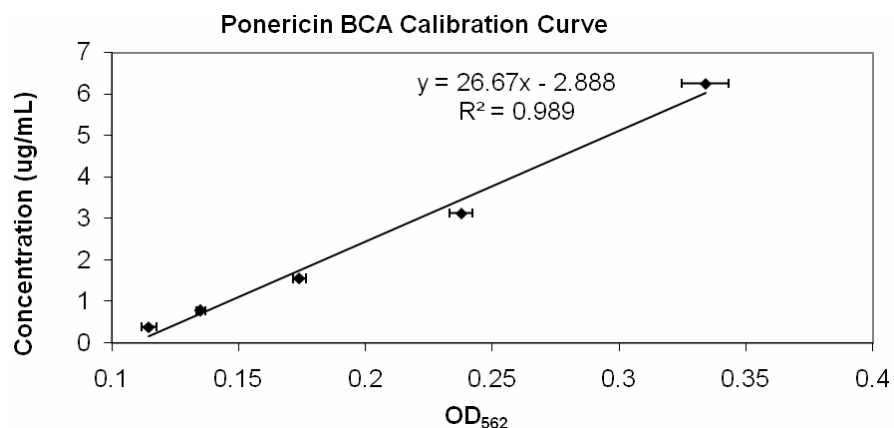
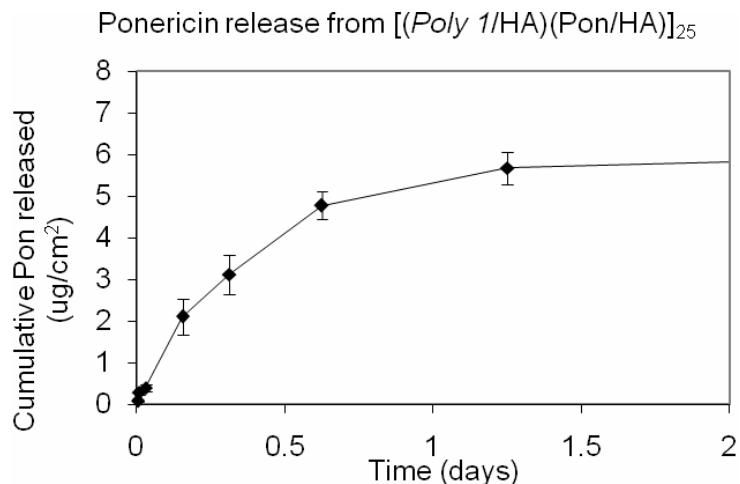
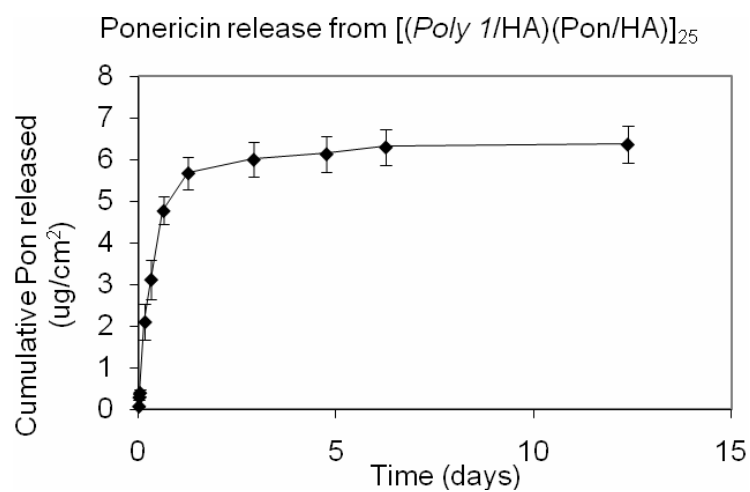


Figure 7.14 – BCA calibration curve for Ponericin.



(a)



(b)

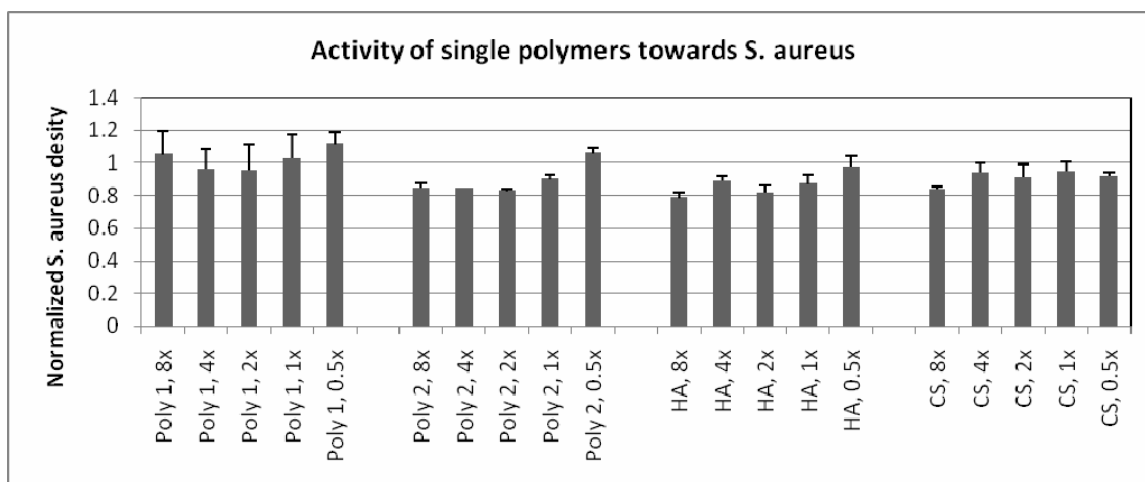
Figure 7.15 - Release of Ponericin (Pon) from $[(Poly\ 1/HA)(Pon/HA)]_{25}$.

(a) release curve zoomed in to the first 2 days to display the 80% release profile, and (b) overall release curve as assessed over 13 days.

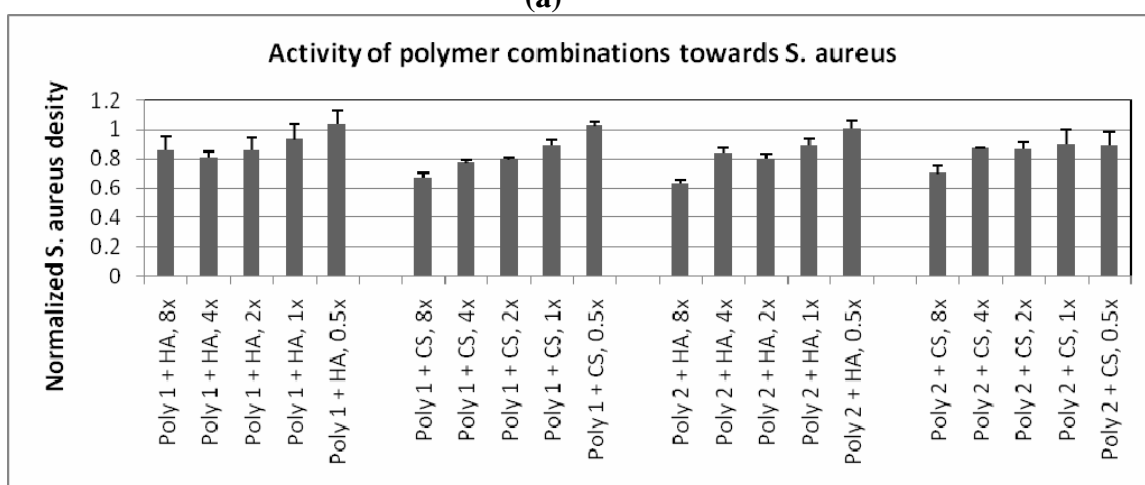
Ponericin-incorporating films are currently under active pursuit by Anita Shukla and Tanguy Chau, and further data will become available on this system.

Activity of polymer co-excipients towards *S. aureus*. To investigate whether the structural components to the film, *i.e.* *Poly X* and the polyanion, could have independent effects on *S. aureus* proliferation, I ran several assays with direct administrations of

single and combinations of polymers to exponentially-growing *S. aureus* cultures and observed their proliferation in comparison to negative controls. These assays were similar to the *Poly 1* + HA assessment performed for gentamicin in Chapter 5, but the present study was more extensive with *Poly 2*, heparin, and chondroitin sulfate added. Polymers were administered at various increments of charge ratios to the model AmP Ponericin. For example, a “1x” concentration of *Poly 1* was a concentration necessary to have a 1:1 charge ratio with Ponericin at its MIC of 4 µg/mL. Hence, for each polymer species, the 1x value would represent a different level of absolute concentration in µg/mL, depending its charge density. The effects of various levels and combinations of polymer treatments on *S. aureus* proliferation are shown in Figure 7.16. Note that in part (b), a polycation + polyanion pair at 1x concentration would mean that each of the two polymers was administered at 1x charge ratio, and hence the overall polymer content of the culture was essentially 2x.



(a)



(b)

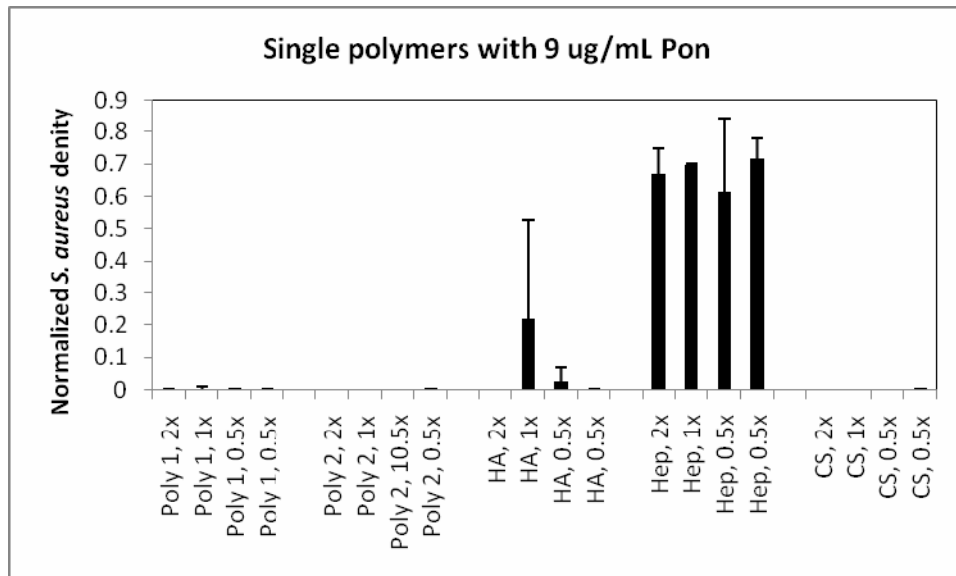
Figure 7.16 – Activity of various levels and combinations of polymers on proliferation of *S. aureus*, normalized to negative controls.

(a) single polymers at various concentrations, (b) combinations of polycations and polyanions at various concentrations. HA stands for hyaluronic acid, and CS stands for chondroitin sulfate, another model biocompatible polyanion.

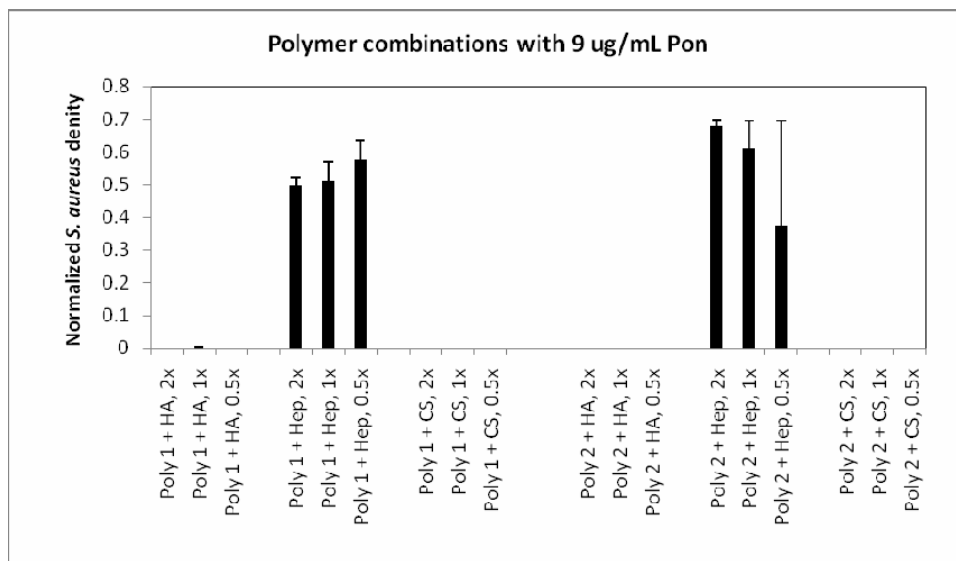
Poly 1 appeared to have little effect on *S. aureus* even at 8x charge ratio to Ponericin, while the other three polymers (*Poly 2*, HA, and chondroitin sulfate (CS)) may have some effect especially at higher concentrations. Among the polymer pairs, *Poly 1* + HA was least inhibitory to *S. aureus* proliferation, while most of the other combinations resulted in 10-40% reduction in *S. aureus* density over the range of 1-8x concentrations. Hence, for *in vitro* assessment purposes, *Poly 1* and HA appeared to be the best polymer pair

among those examined, as they would not complicate the interpretation of antimicrobial activity from the films. For application purposes, however, the potential antimicrobial effects of other polymer pairs could be beneficial, assuming that they do not interfere with the AmP's activity. The potential inhibitory effect of film co-excipients on AmP activity was subsequently investigated.

Effect of polymer co-excipients on AmP activity. Ponericin G1 continued serving as the model AmP. For investigation into the potential inhibitory effect of polymers on AmP activity, various charge ratios of single and combinations of polymers were co-administered with Ponericin at $\sim 2x$ MIC ($9 \mu\text{g/mL}$). The results are shown in Figure 7.17.



(a)



(b)

Figure 7.17 – Effect of various levels and combinations of polymers on activity of Ponericin at 2x MIC towards *S. aureus*, normalized to positive and negative controls:

(a) single polymers at various concentrations, (b) combinations of polycations and polyanions at various concentrations. HA stands for hyaluronic acid, and CS stands for chondroitin sulfate.

The data showed that heparin had a striking inhibitory effect on Ponericin activity. Even at 0.5x charge ratio to Ponericin, heparin essentially took away all of Ponericin’s antimicrobial activity, with the resulting *S. aureus* culture proliferating to 70% of the negative control. As a consequence, any polymer pair containing heparin was also inhibitory, though the effect appeared to be attenuated by the presence of the polycation possibly due to the removal of heparin through complexation.

The mechanism of heparin’s inhibitory activity was unknown. Heparin could either interact directly with Ponericin to interfere with the latter’s binding and penetration into *S. aureus* membranes, or it could interact with *S. aureus* and somehow “toughen” the microorganism against Ponericin. In either case, heparin was clearly not a good

candidate for LbL films for AmP delivery. While HA by itself showed a slight amount of inhibitory effect, its combinations with *Poly 1* and *Poly 2* was non-interfering.

Antimicrobial activity of Ponericin as released from LbL assemblies. *In vitro* activity of Ponericin, both in dipping solution and as released from films, were assessed against *S. aureus*. Serial dilutions of free Ponericin in 0.1M sodium acetate and elution buffers from $[(Poly\ 1/HA)(Pon/HA)]_{100}$ films were administered to *S. aureus* cultures under standard macrodilution protocol. The results are shown in Figure 7.18.

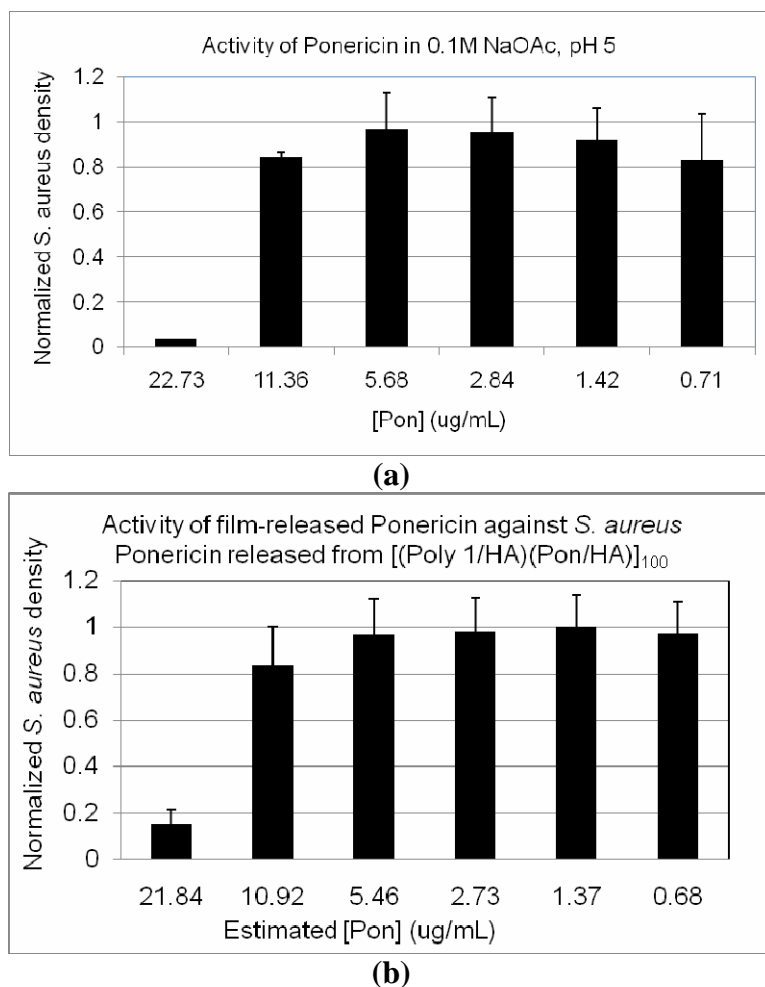
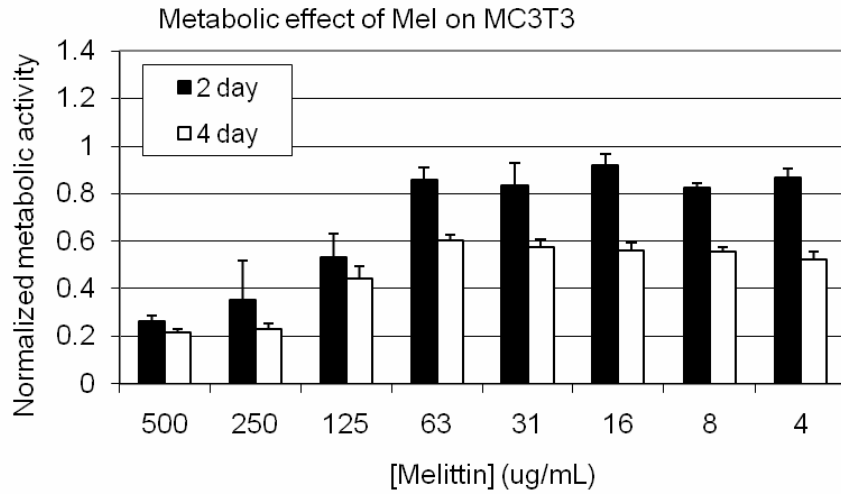


Figure 7.18 – Activity of Ponericin against *S. aureus* proliferation as administered in two forms.

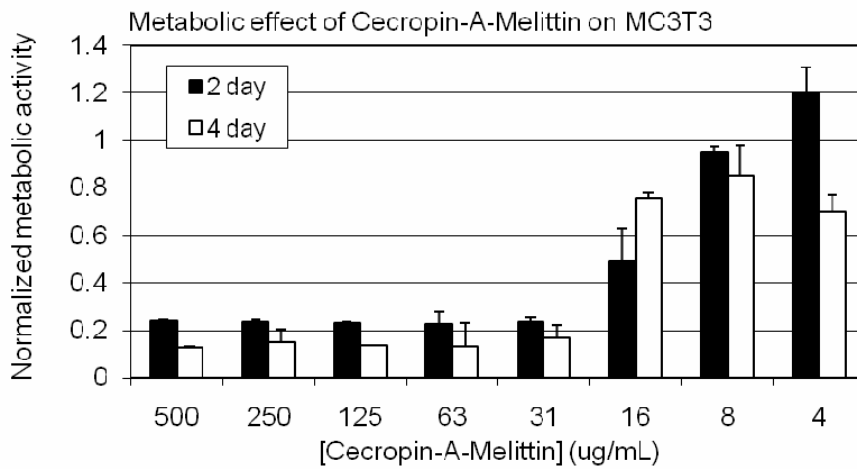
(a) in a free solution of 0.1M sodium acetate, mimicking dipping solution condition, (b) from an elution buffer of $[(Poly\ 1/HA)(Pon/HA)]_{100}$.

As suggested by Figure 7.18, a concentration of ~11-22 µg/mL of both dipping solution or film-released Ponericin was needed to inhibit *S. aureus* proliferation. This range was higher than the reported MIC of 4-8 µg/mL for free Ponericin. Given the similarity of results between dipping solution and film-released Ponericin, the most likely explanation for the higher MIC was that the 0.1M sodium acetate dipping condition was sufficiently harsh to remove some of the Ponericin activity. However, once incorporated into the film, the active fraction retained its activity, and the co-excipients *Poly 1* and HA did not appear to interfere with Ponericin action (echoing results from Figure 7.17). Hence, a necessary investigation on this project would be to optimize the dipping protocol preserve AmP activity while maintaining *Poly 1* integrity and film build-up.

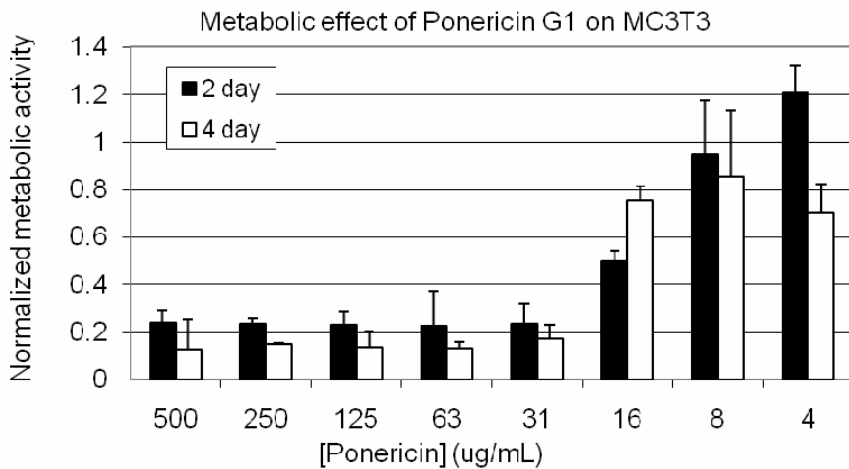
Compatibility of AmPs towards MC3T3. MC3T3, a murine pre-osteoblast, served as the model mammalian cell line for biocompatibility assessment due to previous experience from gentamicin studies (see Chapters 5 and 6). Compatibility was interpreted from the level of metabolic activity of the cell cultures. Various dilutions of Melittin, Cecropin-A-Melittin, and Ponericin were administered to MC3T3 cultures over periods of 2-4 days. The results are shown in Figure 7.19.



(a)



(b)



(c)

Figure 7.19 - Effect of various AmP treatments on MC3T3 metabolic activity level at various concentrations: (a) Melittin, (b) Cecropin-A-Melittin, and (c) Ponericin.

For the three AmPs, toxicity towards MC3T3 over a 2-day treatment appeared in the ranges of 63-125 $\mu\text{g}/\text{mL}$ for Melittin and 8-16 $\mu\text{g}/\text{mL}$ for Cecropin-A-Melittin and Ponericin. Over 4 days, the compatibility limit lowered to beneath 4 $\mu\text{g}/\text{mL}$ for Melittin (lowest dilution tested). For Cecropin-A-Melittin and Ponericin, the MC3T3 cells appeared to recover a little and displayed sufficient metabolic activity up to 16-32 $\mu\text{g}/\text{mL}$. In comparison, the HC_{50} values, or the maximum concentration at which < 50% of human red blood cells were hemolysed over a 1-hr treatment period, were 8, 64, and > 512 $\mu\text{g}/\text{mL}$ for Melittin, Cecropin-A-Melittin, and Ponericin, respectively (data from Tanguy Chau). There appeared to be a slight correlation between HC_{50} values and 4-day treatments on MC3T3, although more assessments towards additional mammalian cell lines are needed, especially on system relevant to the applications identified for AmP-release films, *e.g.* wound dressing. Given the data so far, the biocompatibility of AmPs could be a concern, as the toxicity limits were close to or even lower than the concentrations necessary for AmP action against *S. aureus*.

7.4 Conclusion.

Hydrolytically degradable LbL assemblies for encapsulation and release of antimicrobial peptides (AmPs) were successfully constructed using the familiar heterostructure, $[(\text{Poly } X/\text{HA})(\text{AmP}/\text{HA})]_n$, that was used for gentamicin incorporation. High dosage and multi-day release were achieved for several AmPs of various lengths and charge densities. Release rate could be tuned by the choice of *Poly X* and the use of $[(\text{Poly } X/\text{heparin})(\text{protein}/\text{heparin})]_n$ underlayers. The films were found to be *in vitro* active

against the proliferation of *S. aureus*. Compatibility towards mammalian cells needs further assessment.

In the course of this study, several critical findings were made regarding the design of AmP films. Heparin was found to be highly inhibitory on Ponericin's *in vitro* activity against *S. aureus*, highlighting the importance in selecting appropriate polymers as "inactive" co-excipients of the film. In addition, the standard LbL dipping solution, 0.1M sodium acetate, was found to have a mild effect on AmP activity as well, indicating the need to define a new dipping protocol. Difficulties encountered in batch-to-batch variability in custom-synthesized AmPs and instability of their fluorescent tags pointed out the need to develop a reproducible quantification method for any new therapeutic before extensive film release studies could be undertaken.

Future investigations will focus on one or two specific AmPs, to be selected based on their activity against *S. aureus* and other device-related microorganisms, and on their compatibility towards mammalian cells through hemolysis and other toxicity assessments. In particular, Ponericin G1 is an attractive candidate due to its low MIC against *S. aureus* and low hemolytic action on human erythrocytes. Specific applications for AmP-releasing films will be defined so that the appropriate toxicity assays can be established. UV-vis detection will be developed to quantify the amount of Ponericin encapsulation and release, and will be used in supplement or substitute to the BCA assay.

Acknowledgements.

I would like to thank Chris Loose, now at SteriCoat, for initiating this collaborative effort and being a diligent collaborator and consultant throughout the project. I also wish to thank Tanguy Chau for taking over this effort from Chris and working with me on AmP selection and acquisition, and Professor Gregory Stephanopoulos for devoting resources towards this effort. Within the Hammond group, I would like to thank Anita Shukla for working closely with me and helping out on experiment planning and execution in her process of taking over this project, Mara Macdonald for guidance on the BCA assay, and my UROPs Jeffrey Easley and Michelle Wilson for the efforts they devoted towards these experiments.

References.

- (1) Hancock, R. E. *Drugs*, **1999**, *57*, 469-473
- (2) Tiozzo, E., Rocco, G., Tossi, A. and Romeo, D. *Biochemical and Biophysical Research Communications*, **1998**, *249*, 202-206
- (3) Loose, C., Jensen, K., Rigoutsos, I. and Stephanopoulos, G. *Nature*, **2006**, *443*, 867-869
- (4) Loose, C. R., Langer, R. S. and Stephanopoulos, G. N. *Biotechnol. Prog.*, **2007**, *23*, 444-451
- (5) Etienne, O., Picart, C., Taddei, C., Haikel, Y., Dimarcq, J. L., Schaaf, P., Voegel, J. C., Ogier, J. A. and Egles, C. *Antimicrob. Agents Chemother.*, **2004**, *48*, 3662-3669
- (6) Boulmedais, F., Frisch, B., Etienne, O., Lavalle, P., Picart, C., Ogier, J., Voegel, J.-C., Schaaf, P. and Egles, C. *Biomaterials*, **2004**, *25*, 2003-2011
- (7) Etienne, O., Gasnier, C., Taddei, C., Voegel, J.-C., Aunis, D., Schaaf, P., Metz-Boutigue, M.-H., Bolcato-Bellemin, A.-L. and Egles, C. *Biomaterials*, **2005**, *26*, 6704-6712

- (8) Guyomard, A., Dé, E., Jouenne, T., Malandain, J.-J., Muller, G. and Glinel, K. *Advanced Functional Materials*, **2008**, *18*, 758-765
- (9) Orivel, J., Redeker, V., Le Caer, J.-P., Krier, F., Revol-Junelles, A.-M., Longeon, A., Chaffotte, A., Dejean, A. and Rossier, J. *J. Biol. Chem.* %R 10.1074/jbc.M100216200, **2001**, *276*, 17823-17829
- (10) Lynn, D. M. and Langer, R. *J. Am. Chem. Soc.*, **2000**, *122*, 10761-10768
- (11) Decher, G. *Science*, **1997**, *277*, 1232-1237
- (12) Ayako Oyane, H.-M. K., Takuo Furuya, Tadashi Kokubo, Toshiki Miyazaki, Takashi Nakamura, *Journal of Biomedical Materials Research Part A*, **2003**, *65A*, 188-195
- (13) Standards, N. C. f. C. L. Journal, **1999**, *Approved standard M26-A*,
- (14) Standards, N. C. f. C. L. Journal, **1997**, *Approved standard M7-A4*,
- (15) Chuang, H. F., Smith, R. and Hammond, P. T. Journal, **2008**,
- (16) Balaban, N., Gov, Y., Giacometti, A., Cirioni, O., Ghiselli, R., Mocchegiani, F., Orlando, F., D'Amato, G., Saba, V., Scalise, G., Bernes, S. and Mor, A. *Antimicrob. Agents Chemother.* %R 10.1128/AAC.48.7.2544-2550.2004, **2004**, *48*, 2544-2550
- (17) Picart, C., Mutterer, J., Richert, L., Luo, Y., Prestwich, G. D., Schaaf, P., Voegel, J.-C. and Lavalle, P. *PNAS*, **2002**, *99*, 12531-12535
- (18) Zacharia, N. S., DeLongchamp, D. M., Modestino, M. and Hammond, P. T. *Macromolecules*, **2007**, *40*, 1598-1603
- (19) Wood, K. C., Boedicker, J. Q., Lynn, D. M. and Hammond, P. T. *Langmuir*, **2005**, *21*, 1603-1609
- (20) Wood, K. C., Chuang, H. F., Batten, R. D., Lynn, D. M. and Hammond, P. T. *PNAS*, **2006**, *103*, 10207-10212
- (21) Kujawa, P., Moraille, P., Sanchez, J., Badia, A. and Winnik, F. M. *J. Am. Chem. Soc.*, **2005**, *127*, 9224-9234
- (22) Porcel, C., Lavalle, P., Ball, V., Decher, G., Senger, B., Voegel, J. C. and Schaaf, P. *Langmuir*, **2006**, *22*, 4376-4383
- (23) Porcel, C., Lavalle, P., Decher, G., Senger, B., Voegel, J. C. and Schaaf, P. *Langmuir*, **2007**, *23*, 1898-1904

Chapter 8. In vivo evaluation: design and development of model

8.1 Introduction.

Given positive *in vitro* data on efficacy against *S. aureus* and nontoxicity towards MC3T3, we believed that *in vivo* evaluation should be initiated to advance the development of [(Poly I/HA)(GS/HA)]_n coatings towards device infection controls. The objective of the *in vivo* study is to evaluate the safety and efficacy of the gentamicin coatings in treating a clinically relevant osteomyelitis model.

Osteomyelitis can be broadly classified into two types: acute and chronic. Acute osteomyelitis is commonly associated with bone fraction as introduced during a joint replacement procedure and typically manifest itself within 1-4 weeks after surgery²⁴⁷. If left untreated, the osteomyelitis may evolve into a chronic one, resulting in *sequestra* (necrotic bone tissues) and formation of *involucrum* (new bone) around the infected site.

The first step in planning an *in vivo* study is selection of the animal model, since most other design parameters hinge upon this choice. Under Drs. Hu-Ping Hsu's and Myron Spector's advice, we chose rabbits as our pilot model as they constituted the smallest system available without causing difficulty in manipulating the bones. If we were to observe positive results in rabbits, we would then further our study in goats, which is one of the most accurate animal models in mimicking human bone physiology²⁴⁸⁻²⁵⁰.

After the decision was made on a rabbit model, I surveyed the literature on rabbit osteomyelitis models and found two distinct types: one-step versus two-step procedures. In a one-step procedure, the bacteria inoculum was introduced at the same time as the test material, *e.g.* control or antimicrobial material, and animals were sacrificed after a defined time period for comparison between different test groups. In a two-step procedure, the bacteria inoculum was introduced in a first procedure, usually along with an implant mimic, *e.g.* a cement rod, that simulates the presence of a foreign material. The infection was allowed to develop for a certain amount of time, after which a second procedure was performed to insert the test substrate. While there was consensus that a two-step procedure resulted in a more realistic model for chronic osteomyelitis, there was debate as to whether a one-step or two-step would be a better model for acute implant-related osteomyelitis. A summary of example models from the literature, specific to rabbits, demonstrates the variation in number of procedures, infection site, bacteria burden, and incubation periods:

ONE STEP:

Alt *et al.*¹⁴¹ evaluated their gentamicin-coated steel K-wires through a one-step procedure. Osteomyelitis induction and wire insertion were performed in a single procedure in the intramedullary cavity, in which the tibial tuberosity was perforated and 2 mm-diameter K-wire was driven through the cavity to the distal part of the intramedullary canal. 20 µL of *S. aureus* with 10⁷ total CFUs was then injected into the midshaft area of the canal. Simultaneous osteomyelitis

development and wire treatment proceeded for four weeks, and an infection rate of 88% (7 of 8 animals) was observed for the uncoated K-wire. In all infected animals there was approximately 5×10^8 CFUs/g bone as determined by microbiological evaluation

Gursel *et al.*²⁵¹ used a one-step procedure with osteomyelitis created in an intramedullary aperture in the proximal cortex of the right tibia of albino rabbits (1.5-3kg). An aperture 1.0 cm long was created in the proximal cortex of the right tibia, and stainless steel rods were implanted into the intramedullary area through this aperture. 0.5 mL of *S. aureus* inoculum (hemolytic strain obtained from a chronic osteomyelitis patient) at 5×10^6 CFU/mL (2.5×10^6 CFU total) was introduced into the medullar cavity at the same time. Osteomyelitis was incubated for three weeks, and subsequent treatment by antibiotic-loaded rods was allowed to run for six weeks. The authors noted that among fifty-five animals, five died due to pathological fracture at infection site (1) or diarrhea (4).

Craig *et al.*²⁵² used a one-step procedure with osteomyelitis created in the lateral femoral condyle in NZW rabbits, 4.2 kg on average. Notably, methicillin-resistant *S. aureus* (MRSA, clinical isolate) was used to induce osteomyelitis, and each rabbit received two defects, one on each leg. Defects 4 mm in diameter were drilled transversely into the lateral femoral condyle, anterior to the LCL. This resulted in an intra-articular defect in the nonweightbearing, non-articulating aspect of the lateral femoral condyle. Approximately 0.1 mL of bone cement was

injected into each defect, followed by insertion of a stainless-steel cannulated screw (4.0 mm diameter x 15 mm long) and UHMWPE washer. The defect site was then injected with 100 µL of either saline or inoculum. One group of animals received sterile saline in one knee and 10⁴ CFUs of MRSA in the contralateral knee. A second group of animals received 10² CFU MRSA in one knee and 10³ CFU MRSA in the contralateral knee. Osteomyelitis was developed for seven days.

Darouiche *et al.*²⁵³ used a one-step procedure in which infection was induced in a tibia fracture model in NZW rabbits (4-5 kg). The tibia fracture was made 0.5 cm distal with a fracture-fixation nail in the intramedullary canal. 0.1 mL of *S. aureus* Newman²⁵⁴ at 10⁷ CFU/mL (10⁶ CFU total) was then injected into the intramedullary canal adjacent to the fracture-fixation device. Infection was allowed to develop for six weeks.

TWO STEP:

Nelson *et al.*²⁵⁵ employed a two-step procedure with osteomyelitis created in the radius (bone of the forearm that extends from the outside of the limb to the phlangx (lateral) of the elbow to the thumb side of the wrist). A 1 cm segment of the radius was removed and injected with 10 µL of suspended *Staphylococcus aureus* (ATCC 49230) at 10⁶ CFUs total. The segment was then replaced, the osteomyelitis was allowed to develop for four weeks. In the second procedure,

the infection site was debrided, and tobramycin-loaded pellets were placed in the defect. The treatment proceeded for four weeks prior to sacrifice.

Nijhof *et al.*²⁵⁶ used a two-step procedure with osteomyelitis created in the medullary canal of the tibia of NZW rabbits, 3-3.5 kg. The medullary canal was reamed with drills and fraises up to a length of at least 25 mm and a width of 3.9 mm, and 0.1 mL of *S. aureus* inoculums at a dose of either 10^5 CFU was injected into the tibial canal prior to press-fitting the implant (preformed cement on a central metal wire, 25 mm in length, 3.9 mm in diameter). After four weeks of osteomyelitis development, the site was debrided, rinsed, and filled with test material. Treatment was allowed to proceed for two weeks. The authors noted that inoculation at 10^6 CFU caused too many incidences of sepsis and subsequently reduced the burden down to 10^5 CFU.

Koort *et al.*²⁵⁷ claimed to establish a stage IIIA osteomyelitis in the medullary cavity of NZW rabbits (2.5-3.5 kg) using a two-step procedure. A cortical bone window (6 x 2.7 mm) was drilled into the proximal medial metaphysis of the right tibia, and a defect created in the medullary cavity was filled with a small block of polymerized bone cement. The periosteal and fascial layers were closed first prior to injection of 0.1 mL of *S. aureus* (strain 52/52A/80) at 10^5 CFU/mL (10^4 CFU total) was injected into the medullary space surrounding the bone cement. Infection was allowed to develop for 2 weeks, after which the animals had the

infected medullary space was filled with a composite with or without antibiotic. Treatment proceeded for six weeks.

Some observations from the literature were:

- Intramedullary canal of the tibia appeared to be the most common model site, though other locations such as the lateral femoral condyle or radial canal were also used.
- Bacteria burden varied between 10^3 - 10^7 CFU, with a typical injection volume of 0.1 mL.
- Osteomyelitis was allowed to develop between 3-6 weeks, with the exception of Craig *et al.*'s at one week.
- In two-step models, treatment during the second stage varied between two to six weeks.

Based on Dr. Larry Madoff's input, we chose the two-step model as it was thought to be a more accurate model of treating clinical osteomyelitis that resulted from orthopedic implants. Craig *et al.*²⁵²'s procedure was adopted for our first stage, with a modification to create osteomyelitis in the *medial* femoral condyle rather than lateral. The femoral condyle site was chosen over the intramedullary cavity model for the ease of operation. We wanted to keep our pilot study at a low bacteria burden to minimize distress to the animal and not over-challenge the antimicrobial coating to be tested. Hence, we selected a 10^4 CFU total burden with a three-week infection development, followed by a two-week treatment period.

8.2 Materials and Methods

Materials. All medications, including Ketamine, Xylazine, Buprenex, Meloxicam, and Fentanyl, and standard anesthesia supplies such as syringes, catheters, endotracheal tube, and sterilizing agents, were supplied by the E25 animal facility. Surgical supplies such as drill, saw, blades, scalpels, scissors, and clips, were supplied by Dr. Hu-Ping Hsu. Bio-Gide® was purchased from Luitpold Pharmaceuticals, Inc, (Shirley, NY). Small bone cement rods were made by Dr. Hsu via extrusion using Palacos® by Zimmer (Warsaw, IN), while PMMA rods were custom made by the MIT Machine Shop. New Zealand White rabbits (male, 2-3 kg, generally 3 months old) were ordered from Covance (Princeton, NJ) and allowed to acclimatize for at least one week at the facility before any procedure was performed.

General logistics. All procedures, including animal housing, pre-surgical care, surgical preparation, surgery, radiography, post-surgical care, and tissue harvest, were performed in the E25 facility under supervision of veterinarian Dr. Alison Hayward and veterinary technicians Katie Madden, Chris Autieri, and Sylvia Lesnikowski. All surgeries, survival or sacrifice, were performed in operation room 1 which was approved for BL2 materials, by Dr. Hu-Ping Hsu. Preparations of *S. aureus* samples, including liquid inoculums and colonized PMMA rods, were done at the BL2 culture facility at the ISN. Microbiological evaluations of harvested tissues were done by the diagnostic lab in MIT Department of Comparative Medicine. For histological evaluations, the tissue fixing and bone decalcification were done at the Veterans Affairs (VA) Hospital in Jamaica Plain, while slicing, staining, and slide preparation were done at both VA and MIT diagnostic lab.

Surgical methods. Please refer to Table 8 for a summary of operating parameters specific to each animal, *e.g.* defect size, bacteria burden, sealing procedure, and timeline. Complete surgical protocol is included in Appendix B and summarized below.

Anesthesia was induced by subcutaneous (SC) doses of 35 mg/kg ketamine and 5 mg/kg xylazine,. The left thigh and leg of the rabbit were shaved, and each lower extremity will be prepared with several 7.5% Povidone Iodine scrubs and final 70% alcohol rinse.

Anesthesia was maintained using 1-3% isoflurane gas with oxygen at 1–1.5 L/min through an endotracheal tube. Endotracheal tubes were lubricated with Xylocaine Viscous^R solution prior to insertion. Throughout each procedure, animal's heart rate, respiratory rate, and oxygen level were monitored and recorded every 5 min. Lactated Ringer's solution was administered through a catheter inserted into a cephalic vein, at an initial rate of 10 mL/kg-hr then tapered according to observed hemodynamic parameters.

The left lower extremity of each animal was draped with sterile adhesive surgical drapes. All surgical procedures were performed under sterile conditions. To minimize variability and ensure a standardized surgical procedure, all operations were performed by Dr. Hu-Ping Hsu. A straight medial side incision, approximately 3.5-4.0 cm, was made, the midpoint of which was centered to the knee joint line. The skin and soft tissue were dissected to the deep investing fascia. A small longitudinal incision was made at the front portion of the superior attachment of MCL, approximately 10 mm above a branch of popliteal artery, to release the periosteum to expose the medial femoral condylar surface. Using a sterile drill bit, a defect of specified dimensions was drilled at

the level of the posterior portion of the anterior edge of medial femur about 10 mm. The entire surgical procedure was kept wet by sterile saline sponges, and irrigation was used and maintained during the drills.

After saline joint lavage and hemostasis, the defect was either injected with a liquid live inoculum of *Staphylococcus aureus* at a specified CFU/mL and volume or press-fit with a colonized PMMA (poly(methyl methacrylate) rod (2.8mm diameter and 8.5mm length, with a 3.0mm diameter cap at the top to seal the defect), prepared by immersing sterilized rods in a 10^6 CFU/mL exponentially-growing culture of *S. aureus* overnight. In the case of liquid inoculums, a sterile PMMA rod (1.5 mm diameter and 6.5 mm length) was loosely inserted into the defect after bacteria injection. The defect site might be further sealed with bone wax and a bioresorbable membrane if specified by the protocol. The surgical site was closed in layers using 3-0 interrupted sutures for the investing fascia, 3-0 sutures for the superficial fascia and subcutaneous tissue, followed by reapproximation of the skin with a subcuticular stitch using a non-absorbable 3-0 monofilament nylon suture.

Postoperatively, AP and lateral radiographs were taken on each animal's surgical site, at a setting of 56 kV and 3.2 mA s^{-1} . Each animal was monitored closely until full recovery from anesthesia was observed. Once in their individual cages, each animal was allowed free access to water and antibiotic-free food. Animals were monitored daily for food intake, stool and urine output, body temperature and behavior.

After a specified time period, rabbits designated for osteomyelitis evaluation were sacrificed. 7-10 cc of blood was drawn from the heart after anesthesia but prior to

ethanasia, and stored in Vacutainers for CBC and microbiological evaluation. Under sterile conditions, the skin of each knee was sharply incised and the joint capsule exposed. Fluid was aspirated from each knee joint. The joint capsule was sharply incised, and biopsies from the joint capsule and synovial tissue and fluid surrounding the rod were obtained. The medial femur was cut out and split in half along the implant site, each stored sterilely, one for microbiological evaluation and another for histology in 10% formaline. The implant was retrieved after bone splitting and stored sterilely for microbiological assay. All harvested tissues were placed in 1 mL of sterile freeze medium and sample tare weights were determined. Each rod was sonicated for 30 min in a 4 °C water bath to detach bacteria. Tissue samples were homogenized under sterile conditions using a Polytron generator (Brinkman Instruments Inc., Westbury, NY) in a BL2 hood. Each homogenate was kept at 4 °C before and after homogenization. All tissue processing was performed in instruments approved for BL2 bacteria use and confined within a BL2 hood if possible. Any sample to be taken out of the BL2 hood was tightly sealed in a leak-proof containing device.

Animals designated for implant evaluation received a second survival surgery after a specified period of recovery and osteomyelitis development. Radiographs of the left femurs were taken prior to the second survival surgery, and the surgical sites of the animals were reopened, following the same sterile surgical procedure and monitoring regimen as described above, and treated with focal debridement followed by saline lavage. The PMMA rod (either sterile or colonized versions) were retrieved and stored sterilely in a vial for microbiological assay. The appropriate implant, according to the test group assignment, was press-fit into the defect. After hemostasis and saline lavage,

the wound was closed in layers using the same procedure as described above. AP and lateral radiographs were taken on each animal's surgical site prior to recovery from anesthesia. Each animal received identical postoperative care as described under the first survival surgery.

Animals receiving a second survival surgery were euthanized after a specified time period after second surgery, according to the approved protocol. An x-ray of the left femur was taken prior to the surgery to confirm position of the implant. 7-10 cc of blood was drawn from the heart after anesthesia but prior to euthanasia for CBC and microbiological evaluation. The PMMA rod, bone around the implant site, synovial tissue, synovial fluid, and joint capsule were harvested under identical procedures as those performed on rabbits for osteomyelitis evaluation.

Round-specific designs. A total of four rounds were conducted, each with a different osteomyelitis model. The specifics for each round are described below.

1st round: animals 07-170 to 07-175

For this initial round, we wanted proof-of-concept results without sacrificing too many animals under our newly proposed protocol. Hence, instead of 3+ animals per group for sufficient statistical significance, we assigned two animals per test group. We proposed three test groups: (1) for osteomyelitis model evaluation – these two animals would be sacrificed without receiving an implant, in order to fully evaluate the degree of infection developed by our model, (2) for negative control – these two animals would receive uncoated implants during second

surgery, and (3) for coating evaluation – these two animals would receive [(Poly I/HA)(GS/HA)]₁₀₀-coated implants during the second surgery. Ideally we would have several more test groups, *e.g.* one for positive control, in which the animals would receive an established antimicrobial treatment such as *Palacos® R+G* bone cement with gentamicin (Zimmer Inc., Warsaw, IN), and one group for negative control on osteomyelitis model, in which the animal would receive a sterile saline instead of *S. aureus* inoculum injection. However, as stated above, in order to streamline the pilot study and minimize the use of animals before establishing confidence in our model, we decided to waive the positive control for this pilot round.

Based on surveyed literature, we decided that a total burden of 10^4 CFU *S. aureus* should be sufficient. Dr. Hsu suggested defect dimensions of 8 mm long by 1.9 mm diameter for a sufficiently large reservoir to hold the inoculum while minimizing disruption to the animal's mobility. The defect also had to be sufficiently large so that the localized osteomyelitis to be developed would not be completely drilled away when the defect site was enlarged to 3 mm diameter in the second procedure.

With the defect dimensions of 1.9 mm diameter \times 8 mm length, the void space should be about 0.023 cm³. To mimic an implant-induced osteomyelitis, we decided to insert a loose-fit bone cement rod into the defect at the first procedure to simulate the presence of a surface-colonizable foreign object. We proposed a

dimension of 1.5 mm diameter by 6.5 mm length, occupying 0.011 cm² of volume within the defect (50%). The proposed defect site, size, and bone cement rod dimensions are shown in Figure 8.1. We assumed the bone to be fairly porous and be able to uptake significantly more than the void space. Hence, 100 µL was proposed as the inoculum volume, with inoculum prepared in the exponential growth phase at 10⁵ CFU/mL and kept at -80°C until ready for injection. The defect was to be sealed externally by bone wax to prevent inoculum leakage into surrounding tissues.



Figure 8.1 - Model femur bone showing: (left) defect site at the medial femoral condyle, along with wired bone cement rods and 8mm drill bit, (right) bone cement rod placed into the model defect to check fit.

In terms of timeline, we decided to allow for three weeks of osteomyelitis development, and two weeks for treatment by coated implant. The chosen amounts of time were meant to balance between sufficiency for model development and while not allowing for the animal's self-recovery.

For post-surgery pain management, we only prescribed the pain killer Buprenex. Other commonly prescribed post-surgical medications included anti-inflammatory

and antibiotics, but we could not allow for antibiotics due to the nature of our model, and anti-inflammatory was eliminated out of precaution that it may interfere with osteomyelitis development as well.

2nd round: animals 07-179 to 07-182

Clinical observations from the first round made obvious the excess of the 100 μ L volume of bacteria inoculum. Hence, for our second round, we decided to both enlarge the defect to 3 mm diameter \times 10 mm length and reduce the inoculum volume to 10 μ L. The defect dimensions were chosen to match that of the implant to be inserted during the second survival surgery, so that additional drilling would not be necessary, though extensive debridement may be needed to remove bone tissue growth within the defect. The defect now had a total volume of 70.7 μ L, which should comfortably accommodate the 10 μ L inoculum and the bone cement rod, while allowing some room for blood backflow. The inoculum would be prepared at 10^6 CFU/mL to maintain our proposed 10^4 CFU burden. We kept external bone wax as the sealing procedure, as we believed that the modified defect and inoculum volume should prevent spillage. In addition, since we observed no definitive osteomyelitis in the first round, the osteomyelitis induction period was extended from three to four weeks. Pain management was modified from Q8hr Buprenex shots to Fentanyl patches, a drug delivery form expected to provide a more consistent dosage.

We wanted to conduct a more comprehensive set of studies involving better controls, and hence proposed 20 animals to be divided into seven groups: (1) osteomyelitis evaluation at 10^4 CFU *S. aureus* inoculum, *i.e.* inoculum at 10^6 CFU/mL, (2) osteomyelitis evaluation at 10^5 CFU *S. aureus* inoculum, (3) positive control with treatment of established osteomyelitis by Palacos® R+G, a gentamicin-impregnated bone cement, (4) negative control with treatment of established osteomyelitis by uncoated titanium rod, (5) sample group with gentamicin-coated titanium rod, (6) sample group with lysostaphin-coated titanium rod, and (7) sample group with gentamicin and lysostaphin-coated titanium rod. Two animals were to be assigned to each of groups (1)-(4), while four animals would be assigned to each of groups (5)-(7). Due to high morbidity rate observed in the previous round, osteomyelitis evaluations on groups (1) and (2) would be completed before initiating the remaining groups.

3rd Round: animals 07-222 and 07-223

As we continued observing extensive soft tissue and even joint infections from the second round, coupled with a lack of osteomyelitis development, we believed that it was necessary to improve the method for sealing the defect. Instead of a loosely applied patch of bone wax on top of the defect, we proposed to pack bone wax into the defect and additionally seal the wax-packed defect with a small piece of Bio-Gide®, a collagen-based resorbable membrane used in orthopedic surgeries to prevent soft tissue growth into bony defects. In our case, it would

function as a barrier to the *S. aureus* inoculum. We also shortened the bone cement rod by 1.5 mm to 5 mm in length, to allow room for bone wax.

Another major modification was the addition of anti-inflammatory shots to post-surgical pain management, specifically meloxicam, a non-steroidal anti-inflammatory drug (NSAID). Dr. Hayward believed that adding meloxicam would significantly reduce pain to the animals and hence morbidity rate, improving reproducibility of our model. An NSAID was not expected to interfere with the development of bone infection, so as long as we administer a consistent amount of meloxicam to all rabbits, the osteomyelitis model should remain viable and reproducible.

An identical set as the 2nd round involving twenty animals divided into seven groups was proposed. We would again begin within only groups (1) and (2) for osteomyelitis model evaluation before proceeding to implant evaluation models.

4th Round: animals 08-042 to 08-045

Despite several rounds of modifications on the inoculums injection and defect sealing methods, we frequently observed infection of surrounding soft tissues and knee joint, without significant infection within the bone itself. This was attributed to the spillage of *S. aureus* inoculum out from the defect, despite the thorough double-sealing procedure. In addition, animals exhibited greater signs of distress than anticipated, often requiring sacrifice before study endpoint. Among the

twelve rabbits investigated thus far, osteomyelitis was observed in a few animals, but the results were inconsistent and high morbidity rate was an unresolved problem.

To reduce incidences of soft tissue infections, improve reproducibility of the osteomyelitis model, we proposed a major modification that eliminated the use of liquid inoculums. Instead, a surface-colonized PMMA rod would serve as the source of infection. The rods were custom-

made by the MIT Machine Shop (see Figure 8.2 and Figure 8.3) and designed to have a loose fit within the defect with a press-fit cap at the top. A small metal wire was attached through a hole to facilitate rod retrieval at sacrifice.

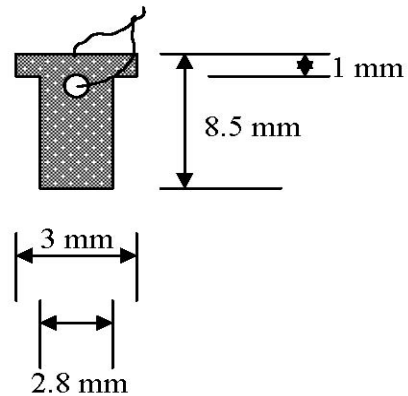


Figure 8.2 - Schematic of the custom-made PMMA rods for Round 4 studies.



Figure 8.3 – Photograph of PMMA rods used to simulate foreign implant object. (Left) custom-made PMMA rod with threaded wire and matching 3 mm drill bit, and (right) insertion into a model 3 mm x 10 mm defect demonstrating good fit.

Surface colonization assays were performed on the PMMA rods to ascertain ability of *S. aureus* to attach and proliferate on this material.

A similar set of seven test groups involving twenty animals as the previous two rounds was proposed, with modified descriptions for groups (1) and (2): (1) osteomyelitis evaluation with PMMA rod colonized in 10^6 CFU/mL culture, (2) osteomyelitis evaluation with PMMA rod colonized in 10^8 CFU/mL culture.

Table 8 summarizes the round-specific operating parameters for each animal.

Table 8 - Summary of schedule and operating parameters

Rabbit	1 st surgery date	Defect size (diameter x length in mm)	Inoculum volume (μ L), concentration (CFU/mL)	Sealing method	2 nd surgery (date, days since last procedure, new defect/implant size)	Sacrifice date (days since last procedure)
07-170	06/05/2007	1.9×8	$20, 10^5$	Loose bone wax	N/A – soft tissue infection	06/13/2007 (8)
07-171	06/06/2007	2.75×8	$40, 10^5$	Loose bone wax	06/27/2007 (21), 3×10	07/11/2007 (14)
07-172	06/06/2007	2.75×9	$50, 10^5$	Loose bone wax	N/A – model evaluation	06/27/2007 (21)
07-174	06/20/2007	2.75×9	$40, 10^5$	Loose bone wax	N/A – too much inflammatory response	06/26/2007 (6)
07-175	06/20/2007	2.75×10	$40, 10^5$	Loose bone wax	07/11/2007 (21), 3×10	07/25/2007 (14)
07-179	07/17/2007	3×10	$10, 10^6$	Loose bone wax	N/A –model evaluation	07/30/2007 (13)
07-180	07/17/2007	3×10	$10, 10^6$	Loose bone wax	N/A –model evaluation	07/30/2007 (13)
07-181	07/18/2007	3×10	$12^\dagger, 10^7$	Loose bone wax	N/A –model evaluation	07/25/2007 (7)

07-182	07/18/2007	3 × 10	10, 10 ⁷	Loose bone wax	N/A –model evaluation	08/15/2007 (28)
Rabbit	1 st surgery date	Defect size (diameter x length in mm)	Inoculum volume (μL), concentration (CFU/mL)	Sealing method	2 nd surgery (date, days since last procedure, new defect/implant size)	Sacrifice date (days since last procedure)
07-222	11/20/2007	3 × 10	10, 10 ⁶	Stuffed bone wax + Bio-Gide®	N/A –model evaluation	12/04/2007 (14)
07-223	11/20/2007	3 × 10	10, 10 ⁶	Stuffed bone wax + Bio-Gide®	N/A –model evaluation	12/04/2007 (14)
08-042	03/19/2008	3 × 10	PMMA rod seeded at 10 ⁶ CFU/mL	None	N/A –model evaluation	04/01/2008 (13)
08-043	03/19/2008	3 × 10	PMMA rod seeded at 10 ⁶ CFU/mL	None	N/A –model evaluation	04/01/2008 (13)
08-044	03/26/2008	3 × 10	PMMA rod seeded at 10 ⁶ CFU/mL	None	N/A –model evaluation	04/23/2008 (28)
08-045	03/26/2008	3 × 10	PMMA rod seeded at 10 ⁶ CFU/mL	None	N/A [‡] – model evaluation	04/23/2008 (28)

[†] an unintentional extra 2 μL was injected.

[‡] Underwent a minor surgery on 04/01/08 to debride incision site and re-sutured.

Bone cement and PMMA rod colonization assessment (non-quantitative). Sterilized rods were immersed into an exponentially-growing culture of *S. aureus* at 10⁵ CFU/mL and incubated overnight. The rods were then thoroughly rinsed with sterile PBS to remove loosely attached bacteria, and placed in a fresh media to incubate overnight. The resulting liquid culture was read at 600 nm for bacteria count.

Clinical observations. Osteomyelitis is indicated by various clinical, radiographic, and surgical observations. However, such signs are merely suggestive and cannot confirm the presence of bone infection without supporting microbiology and histology. Clinical signs

can include fever and local external findings of redness, swelling, and lack of motion or weight bearing. These signs would be monitored on a daily basis after the surgery.

Radiographs. In terms of radiographic evaluation, the telltale sign of osteomyelitis is *radiolucency* (i.e. higher transparency on the x-ray) at the infected site. Radiolucency suggests bone resorption, which is caused by the lytic enzymes released by leukocytes as they attempt to engulf the infectious species. A trained radiologist can also identify necrotic bone tissues and periosteal new bone formation, all suggesting osteomyelitis. Necrotic tissues (“*sequestra*”) and newly formed bone (“*involucrum*”) can both be easily observed during the tissue harvest surgery. Necrotic bone tissues are discolored, spongy, and sometimes fluid-like. Other surgical signs include the presence of brownish granulated soft tissues around the osteomyelitis site²⁴⁷, as well as the presence of *pseudomembranes* within the infected cavity. Pseudomembranes are layers of coagulated fibrin, leukocytes and bacteria overlying a badly damaged mucous membrane and giving the appearance of being a viable tissue.

Microbiological evaluation. This was performed by the MIT Diagnostic Lab in the Department of Comparative Medicine. Standard agar plating procedure was used. Briefly, tissue and pre-ground bone samples were weighed, placed in 1 mL sterile freeze medium (Brucella broth with 20% glycerol), and homogenized by a probe until sample was observed to be completely homogeneous. Implant and joint samples were sonicated in 1 mL sterile PBS. The resulting PBS fluids were diluted (1:1, 1:10; 1:100) and 10 µl of each dilution was streaked on agar plates and cultivated at 37 °C for 24 h. Blood and

urine samples were directly diluted and streaked without processing. Remaining PBS fluids were stored at -20°C, except for blood samples which were discarded after streaking. The number of CFUs was then counted for each agar plate. If the CFU count was too large, the sample was reassessed at 1:1000 dilution. The number of CFUs/g or CFU/mL for each sample was determined by division of the number of CFUs by the initially total weight or volume of the samples. The average of all three dilutions was calculated.

Histology. The remainder of each specimen was fixed in 10% buffered formalin and decalcified in 5% aqueous formic acid solution until total calcium removal was determined by an ammonium oxalate test then processed into paraffin. Paraffin blocks were sectioned at six microns and stained with both standard H&E (hematoxylin and eosin) as well as the Brown-Hopps²⁵⁸ staining method who has been found to be highly selective between gram-positive and gram-negative species²⁵⁹. Briefly, in the Brown-Hopps method, the sample slides undergo deparaffinization, crystal violet staining, fixation in iodine-potassium iodide solution, differentiation in acetone, additional staining in 0.5% basic fuchsin solution, differentiation and fixation in Gellego's solution, staining in Tartrazine solution, differentiation in acetone then picric acid-acetone, and finally xylene to fix and mount.

8.3 Results and Discussion.

Table 9 - Complete blood count (CBC) results for all rabbits

Rabbit	Neutr (%)	Lymphs (%)	Monos (%)	WBC (/mm ³)	RBC (10 ⁶ /mm ³)	HCT (%)	Hgb (g/dl)	Plat Ct (/mm ³)	RBC Indices MCV (fl)
07-170	Blood not collected								
07-171	Blood not collected								
07-172	23	75	2	7.10	6.28	38.1	11.9	238	60.7
07-174	38	60	2	6.30	6.33	36.7	11.8	988	58.0
07-175	58	33	3	5.58	6.6	36.9	11.9	31	55.9
	39	59	2	7.02	6.71	41.0	11.4	524	61.1
07-179	48	48	4	9.22	7.84	47.5	11.8	400	60.6
07-180	51	44	4	9.52	5.91	30.6	8.6	1108	51.7
	57	40	3	14.02	5.23	25.4	7.4	990	48.5
07-181	70	27	3	6.60	6.43	39.0	10.6	194	60.6
	51	47	2	3.88	5.61	35.6	9.0	1041	63.5
07-182	78	21	1	9.50	4.38	23.7	6.6	1082	54.1
07-222	Unable to collect blood								
07-223	72	28	N/A	3.54	5.03	27.5	9.1	1199	54.6
08-042	79	18	3	8.38	6.98	38.5	10.7	1159	55.1
08-043	69	29	2	18.50	5.18	29.3	8.5	1153	56.5
08-044	Blood sample coagulated								
08-045	28	69.00	2	5.8	7.2	40.5	11.7	656.0	56.0

Table 10 - Microbiology results for blood, bone tissues, and implants

Rabbit	Blood (CFU/mL)	Trabecular bone (CFU/g)	Bone around defect (CFU/g)	Materials within defect [†] (CFU/g)	Implant [‡] (CFU)
07-170	N/A	9.24 × 10 ⁵	N/A	N/A	0
07-171	N/A	0	N/A	N/A	0
07-172 (2nd surg.)	0	0	N/A	N/A	0
07-172 (sacrifice)	0	0	N/A	N/A	0
07-174	0	40	N/A	N/A	0
07-175 (2nd surg.)	0	N/A	N/A	N/A	0
07-175 (sacrifice)	0	0	N/A	N/A	0

Rabbit	Blood (CFU/mL)	Trabecular bone (CFU/g)	Bone around defect (CFU/g)	Materials within defect [†] (CFU/g)	Implant [‡] (CFU)
07-179	0	7.72×10^5	N/A	4.20×10^8	1.60×10^7
07-180	0	4.47×10^6	N/A	N/A	3.63×10^6
07-181	0	1.61×10^8	2.07×10^8	3.65×10^9	3.62×10^7
07-182	0	7.94×10^6	N/A	2.13×10^8	1.86×10^8
07-222	N/A	N/A	1000	1.76×10^7	4.00×10^3
07-223	0	N/A	1.5×10^4 , 3.3 $\times 10^4$, 150	2.74×10^7	2.90×10^4
08-042	0	8.70×10^6	N/A	N/A	4.80×10^7
08-043	0	5.93×10^5	N/A	N/A	5.90×10^4
08-044	N/A; N/A	N/A; N/A	0, 526.7, 0; 0, 317, 0	Necrotic tissue: 0; 0, pus: 9.76×10^3 ; 1.50×10^4	0; 0
08-045	0; 0	N/A; N/A	0, 2.04×10^4 ; 0, 1.98×10^4	Pseudomembrane: 3.16×10^7 ; 3.85 $\times 10^7$	0; 20

[†] Could be either bone wax or bone tissue – it was difficult to identify based on visual inspection.

[‡] Implant was sonicated in 1 mL of sterile saline, with resulting saline counted.

Table 11 - Microbiology results for soft tissues and other materials exterior to defect site

Rabbit	Superficial soft tissue (CFU/g)	Superficial soft tissue swab (CFU)	Deep soft tissue (CFU/g)	Periosteum (CFU/g)	Joint Capsule [‡] (CFU)	Others (CFU/g for tissues, CFU/mL for liquids)
07-170	1.56×10^5	20, 0	1.17×10^5	2.28×10^6	4.10×10^2	
07-171	N/A	0	N/A	N/A	N/A	
07-172 (2 nd surg.)	0	0, 0	0	N/A	N/A	
07-172 (sacrifice)	0	N/A	0	N/A	N/A	Synovial tissue = 0,
07-174	0	N/A	N/A	N/A	N/A	
07-175 (2 nd surg.)	N/A	0	0	N/A	N/A	
07-175 (sacrifice)	0	0, 0	7.75×10^3	N/A	N/A	Tendon = 0,
07-179	8.88×10^2	0, 0	2.56×10^2	8.02×10^6	1.12×10^2	
07-180	8.16×10^5 , 1.50×10^8	TNTC*	2.37×10^6	N/A	6.71×10^5	
07-181	9.93×10^4	TNTC*, 127	0	6.22×10^9	N/A	Joint swab = 0,
07-182	1.80×10^3	8	1.02×10^3	N/A	N/A	Synovial tissue = 4.57×10^6 , Joint swab = 26,

Rabbit	Superficial soft tissue (CFU/g)	Superficial soft tissue swab (CFU)	Deep soft tissue (CFU/g)	Periosteum (CFU/g)	Joint Capsule [‡] (CFU)	Others (CFU/g for tissues, CFU/mL for liquids)
07-222	9.17×10^8 , 1.41×10^4	9, TNTC*	3.58×10^5	N/A	N/A	Abscess = 4.56×10^8 ,
07-223	9.43×10^4	60	1.10×10^5	N/A	N/A	Abscess = 1.47×10^3 , urine = 600 (<i>Strep sp.</i> , not <i>S. aureus</i>)
08-042	1.23×10^8	TNTC	6.93×10^7	N/A	N/A	
08-043	7.96×10^6	TNTC	1.60×10^7	N/A	N/A	
08-044	0; 0	0; 0	Granulated : 0; 0	N/A; N/A	0; 0	
08-045	0; 0	0; 0	Granulated : 0; 0	N/A; N/A	0; 0	

* TNTC = too numerous to count

[‡] Joint capsule was sonicated in 1 mL of sterile saline, with resulting saline counted.

1st Round

Bone cement rod colonization assessment. To ensure that the bone cement rod can be surface-colonized by *S. aureus* to simulate an implant infection, an *in vitro* surface colonization assay was performed. However, it was later pointed out by Dr. Lee that the colonization assay used here was not quantitative, so results here should only be taken as a qualitative indication of the surface colonizability of the rods, rather than a quantitative indication of degree of colonizability. Figure 8.4 shows the result from the colonization assay, with five replicates of rods assessed. The mean colony count among the five rods is 1.78×10^8 CFU/mL, with a standard deviation of 0.118 CFU/mL (6.65%). The data indicate that these rods can indeed be surface colonized in a fairly consistent manner.

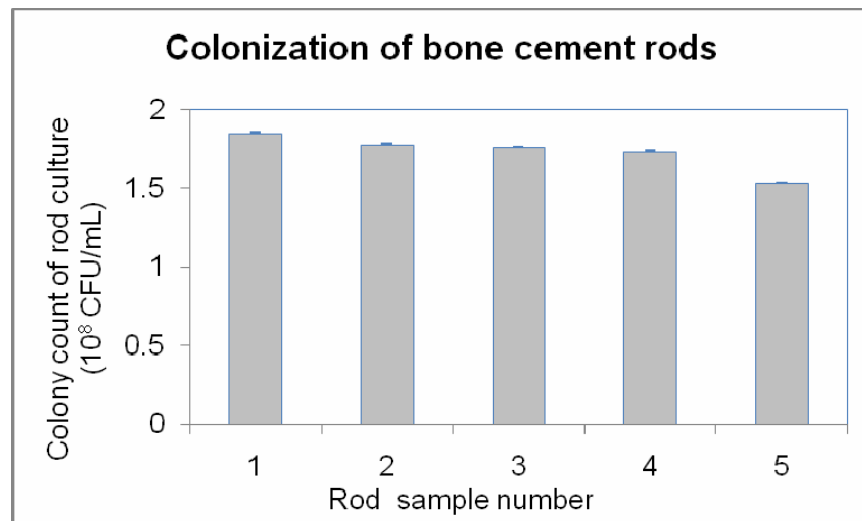


Figure 8.4 - Result of the assessment on surface colonization of bone cement rods by *S. aureus*. Error bars represent standard deviations over triplicate sampling of each culture (values are very small).

Clinical observations. Rabbit 07-173 unfortunately died from anesthesia before the first survival surgery was performed, and hence reduced our pilot study down to five rabbits. For the remaining animals, the cylindrical defects were consistently established in the medial femoral condyle site. However, after the performing the initial surgery on the first

rabbit 07-170, it was immediately obvious that the proposed defect could not accommodate 100 μL of inoculums, especially given the amount of blood backflow out from the defect. With only 20 μL inoculum injected, we already observed spillage out of the defect. Hence, we immediately modified our protocol to enlarge the defect to 2.75 mm diameter \times 8 mm length (47.5 μL of volume), while scaling down the inoculum to 40 μL at the same concentration of 10^5 CFU/mL. Hence, rabbits 07-171 through 07-175 only received 4.0×10^3 CFU *S. aureus* each, but overflow was still observed in some cases. Throughout the next few procedures, the defect was gradually lengthened from one animal to the next, until we reached 10 mm which allowed for complete accommodation of the 40 μL inoculum. For the most part, this modified model appears to work (see Figure 8.5 and Figure 8.6).



Figure 8.5 – Images from 07-174's 1st survival surgery.

(Left) the 2.75 mm \times 9 mm defect, and (right) placement of bone cement rod into the defect after 40 μL inoculum injection.

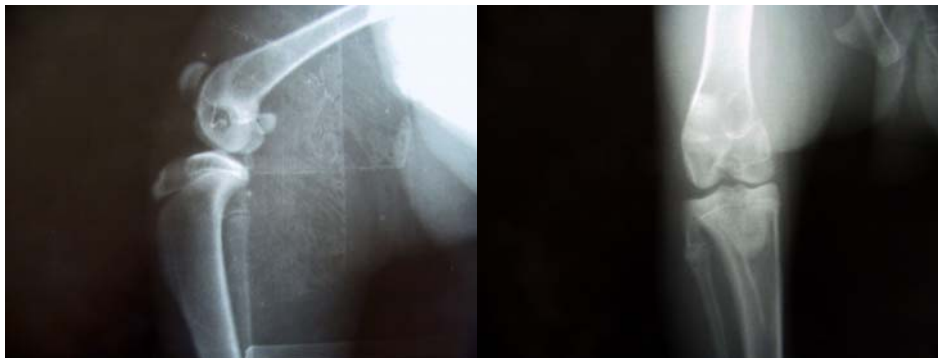


Figure 8.6 – Lateral (left) and AP (anterior-posterior, right) radiographs of rabbit 07-174 after 1st survival surgery, showing drilled defect and inserted bone cement rod.

Another problem we observed was that the defect sealing by bone wax was unsuccessful. Due to a combination of blood and inoculum spillage, bone wax placed on top of the defect would easily fall off even before the skin layers were closed over the defect. All five rabbits likely experienced leakage of most of the inoculum into surrounding soft tissues.

Post operation, rabbits displayed more tissue reactions and signs of distress than anticipated, and many had to be sacrificed before specified study end point due to excessive weight loss or presence of abscess. Instead of the planned three-week osteomyelitis development prior to tissue harvest, 07-170 was sacrificed eight days after first surgery. Indeed, during its sacrifice, we observed extensive infections within the soft tissues (see Figure 8.7), but unfortunately no definitive sign of infection within the defect. A successful bone infection should display a loose, spongy, fluid, and discolored bone material. For a severe infections, visible pus could also be observed¹⁴¹.



Figure 8.7 – Images from 07-170’s tissue harvest, showing (left) visible soft tissue infection but (middle) no definitive sign of bone infection.

A successful bone infection showing yellow pus formation in the intramedullary cavity (from Alt *et al.*¹⁴¹) is shown on the right as a reference.

07-174 was also sacrificed early at six days post-surgery due to inflammatory response observed by Dr. Hayward. However, its tissue harvest indicated neither soft tissue infection nor visible sign of bone infection. 07-171, 172, and 175 fared better and were allowed to survive until defined study endpoints. 07-172 was sacrificed after three weeks for osteomyelitis evaluation. Even after three weeks, we saw no definitive sign of bone infection, and instead observed significant bone re-growth into the defect (see Figure 8.8).



Figure 8.8 – Images from 07-172’s sacrifice. (Left) no sign of soft tissue infection, and (right) bone tissue growth around bone cement rod but no definitive sign of infection.

07-171 and 07-175 were designated to receive a second survival surgery in which coated implants were inserted into an enlarged defect. Since we only had two rabbits for implant evaluation, both rabbits received $[(Poly\ I/HA)(GS/HA)]_{100}$ -coated implants in order to obtain proof-of-concept results on *in vivo* efficacy and biocompatibility of these coatings. However, in both rabbits’ second procedures, there was some difficulty in pulling the bone cement rod out of the defect, suggesting bone tissue growth within the defect. This observation implies that little or no osteomyelitis developed, or we would expect looser bone materials within an infected defect. During the debridement process, Dr. Hsu also

observed that the bone tissues felt dense and uninfected. These tissues were sterilely stored for microbiological evaluation.

Despite the lack of clinical signs for osteomyelitis, second survival surgeries proceeded and the coated glass implants were found to fit well into the defect now enlarged to $3\text{ mm} \times 10\text{ mm}$ (see Figure 8.9 and Figure 8.10).



Figure 8.9 - Images from 07-175's 2nd survival surgery.

(Left) re-opened defect site with bone cement rod still in place, (middle) newly drilled defect at $3\text{ mm} \times 10\text{ mm}$, (right) new defect press-fit with a coated glass rod implant.



Figure 8.10 – Later (left) and AP (right) radiographs of rabbit 07-175 after 2nd survival surgery, showing enlarged defect with a form-fitting implant in place.

After the two-week treatment period, rabbits 07-171 and 175 were sacrificed for tissue harvest. In both rabbits, we observed loose, fluid tissue immediately around the glass implant, and the implant pulled out very easily (see Figure 8.11). We suspected that the combination of film degradation and smoothness of the glass surface discouraged bone

tissue growth onto the implant. Based on this hypothesis, we decided that upcoming studies should use either bone cement or titanium as the implant to be coated to result in a more regenerative surface.

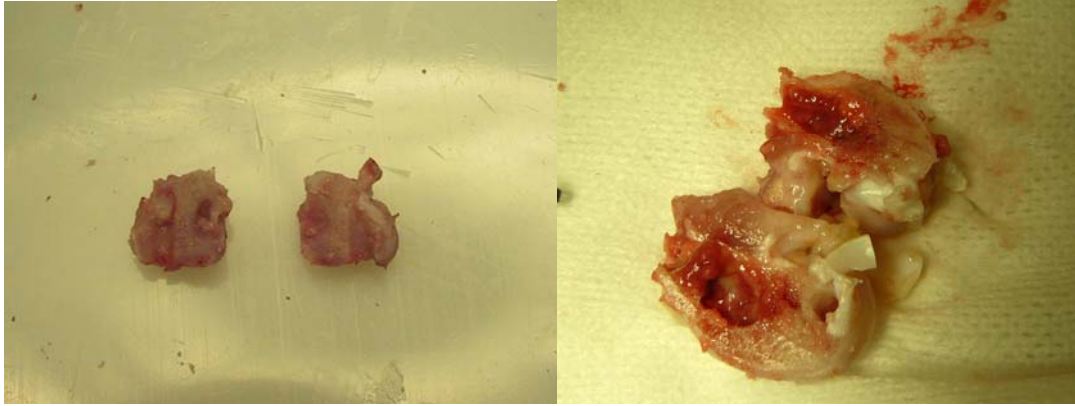


Figure 8.11 – Images of split bone from tissue harvests of 07-171 (left) and 07-175 (right), both of which received a coated implant at 2nd survival surgery.

There were signs of bone resorption suggesting that bone tissues could not grow onto the glass surface.

Neither 07-171 nor 175 was thought to have osteomyelitis based on visual observations during the second survival surgery and results from microbiology (see Table 10). Hence, no conclusion could be drawn on the efficacy of the $[(Poly\ I/HA)(GS/HA)]_{100}$ coatings.

Microbiological evaluation. Table 10 and Table 11 summarize results from quantitative microbiological evaluations on the tissue and implant samples from all rabbits. One immediate observation was that little to no bacteria was found in any of the bone or implant samples of rabbits from Round I, with the exception of 07-170 which had 9.24×10^5 CFU/g of *S. aureus* in its trabecular bone sample. This finding suggests that none of the rabbits from the first round developed clinically relevant osteomyelitis. On the other hand, two of the rabbits, 07-170 and 07-175, experienced a significant amount of soft tissue infection, with 07-170 having high *S. aureus* counts in all its superficial and deep

soft tissue samples. The microbiological results on 07-170 were consistent with the visual observations made during its tissue harvest (see Figure 8.7). Given these results, we believed that our pilot osteomyelitis model was suboptimal, as there was a lack of both osteomyelitis development and reproducibility between animals.

As to be seen throughout this animal study, none of any rabbit blood sample returned any bacteria count. This was the desirable outcome, as the model was not intended to cause bacteremia or sepsis in the animals.

Histology. Brown-Hopps staining was used to stain for *S. aureus* in the tissues. In a Brown-Hopps stained specimen, gram-positive microorganisms such as *S. aureus* would show up as dark blue or purple spots. As a reference, infected tissue samples from Alt *et al.*¹⁴¹ are reproduced in Figure 8.12 to demonstrate histological signs of *S. aureus* in histopathology.

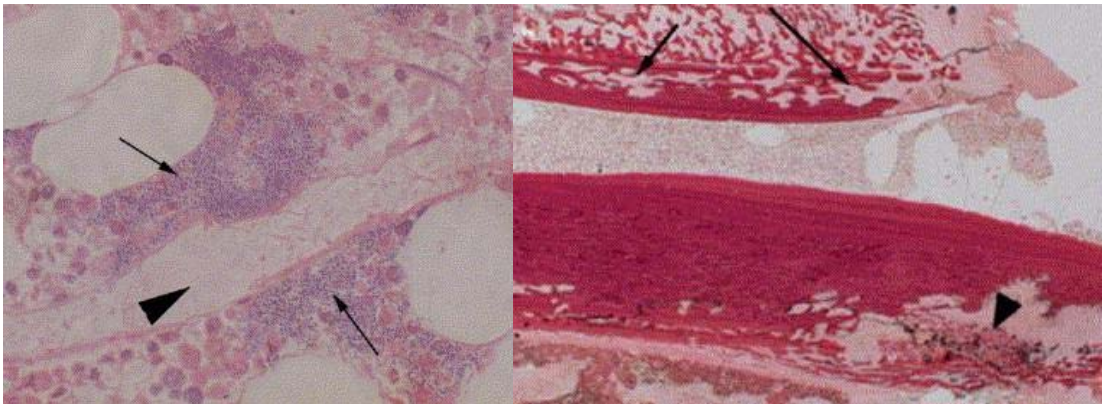


Figure 8.12 – Reference samples from Alt *et al.*¹⁴¹ to demonstrate signs of osteomyelitis under histology. (Left, objective 100x) presence of *S. aureus* (arrow) as indicated by purple-blue color under gram stain, and bone necrosis (arrowhead), and (right, objective 1.5x) signs of cortical lysis (arrow) and abscess formation (arrowhead), both indicative of bone infection.

Joint capsule and soft tissue samples from rabbits 07-170 to 175 showed apparent signs of *S. aureus* in the form of dense dark-purple spots (see Figure 8.13 and Figure 8.14).

However, upon consultation with clinical pathologist Dr. Daniel Milner, we were instructed that the dark spots were artifacts arising from the staining process. Dr. Milner made this assessment based on the streaky morphology of each spot. Hence, the histology did not positively affirm the presence of bacteria in the tissue samples.

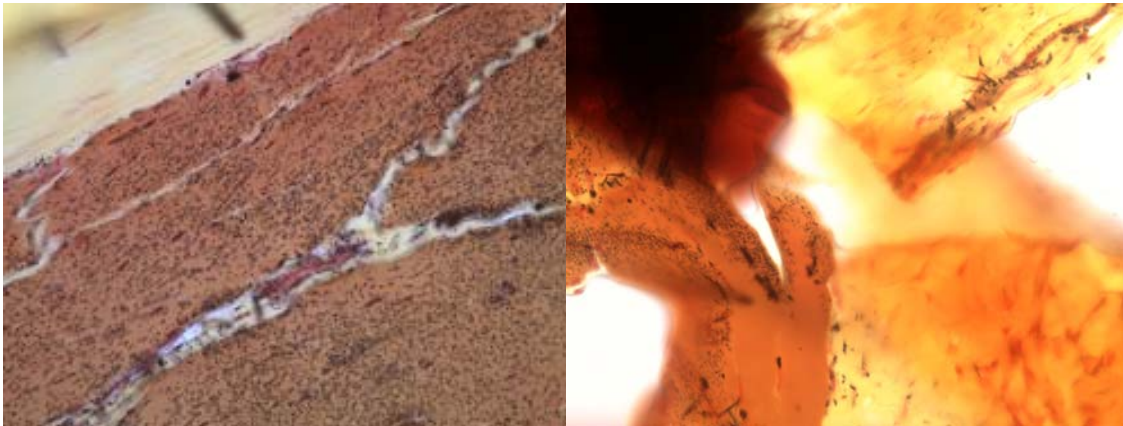


Figure 8.13 – Sample histology on 07-170’s joint capsule slices.

(Left) a low-magnification image showing apparent proliferation of purple colonies, and (right) a high-magnification image showing the purple colonies in greater detail.

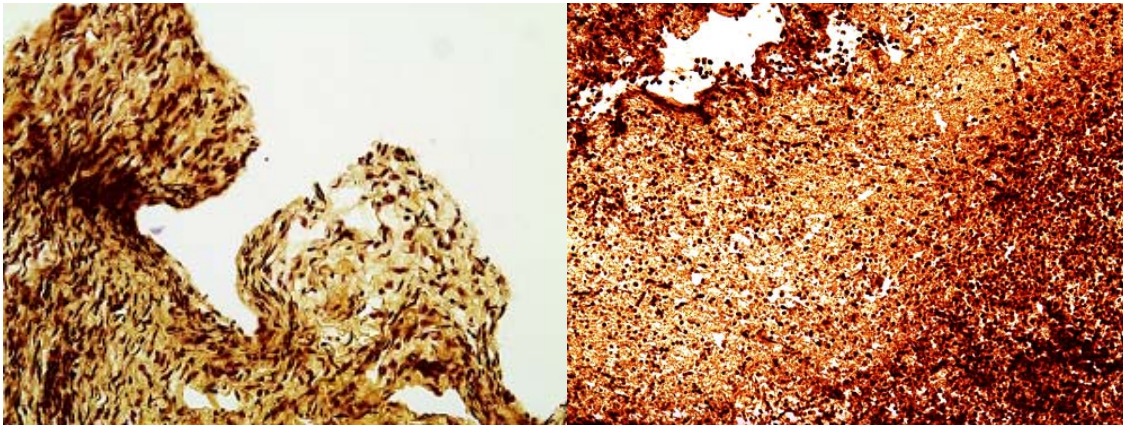


Figure 8.14 – Sample histology on 07-172’s deep soft tissue (left) and 07-174’s superficial soft tissue (right), both of which displaying dense presence of dark colonies similar to those observed in 07-170’s joint capsule staining (Figure 8.13).

2nd Round

Clinical observations. In this round, the defect was enlarged and *S. aureus* inoculum volume was reduced to minimize spillage into surrounding tissues. While no visible

leakage was observed during the first surgery of every animal within this around, we suspected that leakge could occur after suturing due to the looseness of the bone wax sealing.

Because of the significant illnesses observed among rabbits in the previous round, weight loss and temperature of the rabbits were diligently monitored post operation (see Figure 8.15). Steady and significant weight loss was observed among all four rabbits, consistent with our observation of the lack of appetite. Temperatures fluctuated but were generally within the acceptable range after 1-2 days of post-op fever.

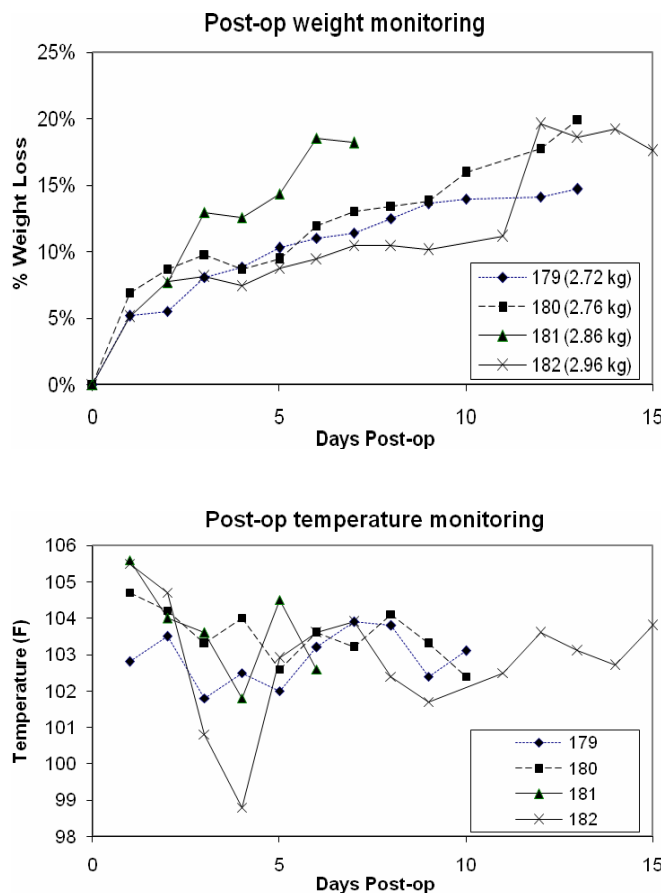


Figure 8.15 - Post-op health stats of rabbits 07-179 to 07-182

Based on the 15% weight loss limit, most rabbits were sacrificed within 7-15 days post operation. Force-feeding was attempted on rabbit 07-182 through syringe injection of a combination of Nutra-Cal™, ground rabbit feed, and water into the rabbit mouth once or twice per day. While its weight appeared to maintain under the force-feeding regimen, the method was not encouraged for the long term. Therefore, even if the present model was efficacious in establishing osteomyelitis, it would not eliminate the problem of animal morbidity and hence irreproducibility stemming from unpredictability of study endpoint.

All four animals were sacrificed for osteomyelitis model evaluation, some before the study endpoint. Radiographs were taken prior to tissue harvest, and we looked for signs of infections such as radiolucency, periosteal elevation, architectural deformation, bone shaft widening, new bone formation (“*involucrum*”) and soft tissue deformation²⁵¹. As an example, 07-179’s radiograph (Figure 8.16) displayed radiolucency around the defect site, suggesting that osteomyelitis did occur to cause alterations in tissue density.



Figure 8.16 – Lateral radiograph of 07-179 prior to sacrifice. Radiolucent lines are evident around the implant, suggesting osteomyelitis development.

Clinical observations during all four animals' tissue harvests suggested that while soft tissue infection still occurred, osteomyelitis was established as well (see Figure 8.17 and Figure 8.18). In particular, significant discoloration was seen, and tissue around the defect felt spongy. The observed tissue texture was consistent with the radiographic finding. The strong clinical findings of osteomyelitis were later confirmed by microbiological evaluations.

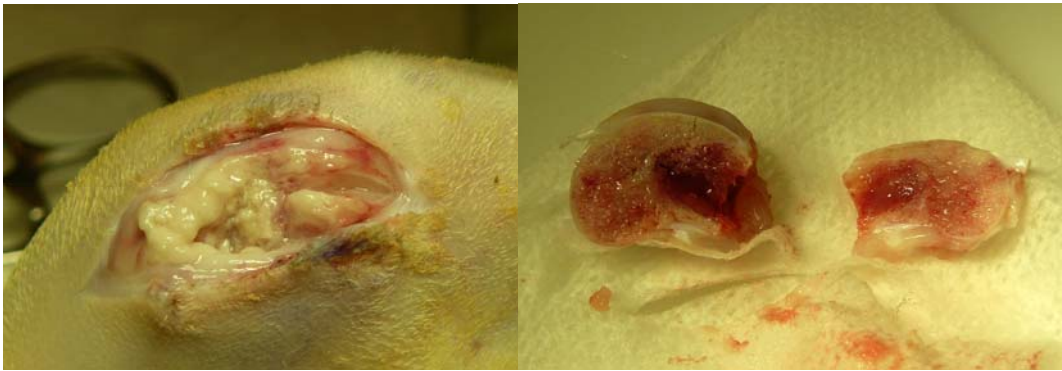


Figure 8.17 – Images from 07-181's sacrifice. Soft tissue infection still developed (left), though bone infection appeared to be established as well (right) based on the softness and discoloration.

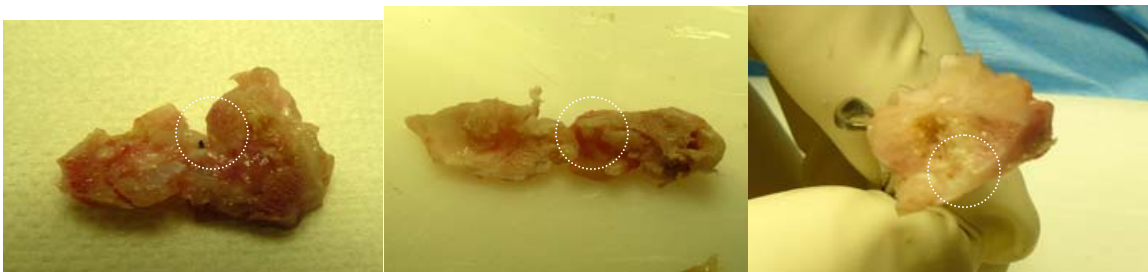


Figure 8.18 – Images from 07-179, 07-180, and 07-182's sacrifices (from left to right), showing split femur bones revealing the defect site (circled).

All three bone samples, along with 07-181's as shown in Figure 8.17, display signs of softness and discoloration indicative of infection.

Microbiology. As data from Table 10 and Table 11 suggest, significant *S. aureus* counts were found in bone tissue samples from all four rabbits in this round. In addition, all the

retrieved implants had high levels of surface colonization. However, at the same time, all four animals displayed high bacteria counts in the soft tissue samples as well, confirming our visual observation of soft tissue infection around the defect (see Figure 8.17). Dr. Hayward indicated that infection of the periosteum (fourth sample column of Table 11), a membrane that lines the outer surfaces of bones, would be particularly painful and result in higher morbidity. For animals with periosteum samples available (07-179 and 07-181), the *S. aureus* counts were indeed high (8×10^6 and 6×10^9 CFU/mL, respectively), and this periosteal infection may explain the significantly weight loss we observed among these animals. We continued to see no bacteria count in blood, indicating that none of the rabbits developed bacteremia.

As the microbiological evaluation suggests, using smaller inoculum at higher concentration did increase the chances for osteomyelitis development. However, it did not resolve the problem of inoculum spillage into the surrounding tissues that caused undesirable soft tissue reactions.

3rd Round

In the third round, we went beyond mere reduction in inoculum volume and implemented a modified defect sealing procedure. Instead of loosely sealing the inoculated defect with a piece of bone wax, the wax was to be packed into the defect followed by coverage of the plugged defect with a bioresorbable membrane. Similar to the previous rounds, the osteomyelitis model needed to be verified prior to an actual sample evaluation, so two rabbits were investigated on this new design. Observations during the surgery suggest

that this modified procedure did contain the liquid inoculum better but not perfectly. Small amounts of leakage were still seen. Post-surgical radiographs (see Figure 8.19, left) showed the positioning of the PMMA rod within the drilled defect. Radiographic evaluation on the same animal two weeks after the inoculation (Figure 8.19, right) displayed radiolucent lines suggestive of osteomyelitis.



Figure 8.19 – Lateral radiographs of 07-223. (Left) right after 1st survival surgery, showing 3 mm defect with inserted bone cement rod, (right) two weeks after 1st surgery, showing radiolucent lines.

Visual evaluations of rabbits 07-222 and 07-223 yielded very similar results as those seen for Round II. While signs of osteomyelitis such as discoloration and sponginess of the bone were present, there was also a significant degree of soft tissue infections. During the two-week incubation period, the two animals experienced about 10% weight loss each – not as severe as the previous round, although their health conditions were not ideal either.

Microbiology. Similar to the previous round (animals 07-179 to 07-182), the two animals from this round had high *S. aureus* counts in both bone and soft tissue samples. Hence, while the desirable osteomyelitis was achieved, the new sealing procedure did not

eliminate the problem of soft tissue infections. In fact, in comparing the *S. aureus* counts between the 2nd and 3rd rounds of animals, the latter had a higher mean count of *S. aureus* in soft tissues. In addition, noticeable abscess was observed on both 07-222 and 07-223.

4th Round

PMMA rod colonization assessment. Similar colonization assessments as those done on bone cement rods were performed on the custom-made PMMA rods, but with higher CFU count in the seeding culture to further promote denser colonization and possibly biofilm formation. We also wanted to ascertain that the adhered bacteria can survive -80°C storage. Figure 8.20 shows data from these assays. As stated previously, this assay was later found to be non-quantitative based on Dr. Lee's input, so that the results in Figure 8.20 should only be taken as a qualitative indication of bacteria survivability.

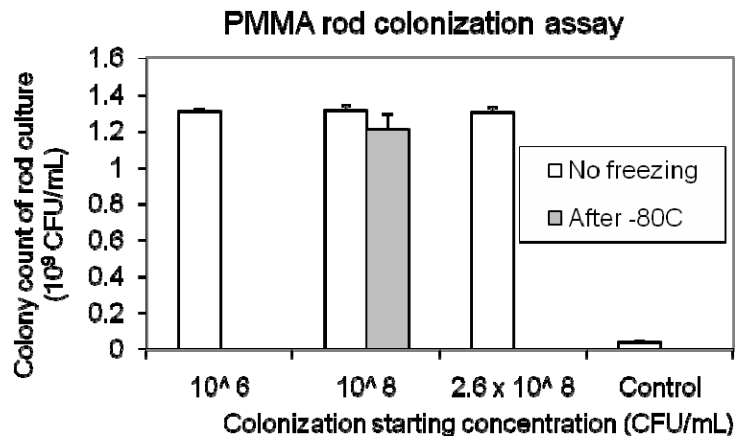


Figure 8.20 - Result of the assessment on surface colonization of bone PMMA rods by *S. aureus*. Error bars represent standard deviations over triplicate rod samples.

Similar to the bone cement rods, we observed colonization of all PMMA rods, and at least a fraction of the colonizing bacteria remained viable after -80°C storage. Ideally we would also assess degree of biofilm formation through a count under the microscope, a

procedure which would involve fixing the adhered bacteria, staining them using an agent like crystal violet, then visualizing them under oil-immersion microscopy. However, there were difficulties in locating all the necessary resources, so these assays were not performed for the time being.

In the study protocol, we proposed osteomyelitis model evaluation with PMMA rods colonized at 10^6 and 10^8 CFU/mL for two separate test groups. However, after the colonization assay, we decided to use 10^6 CFU/mL as the seeding concentration for all four test animals, since it was observed to be sufficient to result in an infectious rod. We wanted to focus on establishing consistency and confidence with this one model.

Surgical and post-op observations. Observations from the first survival surgery were positive: the custom-made implants fit snugly into the defect, with the top of the implant flush against the bone (see Figure 8.21). A lateral radiograph taken immediately after surgery confirmed the placement the implant (see Figure 8.22).

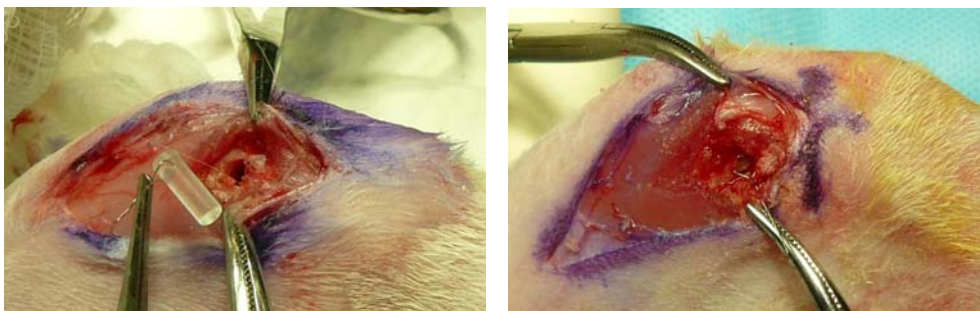


Figure 8.21 - 3mm x 10mm defect at the medial femoral condyle before (left) and after (right) colonized rod insertion, showing good fit of the model.

Pictures are from the first survival surgery of rabbit 08-042.



Figure 8.22 - Post-op lateral radiograph of the defect site from rabbit 08-042, showing placement of the implant with the small wire at the top.

Animals 08-042 and 08-043 exhibited non-weight bearing lameness on the left femur, but both animals showed better activity and appetite than animals from previous rounds.

However, eight days after surgery, 08-042's incision was found to be slightly concertinaed, moist, and necrotic at the margins (see Figure 8.23, left). There was a pea sized swelling and the skin around the site was warm and erythematous. The observed symptom was suspected to be an abscess stemming from either the colonized implant, contamination of the site at surgery, or the exposed suture. At sacrifice, significant superficial soft tissue infection was observed. Both radiographic and visual observations of the bone around defect site (see Figure 8.23, middle and right) suggest presence of osteomyelitis. In addition, the PMMA implant was very easily pulled out, again suggesting the presence of bone infection which resulted in tissue necrosis. Similar visual and radiographic observations were made on 08-043, although this animal experienced deep soft tissue infection rather than superficial, and its implant was more difficult to pull out, suggesting better bone tissue growth within the defect.



Figure 8.23 – Images from 08-042’s tissue harvest, 13 days after first surgery.

(Left) abscess and tissue necrosis at incision site, (middle) radiograph prior to tissue harvest, and (right) trabecular bone around defect site; significant vasculature was observed, suggesting osteomyelitis.

In contrast to 08-042 and 08-043, 08-044 and 08-045 showed good weight bearing on the operated leg almost immediately upon recovery from anesthesia. 08-045 exhibited almost no sign of lameness. Dr. Hayward believed that better suturing on these two animals helped with their recovery. Both rabbits fared well based on behavioral signs, although 08-045 was observed to have significant skin necrosis around the incision on Day 6, and the animal underwent a minor surgery to debride and resuture. 08-044 had an excellent incision recovery – clean, dry, intact, and no redness or bruising. However, a marble-sized swelling was found starting from Day 6, which subsided after a few days. Similar type of temporary swelling was found on 08-045 at the incision site. Neither rabbit required additional medication beyond those prescribed for the first 24 hours post surgery.

Both rabbits survived to their study end point at 4 weeks without weight loss or health issues. Rabbits were bright, alert, and responsive throughout the 4 weeks, with normal outputs. At sacrifice, 08-044 was 2.44 kg (6.2% loss from pre-surgical weight) and 08-045 was 2.76 kg (0% loss). Hence, the morbidity issue appeared to be lessened in this new model.

Radiographic and visual observations at the tissue harvest suggest significant bone infection without any infection of the deep and soft tissues (see Figure 8.24 and Figure 8.25). Both rabbits exhibited radiolucency around defect site on their lateral x-rays, suggesting bone resorption resulting from infection. Visual inspections during the tissue harvests indicated that the degree of bone infection was higher than all previous animals, as the bone surrounding defect was significantly discolored and spongy. For the first time, we observed the presence of *involucrum* (new bone growth) over the defect, suggesting the bone's attempt to recover from the necrosis caused by the infection. We also saw brownish soft tissues suggesting the presence of granules, another sign of possible infection. More importantly, a layer of *pseudomembrane* was found coating the interior of both rabbits' defects. While visual inspection could not confirm that the loosely-adhered white films were indeed pseudomembranes, these were our very first observations of such white films. Based on the degree and extent of infection, Dr. Hsu hypothesized that the rabbits actually progressed to chronic osteomyelitis.

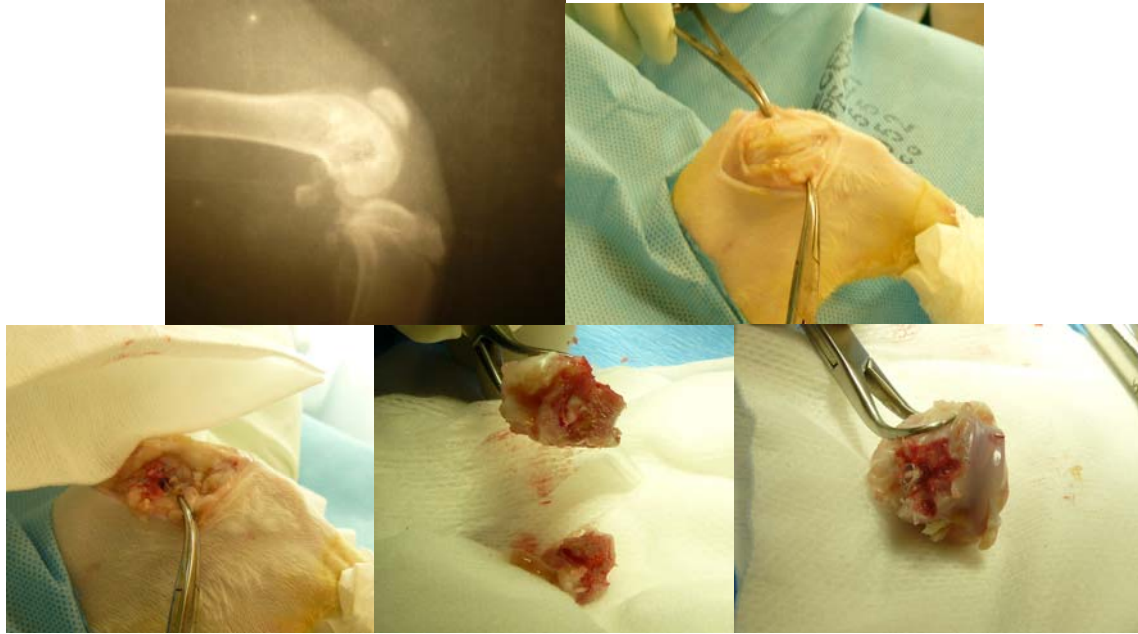


Figure 8.24 – Images from 08-044’s tissue harvest.

Clockwise from the top left: (1) lateral radiograph taken prior to tissue harvest displaying radiolucency, (2) skin incision at tissue harvest revealing no soft tissue infection, (3) new bone growth over the defect area, (4) after debridement of the newly formed bone, the implant could be easily pulled out, and (5) white pseudomembrane found coating the defect interior, further suggesting infection.

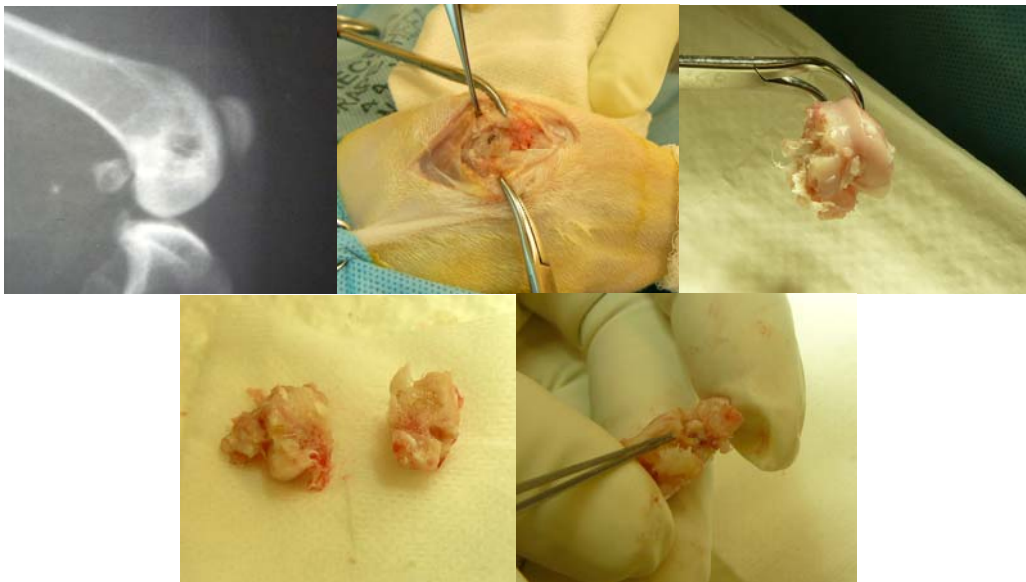


Figure 8.25 - Images from 08-045’s tissue harvest.

Clockwise from the top left: (1) lateral radiograph taken prior to tissue harvest displaying radiolucency, (2) new bone growth over the defect area, (3) after debridement, the implant could be easily pulled out, (4) white pseudomembrane found coating the defect interior, and (5) bone split across the defect site revealing significant discoloration and sponginess.

Microbiological evaluation. For rabbits 08-042 and 043, we expectedly saw high counts of *S. aureus* in bone and implant samples. However, superficial and deep soft tissues also had high counts, suggesting the same tissue infection problem that we saw in previous models. Nevertheless, given the more promising clinical osteomyelitis signs observed during the tissue harvest (Figure 8.24 and Figure 8.25), we believed that the model under this round was an improvement over the previous.

Clinical signs of gross infection as observed for 08-044 and 08-045 strongly suggested that these two animals developed severe and possibly chronic osteomyelitis. The pseudomembrane, pus within defect, and extensive discoloration & decalcification of the bone found in these two animals were not previously observed. Most surprisingly, however, microbiological evaluations revealed little *S. aureus* count in the bone samples of these animals. Several sequestra and other necrotic bone samples from within the defect gave no bacteria count, and neither of the implant yielded any surface-attached bacteria after sonication. However, the pus from 08-044 and a sequestrum and pseudomembrane samples from 08-045 did give relatively high bacteria count, indicating that some live *S. aureus* was present, but not nearly as extensive as expected.

There were several potential explanations for this anomaly: (1) that the animals did experience severe osteomyelitis at some point, but have begun recovering and clearing out the bacteria, (2) that the clinical signs were actually other tissue complications not strictly caused by infection, and (3) that the microbiological evaluation by the Diagnostic Lab was not properly performed this time. Given the consistency and severity of clinical

signs suggestive of osteomyelitis, hypothesis (2) did not seem likely. However, Dr. Spector and Dr. Hsu did not find hypothesis (1) likely given the robustness of *S. aureus*. Several conversations with Kim Dufour at the Diagnostic Lab did not reveal any deviation in evaluation protocol from the previous.

To further troubleshoot, I obtained additional inputs from our new infectious diseases consultant Dr. Jean Lee, an associate microbiologist at Brigham and Women's Hospital. She also found the inconsistency between observed gross infections and lack of microbiology evidence to be confusing, and indicated that while it was possible for osteomyelitis to have developed but then subsided, such a scenario was unlikely given *S. aureus*' ability to proliferate within essentially any tissue, necrotic or not. Dr. Lee made the following recommendations:

1. *Change the strain of S. aureus used.*

Thus far we had used ATCC 25923®, a clinical isolate that was an accepted standard for *in vitro* testing of antibiotic activity. This was not necessarily the most representative candidate for human osteomyelitis. Instead, strain UAMS-1 (ATCC 49230), another clinical isolate of a different genotype, should be used. UAMS-1 carried the gene (*cna*) encoding the collagen binding protein, a protein associated with strains that cause arthritis or infect bone. The culturing techniques would remain the same as that used for strain 25923.

2. *Characterize PMMA rod colonization in a more quantitative manner.*

The previous method used to assess surface colonization of PMMA rods was not quantitative: whether the inoculum on the rod surface was 10^2 or 10^7 , the overnight culture would grow up to 10^9 CFU/mL regardless. Instead, the following kinds of assays should be undertaken to quantify degree of surface colonization:

- a. Sonication in sterile PBS in a *polypropylene* tube (not polystyrene, as *S. aureus* could easily adhere to this material), followed by quantitative plating at serial dilutions of the PBS. Sonication should be done on ice in 20-second spurts to avoid killing *S. aureus* by the heat generated during sonication.
- b. Rolling of sonicated rod on blood agar plate and leaving it there to verify removal of adherent bacteria by sonication.

With the procedures performed so far, I had assumed that storage of a colonized rod at -80C should maintain the viability of the adherent bacteria. Hence, both batches of rabbits received rods that were colonized at the same time, with 08-044 and 08-045 receiving rods that had been stored for additional two weeks. However, Dr. Lee indicated that bacteria in the dry state, *i.e.* not in a glycerol-based freeze medium, could lose viability in -80C storage, and a quantitative assessment at various storage time periods was needed.

3. *Verify methods of microbiology evaluation at the MIT Diagnostic Lab*

Check with the technician to see if small colonies were observed after at least 48 hours of incubation. Chronic infection could result in internalization of *S. aureus*

by eukaryotic cells or the production of *S. aureus* “small colony variants.” These variants would form small, atypical colonies on blood agar plates, and the colonies would only be seen after 48 hours of incubation. The colonies would be tiny and nonhemolytic, and hence would bear no resemblance to typical *S. aureus* colonies. However, they could also easily revert *in vitro*, and so the culture might look mixed. Thorough homogenization of the tissue samples should have released intracellular *S. aureus* and eliminated the occurrence of small colony variants. For future evaluations, I should consider asking the Diagnostic Lab to adding a detergent like 1-2% Triton X-100 to facilitate lysing of the bone cells and hence release of intracellular *S. aureus*.

The Diagnostic Lab technician Kim Dufour indicated that all cultures were grown for at least 48 hours, since no colonies were observed after 24 hours. She stated that no colony of any size was seen, and that all samples were homogenized thoroughly under the method that had been used on our previous samples. Hence, the occurrence of small colony variants may not explain the results seen for 08-044 and 08-045.

Given these recommendations, I obtained *S. aureus* UAMS-1 from Dr. Lee for the quantitative evaluation of PMMA surface colonization as described above. Colonization was performed in an identical fashion as previous round, *i.e.* by immersing the PMMA rods in an exponentially growing culture of *S. aureus* UAMS-1 overnight. Quantitative evaluation was done by the MIT Diagnostic Lab. As a reference and retrospective

assessment, the previous strain (*S. aureus* 25923) was underwent an identical set of assays. The results are summarized in Table 12 and Figure 8.26.

Table 12 – Summary of quantitative PMMA rod colonization evaluation.

Rods were colonized by immersion in 10^5 CFU/mL of exponentially growing *S. aureus* overnight. Rods were stored in a dry, sterile state at -80°C .

<i>S. aureus</i> UAMS-1	Average surface count (CFU/mL)	Rolling assay result
Fresh culture	$2.30 \times 10^5 \pm 60.3\%$	TNTC [†]
2-day storage	$7.90 \times 10^5 \pm 35.7\%$	TNTC
1-week storage	$4.10 \times 10^4 \pm 14.6\%$	TNTC
2-week storage	$4.13 \times 10^4 \pm 26.5\%$	TNTC
<i>S. aureus</i> 25923	Average surface count (CFU/mL)	Rolling assay result
Fresh culture	$7.20 \times 10^4 \pm 41.4\%$	TNTC
2-day storage	$8.33 \times 10^4 \pm 28.8\%$	TNTC
1-week storage	$1.35 \times 10^5 \pm 76.5\%$	TNTC
2-week storage	$1.24 \times 10^5 \pm 8.06\%$	TNTC

[†]Too numerous to count.

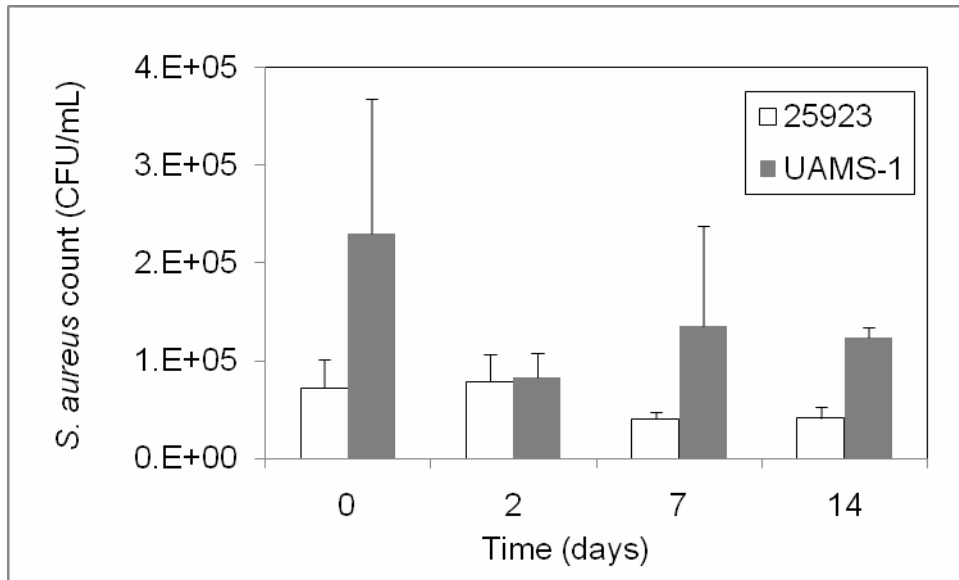


Figure 8.26 – Average saline count of *S. aureus* as sonicated off surfaces of colonized PMMA rods after various lengths of storage at -80°C .

Overall, it appears that both strains were able to survive dry storage at -80°C for at least two weeks. Strain 23923 was more consistent among triplicates in terms of sonicated

saline count and exhibited a decline in viability over time. Strain UAMS-1 had higher saline counts but also with larger variability among triplicates, suggesting that this strain may be more proliferative. However, all 24 rod samples resulted in numerous colony growths when rolled onto a blood agar plate after extensive sonication (several minutes done in spurts), indicating that the saline count may not be reflective of the actual degree of surface colonization, but rather the amount of more loosely attached bacteria. It appears that both strains were able to colonize PMMA surface with very tight adhesion, resulting in colonies that remain attached on the surface even after sonication. The variability in each set of saline counts, as shown by the error bars in Figure 8.26, did not necessarily reflect variations in the viability of the *S. aureus* on the surface, but rather variations in the amount that could be sonicated off the surface. Hence, changes in both viability and adhesion capability were reflected in the saline count. Regardless of the exact characteristics represented by the data, the results presented in Figure 8.26 and Table 12 suggest that *S. aureus* 25923 and UAMS-1 remain sufficiently viable in a dry state on PMMA surface at -80°C over at least two weeks. Therefore, a stored implant should be able to induce osteomyelitis.

Looking back at observations made for rabbits 08-044 and 08-045, it now appears more likely that osteomyelitis did develop in these animals, as we would expect the 25923-colonized PMMA implants to have adequate numbers of viable bacteria on the surface upon insertion. The rabbits' immune systems could be sufficiently robust to clear away the *S. aureus* within four weeks. This hypothesis would suggest that a 2-3 week

incubation period may be optimal for our osteomyelitis model. Further assessment of this osteomyelitis model should be undertaken.

8.4 Conclusion.

In vivo evaluation to evaluate the efficacy and biocompatibility of [(*Poly I/HA*)(*GS/HA*)]_n coatings was proposed, but the actual coating evaluation had not been performed due to the unforeseen challenge in establishing a reproducible osteomyelitis model. The initial model adopted from the literature, which involved injection of a liquid *S. aureus* inoculum into a bone defect, was problematic due to inoculum leakage, causing soft tissue infections, lack of sufficient osteomyelitis development, and high animal morbidity. Several modifications to the injection model, such as reduction in inoculum volume and an improvement on defect sealing procedure, were not successful in achieving a reproducible osteomyelitis model. Only a major update to the procedure, eliminating liquid inoculums in favor of a colonized implant, resulted in the desired clinical signs for osteomyelitis without the undesired morbidity. However, this new model was inconsistent in its microbiology evaluations, and another modification to the model – switching the inoculating *S. aureus* from strain 25923 to UAMS-1, was evaluated. UAMS-1 was observed to survive -80°C storage better, although its surface count was also less consistent among triplicates, suggesting that UAMS-1 might have a higher proliferative ability which would result in both robustness and variability. Compiling all the observations made throughout the four rounds of model, I believe that induction by a colonized rod followed by a 2-3 week incubation would be the optimal osteomyelitis model.

Overall, a major lesson learned is that as laboratory assessments progress into clinical evaluations, one should anticipate higher variability and hence greater challenge in establishing the desired set of results. A “take it from the literature” approach may not work at the *in vivo* level, and significant amounts of human . I believe that we are close to establishing a working model of osteomyelitis, and I look forward to seeing evaluations of [(*Poly I/HA*)(*GS/HA*)]_n and other antimicrobial LbL coatings to be developed.

Acknowledgements.

Many thanks go to Dr. Hu-Ping Hsu, for performing the surgeries and preparing the histology samples, and Dr. Myron Spector for his guidance throughout the study. Drs. Larry Madoff and Jean Lee were both very helpful with inputs on our infection model. Drs. Scott Martin and Mitch Harris helped to shape the overall approach to the model. I also wish to acknowledge to all the staff at the E25 animal facility and MIT DCM, especially Dr. Alison Hayward and Sylvia Lesnikowski, for their mentorship and assistance on animal handling procedures, logistics, and data evaluation.

References.

- (1) Fluckiger, U. and Zimmerli, W. *Orthopade*, **2004**, 33, 416
- (2) Mendes, S. C., Reis, R. L., Bovell, Y. P., Cunha, A. M., van Blitterswijk, C. A. and de Bruijn, J. D. *Biomaterials*, **2001**, 22, 2057-2064
- (3) Mark J. Curtis, P. R. B. J. D. D. R. H. J. *Journal of Orthopaedic Research*, **1995**, 13, 286-295
- (4) Salgado, C., Jamali, A., Mardini, S., Buchanan, K. and Veit, B. *Clinical Orthopaedics And Related Research*, **2005**, 436, 246-250
- (5) Alt, V., Bitschnau, A., Osterling, J., Sewing, A., Meyer, C., Kraus, R., Meissner, S. A., Wenisch, S., Domann, E. and Schnettler, R. *Biomaterials*, **2006**, 27, 4627-4634
- (6) Gursel, I., Korkusuz, F., Turesin, F., Gurdal Alaeddinoglu, N. and Hasirci, V. *Biomaterials*, **2001**, 22, 73-80
- (7) Craig, M. R., Poelstra, K. A., Sherrell, J. C., Kwon, M. S., Belzile, E. L. and Brown, T. E. *Journal of Orthopaedic Research*, **2005**, 23, 1100-1104
- (8) DAROUICHE, R. O., FARMER, J., CHAPUT, C., MANSOURI, M., SALEH, G. and LANDON, G. C. *J Bone Joint Surg Am*, **1998**, 80, 1336-1340

- (9) Darouiche, R. O., Landon, G. C., Patti, J. M., Nguyen, L. L., Fernau, R. C., McDevitt, D., Greene, C., Foster, T. and Klima, M. *J Med Microbiol*, **1997**, *46*, 75-79
- (10) Nelson, C. L., McLaren, S. G., Skinner, R. A., Smeltzer, M. S., Roby Thomas, J. and Olsen, K. M. *Journal of Orthopaedic Research*, **2002**, *20*, 643-647
- (11) Marc W. Nijhof, A. F., Karin Hardus, H. Charles Vogely, Leo M. Schouls, Abraham J. Verbout, Wouter J. A. Dhert,. *Journal of Biomedical Materials Research*, **2001**, *58*, 747-753
- (12) Koort, J. K., Makinen, T. J., Suokas, E., Veiranto, M., Jalava, J., Knuuti, J., Tormala, P. and Aro, H. T. *Antimicrob. Agents Chemother. %R 10.1128/AAC.49.4.1502-1508.2005*, **2005**, *49*, 1502-1508
- (13) Brown, R. C. and Hopps, H. C. *American journal of clinical pathology*, **1973**, *60*, 234-240
- (14) Engbaek, K., Johansen, K. S. and Jensen, M. E. *Journal of Clinical Pathology*, **1979**, *32*, 187-190

Chapter 9. Incorporation of siRNAs

9.1 Introduction

Layer-by-layer assemblies incorporating poly(β -amino esters) for tunable release of DNAs have been extensively characterized by Lynn *et al.*^{111-115, 117, 118, 260} They have demonstrated applicability to a variety of plasmids, tunability of release dosage and rate, and high efficiency in *in vitro* transfection. However, as of early 2006, no work had been reported on the delivery of siRNAs from an LbL assembly, whether hydrolytically degradable or not. Given the successes with DNAs, such a was anticipated to also work with RNAs. Early contemplations on the incorporation of siRNAs did not materialize due to cost and resource considerations.

In late 2005, James Quattrochi of Harvard Medical School approached us for a potential collaborative project on the incorporation of siRNA and carbachol into LbL assemblies for the sequential release of the two substances from the surface of a nanosphere. The purpose of the dual release was to study the mechanism of potential sleep aid medication.

The following is a brief background on Quattrochi *et al.*'s research:

Pons Genicualte Occipital (PGO) waves are phasic electrical bursts of neural activity that occur right before the onset of rapid eye movement (REM) sleep in areas of the brain responsible for eye movements, visual information and visual processing of that information. PGO waves are thought to be responsible for the vivid visual experience of dreams and the rapid eye movements typical of REM stage.

Through carbachol injection into the parabrachial nuclei (PBN) area of the feline brain stem, Quattorchi *et al.* was able to enhance pontogeniculooccipital (PGO) wave without altering any activities within the brain associated with sleep, *e.g.* REM or sleep stages. Hence, they demonstrated that PGO waves could be separated from REM and sleep in general.

Quattorchi *et al.* subsequently designed an siRNA that targets against *c-fos*, an IEG (immediate early gene) that is hypothesized by them to be one of the switches that initiate and/or maintain PGO wave enhancement following carbachol stimulation. The siRNA therapy should not affect sleep itself, but instead disrupts the initiation and maintenance of PGO waves, hence nullifying the effect of carbachol. Up to this point in discussion, Quattorchi *et al.* were not sure what siRNA would do by itself, because they had always co-administered it with carbachol to the feline brain stem.

Instead of direct injection of carbachol and siRNA in free solution in the feline brain, Quattorchi *et al.* desired to have a sequential release of carbachol followed by siRNA inside a neuron, with a 6+ hr time gap between the two releases. Hence, they envisioned a nanobead capable of uptake by neurons, followed by a retrograde travel up the neuronal dendrite into the central intracellular space to sequentially release carbachol and siRNA. Specifically, the nanobead would be LumaFluor's Retrobead™, which were 100-nm polystyrene beads with carboxylated surface and fluorescent tags impregnated throughout the bead body that have been shown to be consistently uptaken by neurons.

The target system would be degradable PEMs deposited onto Retrobeads that would sequentially release carbachol then siRNA with the correct dosage and timing, though we were not sure what the “correct” dosages would be. As a proof-of-concept, we wanted to show PEM encapsulation of siRNA on macroscale planar substrates with tunable release. Concurrent with this effort, we also studied PEM deposition onto Retrobeads and pursued strategies for incorporating small-molecule drugs like carbachol.

While abundant literature exists on polymer-based delivery vehicles for siRNA, very few have reported on PEM incorporation of siRNA as of spring 2008. Recksiedler *et al.*'s work on (PABA/RNA) multilayers with electrochemically triggered release is the only publication that we have found so far²⁶¹, although several conference proceedings on the subject have begun to appear. They include Kidambi *et al.*'s (PLL/siRNA) that deconstructs under physiological salt condition of 0.25M NaCl with *in vitro* uptake by fibroblasts and primary hepatocytes²⁶², and Soto *et al.*'s yeast cell wall particle system²⁶³. While all of the above are promising PEM systems for siRNA, there is plenty of room for additional developments towards higher tunability in dosage, release rate, and pendant functionalities.

9.2 Materials and Methods

Materials. Poly(β -amino esters) (referred to as *Poly X*, $X = 1$ and 6) were synthesized as previously described²³. Silicon wafers (test grade n-type) were purchased from Silicon

Quest (Santa Clara, CA). Linear poly(ethylenimine) (LPEI, $M_n = 25k$) was received from Polysciences, Inc. Poly (sodium 4-styrenesulfonate) (PSS, $M_n = 1M$) and sodium alginate (or alginic acid) were purchased from Sigma-Aldrich (St. Louis, MO). Sodium hyaluronate (or hyaluronic acid (HA), $M_n = 1.76 MDa$) was purchased from Lifecore Biomedical, Inc. (Chaska, MN). FITC- and Cy5-labeled siRNA (sequence GGAGACAGAUCAACUAGAAAdTdT, 13.8kDa) was custom ordered by Quattrochi *et al.* from Dharmacon (Lafayette, CO) with *in vivo* purity, preserved in 0.9% saline at a concentration of 0.2 $\mu\text{mol/mL}$ (2.76 mg/mL). RNaseZap, RNase-free water, and other RNAase-free disposable supplies (*e.g.* pipette tips) were ordered from Ambion. All materials and solvents were used as received without further purification.

General considerations. Silicon wafers and quartz slides were cut into rectangular substrates approximately 1.0 cm \times 1.0 cm each. The substrates were rinsed with methanol and deionized water, dried under nitrogen, and plasma etched in oxygen using a Harrick PDC-32G plasma cleaner at high RF power for 1 min. Layer-by-layer thin film deposition for the (LPEI/PSS)₁₀ base layers was performed using a Carl Zeiss HMS Series Programmable Slide Stainer, while films containing siRNA were made and handled in a biosafety cabinet that had been wiped down by RNaseZap. Dry state ellipsometric measurements were conducted using a Gaertner Variable Angle Ellipsometer (6328 nm, 70° incident angle) and accompanying Gaertner Ellipsometer Measurement Program (GEMP) Version 1.2 software interface. UV-vis readings, both of films deposited onto a quartz substrate or of free-solution siRNA in a quartz cell, were taken on a Cary 500 UV-Vis Spectrophotometer at 260 nm. Any glassware, tweezers,

other tools, and equipment parts that would come in contact with the substrate was wiped with RNaseZap prior to use.

Preparation of Polyelectrolyte Solutions. Dipping solutions containing *Poly X* and siRNA were made at a concentration of 10 mM with respect to the polymer repeat unit in 100 mM sodium acetate buffer (pH 5.1 by glacial acetic acid) prepared with RNase-free water in a biosafety cabinet. Nondegradable base layers were deposited from dipping solutions of LPEI and PSS in deionized water pH adjusted to 4.25 and 4.75, respectively. Deionized water used to prepare LPEI and PSS solutions was obtained using a Milli-Q Plus (Bedford, MA) at 18.2 M Ω .

Polyelectrolyte Deposition. LBL thin films were constructed on a slide stainer for the base layers and manually in a biosafety cabinet for the degradable layers. A ten-bilayer nondegradable base film ((LPEI/PSS)₁₀) was deposited by submerging plasma treated silicon substrates in an LPEI dipping solution for 5 minutes, then a cascade rinse cycle consisting of three deionized water rinsing baths (15, 30, and 45 seconds, respectively). Substrates were then submerged in a PSS dipping solution for 5 minutes followed by the same cascade rinsing cycle, and the entire process was repeated ten times. The substrate with base layers was then thoroughly but gently wiped with ethanol to remove as much RNase as possible without disturbing the base layers. Next, degradable films were deposited on the existing polyanion-terminated base layer by repeating the above procedure manually in a biosafety cabinet wiped down with RNaseZap, with the (*Poly X*/siRNA)_n architecture, dipping for 10 min in each of the *Poly X* and siRNA solutions,

with thorough rinsing in between by a gentle stream of RNAase-free water from a squirter. *Poly X* solutions were re-made every 24 hours, and siRNA dipping solution and unfinished films were stored in RNAase-free vials wrapped in foil in the freezer. Films were air dried inside the biosafety cabinet before storage. Silicon substrate film buildup was monitored by ellipsometry at ten different predetermined locations on the film surface, while quartz substrate film buildup was monitored by Abs₂₆₀ of the coated substrate. All measurements were performed in triplicate.

Measurement of Drug Release. Abs₂₆₀ calibration curve for siRNA in 1x PBS was established for by running a set of standards at known concentrations within a range relevant to our observed release concentrations, and performing linear regression on the concentration *vs.* Abs₂₆₀ reading to establish a calibration curve. For drug release assessment, (*Poly X*/siRNA)_n films were immersed in 1 mL of 37C nuclease-free 1x PBS in a tightly capped, nuclease-free vial wrapped with aluminum foil to block out light. Vials were kept in cell incubators to maintain 37C. At pre-determined time periods, 0.10 mL of the release buffer would be withdrawn from the vial and transferred into a quartz microcuvette, and the cuvette would be capped with a fitted plastic cap then taken to a Cary50 UV-vis spectrophotometer to collect Abs₂₆₀. If the substrate was quartz, the substrate itself would be dried and mounted onto a nuclease-free support to be read in the UV-Vis spectrophotometer. Pure 1x PBS buffer and quartz substrate with (LPEI/PSS)₁₀ base layer were used as the blanks. All procedures requiring opening of the vial were performed in nuclease-free biosafety cabinets. After reading, all buffer samples would be returned to the vial to maintain 1 mL of total release buffer. If the buffer Abs₂₆₀ reading

was beyond the linear range of the calibration curve, the entire release buffer would be diluted two-, four-, or eight-fold until a value within the linear range was obtained. If the substrate was silicon, thickness reading would be taken on an ellipsometer, with a nuclease-free platform, at each release time point to establish the erosion profile. Blanks were used for all measurements; these were either quartz cuvette filled with blank PBS, or quartz substrate with (LPEI/PSS)₁₀ base layer.

Microscopy. Atomic force microscope (AFM) images were collected on a Dimension 3100 model from Digital Instruments in tapping mode at an amplitude set point of 0.8 V under dry conditions. Height and phase images were taken at scanning rates of approximately 1.5 Hz. Optical microscope images were collected on a Leica Leitz DMRX microscope with images taken by a Nikon Digital Camera DMX1200F.

9.3 Results and Discussion

Quantification of siRNA. Initial experiments were performed with FITC-labeled siRNA, as supplied by Quattrochi *et al.* Instead of using fluorescent signal from FITC, quantity of siRNA was determined based on UV absorption at 260 nm, a signature for nucleic acids. Figure 9.1 shows the UV-vis calibration curve. For a better fit within the working range, only the portion lying in within $Abs_{260} = 0.15-0.40$ was used for the calibration equation. PBS solutions of *Poly 1* and *Poly 6* up to 1 mg/mL were verified to not have detectable absorption at 260 nm.

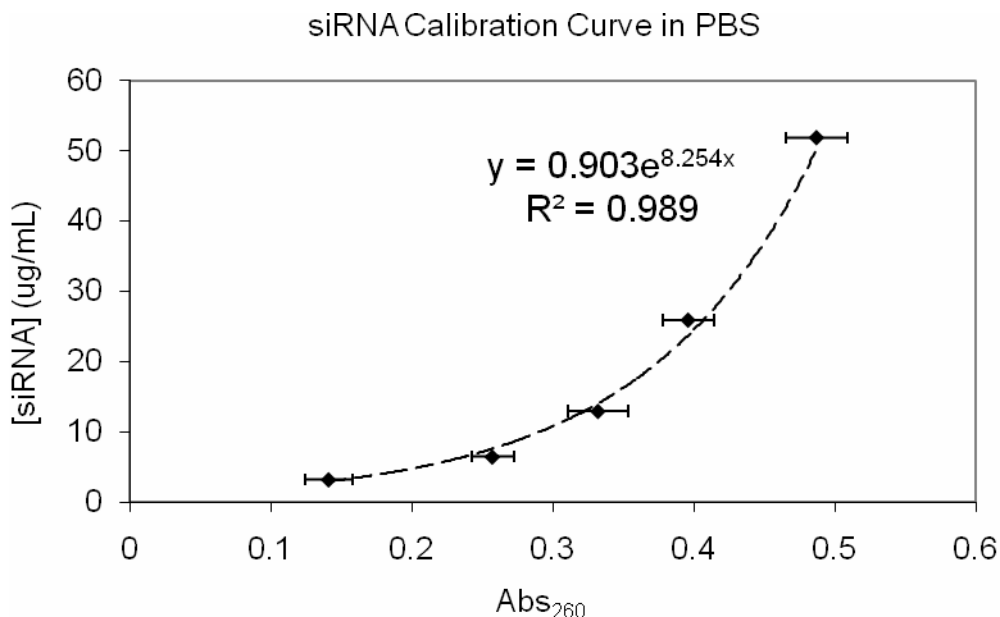


Figure 9.1 - siRNA calibration by UV absorbance.

(Poly X/siRNA)_n film buildup. Initial attempts at constructing (Poly X/siRNA)_n films were made with *Poly X* dipping solution in 0.1M sodium acetate and siRNA dipping solution in deionized nuclease-free water. However, no noticeable film growth was observed by ellipsometry or UV absorption after twenty deposition cycles. The siRNA dipping solution was then switched to 0.1M sodium acetate, and film growth began to occur (see Figure 9.2). This influence of siRNA dipping condition on film build-up was consistent with what Zhang *et al.* reported for (Poly I/pGFP)_n film buildup¹¹¹, and the authors hypothesized that the reduced pH in the pGFP dipping solution helped to maintain higher cationic charge on *Poly I* molecules residing on the topmost layer of the film, hence facilitating pGFP deposition. The authors believed that the effect was not due to a higher ionic strength, as they demonstrated with equivalent strengths of NaCl.

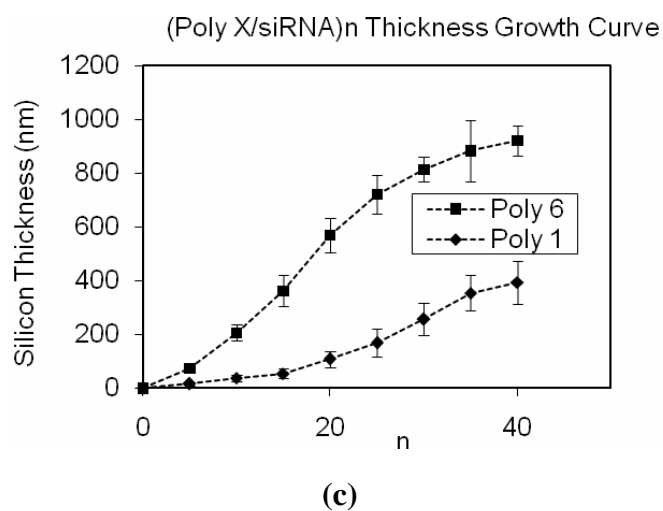
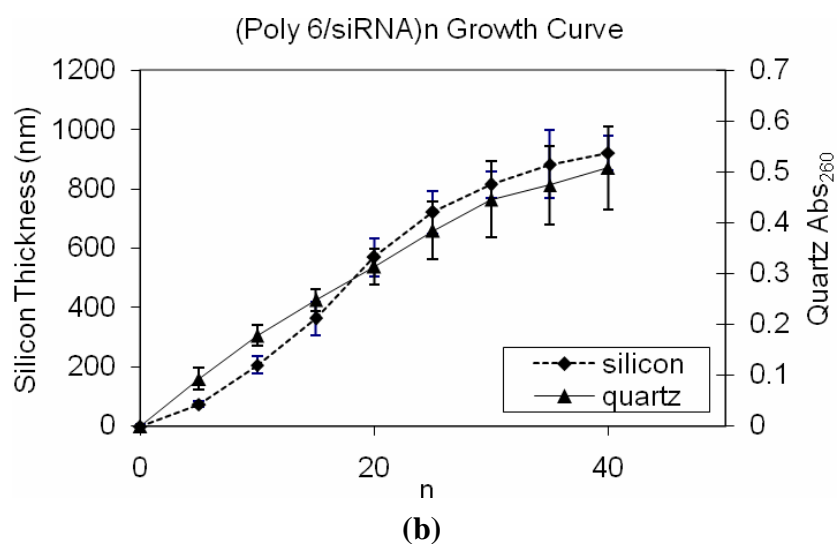
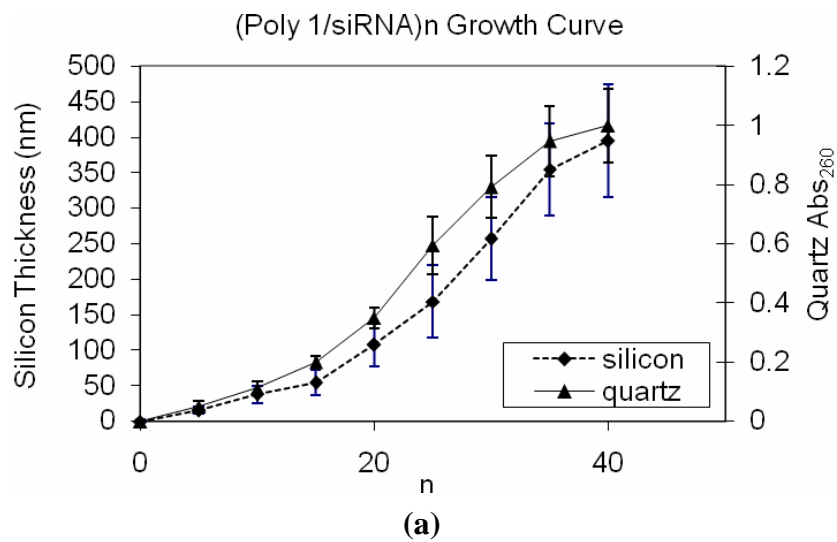


Figure 9.2 - $(Poly X/siRNA)_n$ growth curves in thickness and Abs_{260} .
 (a) $(Poly 1/siRNA)_n$, (b) $(Poly 6/siRNA)_n$, (c) combining thickness growth curves from (a) and (b).

Both *Poly X*'s were able to bilayer with the siRNA with steady monotonic growth. Figure 9.2(c) reveals that *Poly 6* films grew in thickness at a faster growth rate than the *Poly 1* equivalents. The higher growth rate of *Poly 6* film had been observed for the encapsulation of other therapeutics, especially highly charged species, and was expected due to *Poly 6*'s higher hydrophobicity and lower charge density. These properties resulted in looser ionic crosslinking with the highly charged siRNA, causing loopier films that grew faster in observed thickness but could be less dense within the film mass.

In contrast to the thickness growth behavior, *Poly 6* films grew slower in siRNA absorption signal than *Poly 1* films. However, as revealed later by the siRNA release data, (*Poly 6*/siRNA)₄₀ actually contained more siRNA per unit area than the *Poly 1* equivalent. It is unclear why the (*Poly 6*/siRNA)₄₀ film exhibited lower Abs₂₆₀ given identical quartz substrate as the *Poly 1* film. This observation suggests that if Abs₂₆₀ was to be used to quantify amount of siRNA buildup within the film, separate calibration parameters would need to be established for different *Poly X* species.

Both films exhibited an apparent asymptote in growth. Due to the labor-intensive nature of film construction (manually done and had to remain in RNase-free biosafety cabinet), film growths beyond 40 bilayers were not examined. One hypothesis for this asymptotic phenomenon was that the rinsing method in the manual dipping process, in which the substrate was gently rinsed with a stream of water from a squirt bottle, produced mechanical stress that discouraged film growth beyond a certain thickness. However,

under this hypothesis we would expect that *Poly 1* and *Poly 6* films would saturate to similar thicknesses, yet the data suggest that $(Poly\ 1/siRNA)_n$ would saturate around 400 nm and $(Poly\ 6/siRNA)_n$ around 1000 nm. Another potential explanation was that each *Poly X* or siRNA layer only adsorbed very little beyond charge neutralization, discouraging further film growth. This lack of adsorption could arise from *Poly X* and siRNA's conformations and orientations within the film that might somehow result in fewer non-ionic interactions such as van der Waals.

Film morphology. $(Poly\ X/siRNA)_n$ films were inspected under an optical microscope during their build-up process. A distinct island formation build-up process was observed from $(Poly\ 1/siRNA)_n$ films (see Figure 9.3(a)), while $(Poly\ 6/siRNA)_n$ films built up in a smooth, conformal fashion (see Figure 9.3(b)). The μm -scale islands of $(Poly\ 1/siRNA)_n$ were different from the kind of nanostructures observed by Fredin *et al.* during the erosion of $(Poly\ X/p\text{-GFP})_n$ films¹¹⁵ due to the differences in size scales. Such islands were most likely caused by unfavorable interactions between the substrate surface and the deposited polyelectrolytes. One hypothesis was that the $(LPEI/PSS)_{10}$ base layer, despite being nondegradable, might not be able to withstand the mechanical stress imposed by the process of wiping the substrate with Kimwipe. Hence, the surface became less hydrophilic, and *Poly 6*'s more hydrophobic nature might actually promote non-electrostatic interaction with the silicon surface to result in more uniform deposition. Interestingly, erosions of $(Poly\ 1/siRNA)_n$ and $(Poly\ 6/siRNA)_n$ films followed similar morphological progressions as the buildup in reverse.

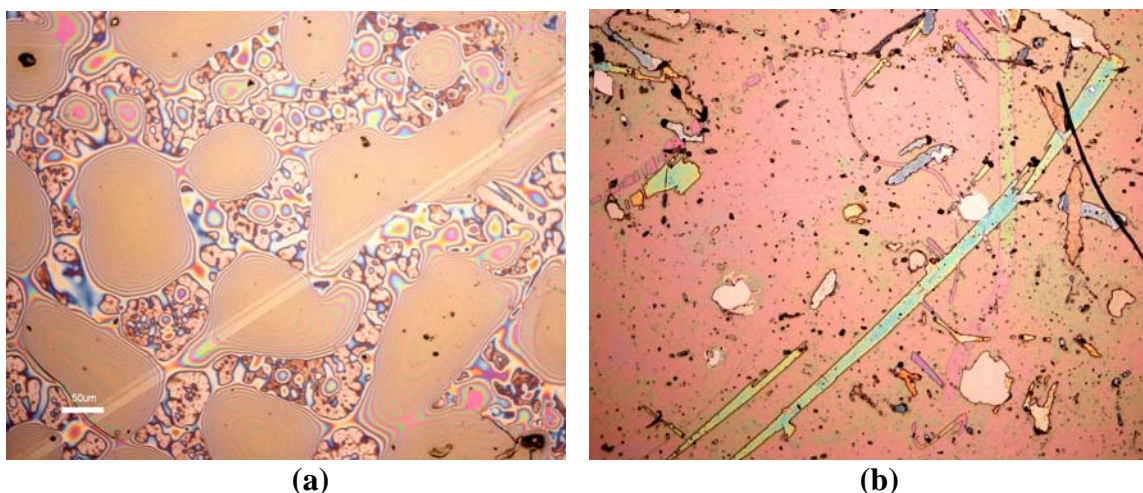
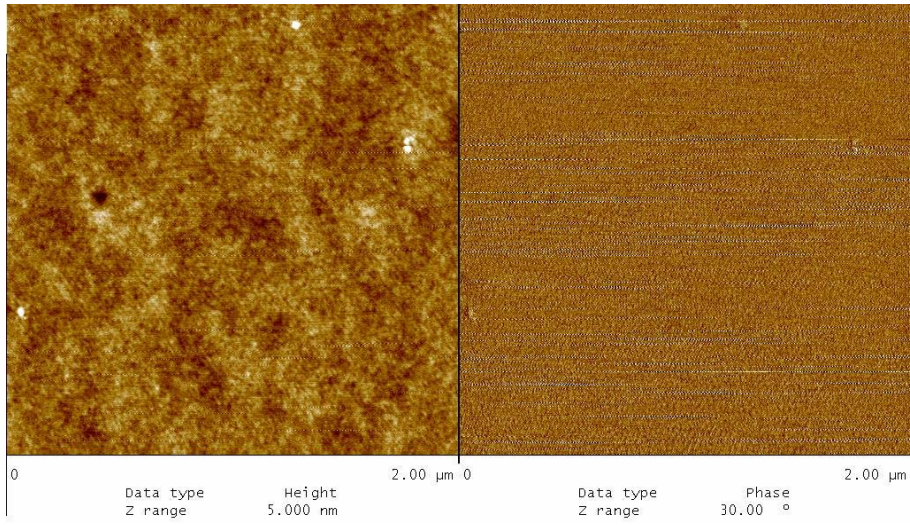


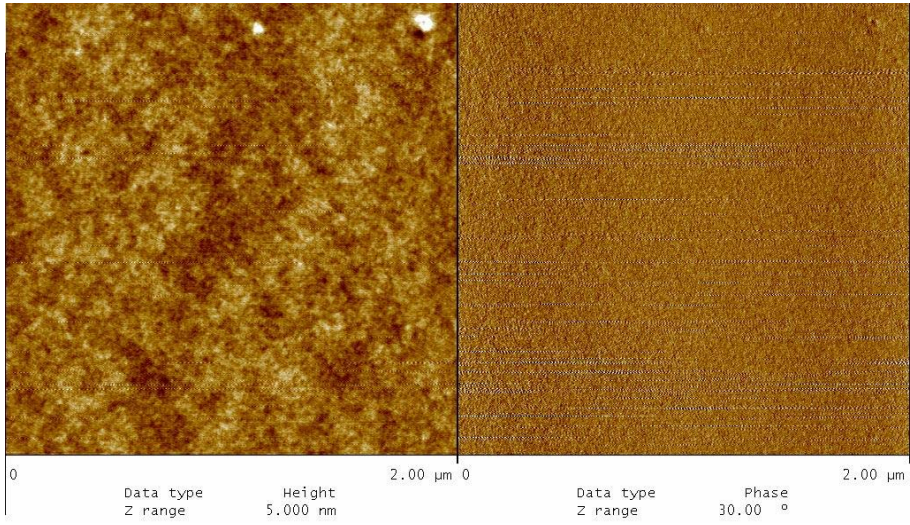
Figure 9.3 - Reflection optical image of $(Poly X/siRNA)_{40}$ deposited on silicon.

(a) $(Poly I/siRNA)_{40}$ - each “island” is approximate 100-200 μm in size, (b) $(Poly 6/siRNA)_{40}$

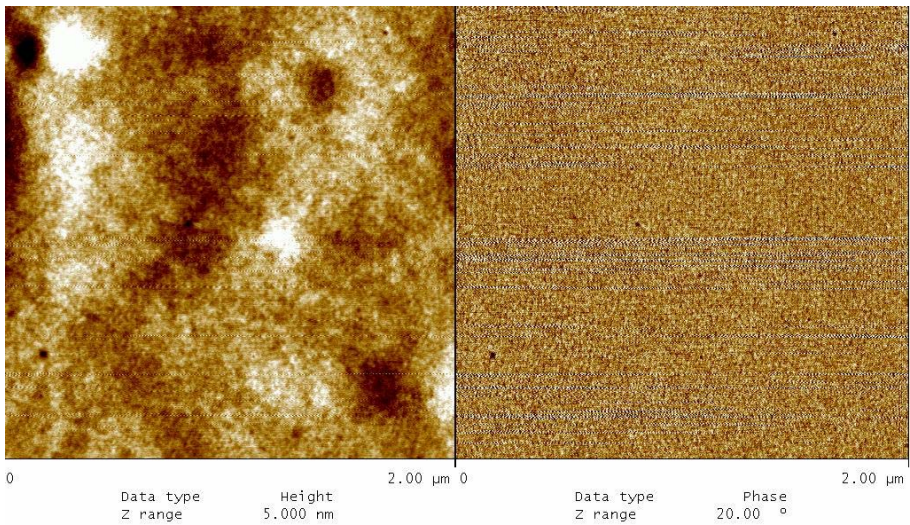
Since Lynn *et al.* observed nanoscale rearrangements of $(Poly I/DNA)_n$ films over a course of incubation in PBS buffer^{112, 115}, I investigated whether a similar phenomenon took place with $(Poly I/siRNA)_n$ films. AFM images of a $(Poly I/siRNA)_{40}$ film incubated for various amounts of time in RNase-free PBS at 37°C are presented in Figure 9.4. Since $(Poly I/siRNA)_{40}$ films were observed to coalesce and degrade in islands on a micrometer scale, all the AFM images were collected towards the middle of an island. As the evolution of images in Figure 9.4 suggests, no nanoscale rearrangement with nanoparticle formation was observed in the course of $(Poly I/siRNA)_{40}$ film erosion. The film did become increasingly rougher and more pitted, but no regular or distinctive feature emerged. I suspect that due to the less polymeric nature of siRNAs as compared to DNAs, *Poly I* was not able to complex the former as well, and hence was not able to form nanoparticles budding off from film surface.



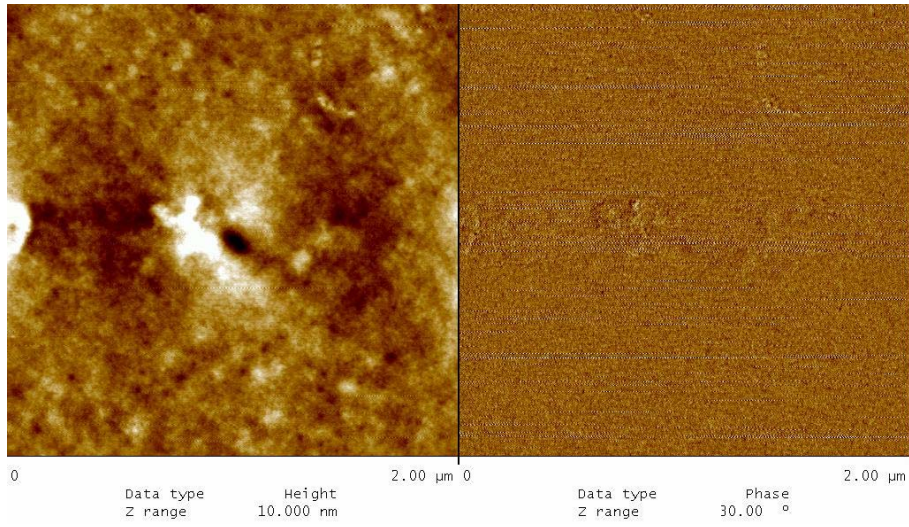
0 min



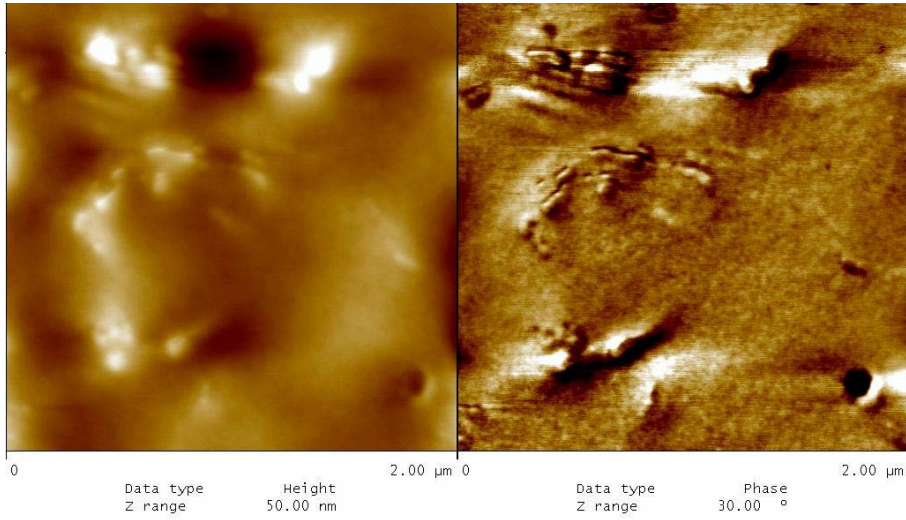
15 min



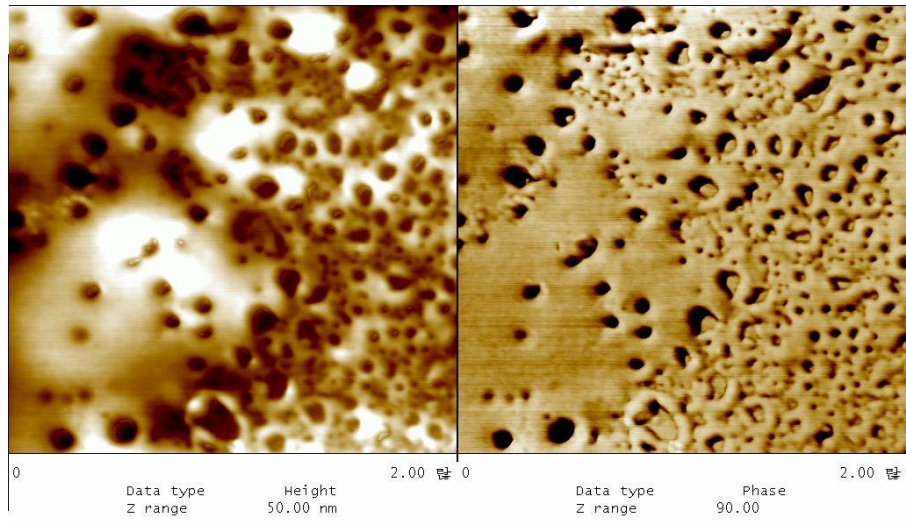
30 min



1 hr



2 hr



9 hr

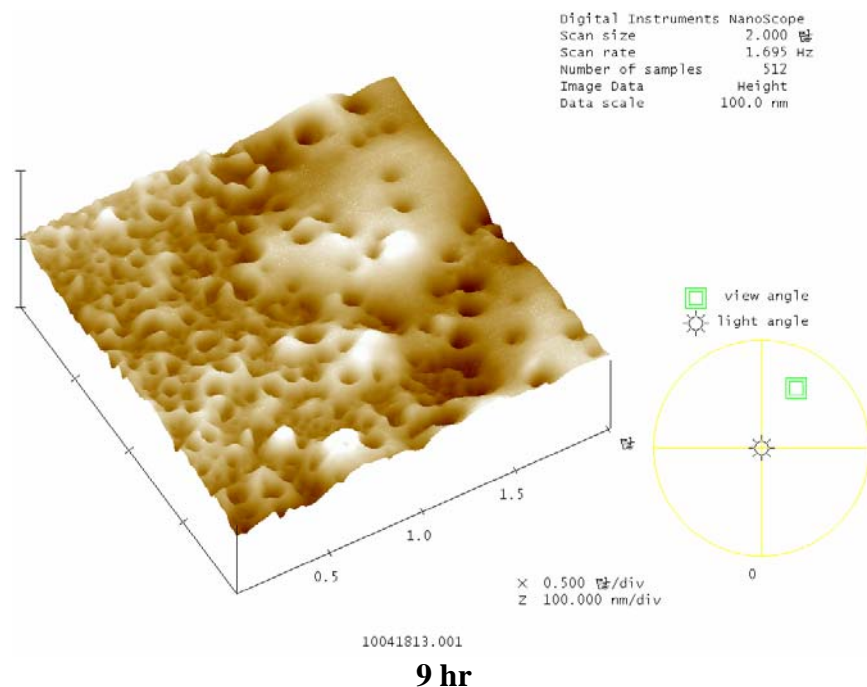


Figure 9.4 – AFM images of *(Poly I/siRNA)*₄₀ (on island portions of the film) over a course of incubation in nuclease-free PBS buffer at 37°C.

Incubation times are indicated right beneath each image. Within each image, the left represents height image and the right phase contrast. The last image is a 3D representation of 9 hr incubation.

Assessment of siRNA release. The dosage and kinetics of siRNA release were assessed on all four types of films (*Poly 1* vs. *Poly 6*, and silicon vs. quartz substrates) through immersion in nuclease-free PBS at 37°C. Film erosion was monitored via ellipsometric thickness on silicon or Abs₂₆₀ on quartz substrate, while siRNA release was monitored by Abs₂₆₀ of release buffer. If the release buffer had Abs₂₆₀ readings beyond the linear range of the calibration curve, the entire sample was diluted 1:2^x to the desired reading range.

Figure 9.5 show the film erosion and siRNA release curves of *(Poly I/siRNA)*₄₀ films from silicon and quartz substrates. A total of 80 µg/cm² of siRNA was released from *(Poly I/siRNA)*₄₀ on silicon over the course of 10 hours, with 50% of content released within 30 min. The concomitant film erosion was more sustained, with 50% erosion

observed around 1 hour. The mismatch between siRNA release and film erosion rates could be due to the partitioning of siRNA to the top of the film that arose from differential interactions with *Poly I* versus the solvent. A residual film approximately 50 nm in thickness would not erode away even after 100 hours of incubation. The material make-up of this residual film was unknown.

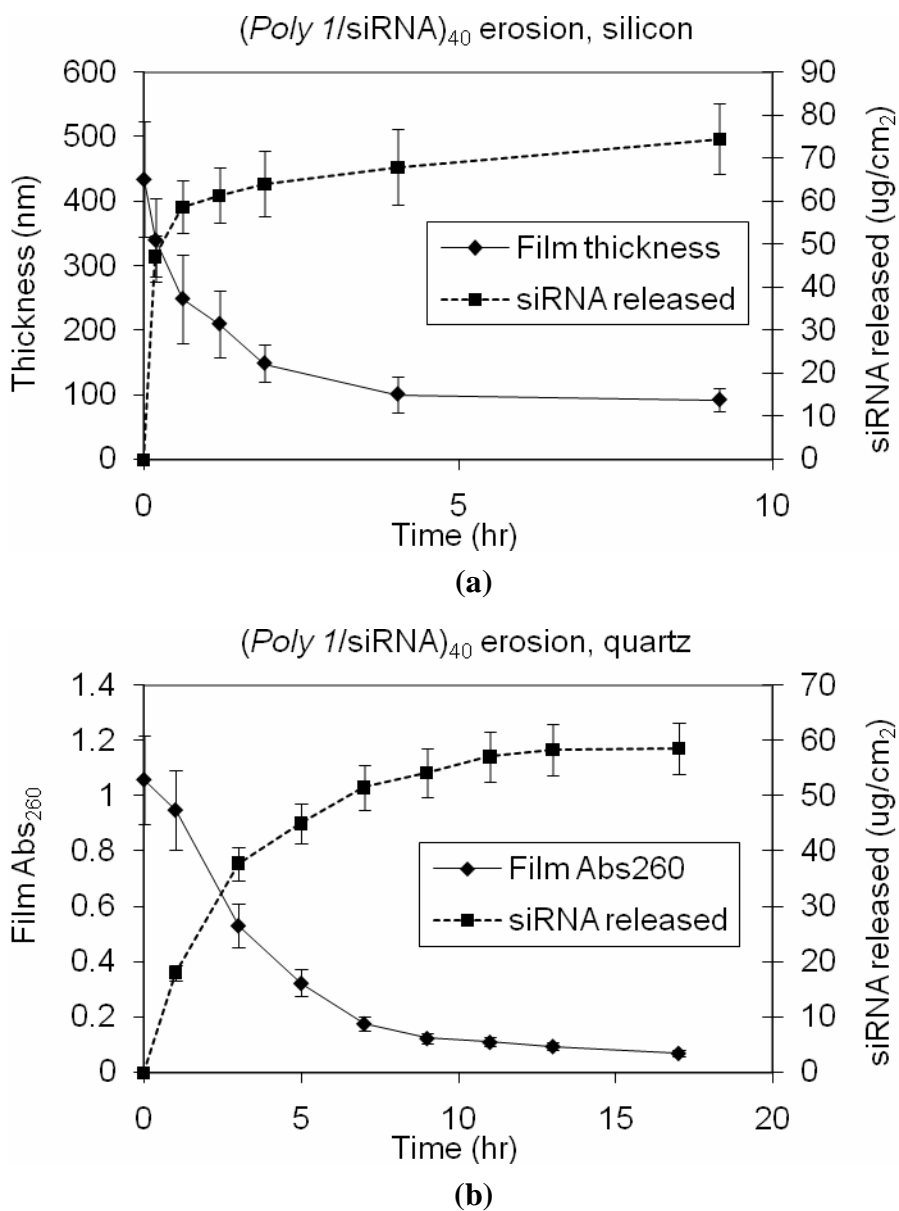
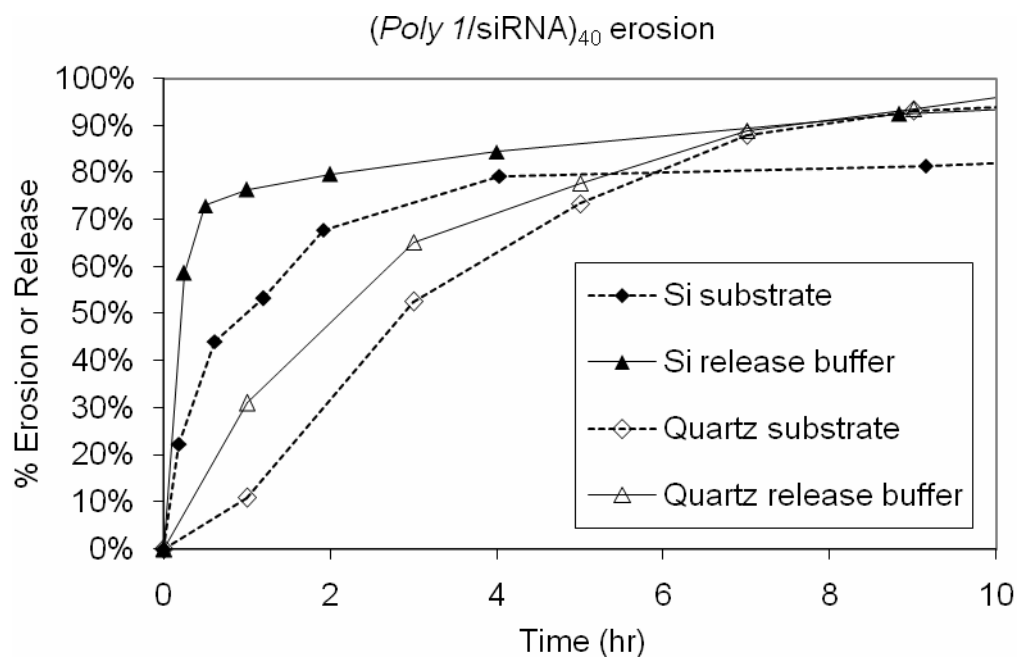


Figure 9.5 – (Poly I/siRNA)₄₀ film erosion and siRNA release.

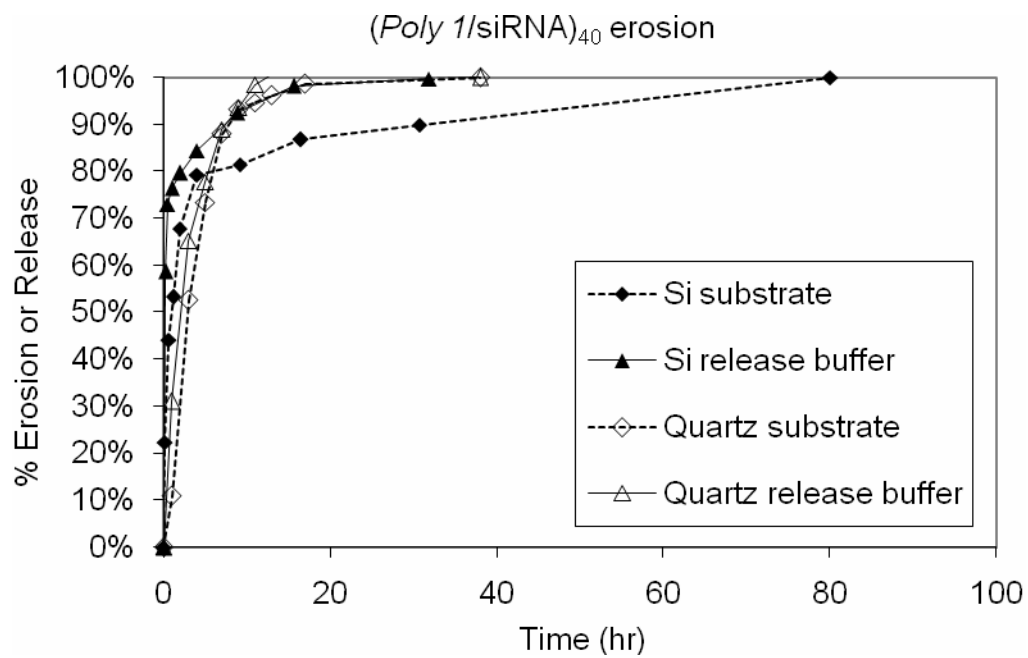
(a) from a film deposited on silicon substrate, with film erosion measured by ellipsometric thickness, and (b) from a film deposited on quartz substrate, with film erosion measured by Abs₂₆₀ of the film.

A smaller but comparable amount of siRNA was released from the quartz substrate ($60 \mu\text{g}/\text{cm}^2$), but in a more sustained fashion with matching rates of siRNA loss from the film and that of siRNA released into the buffer. It was surprising to see the difference in release behaviors from hypothetically identical films deposited on different substrate materials. One potential explanation was that $(Poly\ I/\text{siRNA})_{40}$ had a more favorable interaction with the quartz surface due to a more intact $(\text{LPEI}/\text{PSS})_{10}$ base layer that was more robust against the wiping; the robustness could stem from the longer plasma etch time on the quartz substrate, as quartz could withstand longer etch time than silicon. Unfortunately the examination of quartz substrates under transmission microscopy did not produce observable images that could identify island vs. uniform film formation.

Figure 9.6 presents data from Figure 9.5 in a different format, presenting both erosion and release as % of total progress to facilitate rate comparisons. As the figure shows, quartz substrates resulted in $(Poly\ I/\text{siRNA})_{40}$ films with less burst release within the first several hours. Interestingly, film erosion from a silicon substrate was the most sustained overall (see Figure 9.6 (b)), extending long beyond complete release of siRNA. This observation suggested that siRNA release was partially driven by diffusion out of the film, and that some siRNA-free film mass was left in the end – possibly composed of *Poly I* held in place with some counteranions from the buffer.



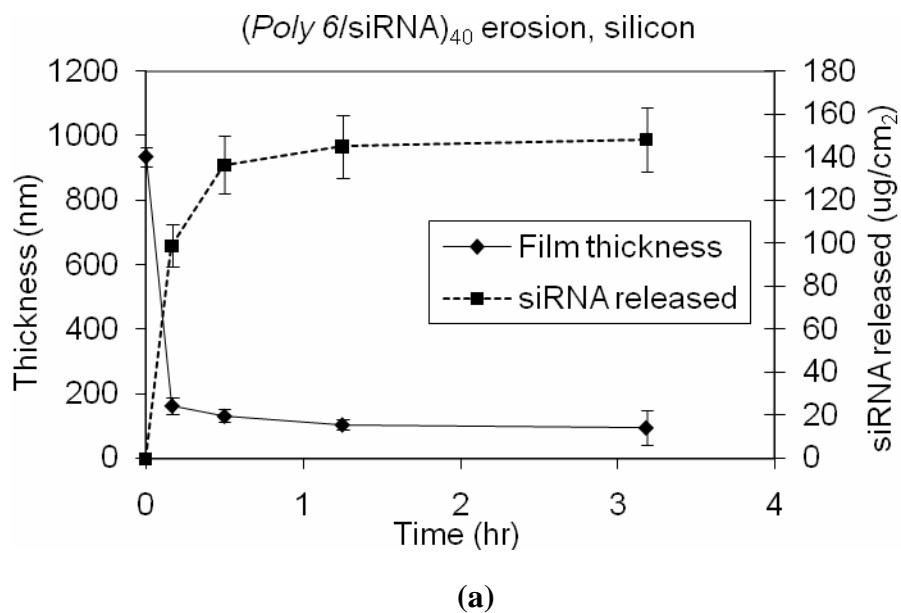
(a)



(b)

Figure 9.6 - Comparing erosion and release of (*Poly 1*/siRNA)₄₀ films on silicon vs. quartz substrates. (a) zoomed into the first 10 hours, and (b) displayed over the entire sampling period.

Figure 9.7 presents analogous data for $(Poly\ 6/siRNA)_{40}$ films. In contrast to $(Poly\ 1/siRNA)_{40}$, both silicon- and quartz-based $(Poly\ 6/siRNA)_{40}$ films completed their siRNA release within half an hour. Faster release from $Poly\ 6$ -based film was expected based on the same reasoning as that for its faster growth rate: the higher hydrophobicity and lower charge density resulted in looser ionic crosslinks. Based on this observation, I hypothesized that the release of siRNA from these $Poly\ X$ films was dominated by bulk deconstruction of the film, as opposed to being driven by hydrolysis of $Poly\ X$. If hydrolysis was predominantly at play, we would expect the hydrophobicity of $Poly\ 6$ to retard its hydrolysis and hence result in slower release of siRNA in comparison to $Poly\ 1$.



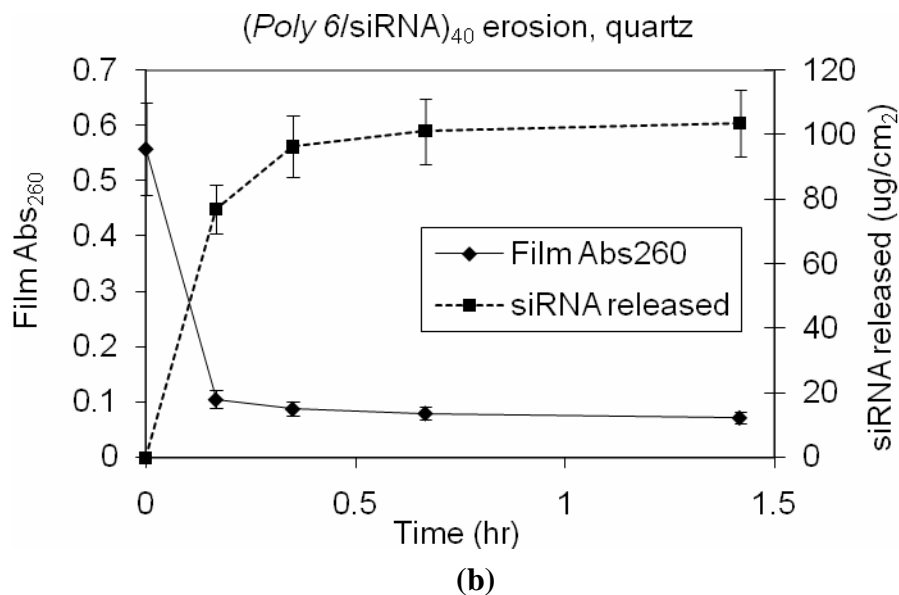
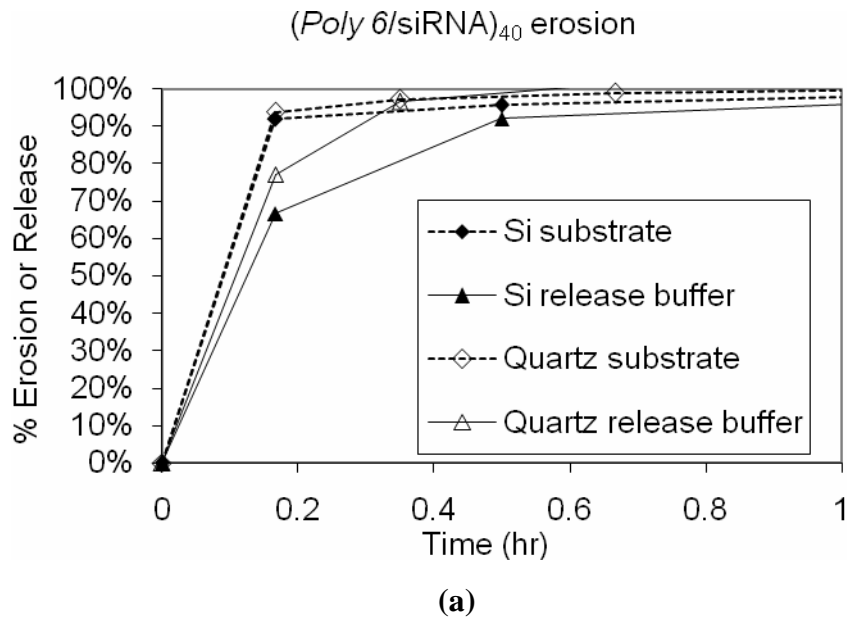


Figure 9.7 – (*Poly 6*/siRNA)₄₀ film erosion and siRNA release.

(a) from a film deposited on silicon substrate, with film erosion measured by ellipsometric thickness, and (b) from a film deposited on quartz substrate, with film erosion measured by Abs₂₆₀ of the film.

siRNA loading of *Poly 6* was higher at 40 bilayers – 140 $\mu\text{g}/\text{cm}^2$ for the silicon substrate and 80 $\mu\text{g}/\text{cm}^2$ for the quartz substrate, as compared to 80 $\mu\text{g}/\text{cm}^2$ and 60 $\mu\text{g}/\text{cm}^2$ respectively for *Poly 1*. The discrepancy between silicon and quartz substrate loadings was also larger for the (*Poly 6*/siRNA)₄₀ films, suggesting a sensitivity of drug dosage to the base substrate. The cause of such a discrepancy was unknown, but likely due to the balance between polyelectrolyte-substrate and polyelectrolyte-polyelectrolyte interactions. As hypothesized previously, the quartz substrate might have a more intact base layer to promote better adhesion of the *Poly X*. This in turn would compete with ionic interaction with *Poly X* and siRNA, leading to less encapsulation of siRNA overall.

Similar to Figure 9.6, Figure 9.8 presents an identical set of data as those from Figure 9.7 but in a % total progress format. For $(Poly\ 6/siRNA)_{40}$, less difference was seen between the two substrates, as the films all deconstructed rather quickly. In the first 0.5 hour, siRNA release from silicon was observed to occur more quickly than film thickness erosion, suggesting that the burst release was partially driven by siRNA diffusion out of the film. A similar conclusion for $(Poly\ 1/siRNA)_{40}$ was drawn. However, in *Poly 1*'s case, film erosion was observed to sustain far beyond completion of siRNA release, whereas in *Poly 6* film's case, both siRNA release and film thickness erosion were found to complete in about 1.5 hours. It appears that $(Poly\ 6/siRNA)_{40}$ deconstructed so rapidly that no residual *Poly 6* was left behind to slowly erode by hydrolysis.



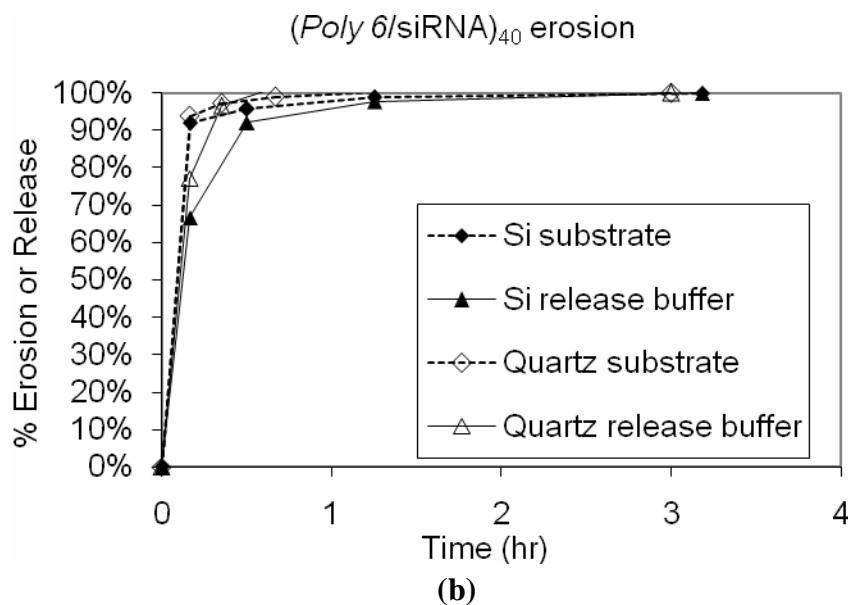


Figure 9.8 - Comparing erosion and release of (*Poly 6*/siRNA)₄₀ films on silicon vs. quartz substrates. (a) zoomed into the first 10 hours, and (b) displayed over the entire sampling period.

9.4 Conclusion.

Naked siRNAs were incorporated into LbL assemblies through simple bilayering with a poly(β -amino ester). By tracking both film thickness and Abs₂₆₀ of the films, I observed a steady and sigmoidal growth of (*Poly X*/siRNA)_n films up to n = 40. Subsequent release of siRNAs from these films under model physiological conditions was also monitored by both film thickness and Abs₂₆₀, and indicated good correlation between rates of siRNA release into the buffer and of film erosion. Both the thickness growth rate and the subsequent rate of siRNA release from these films were highly dependent on *Poly X*, with *Poly 6* films growing notably faster than *Poly 1* films and releasing their siRNAs in a much less sustained fashion. Both observations could be attributed to *Poly 6*'s higher hydrophobicity and lower charge density, which would result in looser ionic crosslinking with the siRNAs. Release appeared to be driven by a variety of mechanisms – siRNA

diffusion, *Poly X* hydrolysis, and bulk delamination of polymers. In the case of *Poly 6*, bulk delamination was thought to be most dominant.

This study provided proof-of-concept support for the ability of hydrolytically-degradable LbL assemblies to deliver siRNAs in a tunable fashion. While dosage tunability was not directly demonstrated at various numbers of layers, the smooth Abs₂₆₀ growth curves suggest that these films can be easily tuned on the amount of encapsulated siRNAs. A major next step for this project would be to assess the *in vitro* activity of the siRNAs released from these films through some kind of knockdown assay. In designing *in vitro* and *in vivo* studies on siRNA activity, one must include all necessary controls to distinguish between immunostimulatory versus gene silencing effect of the siRNA²⁶⁴.

Acknowledgments.

I would like to thank Dr. James Quattrochi and Wendy Ham at Harvard Medical School for providing the siRNAs and guidance on handling them; Dr. David Lynn at University of Wisconsin, Madison for providing input on the data; and Kevin Krogman for training and assistance on UV-vis measurements.

References.

1. Langer, R., Polymer-Controlled Drug Delivery Systems. *Acc. Chem. Res.* **1993**, 26, 537-542.
2. Urich, K. E.; Cannizzaro, S. M.; Langer, R. S.; Shakesheff, K. M., Polymeric Systems for Controlled Drug Release. *Chemical Reviews* **1999**, 99, (11), 3181-3198.
3. Falk, R.; Randolph, T. W.; Meyer, J. D.; Kelly, R. M.; Manning, M. C., Controlled release of ionic compounds from poly (-lactide) microspheres produced by precipitation with a compressed antisolvent. *Journal of Controlled Release* **1997**, 44, (1), 77-85.
4. Johnson, O. L.; Cleland, J. L.; Lee, H. J.; Charnis, M.; Duenas, E.; Jaworowicz, W.; Shepard, D.; Shihzamani, A.; Jones, A. J. S.; Putney, S. D., A month-long effect from a single injection of microencapsulated human growth hormone. *Nature Medicine* **1996**, 2, (7), 795-799.
5. Chluba, J.; Voegel, J.-C.; Decher, G.; Erbacher, P.; Schaaf, P.; Ogier, J., Peptide Hormone Covalently Bound to Polyelectrolytes and Embedded into Multilayer Architectures Conserving Full Biological Activity. *Biomacromolecules* **2001**, 2, (3), 800-805.
6. Misra, G. P.; Siegel, R. A., New mode of drug delivery: long term autonomous rhythmic hormone release across a hydrogel membrane. *Journal of Controlled Release* **2002**, 81, (1-2), 1-6.
7. McGee, J. P.; Davis, S. S.; O'Hagan, D. T., The immunogenicity of a model protein entrapped in poly(lactide-co-glycolide) microparticles prepared by a novel phase separation technique. *Journal of Controlled Release* **1994**, 31, (1), 55-60.
8. Qiu, L. Y.; Zhu, K. J., Design of a core-shelled polymer cylinder for potential programmable drug delivery. *International Journal of Pharmaceutics* **2001**, 219, (1-2), 151-160.
9. Dang, W.; Colvin, O. M.; Brem, H.; Saltzman, W. M., Covalent coupling of methotrexate to dextran enhances the penetration of cytotoxicity into a tissue-like matrix. *Cancer Research* **1994**, 54, (7), 1729-1735.
10. Brem, H.; Gabikian, P., Biodegradable polymer implants to treat brain tumors. *Journal Of Controlled Release: Official Journal Of The Controlled Release Society* **2001**, 74, (1-3), 63-67.
11. Conforti, A.; Bertani, S.; Lussignoli, S.; Grigolini, L.; Terzi, M.; Lora, S.; Caliceti, P.; Marsilio, F.; Veronese, F. M., Anti-inflammatory activity of polyphosphazene-based naproxen slow-release systems. *Journal of Pharmacy and Pharmacology* **1996**, 48, (5), 468-473.
12. Benkirane-Jessel, N.; Schwinte, P.; Falvey, P.; Darcy, R.; Haikel, Y.; Schaaf, P.; Voegel, J.-C.; Ogier, J., Build-up of Polypeptide Multilayer Coatings with Anti-Inflammatory Properties Based on the Embedding of Piroxicam-Cyclodextrin Complexes. *Advanced Functional Materials* **2004**, 14, (2), 174-182.
13. Gopferich, A., Bioerodible implants with programmable drug release. *Journal of Controlled Release* **1997**, 44, (2-3), 271-281.
14. Sershen, S.; West, J., Implantable, polymeric systems for modulated drug delivery. *Advanced Drug Delivery Reviews* **2002**, 54, (9), 1225-1235.

15. Brekke, J. H.; Gubbe, J. H. Device and methods for sequential, regional delivery of multiple cytotoxic agents and directed assembly of wound repair tissues. WO2004037311, May 6, 2004, 2004.
16. Caruso, F.; Schuler, C., Enzyme Multilayers on Colloid Particles: Assembly, Stability, and Enzymatic Activity. *Langmuir* **2000**, 16, (24), 9595-9603.
17. Schuler, C.; Caruso, F., Decomposable Hollow Biopolymer-Based Capsules. *Biomacromolecules* **2001**, 2, (3), 921-926.
18. Shi, X.; Caruso, F., Release Behavior of Thin-Walled Microcapsules Composed of Polyelectrolyte Multilayers. *Langmuir* **2001**, 17, (6), 2036-2042.
19. Khopade, A. J.; Caruso, F., Electrostatically Assembled Polyelectrolyte/Dendrimer Multilayer Films as Ultrathin Nanoreservoirs. *Nano Letters* **2002**, 2, (4), 415-418.
20. Cohen, S.; Yoshioka, T.; Lucarelli, M.; Hwang, L. H.; Langer, R., Controlled Delivery Systems for Proteins Based on Poly(Lactic/Glycolic Acid) Microspheres. *Pharmaceutical Research* **1991**, 8, (6), 713-720.
21. Sukhorukov, G. B.; Brumen, M.; Donath, E.; Möhwald, H., Hollow Polyelectrolyte Shells: Exclusion of Polymers and Donnan Equilibrium. *J. Phys. Chem. B* **1999**, 103, (31), 6434-6440.
22. Sukhorukov, G. B., Multilayer Hollow Microspheres. In *Dendrimers, Assemblies, Nanocomposites*, 1 ed.; Arshady, R.; Guyot, A., Eds. Citrus Reference Books: London, 2002; Vol. 5, pp 111-147.
23. Lynn, D. M.; Langer, R., Degradable Poly(amino esters): Synthesis, Characterization, and Self-Assembly with Plasmid DNA. *J. Am. Chem. Soc.* **2000**, 122, (44), 10761-10768.
24. Lim, Y.-b.; Kim, C.-h.; Kim, K.; Kim, S. W.; Park, J.-s., Development of a Safe Gene Delivery System Using Biodegradable Polymer, Poly[-(4-aminobutyl)-L-glycolic acid]. *J. Am. Chem. Soc.* **2000**, 122, (27), 6524-6525.
25. Sukhishvili, S. A.; Granick, S., Layered, Erasable Polymer Multilayers Formed by Hydrogen-Bonded Sequential Self-Assembly. *Macromolecules* **2002**, 35, (1), 301-310.
26. Etienne, O.; Schneider, A.; Taddei, C.; Richert, L.; Schaaf, P.; Voegel, J.-C.; Egles, C.; Picart, C., Degradability of Polysaccharides Multilayer Films in the Oral Environment: an in Vitro and in Vivo Study. *Biomacromolecules* **2005**, 6, (2), 726-733.
27. Hiller, J. A.; Rubner, M. F., Reversible Molecular Memory and pH-Switchable Swelling Transitions in Polyelectrolyte Multilayers. *Macromolecules* **2003**, 36, (11), 4078-4083.
28. Tanaka, S.; Yamakoshi, K.; Kamiya, A.; Shimazu, H.; Togawa, T., Osmotically powered drug-delivery pump using semipermeable hollow fiber. *Medical & Biological Engineering & Computing* **1986**, 24, (4), 371-374.
29. DeLongchamp, D. M.; Hammond, P. T., High-Contrast Electrochromism and Controllable Dissolution of Assembled Prussian Blue/Polymer Nanocomposites. *Advanced Functional Materials* **2004**, 14, (3), 224-232.
30. Hsieh, D. S.; Langer, R.; Folkman, J., Magnetic modulation of release of macromolecules from polymers. *Proceedings Of The National Academy Of Sciences Of The United States Of America* **1981**, 78, (3), 1863-1867.

31. Kost, J.; Leong, K.; Langer, R., Ultrasound-enhanced polymer degradation and release of incorporated substances. *Proceedings Of The National Academy Of Sciences Of The United States Of America* **1989**, 86, (20), 7663-7666.
32. Bernard, L.; Hoffmeyer, P.; Assal, M.; Vaudaux, P.; Schrenzel, J.; Lew, D., Trends in the treatment of orthopaedic prosthetic infections. *J. Antimicrob. Chemother.* **2004**, 53, (2), 127-129.
33. Bauer, T. W.; Schils, J., The pathology of total joint arthroplasty. *Skeletal Radiology* **1999**, 28, (9), 483-497.
34. Lavernia, C. J.; Drakeford, M. K.; Tsao, A. K.; Gittelsohn, A.; Krackow, K. A.; Hungerford, D. S., Revision and primary hip and knee arthroplasty. A cost analysis. *Clin. Orthop.* **1995**, 311, 136-141.
35. Saleh, K. J.; Rand, J. A.; McQueen, D. A., Current Status of Revision Total Knee Arthroplasty: How Do We Assess Results? *J Bone Joint Surg Am* **2003**, 85, (90001), S18-20.
36. Bourne, R. B., Prophylactic use of antibiotic bone cement: an emerging standard--in the affirmative. *The Journal of Arthroplasty* **2004**, 19, (4, Supplement 1), 69-72.
37. Fluckiger, U.; Zimmerli, W., Diagnostestellung und Verlaufsmonitoring der postoperativen bakteriellen Osteitis. *Der Orthopade* **2004**, 33, (4), 416-423.
38. Bottner, F.; Sculco, T. P.; Sharrock, N. E.; Westrich, G. H.; Steinbeck, J., Thromboseprophylaxe in der Huftendoprothetik. *Der Orthopade* **2001**, 30, (11), 890-896.
39. Heisel, C.; Clarius, M.; Schneider, U.; Breusch, S. J., Thromboembolic complications related to the use of bone cement in hip arthroplasty--pathogenesis and prophylaxis. *Zeitschrift fur Orthopadie und ihre Grenzgebiete* **2001**, 139, (3), 221-228.
40. Dahl, O. E., Orthopaedic surgery as a model for drug development in thrombosis. *Drugs* **2004**, 64, (Supplement 1), 17-25.
41. Patil, S.; Allan, D. B.; Quin, R., Effect of total knee arthroplasty on blood flow to the lower limb. *The Journal of Arthroplasty* **2002**, 17, (7), 882-886.
42. Cole, B. J.; Schultz, E.; Smilari, T. F.; Hajdu, S. I.; Krauss, E. S., Malignant fibrous histiocytoma at the site of a total hip replacement: review of the literature and case report. *Skeletal Radiology* **1997**, 26, (9), 559-563.
43. Ganapathi, M.; Lake, D. N. W.; Griffiths, A. P., Periprosthetic high-grade B-cell lymphoma complicating an infected revision total hip arthroplasty. *The Journal of Arthroplasty* **2001**, 16, (2), 229-232.
44. Korkala, O.; Syrj nen, K. J., Intrapelvic cyst formation after hip arthroplasty with a carbon fibre-reinforced polyethylene socket. *Archives of Orthopaedic and Trauma Surgery* **1998**, 118, (1 - 2), 113-115.
45. Grayson, A. C. R.; Voskerician, G.; Lynn, A.; Anderson, J. M.; Cima, M. J.; Langer, R., Differential degradation rates *in vivo* and *in vitro* of biocompatible poly(lactic acid) and poly(glycolic acid) homo- and co-polymers for a polymeric drug-delivery microchip. *Journal of Biomaterials Science. Polymer Edition* **2004**, 15, (10), 1281-1304.
46. Richards-Grayson, A. C.; Choi, I. S.; Tyler, B. M.; Wang, P. P.; Brem, H.; Cima, M. J.; Langer, R., Multi-pulse drug delivery from a resorbable polymeric microchip device. *Nature Materials* **2003**, 2, 767-772.
47. Santini, J. T.; Cima, M. J.; Langer, R., A Controlled-Release Microchip. *Nature* **1999**, 397, 335-338.

48. Santini, J. T.; Richards, A. C.; Scheidt, R.; Cima, M. J.; Langer, R., Microchips as Controlled Drug-Delivery Devices. *Angewandte Chemie International Edition* **2000**, *39*, (14), 2396-2407.
49. Richardson, T. P.; Peters, M. C.; Ennett, A. B.; Mooney, D. J., Polymeric System for Dual Growth Factor Delivery. *Nature Biotechnology* **2001**, *19*, (11), 1029-1034.
50. Raiche, A. T.; Puleo, D. A., In vitro effects of combined and sequential delivery of two bone growth factors. *Biomaterials* **2004**, *25*, (4), 677-685.
51. Decher, G.; Hong, J. D., Buildup of ultrathin multilayer films by a self-assembly process. 1. Consecutive adsorption of anionic and cationic bipolar amphiphiles on charged surfaces. *Makromolekulare Chemie, Macromolecular Symposia* **1991**, *46*, 321-327.
52. Decher, G.; Hong, J. D., Buildup of ultrathin multilayer films by a self-assembly process: II. Consecutive adsorption of anionic and cationic bipolar amphiphiles and polyelectrolytes on charged surfaces. *Berichte der Bunsen-Gesellschaft* **1991**, *95*, (11), 1430-1434.
53. Decher, G., Fuzzy Nanoassemblies: Toward Layered Polymeric Multicomposites. *Science* **1997**, *277*, (5330), 1232-1237.
54. Stroeve, P.; Vazquez, V.; Coelho, M. A. N.; Rabolt, J. F., Gas transfer in supported films made by molecular self assembly of ionic polymers. *Thin Solid Films* **1996**, *285*, 708-712.
55. Balasubramanian, S.; Wang, X.; Wang, H. C.; Yang, K.; Kumar, J.; Tripathy, S. K., Azo Chromophore-Functionalized Polyelectrolytes. 2. Acentric Self-Assembly through a Layer-by-Layer Deposition Process. *Chemistry of Materials* **1998**, *10*, (6), 1554-1560.
56. Lindsay, G. A.; Roberts, M. J.; Chafin, A. P.; Hollins, R. A.; Merwin, L. H.; Stenger-Smith, J. D.; Yee, R. Y.; Zarras, P.; Wynne, K. J., Ordered Films by Alternating Polyelectrolyte Deposition of Cationic Side Chain and Anionic Main Chain Chromophoric Polymers. *Chemistry of Materials* **1999**, *11*, (4), 924-929.
57. Joly, S.; Kane, R.; Radzilowski, L.; Wang, T.; Wu, A.; Cohen, R. E.; Thomas, E. L.; Rubner, M. F., Multilayer Nanoreactors for Metallic and Semiconducting Particles. *Langmuir* **2000**, *16*, (3), 1354-1359.
58. Caruso, F.; Niikura, K.; Furlong, D. N.; Okahata, Y., Assembly of alternating polyelectrolyte and protein multilayer films for immunosensing. *Langmuir* **1997**, *13*, 3427-3433.
59. Constantine, C. A.; Mello, S. V.; Dupont, A.; Cao, X.; David Santos, J.; Osvaldo N. Oliveira, J.; Strixino, F. T.; Pereira, E. C.; Cheng, T.-C.; Defrank, J. J.; Leblanc, R. M., Layer-by-Layer Self-Assembled Chitosan/Poly(thiophene-3-acetic acid) and Organophosphorus Hydrolase Multilayers. *J. Am. Chem. Soc.* **2003**, *125*, (7), 1805-1809.
60. Forzani, E. S.; Otero, M.; Pérez, M. A.; Tejel, M. L.; Calvo, E. J., The Structure of Layer-by-Layer Self-Assembled Glucose Oxidase and Os(Bpy)₂CIPyCH₂NH-Poly(allylamine) Multilayers: Ellipsometric and Quartz Crystal Microbalance Studies. *Langmuir* **2002**, *18*, (10), 4020-4029.
61. Sukhorukov, G. B.; Montrel, M. M.; Petrov, A. I.; Shabarchina, L. I.; Sukhorukov, B. I., Multilayer films containing immobilized nucleic acids. Their structure and possibilities in biosensor applications. *Biosensors and Bioelectronics* **1996**, *11*, 913-922.

62. DeLongchamp, D. M.; Hammond, P. T., Highly Ion Conductive Poly(ethylene oxide)-Based Solid Polymer Electrolytes from Hydrogen Bonding Layer-by-Layer Assembly. *Langmuir* **2004**, 20, (13), 5403-5411.
63. Rouse, J. H.; Lillehei, P. T., Electrostatic Assembly of Polymer/Single Walled Carbon Nanotube Multilayer Films. *Nano Letters* **2003**, 3, (1), 59-62.
64. Fulda, K.-U.; Kampes, A.; Krasemann, L.; Tieke, B., Self-assembled mono- and multilayers of monodisperse cationic and anionic latex particles. *Thin Solid Films* **1998**, 327-329, 752-757.
65. Iler, R. K., Multilayers of colloidal particles. *Journal of Colloid Interface Science* **1966**, 21, (6), 569-594.
66. Dokoutchaev, A.; James, J. T.; Koene, S. C.; Pathak, S.; Prakash, G. K. S.; Thompson, M. E., Colloidal Metal Deposition onto Functionalized Polystyrene Microspheres. *Chemistry of Materials* **1999**, 11, (9), 2389-2399.
67. Liu, Y. J.; Wang, Y. X.; Claus, R. O., Layer-by-layer ionic self-assembly of Au colloids into multilayer thin-films with bulk metal conductivity. *Chemical Physics Letters* **1998**, 298, 315-319.
68. Hammond, P. T.; Whitesides, G. M., Formation of Polymer Microstructures by Selective Deposition of Polyion Multilayers Using Patterned Self-Assembled Monolayers as a Template. *Macromolecules* **1995**, 28, (22), 7569-7571.
69. Clark, S. L.; Hammond, P. T., Engineering the Microfabrication of Layer-by-Layer Thin Films. *Advanced Materials* **1998**, 10, (18), 1515-1519.
70. Lvov, Y. M.; Sukhorukov, G. B., Protein architecture: Assembly of ordered films by means of laternated adsorption of oppositely charged macromolecules. *Membrane Cell Biology* **1997**, 11, 277-303.
71. Onda, M.; Lvov, Y. M.; Ariga, K.; Kunitake, T., Sequential actions of glucose oxidase and peroxidase in molecular films assembled by layer by layer adsorption. *Biotechnology and Bioengineering* **1996**, 51, 163-166.
72. Groth, T.; Lendlein, A., Layer-by-Layer Deposition of Polyelectrolytes - A Versatile Tool for the In Vivo Repair of Blood Vessels. *Angewandte Chemie International Edition* **2004**, 43, (8), 926-928.
73. Berg, M. C.; Yang, S. Y.; Hammond, P. T.; Rubner, M. F., Controlling Mammalian Cell Interactions on Patterned Polyelectrolyte Multilayer Surfaces. *Langmuir* **2004**, 20, (4), 1362-1368.
74. Pavor, P. V.; Gearing, B. P.; Bellare, A.; Cohen, R. E., Tribological characteristics of polyelectrolyte multilayers. *Wear* **2004**, 256, (11-12), 1196-1207.
75. van de Belt, H.; Neut, D.; Schenk, W.; van Horn, J. R.; van der Mei, H. C.; Busscher, H. J., Infection of orthopedic implants and the use of antibiotic-loaded bone cements. A review. *Acta Orthopaedica Scandinavica* **2001**, 72, (6), 557-571.
76. Ono, I.; Tateshita, T.; Inoue, M.; Kuboki, Y., In vivo strength enhancement of hydroxyapatite combined with rhBMP-2. *Journal of Bone and Mineral Metabolism* **1998**, 16, (2), 81-87.
77. Li, R. H.; Boussein, M. L.; Blake, C. A.; D'Augusta, D.; Kim, H.; Li, X. J.; Wozney, J. M.; Seeherman, H. J., rhBMP-2 injected in a calcium phosphate paste ([alpha]-BSM) accelerates healing in the rabbit ulnar osteotomy model. *Journal of Orthopaedic Research* **2003**, 21, (6), 997-1004.

78. Geiger, M.; Li, R. H.; Friess, W., Collagen sponges for bone regeneration with rhBMP-2. *Advanced Drug Delivery Reviews* **2003**, *55*, (12), 1613-1629.
79. Keskin, D. S.; Tezcaner, A.; Korkusuz, P.; Korkusuz, F.; Hasirci, V., Collagen-chondroitin sulfate-based PLLA-SAIB-coated rhBMP-2 delivery system for bone repair. *Biomaterials* **2005**, *26*, (18), 4023-4034.
80. Kroese-Deutman, H. C.; Ruhe, P. Q.; Spauwen, P. H. M.; Jansen, J. A., Bone inductive properties of rhBMP-2 loaded porous calcium phosphate cement implants inserted at an ectopic site in rabbits. *Biomaterials* **2005**, *26*, (10), 1131-1138.
81. Kaito, T.; Myoui, A.; Takaoka, K.; Saito, N.; Nishikawa, M.; Tamai, N.; Ohgushi, H.; Yoshikawa, H., Potentiation of the activity of bone morphogenetic protein-2 in bone regeneration by a PLA-PEG/hydroxyapatite composite. *Biomaterials* **2005**, *26*, (1), 73-79.
82. Tabata, Y.; Miyao, M.; Ozeki, M.; Ikada, Y., Controlled release of vascular endothelial growth factor by use of collagen hydrogels. *Journal of Biomaterials Science, Polymer Edition* **2000**, *11*, (9), 915-930.
83. Yamamoto, M.; Ikada, Y.; Tabata, Y., Controlled release of growth factors based on biodegradation of gelatin hydrogel. *Journal of Biomaterials Science, Polymer Edition* **2001**, *12*, (1), 77-88.
84. Carano, R. A. D.; Filvaroff, E. H., Angiogenesis and bone repair. *Drug Discovery Today* **2003**, *8*, (21), 980-989.
85. Gu, F.; Amsden, B.; Neufeld, R., Sustained delivery of vascular endothelial growth factor with alginate beads. *Journal of Controlled Release* **2004**, *96*, (3), 463-472.
86. Kotov, N. A., Layer-by-layer self-assembly: The contribution of hydrophobic interactions. *Nanostructured Materials* **1999**, *12*, (5-8), 789-796.
87. Wadood, A. C.; Armbrecht, A. M.; Aspinall, P. A.; Dhillon, B., Safety and efficacy of a dexamethasone anterior segment drug delivery system in patients after phacoemulsification. *Journal of Cataract & Refractive Surgery* **2004**, *30*, (4), 761-768.
88. Baeyens, V.; Percicot, C.; Zignani, M.; Deshpande, A. A.; Kaltsatos, V.; Gurny, R., Ocular drug delivery in veterinary medicine. *Advanced Drug Delivery Reviews* **1997**, *28*, (3), 335-361.
89. Chan, A. T. C.; Ma, B. B. Y.; Lo, Y. M. D.; Leung, S. F.; Kwan, W. H.; Hui, E. P.; Mok, T. S. K.; Kam, M.; Chan, L. S.; Chiu, S. K. W.; Yu, K. H.; Cheung, K. Y.; Lai, K.; Lai, M.; Mo, F.; Yeo, W.; King, A.; Johnson, P. J.; Teo, P. M. L.; Zee, B., Phase II Study of Neoadjuvant Carboplatin and Paclitaxel Followed by Radiotherapy and Concurrent Cisplatin in Patients With Locoregionally Advanced Nasopharyngeal Carcinoma: Therapeutic Monitoring With Plasma Epstein-Barr Virus DNA. *J Clin Oncol* **2004**, *22*, (15), 3053-3060.
90. Herzog, T. J., Recurrent Ovarian Cancer: How Important Is It to Treat to Disease Progression? *Clin Cancer Res* **2004**, *10*, (22), 7439-7449.
91. Prevention, C. f. D. C. a. *Diphtheria, Tetanus, & Pertussis Vaccines: What You Need to Know*; 42 U.S.C. 300aa-26; CDC National Immunization Program: July 30, 2001, 2001.
92. Matthews, D. R.; Lang, D. A.; Burnett, M. A.; Turner, R. C., Control of pulsatile insulin secretion in man. *Diabetologia* **1983**, *24*, (4), 231-237.

93. Reid, R. L.; Fretts, R.; Van Vugt, D. A., The theory and practice of ovulation induction with gonadotropin-releasing hormone. *American Journal Of Obstetrics And Gynecology* **1988**, 158, (1), 176-185.
94. Kuret, J. A.; Murad, F., In *Goodman and Gilman's the Pharmacological Basis of Therapeutics*, 8 ed.; Gilman, A. G.; Rall, T. W.; Niles, A. S.; Taylor, P., Eds. McGraw-Hill: New York, 1990; pp 1334-1360.
95. Levy, R.; Nichols, M. A.; Miller, T. W., Jr., Encapsulated systems for controlled release and pest management. *ACS Symposium Series* **1993**, 520, 202-212.
96. Bouzeloc, S.; Creutz, S.; Leaym, T. M. Controlled release compositions for use in cosmetics. WO2004084844, 10/07/2004, 2004.
97. Brannon-Peppas, L., Controlled release in the food and cosmetics industries. *ACS Symposium Series* **1993**, 520, 42-52.
98. Dees, C. H. Combination antiperspirant and antimicrobial compositions. EP1362581, 11/19/2003, 2003.
99. Chung, A. J.; Rubner, M. F., Methods of Loading and Releasing Low Molecular Weight Cationic Molecules in Weak Polyelectrolyte Multilayer Films. *Langmuir* **2002**, 18, (4), 1176-1183.
100. Dubas, S. T.; Schlenoff, J. B., Polyelectrolyte Multilayers Containing a Weak Polyacid: Construction and Deconstruction. *Macromolecules* **2001**, 34, (11), 3736-3740.
101. Hahn, S. K.; Hoffman, A. S., Characterization of Biocompatible Polyelectrolyte Complex Multilayer of Hyaluronic Acid and Poly-L-Lysine. *Biotechnology and Bioprocess Engineering* **2004**, 9, (3), 179-183.
102. Sukhorukov, G. B.; Mohwald, H.; Decher, G.; Lvov, Y. M., Assembly of polyelectrolyte multilayer films by consecutively alternating adsorption of polynucleotides and polycations. *Thin Solid Films* **1996**, 284-285, 220-223.
103. Thierry, B.; Winnik, F. M.; Merhi, Y.; Silver, J.; Tabrizian, M., Bioactive Coatings of Endovascular Stents Based on Polyelectrolyte Multilayers. *Biomacromolecules* **2003**, 4, (6), 1564-1571.
104. Sukhishvili, S. A.; Granick, S., Layered, Erasable, Ultrathin Polymer Films. *J. Am. Chem. Soc.* **2000**, 122, (39), 9550-9551.
105. Choksakulnimitr, S.; Masuda, S.; Tokuda, H.; Takakura, Y.; Hashida, M., In vitro cytotoxicity of macromolecules in different cell culture systems. *Journal of Controlled Release* **1995**, 34, (3), 233-241.
106. Zauner, W.; Ogris, M.; Wagner, E., Polylysine-based transfection systems utilizing receptor-mediated delivery. *Advanced Drug Delivery Reviews* **1998**, 30, (1-3), 97-113.
107. Roberts, J. C.; Bhalgat, M. K.; Zera, R. T., Preliminary biological evaluation of polyamidoamine (PAMAM) Starburst™ dendrimers. *Journal of Biomedical Materials Research* **1996**, 30, (1), 53-65.
108. Barrera, D. A.; Zylstra, E.; Peter T. Lansbury, J.; Langer, R., Synthesis and RGD Peptide Modification of a New Biodegradable Copolymer: Poly(lactic acid-co-lysine). *J. Am. Chem. Soc.* **1993**, 115, 11010-11011.
109. Putnam, D.; Langer, R., Poly(4-hydroxy-L-proline ester): Low-Temperature Polycondensation and Plasmid DNA Complexation. *Macromolecules* **1999**, 32, (11), 3658-3662.

110. Vazquez, E.; Dewitt, D. M.; Hammond, P. T.; Lynn, D. M., Construction of Hydrolytically-Degradable Thin Films via Layer-by-Layer Deposition of Degradable Polyelectrolytes. *J. Am. Chem. Soc.* **2002**, 124, (47), 13992-13993.
111. Zhang, J.; Chua, L. S.; Lynn, D. M., Multilayered Thin Films that Sustain the Release of Functional DNA under Physiological Conditions. *Langmuir* **2004**, 20, (19), 8015-8021.
112. Jewell, C. M.; Zhang, J.; Fredin, N. J.; Lynn, D. M., Multilayered polyelectrolyte films promote the direct and localized delivery of DNA to cells. *Journal of Controlled Release* **2005**, 106, (1-2), 214-223.
113. Zhang, J.; Fredin, N. J.; Lynn, D. M., Apparent Dewetting of Ultrathin Multilayered Polyelectrolyte Films Incubated in Aqueous Environments. *Langmuir* **2007**, 23, (23), 11603-11610.
114. Zhang, J.; Montanez, S. I.; Jewell, C. M.; Lynn, D. M., Multilayered Films Fabricated from Plasmid DNA and a Side-Chain Functionalized Poly(β -amino Ester): Surface-Type Erosion and Sequential Release of Multiple Plasmid Constructs from Surfaces. *Langmuir* **2007**, 23, (22), 11139-11146.
115. Fredin, N. J.; Zhang, J.; Lynn, D. M., Surface Analysis of Erodible Multilayered Polyelectrolyte Films: Nanometer-Scale Structure and Erosion Profiles. *Langmuir* **2005**, 21, (13), 5803-5811.
116. Liu, X.; Yang, J. W.; Miller, A. D.; Nack, E. A.; Lynn, D. M., Charge-Shifting Cationic Polymers That Promote Self-Assembly and Self-Disassembly with DNA. *Macromolecules* **2005**.
117. Zhang, J.; Lynn, D. M., Multilayered Films Fabricated from Combinations of Degradable Polyamines: Tunable Erosion and Release of Anionic Polyelectrolytes. *Macromolecules* **2006**, 39, (26), 8928-8935.
118. Jewell, C. M.; Zhang, J.; Fredin, N. J.; Wolff, M. R.; Hacker, T. A.; Lynn, D. M., Release of Plasmid DNA from Intravascular Stents Coated with Ultrathin Multilayered Polyelectrolyte Films. *Biomacromolecules* **2006**, 7, (9), 2483-2491.
119. Wood, K. C.; Boedicker, J. Q.; Lynn, D. M.; Hammond, P. T., Tunable Drug Release from Hydrolytically Degradable Layer-by-Layer Thin Films. *Langmuir* **2005**, 21, (4), 1603-1609.
120. Wood, K. C.; Chuang, H. F.; Batten, R. D.; Lynn, D. M.; Hammond, P. T., Controlling interlayer diffusion to achieve sustained, multiagent delivery from layer-by-layer thin films. *PNAS* **2006**, 103, (27), 10207-10212.
121. Schmidmaier, G.; Lucke, M.; Wildemann, B.; Haas, N. P.; Raschke, M., Prophylaxis and treatment of implant-related infections by antibiotic-coated implants: a review. *Injury* **2006**, 37, (2, Supplement 1), S105-S112.
122. Stigter, M.; Bezemer, J.; de Groot, K.; Layrolle, P., Incorporation of different antibiotics into carbonated hydroxyapatite coatings on titanium implants, release and antibiotic efficacy. *Journal of Controlled Release* **2004**, 99, (1), 127-137.
123. Humphrey, J. S.; Mehta, S.; Seaber, A. V.; Vail, T. P., Pharmacokinetics of a degradable drug delivery system in bone. *Clinical Orthopaedics And Related Research* **1998**, (349), 218-224.
124. L. Meseguer-Olmo, M. J. R.-N., M. Clavel-Sainz, V. Vicente-Ortega, M. Alcaraz-Baños, A. Lax-Pérez, D. Arcos, C. V. Ragel, M. Vallet-Regí, Biocompatibility and Ca^{2+} in

- vivo gentamicin release from bioactive sol-gel glass implants. *Journal of Biomedical Materials Research* **2002**, 61, (3), 458-465.
125. Johannes G.E. Hendriks, D. N., Jim R. van Horn, Henny C. van der Mei, Henk J. Busscher,, The release of gentamicin from acrylic bone cements in a simulated prosthesis-related interfacial gap. *Journal of Biomedical Materials Research Part B: Applied Biomaterials* **2003**, 64B, (1), 1-5.
126. Price, J. S.; Tencer, A. F.; Arm, D. M.; Bohach, G. A., Controlled release of antibiotics from coated orthopedic implants. . *Journal of Biomedical Materials Research* **1996**, 30, (3), 281-286.
127. Nablo, B. J.; Rothrock, A. R.; Schoenfisch, M. H., Nitric oxide-releasing sol-gels as antibacterial coatings for orthopedic implants. *Biomaterials* **2004**, 26, (8), 917-924.
128. Chung, R.-J.; Hsieh, M.-F.; Huang, C.-W.; Perng, L.-H.; Wen, H.-W.; Chin, T.-S., Antimicrobial effects and human gingival biocompatibility of hydroxyapatite sol-gel coatings. *Journal of Biomedical Materials Research Part B: Applied Biomaterials* **2006**, 76B, (1), 169-178.
129. Balaban, N.; Gov, Y.; Bitler, A.; Boelaert, J. R., Prevention of *Staphylococcus aureus* biofilm on dialysis catheters and adherence to human cells. *Kidney International* **2003**, 63, 340-345.
130. Danese, P. N., Antibiofilm Approaches: Prevention of Catheter Colonization. *Chemistry & Biology* **2002**, 9, (8), 873-880.
131. Bayston, R.; Ashraf, W.; Bhundia, C., Mode of action of an antimicrobial biomaterial for use in hydrocephalus shunts. *J. Antimicrob. Chemother.* **2004**, 53, (5), 778-782.
132. Camiel C. L. Peerlings, H. H. L. H., Raymond T. J. Bevers, Erik J. H. Boelen, Bram J. Stelt, Eva J. M. Korthagen, Leo H. Koole,, Heparin release from slippery-when-wet guide wires for intravascular use. *Journal of Biomedical Materials Research* **2002**, 63, (6), 692-698.
133. Belt, H. v. d.; Neut, D.; Schenk, W.; Horn, J. R. v.; Mei, H. C. v. d.; Busscher, H. J., Infection of orthopedic implants and the use of antibiotic-loaded bone cements: A review. *Acta Orthopaedica Scandinavica* **2001**, 72, (6), 557-571.
134. Ramage, G.; Tunney, M. M.; Patrick, S.; Gorman, S. P.; Nixon, J. R., Formation of *Propionibacterium acnes* biofilms on orthopaedic biomaterials and their susceptibility to antimicrobials. *Biomaterials* **2003**, 24, (19), 3221-3227.
135. Harris, L. G.; Richards, R. G., Staphylococci and implant surfaces: a review. *Injury* **2006**, 37, (2, Supplement 1), S3-S14.
136. Lynch, A. S.; Robertson, G. T., Bacterial and Fungal Biofilm Infections. *Annual Review of Medicine* **2008**, 59, (1 %R doi:10.1146/annurev.med.59.110106.132000), 415-428.
137. Costerton, J. W.; Khoury, A. E.; Ward, K. H.; Anwar, H., Practical measures to control device-related bacterial infections. *The International Journal of Artificial Organs* **1993**, 16, (11), 765-770.
138. Esposito, S.; Leone, S., Antimicrobial treatment for Intensive Care Unit (ICU) infections including the role of the infectious disease specialist. *International Journal of Antimicrobial Agents* **2007**, 29, (5), 494-500.

139. Lucke, M.; Schmidmaier, G.; Sadoni, S.; Wildemann, B.; Schiller, R.; Haas, N. P.; Raschke, M., Gentamicin coating of metallic implants reduces implant-related osteomyelitis in rats. *Bone* **2003**, 32, (5), 521-531.
140. Hanssen, A. D.; Spangehl, M. J., Practical applications of antibiotic-loaded bone cement for treatment of infected joint replacements. *Clinical Orthopaedics And Related Research* **2004**, (427), 79-85.
141. Alt, V.; Bitschnau, A.; Osterling, J.; Sewing, A.; Meyer, C.; Kraus, R.; Meissner, S. A.; Wenisch, S.; Domann, E.; Schnettler, R., The effects of combined gentamicin-hydroxyapatite coating for cementless joint prostheses on the reduction of infection rates in a rabbit infection prophylaxis model. *Biomaterials* **2006**, 27, (26), 4627-4634.
142. Cook, G.; Costerton, J. W.; Darouiche, R. O., Direct confocal microscopy studies of the bacterial colonization in vitro of a silver-coated heart valve sewing cuff. *International Journal of Antimicrobial Agents* **2000**, 13, (3), 169-173.
143. Gosheger, G.; Harges, J.; Ahrens, H.; Streitburger, A.; Buerger, H.; Erren, M.; Gonsel, A.; Kemper, F. H.; Winkelmann, W.; von Eiff, C., Silver-coated megaendoprostheses in a rabbit model--an analysis of the infection rate and toxicological side effects. *Biomaterials* **2004**, 25, (24), 5547-5556.
144. Grunlan, J. C.; Choi, J. K.; Lin, A., Antimicrobial Behavior of Polyelectrolyte Multilayer Films Containing Cetrime and Silver. *Biomacromolecules* **2005**, 6, (2), 1149-1153.
145. Hollinger, M. A., Toxicological aspects of topical silver pharmaceuticals. *Critical Reviews in Toxicology* **1996**, 26, (3), 255-260.
146. Sheehan, E.; McKenna, J.; Mulhall, K. J.; Marks, P.; McCormack, D., Adhesion of Staphylococcus to orthopaedic metals, an in vivo study. *Journal of Orthopaedic Research* **2004**, 22, (1), 39-43.
147. Chuang, H. F.; Smith, R.; xe, C; Hammond, P. T., Polyelectrolyte Multilayers for Tunable Release of Antibiotics. *Biomacromolecules* **2008**, ASAP Article.
148. Kim, B.-S.; Park, S. W.; Hammond, P. T., Hydrogen-Bonding Layer-by-Layer-Assembled Biodegradable Polymeric Micelles as Drug Delivery Vehicles from Surfaces. *ACS Nano* **2008**, 2, (2), 386-392.
149. DeLongchamp, D. M.; Hammond, P. T., Multi-hue electrochromism in polymer/inorganic composites from layer-by-layer assembly. *Polymer Preprints* **2003**, 44, (1), 649-650.
150. DeLongchamp, D. M.; Hammond, P. T., Multiple-Color Electrochromism from Layer-by-Layer-Assembled Polyaniline/Prussian Blue Nanocomposite Thin Films. *Chemistry of Materials* **2004**, 16, (23), 4799-4805.
151. Pearce, J., Studies of any toxicological effects of Prussian blue compounds in mammals--A review. *Food and Chemical Toxicology* **1994**, 32, (6), 577-582.
152. Oupick, D.; Parker, A. L.; Seymour, L. W., Laterally Stabilized Complexes of DNA with Linear Reducible Polycations: Strategy for Triggered Intracellular Activation of DNA Delivery Vectors. *J. Am. Chem. Soc.* **2002**, 124, (1), 8-9.
153. Picart, C.; Mutterer, J.; Richert, L.; Luo, Y.; Prestwich, G. D.; Schaaf, P.; Voegel, J.-C.; Lavalle, P., Molecular basis for the explanation of the exponential growth of polyelectrolyte multilayers. *PNAS* **2002**, 99, (20), 12531-12535.

154. Garza, J. M.; Schaaf, P.; Muller, S.; Ball, V.; Stoltz, J.-F.; Voegel, J.-C.; Lavalle, P., Multicompartiment Films Made of Alternate Polyelectrolyte Multilayers of Exponential and Linear Growth. *Langmuir* **2004**, *20*, (17), 7298-7302.
155. BERRY, D.; KWAN, C.-P.; SHRIVER, Z.; VENKATARAMAN, G.; SASISEKHARAN, R., Distinct heparan sulfate glycosaminoglycans are responsible for mediating fibroblast growth factor-2 biological activity through different fibroblast growth factor receptors
10.1096/fj.00-0661fje. *FASEB J.* **2001**, *15*, (8), 1422-1424.
156. Berry, D.; Shriver, Z.; Venkataraman, G.; Sasisekharan, R., Quantitative assessment of FGF regulation by cell surface heparan sulfates. *Biochemical and Biophysical Research Communications* **2004**, *314*, (4), 994-1000.
157. Ayako Oyane, H.-M. K., Takuo Furuya, Tadashi Kokubo, Toshiki Miyazaki, Takashi Nakamura,, Preparation and assessment of revised simulated body fluids. *Journal of Biomedical Materials Research Part A* **2003**, *65A*, (2), 188-195.
158. Berry, D.; Lynn, D. M.; Sasisekharan, R.; Langer, R., Poly([beta]-amino ester)s Promote Cellular Uptake of Heparin and Cancer Cell Death. *Chemistry & Biology* **2004**, *11*, (4), 487-498.
159. Brynda, E.; Houska, M.; Jirouskova, M.; Dyr, J. E., Albumin and heparin multilayer coatings for blood-contacting medical devices. *Journal of Biomedical Materials Research* **2000**, *51*, (2), 249-257.
160. Tana, Q.; Ji, J.; Barbosa, M. A.; Fonseca, C.; Shen, J., Constructing thromboresistant surface on biomedical stainless steel via layer-by-layer deposition anticoagulant. *Biomaterials* **2003**, *24*, (25), 4699-4705.
161. Claudia Sperling, M. H. E. B. U. S. C. W., In vitro hemocompatibility of albumin-heparin multilayer coatings on polyethersulfone prepared by the layer-by-layer technique. *Journal of Biomedical Materials Research Part A* **2006**, *76A*, (4), 681-689.
162. Anderson, D. G.; Lynn, D. M.; Langer, R., Semi-Automated Synthesis and Screening of a Large Library of Degradable Cationic Polymers for Gene Delivery. *Angewandte Chemie International Edition* **2003**, *42*, (27), 3153-3158.
163. Heidel, J. D., Linear cyclodextrin-containing polymers and their use as delivery agents. *Expert Opinion in Drug Delivery* **2006**, *3*, (5), 641-646.
164. Gavrilin, M. V.; Kompantseva, Y. V.; Ushakova, L. S., Dimethyl-b-cyclodextrin for eye drops of dexamethasone. *Khimiko-Farmatsevticheskii Zhurnal* **1994**, *28*, (9), 44-46.
165. Gavrilin, M. V.; Kompantseva, E. V.; Gusova, B. A.; Ushakova, L. S.; Makarov, V. A.; Karpenya, L. I., Dexamethasone eye drops based on the products of its interaction with 2-hydroxypropyl-beta-cyclodextrin: synthesis and study. *Pharmaceutical Chemistry Journal* **1999**, *33*, (3), 45-48.
166. Usayapant, A.; Karara, A. H.; Narurkar, M. M., Effect of 2-Hydroxypropyl- β -cyclodextrin on the Ocular Absorption of Dexamethasone and Dexamethasone Acetate. *Pharmaceutical Research* **1991**, *8*, (12), 1495-1499.
167. Blanchemain, N.; Haulon, S.; Martel, B.; Traisnel, M.; Morcellet, M.; Hildebrand, H. F., Vascular PET Prostheses Surface Modification with Cyclodextrin Coating: Development of a New Drug Delivery System. *European Journal of Vascular and Endovascular Surgery* **2005**, *29*, (6), 628-632.

168. Dhanaraju, M. D.; Kumaran, K. S.; Baskaran, T.; Moorthy, M. S. R., Enhancement of bioavailability of griseofulvin by its complexation with beta-cyclodextrin. *Drug Development and Industrial Pharmacy* **1998**, *24*, (6), 583-587.
169. G., A.; S., M.; E., L.-C.; T., T.; E., A.-V., Antimicrobial activity of beta-lactam antibiotics against clinical pathogens after molecular inclusion in several cyclodextrins. A novel approach to bacterial resistance. *Journal of Pharmacy and Pharmacology* **2003**, *55*, (3), 291-300.
170. Domingues, Z. R.; Cortes, M. E.; Gomes, T. A.; Diniz, H. F.; Freitas, C. S.; Gomes, J. B.; Faria, A. M. C.; Sinisterra, R. D., Bioactive glass as a drug delivery system of tetracycline and tetracycline associated with [beta]-cyclodextrin. *Biomaterials* **2004**, *25*, (2), 327-333.
171. Sanghavi, N. M.; Choudhari, K. B.; Matharu, R. S.; Viswanathan, L., Inclusion complexation of lorazepam with beta-cyclodextrin. *Drug Development and Industrial Pharmacy* **1993**, *19*, (6), 701-712.
172. Jessel, N.; Oulad-Abdelghani, M.; Meyer, F.; Lavallo, P.; Haikel, Y.; Schaaf, P.; Voegel, J. C., Multiple and time-scheduled in situ DNA delivery mediated by beta-cyclodextrin embedded in a polyelectrolyte multilayer. *PNAS* **2006**, *103*, (23), 8618-8621.
173. Uekama, K.; Shiotami, K.; Irie, T.; Ishimaru, Y.; Pitha, J., Protective effects of cyclodextrin sulphates against gentamicin-induced nephrotoxicity in the rat. *Journal of pharmacy and pharmacology* **1993**, *45*, (8), 745-747.
174. Suzuki, I.; Sato, K.; Koga, M.; Chen, Q.; Anzai, J.-i., Polyelectrolyte layered assemblies containing azobenzene-modified polymer and anionic cyclodextrins. *Materials Science and Engineering: C* **2003**, *23*, (5), 579-583.
175. Yang, X.; Johnson, S.; Shi, J.; Holesinger, T.; Swanson, B., Polyelectrolyte and molecular host ion self-assembly to multilayer thin films: An approach to thin film chemical sensors. *Sensors and Actuators B: Chemical* **1997**, *45*, (2), 87-92.
176. Yang, X.; Shi, J.; Johnson, S.; Swanson, B., Molecular host siloxane thin films for surface acoustic wave chemical sensors. *Sensors and Actuators B: Chemical* **1997**, *45*, (1), 79-84.
177. Yang, Y.; Yang, X.; Liu, Y.-L.; Liu, Z.-M.; Yang, H.-F.; Shen, G.-L.; Yu, R.-Q., Optical sensor for lithocholic acid based on multilayered assemblies from polyelectrolyte and cyclodextrin. *Journal of Photochemistry and Photobiology A: Chemistry* **2005**, *171*, (2), 137-144.
178. Sato, K.; Suzuki, I.; Anzai, J.-i., Preparation of Polyelectrolyte-Layered Assemblies Containing Cyclodextrin and Their Binding Properties. *Langmuir* **2003**, *19*, (18), 7406-7412.
179. Bauer, T. W.; Schils, J., The pathology of total joint arthroplasty.II. Mechanisms of implant failure. *Skeletal Radiology* **1999**, *28*, (9), 483-497.
180. Lu, W.; Park, T. G., Protein release from poly(lactic-co-glycolic acid) microspheres: Protein stability problems. *PDA Journal of Pharmaceutical Science and Technology* **1995**, *49*, (1), 13-19.
181. Graul, T. W.; Schlenoff, J. B., Capillaries Modified by Polyelectrolyte Multilayers for Electrophoretic Separations. *Anal. Chem.* **1999**, *71*, (18), 4007-4013.
182. Etienne, O.; Gasnier, C.; Taddei, C.; Voegel, J.-C.; Aunis, D.; Schaaf, P.; Metz-Boutigue, M.-H.; Bolcato-Bellemin, A.-L.; Egles, C., Antifungal coating by

- biofunctionalized polyelectrolyte multilayered films. *Biomaterials* **2005**, 26, (33), 6704-6712.
183. Ai, H.; Jones, S. A.; Lvov, Y. M., Biomedical applications of electrostatic layer-by-layer nano-assembly of polymers, enzymes, and nanoparticles. *Cell Biochemistry And Biophysics* **2003**, 39, (1), 23-43.
184. Schneider, A.; Vodouhe, C.; Richert, L.; Francius, G.; LeGuen, E.; Schaaf, P.; Voegel, J. C.; Frisch, B.; Picart, C., Multifunctional Polyelectrolyte Multilayer Films: Combining Mechanical Resistance, Biodegradability, and Bioactivity. *Biomacromolecules* **2007**, 8, (1), 139-145.
185. Zhu, H.; Ji, J.; Shen, J., Osteoblast growth promotion by protein electrostatic self-assembly on biodegradable poly(lactide). *Journal Of Biomaterials Science. Polymer Edition* **2005**, 16, (6), 761-774.
186. Prouty, M.; Lu, Z.; Leuschner, C.; Lvov, Y., Layer-by-Layer Engineered Nanoparticles for Sustained Release of Phor21- β CG(ala) Anticancer Peptide. *Journal of Biomedical Nanotechnology* **2007**, 3, (2), 184-189.
187. Sax, H.; Lew, D., Osteomyelitis. *Current Infectious Disease Reports* **1999**, 1, (3), 261-266.
188. Waldvogel, F. A.; Papageorgiou, P. S., Osteomyelitis: the past decade. *New England Journal of Medicine* **1980**, 303, (7), 360-370.
189. Goldenberg, D. L., Septic arthritis. *Lancet* **1998**, 351, 197-202.
190. Hamed, K. A.; Tam, J. Y.; Prober, C. G., Pharmacokinetic optimization of the treatment of septic arthritis. *Clinical Pharmacokinetics* **1996**, 31, 156-163.
191. Tam, V. H.; Kabbara, S.; Vo, G.; Schilling, A. N.; Coyle, E. A., Comparative Pharmacodynamics of Gentamicin against *Staphylococcus aureus* and *Pseudomonas aeruginosa*. *Antimicrob. Agents Chemother.* **2006**, 50, (8), 2626-2631.
192. Schafer, J. A.; Hovde, L. B.; Rotschafer, J. C., Consistent rates of kill of *Staphylococcus aureus* by gentamicin over a 6-fold clinical concentration range in an in vitro pharmacodynamic model (IVPDM). *J. Antimicrob. Chemother.* **2006**, 58, (1), 108-111.
193. Stallmann, H. P.; Faber, C.; Bronckers, A. L. J. J.; Nieuw Amerongen, A. V.; Wuisman, P. I. J. M., Osteomyelitis prevention in rabbits using antimicrobial peptide hLF1-11- or gentamicin-containing calcium phosphate cement. *J. Antimicrob. Chemother.* **2004**, 54, (2), 472-476.
194. Schultheis, K. H.; Rehm, K. E.; Voelkel, W.; Schiefer, H. G.; Schulz, A.; Kahl, M., A prolamin-antibiotic compound in local treatment of *Staphylococcus aureus*-induced osteomyelitis - a new therapeutic principle. *Chirurgisches Forum fuer Experimentelle und Klinische Forschung* **1983**, 127-131.
195. Kotlus, B. S.; Wymbs, R. A.; Vellozzi, E. M.; Udell, I. J., In vitro Activity of Fluoroquinolones, Vancomycin, and Gentamicin Against Methicillin-Resistant *Staphylococcus aureus* Ocular Isolates. *American Journal of Ophthalmology* **2006**, 142, (5), 721-726.
196. Edmiston, C. E.; Goheen, M. P.; Seabrook, G. R.; Johnson, C. P.; Lewis, B. D.; Brown, K. R.; Towne, J. B., Impact of selective antimicrobial agents on staphylococcal adherence to biomedical devices. *American Journal of Surgery* **2006**, 192, (3), 344-354.

197. Thierry, B.; Kujawa, P.; Tkaczyk, C.; Winnik, F. M.; Bilodeau, L.; Tabrizian, M., Delivery Platform for Hydrophobic Drugs: Prodrug Approach Combined with Self-Assembled Multilayers. *J. Am. Chem. Soc.* **2005**, *127*, (6), 1626-1627.
198. Caruso, F.; Yang, W.; Trau, D.; Renneberg, R., Microencapsulation of Uncharged Low Molecular Weight Organic Materials by Polyelectrolyte Multilayer Self-Assembly. *Langmuir* **2000**, *16*, (23), 8932-8936.
199. Zacharia, N. S.; DeLongchamp, D. M.; Modestino, M.; Hammond, P. T., Controlling Diffusion and Exchange in Layer-by-Layer Assemblies. *Macromolecules* **2007**, *40*, (5), 1598-1603.
200. Kujawa, P.; Moraille, P.; Sanchez, J.; Badia, A.; Winnik, F. M., Effect of Molecular Weight on the Exponential Growth and Morphology of Hyaluronan/Chitosan Multilayers: A Surface Plasmon Resonance Spectroscopy and Atomic Force Microscopy Investigation. *J. Am. Chem. Soc.* **2005**, *127*, (25), 9224-9234.
201. Porcel, C.; Lavallo, P.; Ball, V.; Decher, G.; Senger, B.; Voegel, J. C.; Schaaf, P., From Exponential to Linear Growth in Polyelectrolyte Multilayers. *Langmuir* **2006**, *22*, (9), 4376-4383.
202. Porcel, C.; Lavallo, P.; Decher, G.; Senger, B.; Voegel, J. C.; Schaaf, P., Influence of the Polyelectrolyte Molecular Weight on Exponentially Growing Multilayer Films in the Linear Regime. *Langmuir* **2007**, *23*, (4), 1898-1904.
203. Richert, L.; Lavallo, P.; Payan, E.; Shu, X. Z.; Prestwich, G. D.; Stoltz, J.-F.; Schaaf, P.; Voegel, J.-C.; Picart, C., Layer by Layer Buildup of Polysaccharide Films: Physical Chemistry and Cellular Adhesion Aspects. *Langmuir* **2004**, *20*, (2), 448-458.
204. Burke, S. E.; Barrett, C. J., Swelling Behavior of Hyaluronic Acid/Polyallylamine Hydrochloride Multilayer Films. *Biomacromolecules* **2005**, *6*, (3), 1419-1428.
205. Burke, S. E.; Barrett, C. J., pH-Responsive Properties of Multilayered Poly(L-lysine)/Hyaluronic Acid Surfaces. *Biomacromolecules* **2003**, *4*, (6), 1773-1783.
206. Miller, M. D.; Bruening, M. L., Correlation of the Swelling and Permeability of Polyelectrolyte Multilayer Films. *Chem. Mater.* **2005**, *17*, (21), 5375-5381.
207. Standards, N. C. f. C. L., *Methods for dilution antimicrobial susceptibility tests for bacteria that grow aerobically*. National Committee for Clinical Laboratory Standards: Wayne, PA, 1997; Vol. Approved standard M7-A4.
208. Traub, W. H.; Leonhard, B., Heat stability of the antimicrobial activity of sixty-two antibacterial agents. *J. Antimicrob. Chemother.* %R 10.1093/jac/35.1.149 **1995**, *35*, (1), 149-154.
209. Mingeot-Leclercq, M.-P.; Glupczynski, Y.; Tulkens, P. M., Aminoglycosides: Activity and Resistance. *Antimicrob. Agents Chemother.* **1999**, *43*, (4), 727-737.
210. Anderson, J. M.; Shive, M. S., Biodegradation and biocompatibility of PLA and PLGA microspheres. *Advanced Drug Delivery Reviews* **1997**, *28*, (1), 5-24.
211. Burton, K. W.; Shameem, M.; Thanoo, B. C.; Deluca, P. P., Extended release peptide delivery systems through the use of PLGA microsphere combinations. *Journal of Biomaterials Science, Polymer Edition* **2000**, *11*, (7), 715-729.
212. Jackanicz, T. M.; Nash, H. A.; Wise, D. L.; Gregory, J. B., Poly(lactic acid) as a biodegradable carrier for contraceptive steroids. *Contraception* **1973**, *8*, (3), 227-234.
213. Ogawa, Y.; Okada, H.; Yamamoto, M.; Shimamoto, T., In vivo release profiles of leuprolide acetate from microcapsules prepared with polylactic acids or

- copoly(lactic/glycolic) acids and in vivo degradation of these polymers. *Chemical & Pharmaceutical Bulletin* **1988**, 36, (7), 2576-2581.
214. Okumu, F. W.; Cleland, J. L.; Borchardt, R. T., The effect of size, charge and cyclization of model peptides on their in vitro release from -PLGA microspheres. *Journal of Controlled Release* **1997**, 49, (2-3), 133-140.
215. Monika Schlapp, W. F., Collagen/PLGA microparticle composites for local controlled delivery of gentamicin. *Journal of Pharmaceutical Sciences* **2003**, 92, (11), 2145-2151.
216. Naraharisetti, P. K.; Lee, H. C. G.; Fu, Y.-C.; Lee, D.-J.; Wang, C.-H., In vitro and in vivo release of gentamicin from biodegradable discs. *Journal of Biomedical Materials Research Part B: Applied Biomaterials* **2006**, 77B, (2), 329-337.
217. Friess, W.; Schlapp, M., Sterilization of gentamicin containing collagen/PLGA microparticle composites. *European Journal of Pharmaceutics and Biopharmaceutics* **2005**, 63, (2), 176-187.
218. Simmons, A. In *Sterilization of Medical Devices*, Medical Device Manufacturing & Technology, 2004; 2004.
219. Health, F. C. f. D. a. R., Submission documentation for sterilization process validation in application for human and veterinary devices. *Guidance for Industry* **1994**.
220. Anderson, J. M.; Bavacqua, B.; Cranin, A. N.; al., e., Implants and Devices. In *Biomaterials Science*, Ratner, B. D.; Hoffman, A. S.; Schoen, F. J.; Lemons, J. E., Eds. Academic Press: London, 1996; pp 415-420.
221. Hooper, K. A.; Cox, J. D.; Kohn, J., Comparison of the effect of ethylene oxide and gamma-irradiation on selected tyrosine-derived polycarbonates and poly(L-lactic acid). *Journal of Applied Polymer Science* **1997**, 63, (11), 1499-1510.
222. Goldman, M.; Gronsky, R.; Pruitt, L., The influence of sterilization technique and aging on the structure and morphology of medical-grade ultrahigh molecular weight polyethylene. *Journal of Materials Science - Materials in Medicine* **1998**, 9, (4), 207-212.
223. Zhang, Y. Z.; Bjursten, L. M.; Freij-Larsson, C.; Kober, M.; Wesslen, B., Tissue response to commercial silicone and polyurethane elastomers after different sterilization procedures. *Biomaterials* **1996**, 17, (23), 2265-2272.
224. Sintzel, M. B.; Merkli, A.; Tabatabay, C.; Gurny, R., Influence of irradiation sterilization on polymers used as drug carriers - a review. *Drug Development and Industrial Pharmacy* **1997**, 23, (9), 857-878.
225. Balazs, E. A.; Davies, J. V.; Phillips, G. O.; Young, M. D., *Radiation Research* **1967**, 31, 243.
226. McDonnell, G.; Russell, A. D., Antiseptics and Disinfectants: Activity, Action, and Resistance. *Clinical Microbiology Review* **1999**, 12, (1), 147-179.
227. CDC, Guidelines for infection control. *MMWR* **2003**, 52, (RR-17), 1-66.
228. Riley, D. J.; Bavastrello, V.; Covani, U.; Barone, A.; Nicolini, C., An in-vitro study of the sterilization of titanium dental implants using low intensity UV-radiation. *Dental Materials* **2005**, 21, (8), 756-760.
229. McDonald, K. F.; Curry, R. D.; Clevenger, T. E.; Unklesbay, K. A. U. K.; Eisenstark, A. A. E. A.; Golden, J. A. G. J.; Morgan, R. D. A. M. R. D., A comparison of pulsed and continuous ultraviolet light sources for the decontamination of surfaces. *Plasma Science, IEEE Transactions on* **2000**, 28, (5), 1581-1587.

230. RD, W.; R, M.; K, R.; JM, H.; WH, C., Sterilization of a new medical device using broad-spectrum pulsed light. *Biomed. Instrum. Technol.* **2001**, 35, (5), 323-330.
231. Krishnamurthy, K.; Demirci, A.; Irudayaraj, J., Inactivation of *Staphylococcus aureus* by Pulsed UV-Light Sterilization. *Journal of Food Protection* **2004**, 67, 1027-1030.
232. Stanford, C. M.; Keller, J. C.; Solursh, M., Bone cell expression on titanium surfaces is altered by sterilization treatments. *J Dent Res* **1994**, 73, (5), 1061-1071.
233. Etienne, O.; Picart, C.; Taddei, C.; Haikel, Y.; Dimarcq, J. L.; Schaaf, P.; Voegel, J. C.; Ogier, J. A.; Egles, C., Multilayer Polyelectrolyte Films Functionalized by Insertion of Defensin: a New Approach to Protection of Implants from Bacterial Colonization. *Antimicrob. Agents Chemother.* **2004**, 48, (10), 3662-3669.
234. Boulmedais, F.; Frisch, B.; Etienne, O.; Lavallo, P.; Picart, C.; Ogier, J.; Voegel, J.-C.; Schaaf, P.; Egles, C., Polyelectrolyte multilayer films with pegylated polypeptides as a new type of anti-microbial protection for biomaterials. *Biomaterials* **2004**, 25, (11), 2003-2011.
235. Dierich, A.; Le Guen, E.; Messaddeq, N.; Stoltz, J. F.; Netter, P.; Schaaf, P.; Voegel, J. C.; Benkirane-Jessel, N., Bone Formation Mediated by Synergy-Acting Growth Factors Embedded in a Polyelectrolyte Multilayer Film. *Advanced Materials* **2007**, 19, (5), 693-697.
236. Diefenbeck, M.; Muckley, T.; Hofmann, G. O., Prophylaxis and treatment of implant-related infections by local application of antibiotics. *Injury Infection in Fracture Fixation. From basic research, to diagnosis, to evidence-based treatment* **2006**, 37, (2, Supplement 1), S95-S104.
237. Lucke, M.; Wildemann, B.; Sadoni, S.; Surke, C.; Schiller, R.; Stemberger, A.; Raschke, M.; Haas, N. P.; Schmidmaier, G., Systemic versus local application of gentamicin in prophylaxis of implant-related osteomyelitis in a rat model. *Bone* **2005**, 36, (5), 770-778.
238. Hancock, R. E., Host defence (cationic) peptides: what is their future clinical potential? *Drugs* **1999**, 57, (4), 469-473.
239. Tiozzo, E.; Rocco, G.; Tossi, A.; Romeo, D., Wide-Spectrum Antibiotic Activity of Synthetic, Amphipathic Peptides. *Biochemical and Biophysical Research Communications* **1998**, 249, (1), 202-206.
240. Loose, C.; Jensen, K.; Rigoutsos, I.; Stephanopoulos, G., A linguistic model for the rational design of antimicrobial peptides. *Nature* **2006**, 443, (7113), 867-869.
241. Loose, C. R.; Langer, R. S.; Stephanopoulos, G. N., Optimization of Protein Fusion Partner Length for Maximizing in Vitro Translation of Peptides. *Biotechnol. Prog.* **2007**, 23, (2), 444-451.
242. Guyomard, A.; Dé, E.; Jouenne, T.; Malandain, J.-J.; Muller, G.; Glinel, K., Incorporation of a Hydrophobic Antibacterial Peptide into Amphiphilic Polyelectrolyte Multilayers: A Bioinspired Approach to Prepare Biocidal Thin Coatings. *Advanced Functional Materials* **2008**, 18, (5), 758-765.
243. Orivel, J.; Redeker, V.; Le Caer, J.-P.; Krier, F.; Revol-Junelles, A.-M.; Longeon, A.; Chaffotte, A.; Dejean, A.; Rossier, J., Ponericins, New Antibacterial and Insecticidal Peptides from the Venom of the Ant *Pachycondyla goeldii*. *J. Biol. Chem.* **2001**, 276, (21), 17823-17829.

244. Standards, N. C. f. C. L., *Methods for determining bactericidal activity of antimicrobial agents*. National Committee for Clinical Laboratory Standards: Wayne, PA, 1999; Vol. Approved standard M26-A.
245. Chuang, H. F.; Smith, R.; Hammond, P. T., Polyelectrolyte multilayers for tunable release of antibiotics. In 2008.
246. Balaban, N.; Gov, Y.; Giacometti, A.; Cirioni, O.; Ghiselli, R.; Mocchegiani, F.; Orlando, F.; D'Amato, G.; Saba, V.; Scalise, G.; Bernes, S.; Mor, A., A Chimeric Peptide Composed of a Dermaseptin Derivative and an RNA III-Inhibiting Peptide Prevents Graft-Associated Infections by Antibiotic-Resistant Staphylococci. *Antimicrob. Agents Chemother.* **2004**, 48, (7), 2544-2550.
247. Fluckiger, U.; Zimmerli, W., Diagnosis and follow-up management of postoperative bacterial osteomyelitis. *Orthopade* **2004**, 33, (4), 416.
248. Mendes, S. C.; Reis, R. L.; Bovell, Y. P.; Cunha, A. M.; van Blitterswijk, C. A.; de Bruijn, J. D., Biocompatibility testing of novel starch-based materials with potential application in orthopaedic surgery: a preliminary study. *Biomaterials* **2001**, 22, (14), 2057-2064.
249. Curtis, M. J.; Brown, P. R.; Dick, J. D.; Jinnah, R. H., Contaminated fractures of the tibia: A comparison of treatment modalities in an animal model. *Journal of Orthopaedic Research* **1995**, 13, (2), 286-295.
250. Salgado, C.; Jamali, A.; Mardini, S.; Buchanan, K.; Veit, B., A model for chronic osteomyelitis using Staphylococcus aureus in goats. *Clinical Orthopaedics And Related Research* **2005**, 436, 246-250.
251. Gursel, I.; Korkusuz, F.; Turesin, F.; Gurdal Alaeddinoglu, N.; Hasirci, V., In vivo application of biodegradable controlled antibiotic release systems for the treatment of implant-related osteomyelitis. *Biomaterials* **2001**, 22, (1), 73-80.
252. Craig, M. R.; Poelstra, K. A.; Sherrell, J. C.; Kwon, M. S.; Belzile, E. L.; Brown, T. E., A novel total knee arthroplasty infection model in rabbits. *Journal of Orthopaedic Research* **2005**, 23, (5), 1100-1104.
253. DAROUICHE, R. O.; FARMER, J.; CHAPUT, C.; MANSOURI, M.; SALEH, G.; LANDON, G. C., Anti-Infective Efficacy of Antiseptic-Coated Intramedullary Nails. *J Bone Joint Surg Am* **1998**, 80, (9), 1336-1340.
254. Darouiche, R. O.; Landon, G. C.; Patti, J. M.; Nguyen, L. L.; Fernau, R. C.; McDevitt, D.; Greene, C.; Foster, T.; Klima, M., Role of Staphylococcus aureus surface adhesins in orthopaedic device infections: are results model-dependent? *J Med Microbiol* **1997**, 46, (1), 75-79.
255. Nelson, C. L.; McLaren, S. G.; Skinner, R. A.; Smeltzer, M. S.; Roby Thomas, J.; Olsen, K. M., The treatment of experimental osteomyelitis by surgical debridement and the implantation of calcium sulfate tobramycin pellets. *Journal of Orthopaedic Research* **2002**, 20, (4), 643-647.
256. Marc W. Nijhof, A. F., Karin Hardus, H. Charles Vogely, Leo M. Schouls, Abraham J. Verbout, Wouter J. A. Dhert,, Tobramycin-containing bone cement and systemic cefazolin in a one-stage revision. Treatment of infection in a rabbit model. *Journal of Biomedical Materials Research* **2001**, 58, (6), 747-753.
257. Koort, J. K.; Makinen, T. J.; Suokas, E.; Veiranto, M.; Jalava, J.; Knuuti, J.; Tormala, P.; Aro, H. T., Efficacy of Ciprofloxacin-Releasing Bioabsorbable Osteoconductive Bone Defect Filler for Treatment of Experimental Osteomyelitis Due to

- Staphylococcus aureus. *Antimicrob. Agents Chemother.* %R 10.1128/AAC.49.4.1502-1508.2005 **2005**, 49, (4), 1502-1508.
258. Brown, R. C.; Hopps, H. C., Staining of bacteria in tissue sections: a reliable gram stain method. *American journal of clinical pathology* **1973**, 60, (2), 234-240.
259. Engbaek, K.; Johansen, K. S.; Jensen, M. E., A new technique for Gram staining paraffin-embedded tissue. *Journal of Clinical Pathology* **1979**, 32, (2), 187-190.
260. Zhang, J.; Fredin, N. J.; Janz, J. F.; Sun, B.; Lynn, D. M., Structure/Property Relationships in Erodible Multilayered Films: Influence of Polycation Structure on Erosion Profiles and the Release of Anionic Polyelectrolytes. *Langmuir* **2006**, 22, (1), 239-245.
261. Recksiedler, C. L.; Deore, B. A.; Freund, M. S., A Novel Layer-by-Layer Approach for the Fabrication of Conducting Polymer/RNA Multilayer Films for Controlled Release. *Langmuir* **2006**, 22, (6), 2811-2815.
262. Kidambi, S.; Mehrotra, S.; Gredell, J. A.; Walton, S. P.; Lee, I.; Chan, C., Polyelectrolyte multilayer films as platforms for efficient siRNA delivery. . In *234th ACS National Meeting*, Boston, MA, 2007.
263. Soto, E. R.; Ostroff, G. R., Characterization of Multilayered Nanoparticles Encapsulated in Yeast Cell Wall Particles for DNA Delivery. *Bioconjugate Chem.* **2008**, 19, (4), 840-848.
264. Schlee, M.; Hornung, V.; Hartmann, G., siRNA and isRNA: Two Edges of One Sword. *Molecular Therapy* **2006**, 14, (4), 463-470.

Chapter 10. Appendices

Appendix A. Acronyms

Acronym	Full Name	Description
AmP	Antimicrobial peptide	A family of short peptides with broad spectrum bacteriocidal activity.
BCA	Bicinchoninic acid	An agent used for colometric quantitation of proteins and peptides.
bFGF	Basic fibroblast growth factor	A class of growth factors that promotes fibroblastic cell proliferation.
BMP	Bone morphogenetic protein	A class of growth factors especially useful for therapeutic osteogenesis
BSA	Bovine serum albumin	A model protein often used in polymer matrix release studies.
Chi	Chitosan	A biocompatible polysaccharide; found to freely diffuse among layers.
Dex	Dexamethasone	A non-steroidal anti-inflammatory drug.
DS	Dextran sulfate	An anionic polysaccharide.
FGF	See bFGF	
FITC	Fluorescein isothiocyanate	A fluorescent tag often used for particle release studies.
FTIR	Fourier Transform Infrared Spectroscopy	An analytical technique that measures the absorption of various infrared light wavelengths by the material of interest.
GS	Gentamicin sulfate	An aminoglycosidic antibiotic.
HA	Hyaluronan	An anionic polysaccharide.
Hep	Heparin	An anionic polysaccharide with anti-coagulant function.
IOL	Intraocular lens	An implant replacing natural lens of the eye after surgical cataract removal
LB	Langmuir-Blodgett	A technique to make multilayered thin films via transfer of preassembled monolayers from a solution interface to the substrate.
LbL	Layer-by-layer	Construction of multilayered films by sequential adsorptions of polyelectrolytes.
MW	Molecular Weight	
PAA	Poly(acrylic acid)	Weak polyanion.
PB	Prussian blue	A transition metal hexacyanoferrate complex; potential candidate for electrochemically-degradable drug delivery device
PDADMAC	Poly(diallyldimethylammonium chloride)	A polycation.
PEI	Poly(ethylene imine)	Commonly used for DNA delivery; has been found to be mildly cytotoxic.
PEL	Polyelectrolytes	Polymers consisting of charged subunits.
PEM	Polyelectrolyte	An LbL-assembled thin film of polyelectrolytes

	multilayers	
PGA	Poly(glycolic acid)	See description for PLA.
PLA	Poly(lactic acid)	A polyester which is a natural metabolite and highly biocompatible.
PLGA	Poly(lactic-co-glycolic acid)	A copolymer commonly used to make micro/nanospheres which can encapsulate a wide range of drugs.
PLL	Poly(L-lysine)	Polypeptide commonly used in LbL assembly.
<i>Poly I</i>	A poly(β -amino ester)	A degradable, biocompatible polymer created by Lynn <i>et al.</i> ²³ ; see Figure 1.
PSS	Poly(styrene sulfonate)	Strong polyanion commonly used for LbL assembly.
QCM	Quartz Crystal Microbalance	A mechanical, surface-specific technique that measures the mechanical properties of an adsorbate, including viscosity, elasticity, density and thickness.
VEGF	Vascular endothelial growth factor	A class of growth factors especially useful for therapeutic angiogenesis

Appendix B. CAC Protocol on surgical procedures.

Surgical Procedures

This form may be submitted in support of a protocol application or separately, as an addendum. If this is an addendum, please also provide a cover letter that includes the following: PI Name/Department; Protocol Number/Title; Contact Person/Contact Details; and PI Signature (required). If submitting a request to add additional surgical procedures to the use of animals that have had, or been approved for, prior surgery, please first review the last section of this form.

Indicate which type(s) of surgery will you be performing:

Single Terminal Surgery Single Survival Surgery Multiple Surgeries on

Objectives

Explain your objectives. If more than one surgical procedure is proposed for individual animals, provide scientific justification. Considerations of reducing the number of animals used or cost are not sufficient justification.

To evaluate biocompatibility and efficacy of polymer-based antibiotic-eluting films on implant surfaces *in-vivo*, for the specific application of delivery from the surfaces of prostheses for revision arthroplasty. This aim will include the determination of compatibility and toxicity in a typical implant environment, and will also involve collaborations with Dr. Myron Spector and his associate, Dr. Hu Ping Hsu, who will perform the animal studies. Infection studies using a rabbit model will be used to determine the remediation of bone infection from implants coated with a single antibacterial agent at doses determined to be efficacious based on *in vitro* studies. The results of these studies will be addressed in consultation with Drs. Larry Madoff and Mitch Harris.

Animal Species to be Used

Animal species (indicate strain and/or genetic modification) and quantities per year:

> 20 New Zealand white rabbits, male, 2-3 kg, 3 months old

Details of Surgery

Describe **details of surgery** including preparation of animal such as fasting (if applicable), surgical approach, intraoperative manipulations, and methods of closure (type of suture or wound clip to close each tissue layer as applicable - muscle wall, subcutaneous tissue and skin). If **multiple surgeries** on individual animals are part of the experimental design, describe each separate surgery, the intended number per animal over its experimental use, and the time interval between procedures.

> All surgical procedures and follow-up care will be done with especial attention to avoid *S. aureus* contamination of the facilities, following the guidelines established in Section 5 of Supplement I of the original application.

Rabbits will be divided into seven groups: (1) osteomyelitis evaluation with PMMA rod colonized in 10^6 CFU/mL culture, (2) osteomyelitis evaluation with PMMA rod colonized in 10^8 CFU/mL culture, (3) positive control with treatment of established osteomyelitis by Palacos® R+G, a gentamicin-impregnated bone cement, (4) negative control with treatment of established osteomyelitis by uncoated titanium rod, (5) sample group with gentamicin-coated titanium rod, (6) sample group with lysostaphin-coated titanium rod, and (6) sample group with gentamicin and lysostaphin-coated titanium rod. Two animals will be assigned to each of groups (1)-(4), while four animals will be assigned to each of groups (5)-(7), and evaluations on groups (1) and (2) will be completed before initiating the remaining groups. Anesthesia will be induced by SC doses of 35 mg/kg ketamine and 5 mg/kg xylazine. The rabbits will also be administered a SQ dose of 0.01-0.05 mg/kg Buprenex and 0.2 mg/kg Meloxicam SC/OP. The back of the rabbit will be shaved and prepared with alternating Betadine scrub and 70% IPA, and 10 mg lidocaine will be administered into the lumbosacral space. The left thigh and leg will be shaved, and each lower extremity will be prepared with several 7.5% Povidone Iodine scrubs

and final 70% alcohol rinse. Anesthesia will be maintained using 1-3% isoflurane gas with oxygen at 1–1.5 L/min through an endotracheal tube. Endotracheal tubes will be lubricated with Xylocaine Viscous^R solution prior to insertion. Throughout each procedure, animal's heart rate, respiratory rate, and oxygen level will be monitored. Lactated Ringer's solution will be administered through a catheter inserted into a cephalic vein, at an initial rate of 10 mL/kg-hr then tapered according to observed hemodynamic parameters.

The left lower extremity of each animal will be draped with sterile adhesive surgical drapes. All surgical procedures will be performed under sterile conditions. To minimize variability and ensure a standardized surgical procedure, all operations will be performed by Dr. Ho-Ping Hsu. A straight medial side incision, approximately 3.5-4.0 cm, will be made, the midpoint of which will be centered to the knee joint line. The skin and soft tissue will be dissected to the deep investing fascia. An SC dose of 2 mg/kg Lidocaine at the surgical site after opening. A small longitudinal incision will be made at the front portion of the superior attachment of MCL, approximately 10 mm above a branch of popliteal artery, to release the periosteum to expose the medial femoral condylar surface. Using a 3.00 mm sterile drill bit, a defect 10 mm in length will be drilled at the level of the posterior portion of the anterior edge of medial femur about 10 mm. Blood loss will be monitored, and animals will receive three times the estimated loss throughout the procedure. The entire surgical procedure will be kept wet by sterile saline sponges, and irrigation is used and maintained during the drills.

After saline joint lavage and hemostasis, a colonized PMMA (poly(methyl methacrylate) rod (2.8mm diameter and 8.5mm length, with a 3.0mm diameter cap at the top to seal the defect), prepared by immersing sterilized rods in a 10^8 CFU/mL exponentially-growing culture of *S. aureus* overnight, will be press-fit into the defect. The surgical site will be closed in layers using 3-0 interrupted sutures for the investing fascia, 3-0 sutures for the superficial fascia and subcutaneous tissue, followed by reapproximation of the skin with a subcuticular stitch using a non-absorbable 3-0 monofilament nylon suture. Postoperatively, AP and lateral radiographs will be taken on each animal's surgical site, and each animal will be monitored closely until full recovery from anesthesia was observed. Once in their individual cages, each animal will be allowed free access to water and antibiotic-free food. Animals will be monitored daily for food intake, stool and urine output, body temperature and behavior.

After four weeks, rabbits from groups (1) and (2) will be sacrificed. The PMMA rod, bone around the implant site, synovial tissue, synovial fluid, and joint capsule will be harvested for histological and microbiological evaluations. 7-10 cc of blood will be drawn from the heart after anesthesia but prior to euthanasia for CBC and microbiological evaluation. We will begin with only one animal for each of groups (1) and (2) to evaluate morbidity, and modify CFU burden, defect size, and/or pain management regime for the second pair of animals accordingly. Based on evaluations on groups (1) and (2), the more appropriate amount of *S. aureus* inoculum will be determined, and this will be the amount used on groups (3) and (4).

Groups (3)-(7) will undergo identical survival procedure as outlined for groups (1) and (2) above. However, these animals will receive a second survival surgery after the two-week recovery. X-rays of the left femurs will be taken prior to the second survival surgery, and the surgical sites of the animals will be reopened, following the same sterile surgical procedure and monitoring regimen as described above, and treated with focal debridement followed by saline lavage. The PMMA rod will be retrieved and stored sterilely in a vial for microbiological assay. The appropriate implant, according to the test group assignment, will be press-fit into the defect. After hemostasis and saline lavage, the wound will be closed in layers using the same procedure as described above. AP and lateral radiographs will be taken on each animal's surgical site prior to recovery from anesthesia. Each animal will receive identical postoperative care as described in the previous paragraph.

Each animal will be euthanized two weeks after second surgery, according to the approved protocol. An x-ray of the left femur will be taken prior to the surgery to confirm position of the implant. 7-10 cc of blood will be drawn from the heart after anesthesia but prior to euthanasia and stored in Vacutainers for CBC and microbiological evaluation. Under sterile conditions, the skin of each knee will be sharply incised and the joint capsule will be exposed. Fluid will be aspirated from each knee joint. The joint capsule will then be sharply incised and the inflammatory reaction of each knee will be graded. Biopsies from the joint capsule and synovial tissue and fluid surrounding the rod, will be obtained. The medial femur will be cut out and split in half along the implant site, each stored sterilely, one for microbiological evaluation and another for histology in 10% formaline. The titanium rod implant will be retrieved after bone splitting and stored sterilely for microbiological assay. All harvested tissues will be placed in 1 mL of sterile freeze medium and sample tare weights will be determined. Each rod will be sonicated for 30 min in a 4 °C water bath to detach bacteria. Tissue samples will be homogenized under sterile conditions using a Polytron generator (Brinkman Instruments Inc., Westbury, NY) in a BL2 hood. Each homogenate will be kept at 4 °C before and after homogenization. All tissue processing will be performed in instruments approved for BL2 bacteria use and confined within a BL2 hood if possible. Any sample to be taken out of the BL2 hood will be tightly sealed in a leak-proof containing device.

Personnel

If survival surgery, these name(s) of surgeon(s) should match survival surgery column in Section 8 of main protocol

Name of surgeon:	Lab and home phone numbers:
> Hu-Ping Hsu, M.D.	> Lab: (857) 364-5343 Cell: (978)987-1591
Name of anesthetist if different:	Lab and home phone numbers:
> Alison Hayward, or Helen Chuang under supervision.	> x2-3629, or x8-7038
Personnel responsible for postoperative care if different:	Lab and home phone numbers:
> Monitoring: Helen Chuang	> Lab: x8-7038 Home: x7-5696 Cell: (617)905-3898 Lab: (617) 253-3050 Home: on file with DCM
Veterinary care: Alison Hayward, DVM	
Building and Room address where surgery will be performed (investigator's lab or DCM facility with room number):	
> E25 OR 1 (approved for BL2 procedure)	

Anesthesia

Premedication (include doses in mg/kg, volume of injection(s), and route of administration):

> SQ dose of 0.01-0.05 mg/kg Buprenex and an SC dose of 2 mg/kg Lidocaine at the surgical site right before surgery

Anesthesia drug and starting dose. For injectables, provide dose in mg/kg, volume of injection(s), and route of administration. For inhalants, indicate delivery mechanism and scavenging method.

> Anesthesia will be induced by SC doses of 35 mg/kg ketamine and 5 mg/kg xylazine and maintained by 1-3% isoflurane with oxygen at 1-1.5 L/min through an endotracheal tube. No vaporizer or bell jar will be used, and the anesthetic circuit will be adapted with a scavenging hose that vents into the non-circulating facility exhaust.

How will depth of anesthesia be monitored?

> Depth of anesthesia will be monitored by:

- Reflexes: including pinnae reflex, palperbral reflex, toe pinch reflex, and corneal reflex.
- Cardiopulmonary function: including heart rate, blood pressure, and respiration.
- Body temperature

Throughout the surgery, the respiration, oxygen, pulse, EKG, and blink response of the animal will be observed and the animal closely examined for signs of distress including flinching.

Use of paralytics under general anesthesia

If you will be using paralytics, provide rationale, drug name, dose in mg/kg, volume of injection(s), route of administration and how anesthesia will be monitored and adjusted.

> N/A

Verification of Aseptic Technique

It is required that aseptic technique be used in all survival surgical procedures. All the aspects of aseptic technique listed below must be addressed. Give rationale if you wish to be exempt from any of these.

Indicate which methods will be used for instrument sterilization:

Autoclave Autoclave with use of Glass Bead Sterilizer between animals

Other (describe along with rationale): EtO, for the surgical marker which is heat sensitive.

Indicate which methods will be used for implant sterilization:

Autoclave Ethylene Oxide Commercially-supplied Sterile Implants

Other (describe along with rationale): immersion in 70% ethanol for 24 hours.

Verify that aseptic preparation of the surgery site will include:

Clipping hair (if present) with #40 blade or using a depilatory agent followed by cleaning the incision site with several cycles of povidine iodine (Betadine scrub), or chlorhexidine scrub, followed by alcohol rinse. Final application of Betadine or chlorhexidine solution is considered optional.

Other (describe along with rationale):

Indicate which methods will be used for maintaining the aseptic/sterile field* (check all that apply):

Sterile Drapes Sterile Gloves Face Mask Sterile Surgical Gown
 Surgeon's Bonnet

Other (describe in detail): goggles and shoe covers.

**Due to visibility problems related to small body size and relative risk of contamination, the use of drapes, gowns, and bonnets may not be practical for some forms of rodent surgery. NIH Guidelines for Aseptic Surgery on Rodents are posted on the CAC website at <https://web.mit.edu/comp-med/Restrict/CAC/sptop11.htm> [CAC Policies/Special Topics].*

Postoperative Procedures,
Analgesia Plan, and
Maintenance of Medical
Records

Procedures known to cause postoperative pain in humans should be considered painful to animals. Analgesia should be routinely administered before anesthetic recovery and continued postoperatively based on the relative invasiveness of the procedure and evaluation of each animal for signs of pain (for example, a thoracotomy is considered sufficiently painful that analgesia should be given for several days irrespective of what appears to be a comfortable postoperative animal). Drugs of choice include buprenorphine, morphine, fentanyl (available as patch for larger species), carprofen, and ketoprofen (injectable drugs with systemic effects); and lidocaine or bupivacaine (longer acting lidocaine) for regional analgesia, such as for a thoracotomy. Consult the Laboratory Animal Users' Handbook and the veterinarian for your animal colony for advice on drug selection, dosage, potential side effects, and duration of pre-emptive analgesia. If analgesia will interfere with your research objectives, you must provide scientific justification.

Describe the postop care plan including how often animals will be monitored and how potential complications such as pain, inflammation or infection will be treated. All drugs (analgesics, anti-inflammatories, antibiotics, others) to be used must be named along with the starting dose in mg/kg and route and timing of administration (supply details even if described elsewhere in the protocol). Pre-emptive dosing with analgesics during surgery prep is optimal to achieve adequate blood levels before anesthesia wears off. Continued dosing should be based on assessment of each animal for signs of pain. Antibiotics should be chosen based on risk assessment in combination with advice from the veterinary staff.

The rabbits will also be administered a SQ dose of 0.01-0.05 mg/kg Buprenex and an SC dose of 2 mg/kg Lidocaine at the surgical site right before surgery. 0.01-0.05 mg/kg Buprenex SQ Q6-12hr will be given in the first 24 hrs then more as necessary. Animals will be monitored for signs of pain, distress, or sepsis based on food and water consumption, breathing and heart rate, stool and urine output, redness or swelling at surgical site, body temperature, abnormal posture and behaviors, respiration, physical movements (including twitching and tremor), response to stimuli, and vocalization. Additional pain management will include 0.2 mg/kg Meloxicam SC/PO Q24hr as necessary..

List any additional follow-up care until healing is judged complete including when you expect to remove skin sutures or wound clips:

> Animals will be monitored daily for signs of pain, distress, or sepsis as described above. In addition, animal weight will be monitored for excessive loss. Animals that appear to be in discomfort will receive 0.01-0.05 mg/kg Buprenex SQ Q6-12hr and 0.2 mg/kg Meloxicam SC/PO Q24hr as necessary. . Animals displaying signs of poor condition postoperatively will be euthanized by IV injection with 120 mg/kg Pentobarbital. These signs of moribund condition include: sepsis (as indicated by signs of septic shock, including fever, rapid breathing, increased heart rate, decreased urine output, and lateral recumbency), excessive weight loss (>15% initial weight within two weeks), lack of responsiveness to stimuli and persistent non-weight bearing lameness. If the animal is experiencing excessive weight loss and an euthanasia is scheduled within 2 days, the animal may be force-fed with wet feed (combination of powdered pellet, Nutracal, and water) for temporary weight maintenance. No suture or clip removal is necessary.

Rodents, birds, amphibians, reptiles and similar species should have DCM-issued white surgery cards posted on their cage with clear documentation to alert the veterinary staff to the date and type of surgery performed. These cage cards should also indicate preemptive analgesia and list ensuing postoperative monitoring entries as needed until healing is complete (7-14 days on average). DCM postoperative care forms for rabbits, ferrets, livestock, nonhuman primates, cats, and dogs must be completed at the time of surgery, with monitoring forms kept in the animal room. Surgery cage cards or DCM-issued surgery forms must remain with the animal until sutures or wound clips are removed and postoperative complications have been resolved. Note that the drug regimens (drug name, dose, route and timing of administration) must be documented on the DCM-issued white surgery cards or in the animal's medical record on the same schedule as approved by the CAC unless veterinary consultation changes the treatment plan.

STOP: The remainder of this supplement is to be filled out only in the case where one needs to request additional, major survival surgical procedures in individual animals beyond the quantity that has been previously approved by the CAC.

Request for Additional Major Survival Surgical Procedures Beyond Previously Approved Number

If this is a request for additional surgical procedures on individual animals beyond the quantity that has been previously approved by the CAC, and the surgical procedures you will perform have been previously described and approved by the CAC for this protocol, please fill out (just) the information below. If the additional surgical procedures and personnel are not identical to descriptions already in your approved protocol, please also fill out the appropriate sections above to indicate changes.

Animal Species and ID (common name, ear tag, tattoo etc.):

>

Describe objectives and scientific justification:

>

Provide brief description of additional surgical procedure(s):

>

Describe surgical history of each animal or, if more appropriate, each experimental group (such as rodents). List major procedures, dates performed, any morbidity encountered, and its resolution.

>

DCM Veterinarian
Endorsement

Date:

Signature of DCM veterinary staff confirming that clinical condition of animal(s) is (are) good to excellent and that additional surgery is expected to be routine.